Title

LABORATORY INVESTIGATIONS OF THERMOMECHANICAL PROPERTIES OF STRIPA GRANITE. PART I: APPARATUS. PART II: APPLICAION AND RESULTS

Authors

Myer, L.
Rachiele, R.

Publication Date

1981-08-01

LBL-13435 c.2
SAC-40
UC-70

SWEDISH-AMERICAN COOPERATIVE PROGRAM ON RADIOACTIVE WASTE STORAGE IN MINED CAVERNS IN CRYSTALLINE ROCK

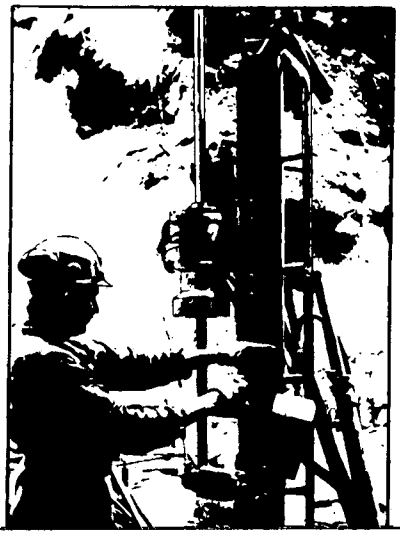

Technical Information No. 40

LABORATORY INVESTIGATIONS OF THERMOMECHANICAL PROPERTIES OF STRIPA GRANITE

Part I: Apparatus
Part II: Application and Results

L. Myer and R. Rachiele
Lawrence Berkeley Laboratory
University of California
Berkeley, CA 94720

August 1981

A Joint Project of

Swedish Nuclear Fuel Supply Co.
Fack 10240 Stockholm, Sweden

Operated for the Swedish
Nuclear Power Utility Industry

Lawrence Berkeley Laboratory
Earth Sciences Division
University of California
Berkeley, California 94720, USA

Operated for the U.S. Department of
Energy under Contract DE-AC03-76SF00098

DISCLAIMER

LBL-13435
SAC-40
UC-70

LABORATORY INVESTIGATIONS OF THERMOMECHANICAL PROPERTIES OF STRIPA GRANITE

Part I: Apparatus

Part II: Application and Results

L. Myer and R. Rachiele

Earth Sciences Division
Lawrence Berkeley Laboratory
University of California
Berkeley, California 94720

August, 1981

This work was supported by the Assistant Secretary for Nuclear Energy, Office of Waste Isolation, U.S. Department of Energy under Contract No. DE-AC03-76SF00098. Funding for this project is administered by the Office of Nuclear Waste Isolation at Battelle Memorial Institute.

PREFACE

This report is one of a series documenting the results of the Swedish-American cooperative research program in which the cooperating scientists explore the geological, geophysical, hydrological, geochemical, and structural effects anticipated from the use of a large crystalline rock mass as a geologic repository for nuclear waste. This program has been sponsored by the Swedish Nuclear Power Utilities through the Swedish Nuclear Fuel Supply Company (SKBF), and the U.S. Department of Energy (DOE) through the Lawrence Berkeley Laboratory.

The principal investigators are L.B. Nilsson and O. Degerman for SKBF, and N.G.W. Cook, P.A. Witherspoon, and J.E. Gale for LBL. Other participants will appear as authors of the individual reports.

Previous technical reports in this series are listed below.

1. Swedish-American Cooperative Program on Radioactive Waste Storage in Mined Caverns by P.A. Witherspoon and O. Degerman. (LBL-7049, SAC-01).

2. Large Scale Permeability Test of the Granite in the Stripa Mine and Thermal Conductivity Test by Lars Lundstrom and Haken Stille. (LBL-7052, SAC-02).

3. The Mechanical Properties of the Stripa Granite by Graham Swan. (LBL-7074, SAC-03).

4. Stress Measurements in the Stripa Granite by Hans Carlsson. (LBL-7078, SAC-04).

5. Borehole Drilling and Related Activities at the Stripa Mine by P.J. Kurfurst, T. Hugo-Persson, and G. Rudolph. (LBL-7080, SAC-05).

6. A Pilot Heater Test in the Stripa Granite by Hans Carlsson. (LBL-7086, SAC-06).

7. An Analysis of Measured Values for the State of Stress in the Earth's Crust by Dennis B. Jamison and Neville G.W. Cook. (LBL-7071, SAC-07).

8. Mining Methods Used in the Underground Tunnels and Test Rooms at Stripa by B. Andersson and P.A. Halen. (LBL-7081, SAC-08).

9. Theoretical Temperature Fields for the Stripa Heater Project by T. Chan, Neville G.W. Cook, and C.F. Tsang. (LBL-7082, SAC-09).

10. Mechanical and Thermal Design Considerations for Radioactive Waste Repositories in Hard Rock. Part I: An Appraisal of Hard Rock for Potential Underground Repositories of Radioactive Waste by N.G.W. Cook; Part II: In Situ Heating Experiments in Hard Rock: Their Objectives and Design by N.G.W. Cook and P.A. Witherspoon. (LBL-7073, SAC-10).

11. Full-Scale and Time-Scale Heating Experiments at Stripa: Preliminary Results by N.G.W. Cook and M. Hood. (LBL-7072, SAC-11).

12. Geochemistry and Isotope Hydrology of Groundwaters in the Stripa Granite: Results and Preliminary Interpretation by P. Fritz, J.F. Barker, and J.E. Gale. (LBL-8285, SAC-12).

13. Electrical Heaters for Thermo-Mechanical Tests at the Stripa Mine by R.H. Burleigh, E.P. Binnall, A.O. DuBois, D.O. Norgren, and A.R. Ortiz. (LBL-7063, SAC-13).

14. Data Acquisition, Handling, and Display for the Heater Experiments at Stripa by Maurice B. McEvoy. (LBL-7063, SAC-14).

15. An Approach to the Fracture Hydrology at Stripa: Preliminary Results by J.E. Gale and P.A. Witherspoon. (LBL-7079, SAC-15).

16. Preliminary Report on Geophysical and Mechanical Borehole Measurements at Stripa by P. Nelson, B. Paulsson, R. Rachiele, L. Andersson, T. Schrauf, W. Hustrulid, O. Duran, and K.A. Magnussen. (LBL-8280, SAC-16).

17. Observations of a Potential Size-Effect in Experimental Determination of the Hydraulic Properties of Fractures by P.A. Witherspoon, C.H. Amick, J.E. Gale, and K. Iwai. (LBL-8571, SAC-17).

18. Rock Mass Characterization for Storage in Nucler Waste in Granite by P.A. Witherspoon, P. Nelson, T. Doe, R. Thorpe, B. Paulsson, J.E. Gale, and C. Forster. (LBL-8570, SAC-18).

19. Fracture Detection in Crystalline Rock Using Ultrasonic Shear Waves by K.H. Waters, S.P. Palmer, and W.F. Farrell. (LBL-7051, SAC-19).

20. Characterization of Discontinuities in the Stripa Granite--Time Scale Heater Experiment by R. Thorpe. (LBL-7083, SAC-20).

21. Geology and Fracture System at Stripa by A. Okliewicz, J.E. Gale, R. Thorpe, and B. Paulsson. (LBL-8907, SAC-21).

22. Calculated Thermally Induced Displacements and Stresses for Heater Experiements at Stripa by T. Chan and N.G.W. Cook. (LBL-7061, SAC-22).

23. Validity of Cubic Law for Fluid Flow in a Deformable Rock Fracture by P.A. Witherspoon, J. Wang, K. Iwai, and J.E. Gale. (LBL-9557, SAC-23).

24. Determination of In-Situ Thermal Properties of Stripa Granite from Temperature Measurements in the Full-Scale Heater Experiments: Methods and Primary Results by J. Jeffry, T. Chan, N.G.W. Cook and P.A. Witherspoon. (LBL-8424, SAC-24).

25. Instrumentation Evaluation, Calibration, and Installation for Heater Tests Simulating Nuclear Waste in Crystalline Rock, Sweden by T. Schrauf, H. Pratt, E. Simonson, W. Hustrulid, P. Nelson, A. DuBois, E. Binnall, and R. Haught. (LBL-8313, SAC-25)

26. Part I: Some Results From a Field Investigation of Thermo-Mechanical Loading of a Rock Mass When Heater Canisters are Emplaced in the Rock by M. Hood. Part II: The Application of Field Data from Heater Experiments Conducted at Stripa, Sweden for Repository Design by M. Hood, H. Carlsson, and P.H. Nelson. (LBL-9392, SAC-26).

27. Progress with Field Investigations at Stripa by P.A. Witherspoon, N.G.W. Cook, and J.E. Gale (LBL-10559, SAC-27).

28. A Laboratory Assessment of the Use of Borehole Pressure Transients to Measure the Permeability of Fractured Rock Masses by C.B. Forster and J.E. Gale. (LBL-8674, SAC-28).

29. Thermal and Thermomechanical Data for In Situ Heater Experiments at Stripa, Sweden by T. Chan, E. Binnall, P. Nelson, O. Wan, C. Weaver, K. Ang, J. Braley, and M. McEvoy. (LBL-11477, SAC-29).

30. The Effect of Radon Transport in Groundwater Upon Gamma Ray Borehole Logs by P.H. Nelson, R. Rachiele, and A. Smith. (LBL-11180, SAC-30).

31. Strength and Permeability Tests on Ultra-Large Stripa Granite Core by R. Thorpe, D.J. Watkins, W.E. Ralph, R. Hsu, and S. Flexser. (LBL-11203, SAC-31).

32. Ultrasonic and Acoustic Emission Results from the Stripa Heater Experiments. Part I: A Cross-Hole Investigation of a Rock Mass Subjected to Heating by B.N.P. Paulsson and M.S. King. Part II: Acoustic Emission Monitoring During Cool-Down of the Stripa Heater Experiment by R. Rachiele. (LBL-10975, SAC-32).

33. Numerical Modeling to Assess Possible Influence of the Mine Openings on Far-Field In Situ Stress Measurements at Stripa by T. Chan, V. Guvanasen, and N. Littlestone (LBL-12469, SAC-33).

34. A Field Assessment of the Use of Borehole Pressure Transients to Measure the Permeability of Fractured Rock Masses by C.B. Forster and J.E. Gale. (LBL-11829, SAC-34).

35. Water Inflow into Boreholes During the Stripa Experiments by P.H. Nelson, R. Rachiele, J.S. Remer and H.S. Carlsson (LBL-12547, SAC-35).

36. Petrology and Radiogeology of the Stripa Pluton by H. Wollenberg, S. Flexser, and L. Andersson. (LBL-11654, SAC-36).

37. Geohydrological Data from the Macopermeability Experiment at Stripa, Sweden by C.R. Wilson, J.C.S. Long, R.M. Galbraith, K. Karasaki, H.K. Endo, A.O. DuBois, M.J. McPherson, and G. Ramqvist. (LBL-12520, SAC-37).

38. Characterization of Discontinuities in the Stripa Granite--Full-Scale Heater Experiments by B.N.P. Paulsson, P.H. Nelson, and P.J. Kurfurst. (LBL-9063, SAC-38).

39. Application of Borehole Geophysics at an Experimental Waste Storage Site by P.H. Nelson, K.A. Magnusson, and R. Rachiele. (LBL-11982, SAC-39).

TABLE OF CONTENTS

LIST OF FIGURES

Page

Page

Page

LIST OF TABLES

PART I

PART II

ABSTRACT

The Stripa material properties investigations were carried out in two phases: (1) development of a laboratory test facility with thermomechanical property measurement capabilities, and (2) determination of thermomechanical properties of Stripa granite for use in modeling the in-situ experiments at Stripa. A stiff triaxial test machine, capable of providing a maximum confining pressure of 70 MPa and a maximum axial load of 1.4 MN, was built. Independent systems for heating and cooling the cell provide a maximum sustained test cell temperature of 200°C. The test cell can accommodate either a 52 mm diameter of 62 mm diameter core with a 3:1 length to diameter ratio. Confining pressure and deviator stress loading paths are independently controlled by an electroservo control system using a PDP 11/44 computer to close the feedback control loop. Automatic data acquisition was integrated into the computer control system. Such a system was necessary to maintain test control for the extended time required to complete the testing of each sample. Calibration tests were performed on individual transducers, and a test duplicating the sequence for rock samples was conducted on an aluminum sample. This latter test provided data on the contribution of friction, or deformations in test machine components, to property measurements.

In the second phase of the study, thermomechanical properties were determined from samples of dry, intact 62 mm diameter core taken from the same instrumentation holes in which measurements of displacements and stresses were made during the in situ experiments. To bracket in situ temperatures and stress conditions, measurements were made over a range of confining pressures from 2 MPa to 55 MPa and a range of temperatures from

25°C to 200°C.

To provide properties at several pressure-temperature states within these ranges while limiting the number of test samples, each sample was subjected to a matrix of pressure-temperature states with the test sequence designed to minimize the accumulation of sample damage.

Test results provided data on the temperature and stress dependence of the volumetric and linear coefficients of thermal expansion (α_V and α_ℓ), tangent Young's modulus (E_T) and Poisson's ratio (ν). To varying degrees, all properties were affected by changes in confining pressure and temperature. The most significant trend in thermal expansion results was the effect of increasing temperature at constant pressure. Average values of α_V at 20°C were from 48% to 61% of those at 180°C, while values of α_ℓ at 20°C ranged from 52% to 70% of those at 180°C. Effects of isothermal pressure increases were less pronounced, resulting in, at most, a 10% to 20% decrease in α_V and a 5% to 10% decrease in α_ℓ. Measurements of E_T were most significantly affected by isothermal increases in confining pressure: E_T increased about 20% over the range of pressures tested. Effects of isothermal temperature increases varied from almost none at high confining pressure to less than a 14% decrease at low confining pressure. For Poisson's ratio results, the most significant trends were due to isobaric temperature changes that caused a 15% to 27% decrease in ν over the temperature range tested.

PART I: APPARATUS

1. INTRODUCTION

In situ electrical heater experiments were conducted in the Stripa iron ore mine in Sweden to understand the response of a granite rock mass to thermal loading produced by buried nuclear waste. An integral part of the experimental analysis was a laboratory investigation of the thermomechanical behavior of the Stripa granite. For this investigation, a small-core test facility, including a triaxial apparatus capable of thermomechanical property measurements, had to be developed. The general design criteria were:

(1) a stiff load frame and axial loading system,

(2) maximum axial load of 1.4 MN and maximum confining pressure of 70 MPa,

(3) maximum sustained test temperature of 200°C,

(4) maximum sample size of 62 mm diameter and a 3:1 length to diameter ratio,

(5) automatic (i.e., computer-based) data acquisition and servocontrol of test conditions.

Figure 1 is a photograph of the principal components of the triaxial test machine. On the extreme left is the stiff load frame with an insulated test cell in place. For safety, a Lexan shield surrounds the frame, and fumes produced during cell heating are removed through the hood above. To the right of the frame is the power pack containing motors and pumps for independent control of axial load and confining pressure. To the far right is the instrumentation rack. The computer, a PDP-11/44, is not shown.

Various components of the facility are described in sections 2 through 5 of Part I of this report. Section 6 describes a system calibration test

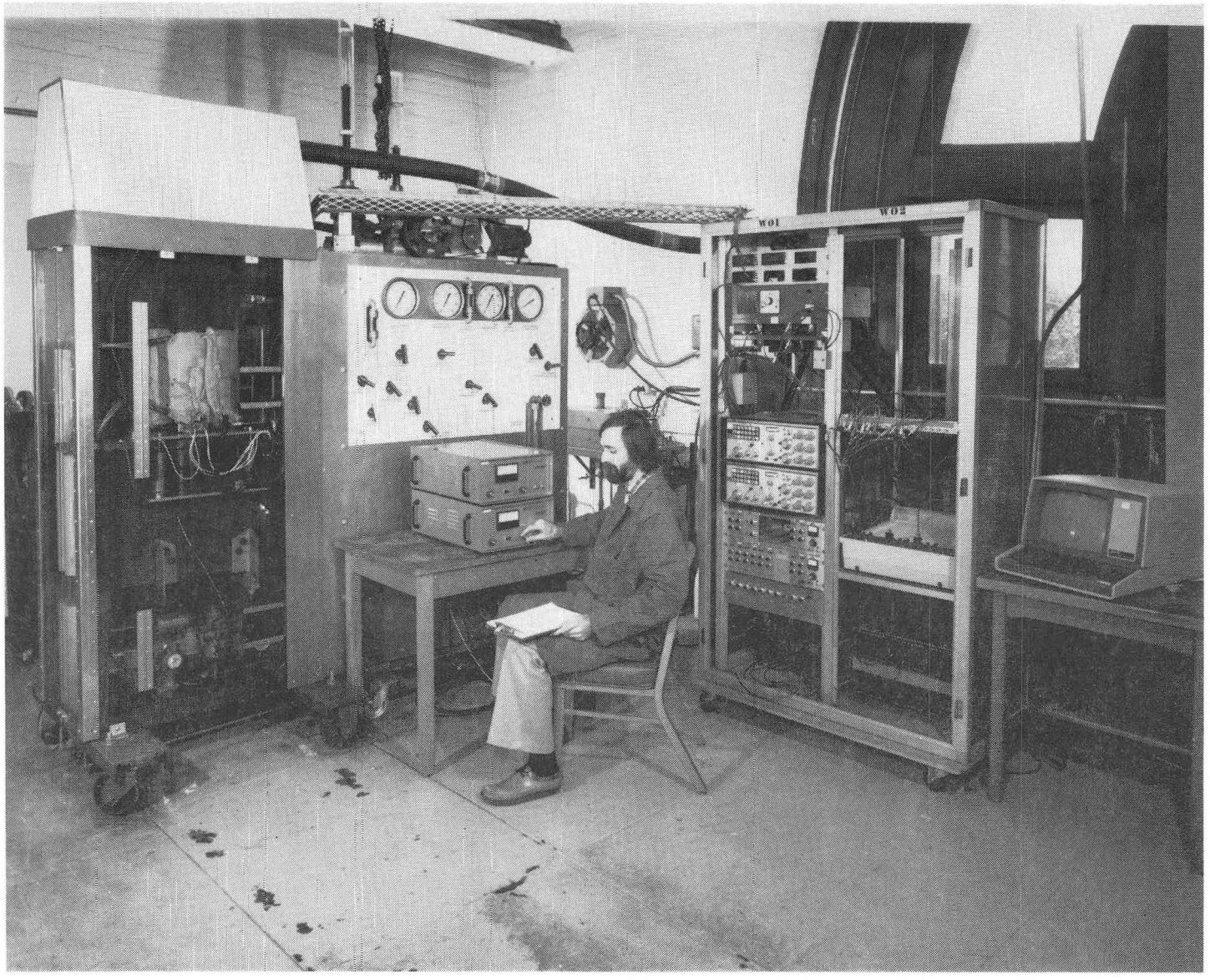

Fig. 1. Components of triaxial test machine, from left to right: stiff load frame with test cell in place, power pack, and instrumentation rack.

in which an aluminum sample of known properties was subjected to a series of temperature-pressure conditions to determine the contribution of system stiffness and thermal expansion to sample deformation measurements.

2. TEST FRAME, ACTUATOR, AND TEST CELL

2.1 Test Frame and Actuator

The load, or test, frame provides the reaction for the axial load on the sample. For rock failure studies, it is desirable to have a test machine stiffness large enough that the elastic energy released by the machine at sample failure will not destroy the sample (Cook, 1981). This stiffness is achieved in part by using a massive load frame. The load frame for this machine was therefore constructed of a steel plate 48 inches high by 28 inches wide by 8 inches thick.

The actuator, housing the 9-inch diameter actuator piston, rests in the cut-out of the frame, as illustrated in Fig. 2. Axial load is transmitted to the sample by the external load cell, which rests upon the actuator piston. The external load cell acts through a hole in the actuator table. This table, which moves along with the actuator piston, supports the test cell.

2.2 Triaxial Test Cell

The test cell is essentially a steel cylinder with threaded top and base pieces (Fig. 3). The cylinder is a sandwich construction consisting of one cylinder heat-shrunk over another. The inner cylinder, under compression, thus adds to the cell strength. Thread strength of the cell base and top limits the confining fluid working pressure to 70 MPa while allowing for a safety factor of 4. All components were machined from 4340 (nickel-chromium) steel.

The test cell is pressure-sealed with two sets of Viton O-rings with brass back-up rings. As shown in Fig. 3, one set of O-rings acts as a seal

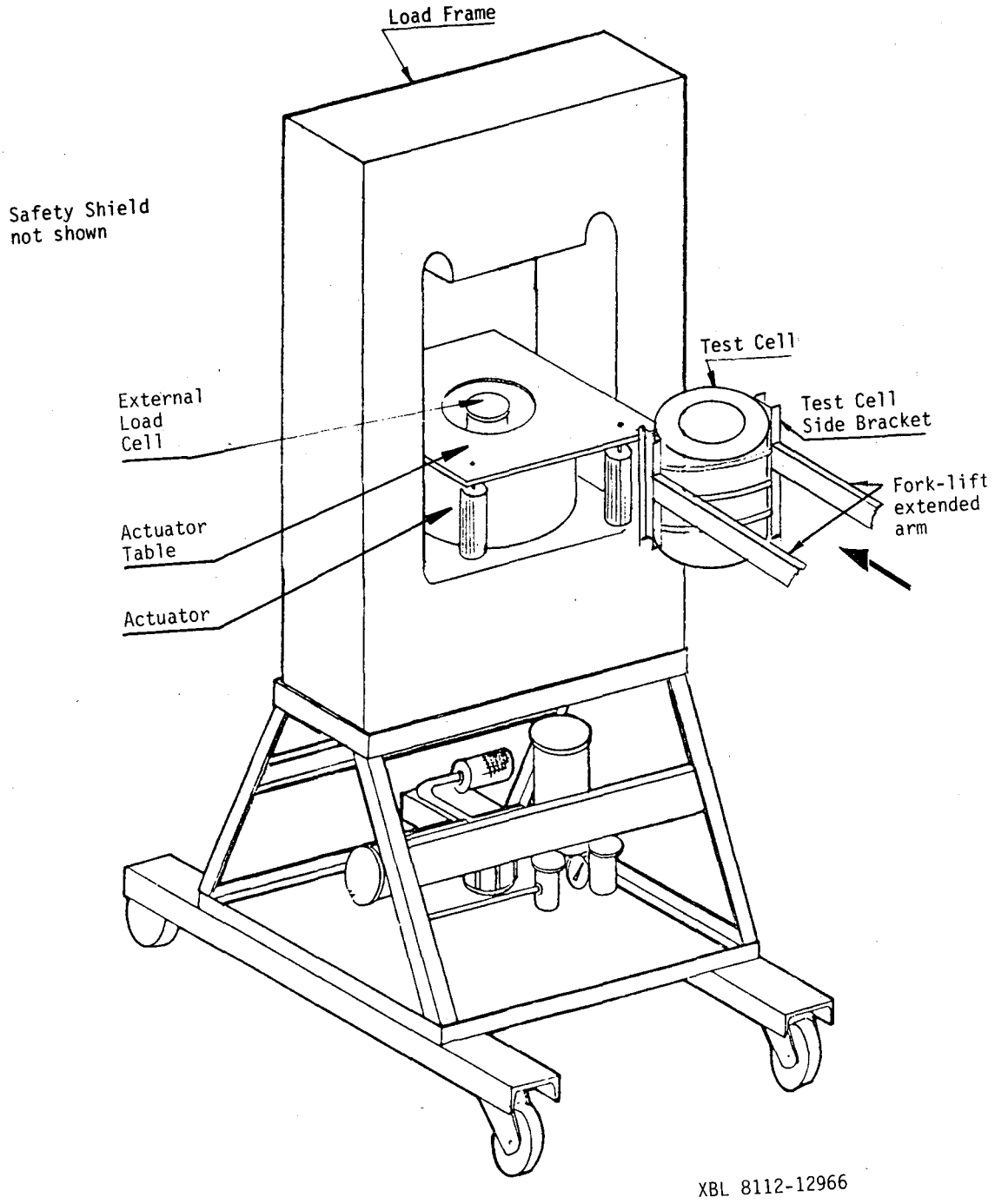

Fig. 2. Stiff load frame and actuator.

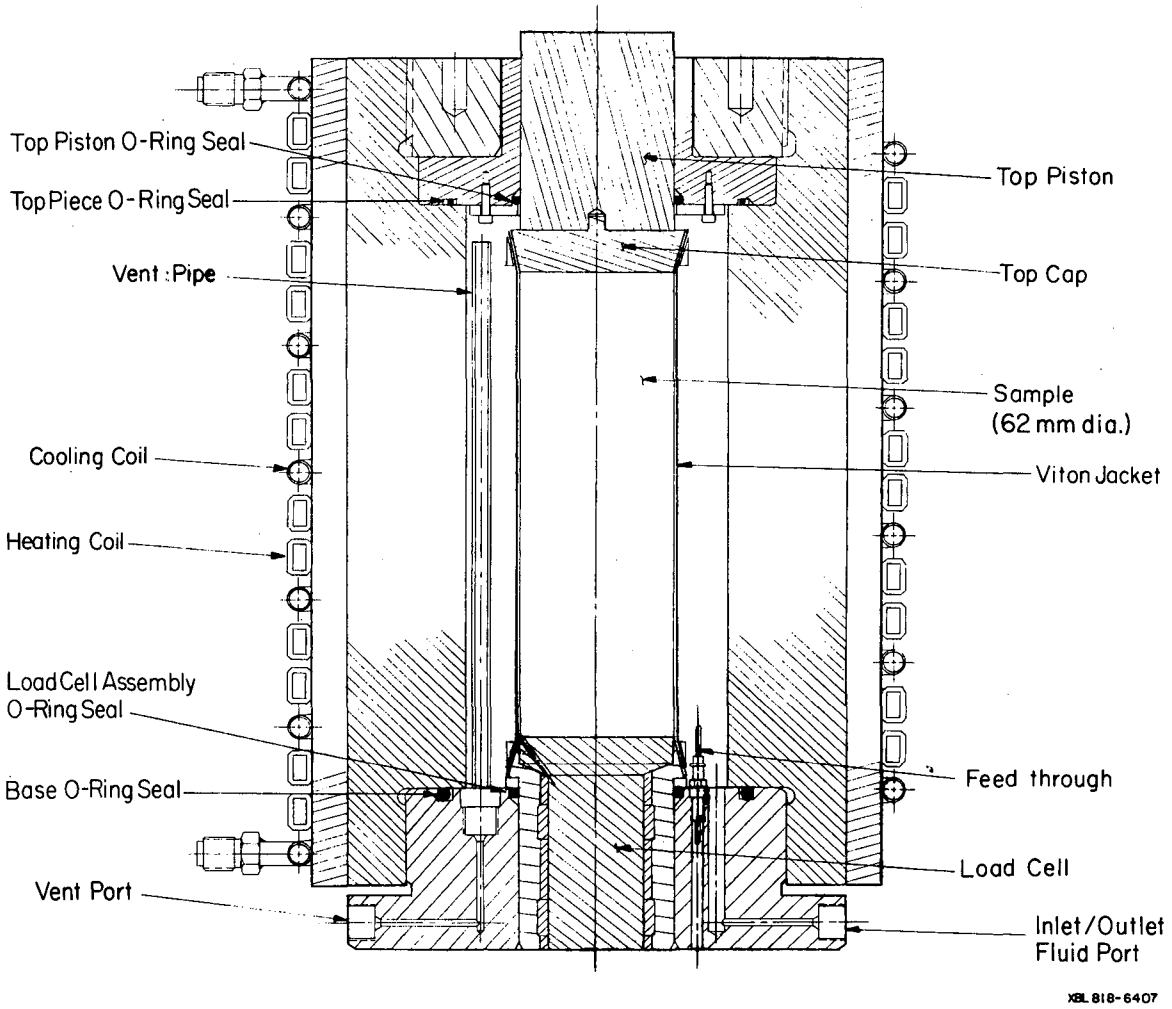

Fig. 3. Cross section of the test cell, illustrating primary components.

between the top and bottom pieces and the cylinder. The other set of O-rings seals against the top piston and internal load cell assembly.

Confining pressure fluid enters the cell through an inlet port in the base, while a vent pipe, also attached to the base, serves as an air bleed for the cell. The internal load cell shown in Fig. 3 rests directly on the external load cell and actuator piston (Fig. 2). After the top piston contacts the load frame, pressure on the actuator piston is transmitted to the sample as axial load. Figure 4 is an exploded view of the internal load cell assembly, showing how it is placed within a shell. The O-ring pressure seal is made against this shell. One reason for this design was to eliminate O-ring friction, which would otherwise have restricted the movement of a solid lower piston and reduced the accuracy of the axial load readings.

An impermeable membrane around the sample prevents penetration of the sample by the confining fluid. Several candidates for this membrane were tested because the cell environment requires the membrane to retain its toughness at 200°C and to be inert to the confining fluid. Teflon FEP heat shrink tubing was tried, but lacked sufficient strength at 200°C. Silicone rubber dissolved in the confining fluid. Ultimately, Viton tubing proved to be satisfactory and readily obtainable. Beveled rings clamp the membrane to the beveled surface of the top cap and shell (Figs. 3 and 4) to achieve a high-pressure seal at the end of the membrane.

Twenty electrical feedthroughs, rated to 200°C and 140 MPa pressure, are located in the cell case (Fig. 3) to transmit transducer signals from inside the test cell to the outside. For strain gauges attached to the sample (and thus enclosed by the sample membrane), a different method of signal transmission was

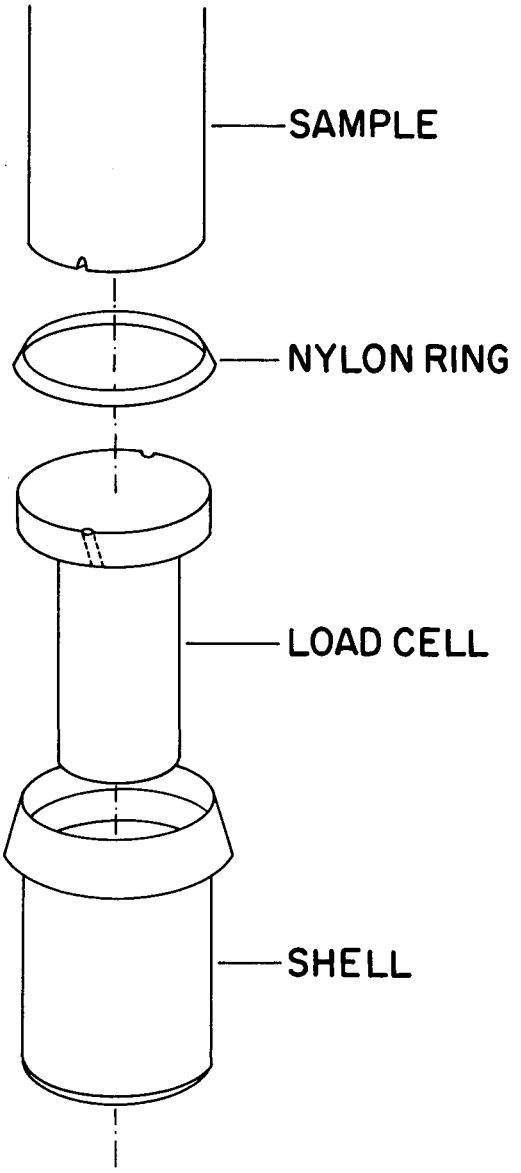

Fig. 4. Exploded view of internal load cell assembly.

developed. Leads from these strain gauges pass through a small groove cut in the edge of the rock into a hole drilled in the flange of the internal load cell and out of the cell (Fig. 4). A beveled nylon ring slipped over the bottom edge of the sample prevents extrusion of the sample membrane into the lead wire hole or into the small space between the outer shell and the top of the load cell.

2.3 Test Cell Temperature Control

Separate systems for heating and cooling the sample were constructed. Heat is provided by a 1-kW resistance element wrapped around the outside of the cell (Fig. 3). Power to the element is turned on or off by a Fenwall 550 thermocontroller, in combination with a type-J thermocouple, placed in the test cell wall (Fig. 5). The thermocouple well is within 1/8 inch of the exterior cell surface to insure that cell temperatures do not exceed the thermostat set-point values. For safety, a switch on the load frame shield door prevents current from passing through the heater coil if the door is open.

The cooling system is also illustrated in Fig. 5. A heat transfer fluid, Dowtherm G, is pumped from a reservoir through cooling coils into a tank filled with antifreeze. From the cooling tank the fluid flows to the test cell, where it absorbs heat from the cell while flowing through a 3/8-inch copper tube soldered to the cell exterior (Fig. 3). The heated fluid is then returned to the reservoir. For cooling below 40°C, dry ice is added to the cooling tank to improve efficiency.

Experiments to date have required only manual, set-point temperature control to prevent damage to samples due to excessively high sample heating

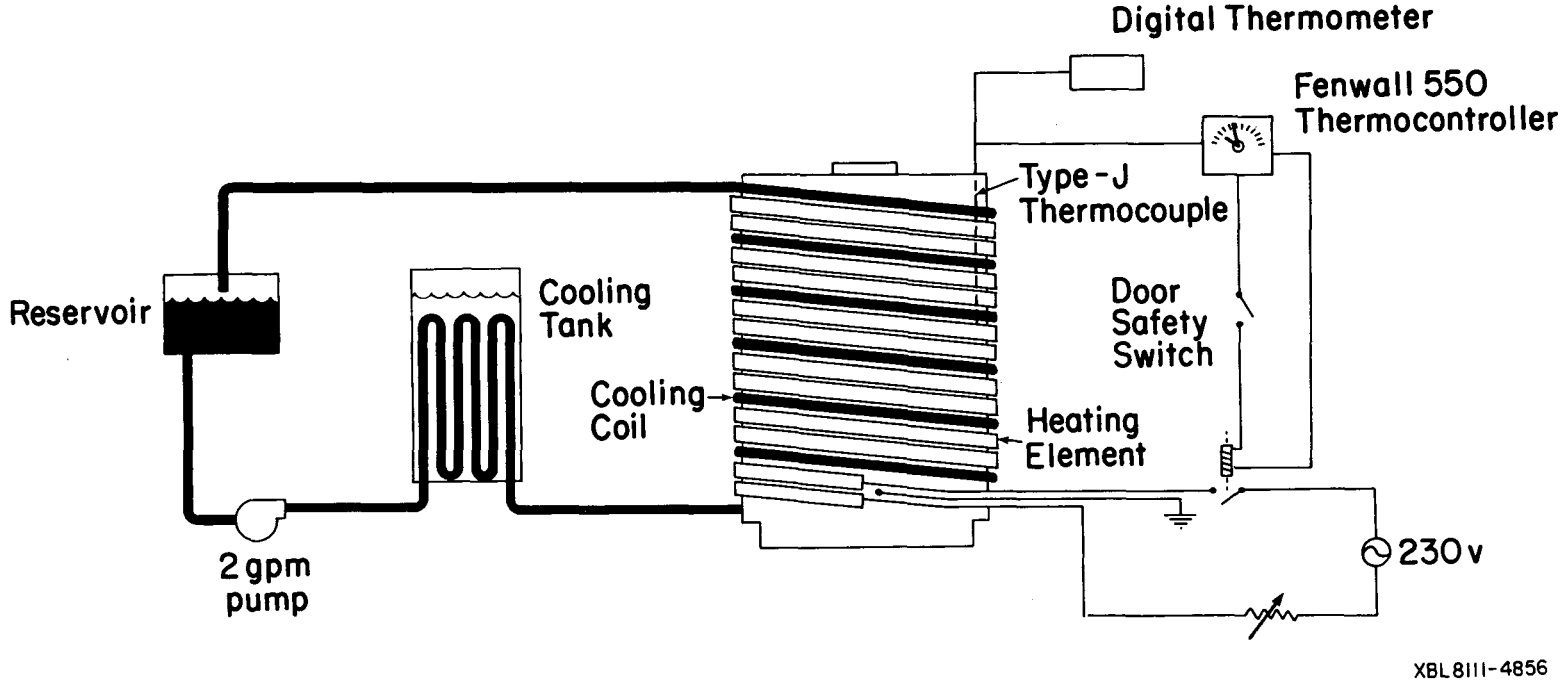

Fig. 5. Test cell temperature control system.

rates. For temperature increases of 25°C in the sample, the rate of increase is limited to 1.5°C per minute. This maximum is set by the thermal properties of the system such as the power output of the heater and the rate of heat loss to the surroundings. To cool the cell, cooling fluid is circulated until the thermocouple in the cell wall indicates that the desired temperature has been reached. Natural heat loss to the surroundings obviates cooling the cell exterior to below target temperatures. For temperature decreases of 25°C in the sample, the rate of decrease is 1.5°C per minute or less.

Automatic (computer-based) temperature control can be implemented using the digital thermometer (Fig. 5). The thermometer sends an analogue signal representing the cell temperature to the computer that controls the power (via relays) for the heating and cooling devices.

3.0 POWER PACK

The power pack contains the test machine's hydraulic system, which supplies fluid at high pressures for the sample confining pressure and axial load. The principal components are the electric-motor-driven pumps for confining pressure and the actuator fluid. Though situated beneath the load frame, the air-oil intensifier is, by function, also part of the power pack. Figure 6 is a schematic representation of the entire hydraulic system.

The air-oil intensifier is an SC Hydraulic Engineering Corp. model 40-500-25 air pressure pump with a flow rate (approximately 29 cu inches/min) much greater than the confining pressure or actuator pumps. The intensifier fills the actuator and the confining pressure pumps, purges the hydraulic system and the test cell of air, and quickly positions the actuator table and piston.

3.1 Actuator and Confining Pressure Pumps

A few guidelines on test machine capabilities were established to select an appropriate pumping system:

(1) The test machine was to be used primarily for studies under quasi-static stress and displacement conditions.

(2) The actuator fluid pressure pump was to be capable of producing controlled axial strain rates ranging from 0.01% per minute to 2% per minute in the sample.

(3) Maximum axial load was to be 1.4 MN and maximum confining pressure, 70 MPa.

(4) To make the machine as stiff as possible, fluid volumes under high pressure were to be minimized.

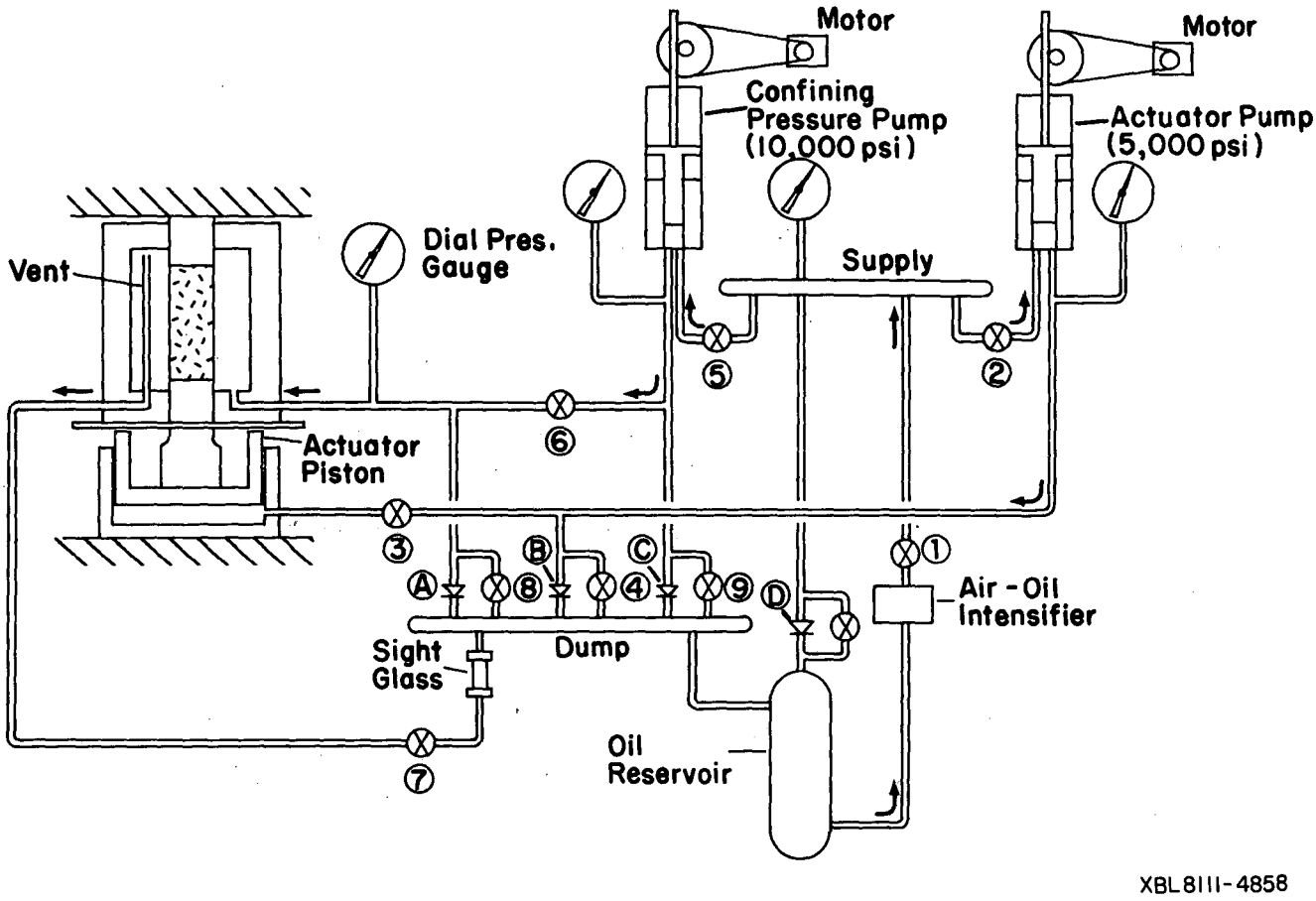

VALVES

1 Air-Oil Intensifier V.
2 Actuator Pump Fill V.
3 Actuator Isolation V.
4 Actuator Manual Relief V.
5 Confining Pres. Pump Fill V.
6 Test Cell Isolation V.
7 Test Cell Purge V.
8 Test Cell Manual Relief V.
9 Conf. Pres. Pump Manual Relief V.

RELIEF VALVES

A Test Cell R.V. - 11,000 psi
B Actuator R.V. - 6,000 psi
C Conf. Pres. R.V. - 11,000 psi
D Supply R.V. - 300 psi

Fig. 6. Schematic representation of test machine hydraulic system.

(5) If positive displacement pumps were to be used, the volume capacity of these pumps was to correspond to the fluid volume displaced by a sample undergoing an axial and radial strain of 15%.

(6) Actuator and confining pressure were to be controlled both manually and automatically.

Electric-motor-driven positive-displacement pumps were chosen because they were best suited for the type of testing to be performed. Figure 7 shows the primary components of the motor-pump systems. The motors are bi-directional Electro-Craft model 670-07-21 generators with rated outputs of 1/2 hp and constant torque over the 0-4000 rpm operating speed. Maximum motor speed is achieved in 0.3 seconds from start. These high-acceleration motors were selected to minimize system response times. The motors are connected to gear reduction boxes and then to Duff Norton ball jacks that translate the rotational motion of the motors to linear piston movement in the pumps. To achieve the very large range in strain rates specified in the guidelines, timing belts and gears connect the various components. Different sizes of gears can be used for different strain rates.

A simplified cross section of a positive-displacement pump is shown in Fig. 7. The actuator pump was rated at 34.5 MPa (5000 psi) working pressure, with a piston diameter of 5.08 cm (2.0 in.) and a volume of 514.8 cu cm (31.4 cu in.). The confining pressure pump was rated to 69 MPa (10,000 psi) working pressure with a 2.85 cm (1-1/2 in.) diameter piston and a 333.9 cu cm (20.4 cu in.) volume. Figure 8 shows the placement of the pumps in the power pack.

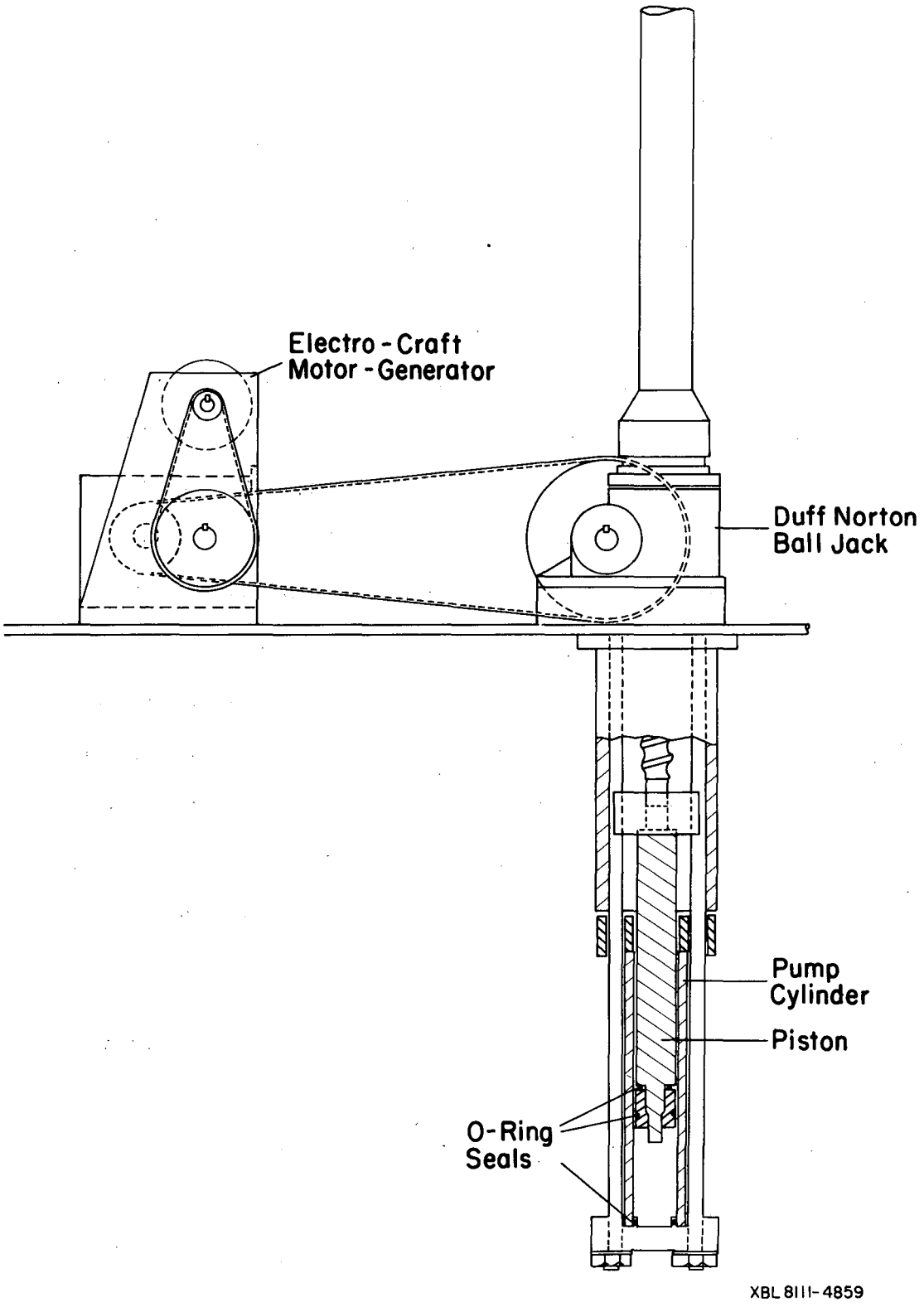

Fig. 7. Illustration of electric motor driven pump showing gearing and a cross-section of the pump piston and cylinder assembly.

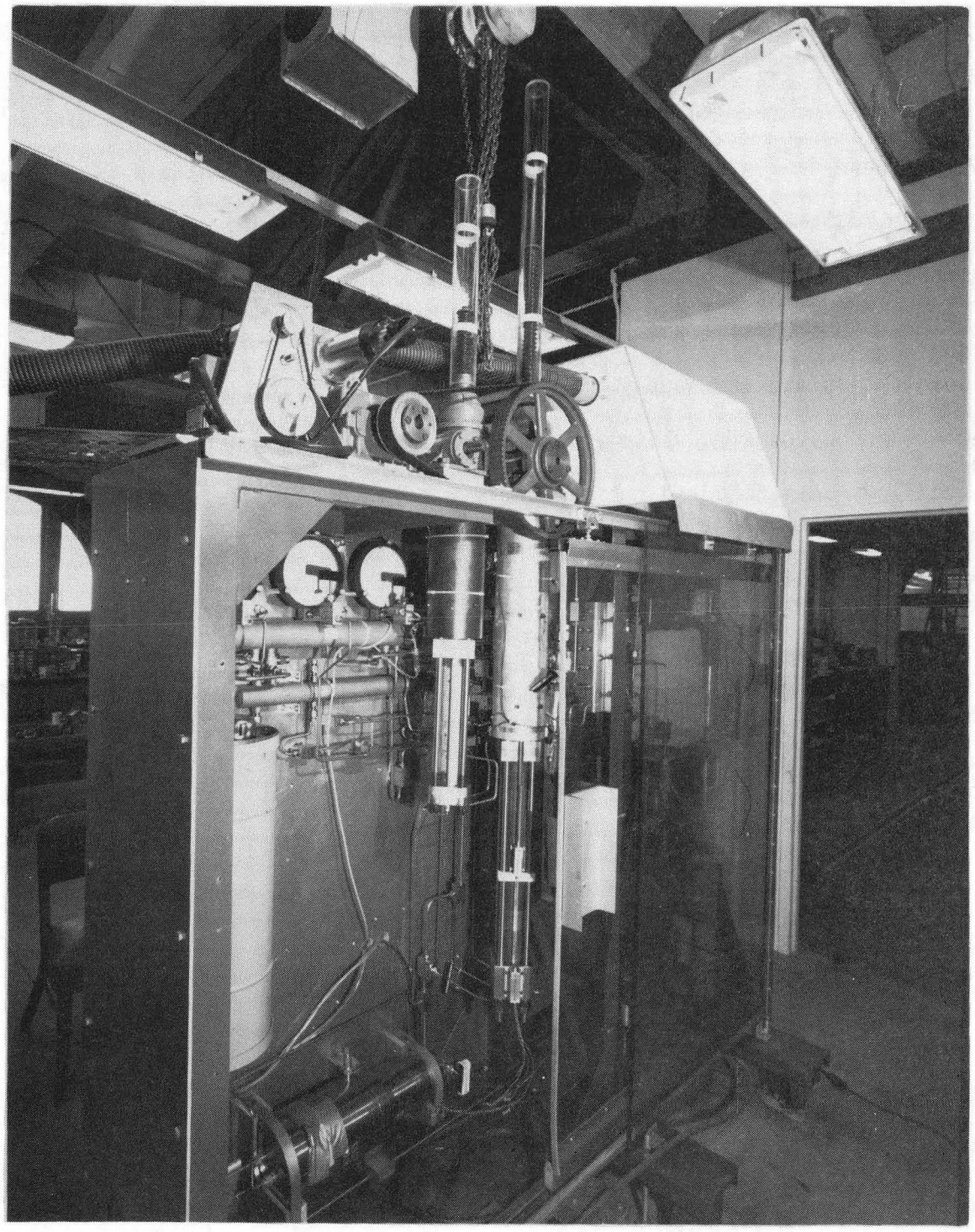

Fig. 8. Rear view of power pack showing position of pumps in hydraulic system.

3.2 System Hydraulics

Except for the following notes, the flow of fluid through the hydraulic system shown in Fig. 6 is self explanatory. The supply manifold is a low-pressure, 3.5 MPa (500 psi), accumulator that supplies fluid for filling the pumps and the test cell; it also applies small loads independently of the high-pressure pumps. When high pressures are desired, valves 5 and 2 are closed to isolate the supply from the high pressure system. After the test cell is purged of air, valve 7 is closed. Thus, during normal operation, fluid flows both into and out of the test cell through the same port. Similarly, a single path is provided for flow into and out of the actuator. Isolation valves 6 and 3 are provided to maintain pressure in the cell and actuator if it is necessary to quickly depressurize the pumps.

Exxon Turbo oil no. 2389 is used throughout the hydraulic system and in the test cell. This fluid has (1) a flash point well above the 200°C maximum operating temperature, important for safety; (2) low viscosity, which allows efficient movement through the 3 mm (1/8-inch) inner diameter hydraulic lines; and (3) lubricating properties that prevent wear in the pumps.

4. INSTRUMENTATION

This section discusses the various transducers used to monitor sample stress, displacement, and temperature conditions. The physical position of the transducers, as well as their connections to the signal conditioning units, is illustrated in Fig. 9.

The transducers are grouped according to four functions: (1) axial load on the sample is monitored directly by two electronic load cells and indirectly by the actuator fluid pressure transducer; (2) confining pressure is monitored by a pressure transducer; (3) sample deformations are monitored directly by strain gauges and indirectly by a linear variable differential transformer (LVDT) mounted on the actuator table and by another LVDT on the confining pressure pump; and (4) sample temperature is monitored by a resistance temperature sensor. Excitation power and signal amplification are supplied by Vishay signal conditioners for the strain gauges and temperature sensors, and by two MTS 442 controllers for the remaining transducers. As seen in Fig. 9, the transducers are also connected to digital volt meters (DVM) mounted in the instrumentation rack. These DVM's facilitate sensor calibration and enable visual monitoring of transducer signals. An X-Y-Y plotter is available for continuous recording of sensor output, e.g., axial and radial strain as a function of axial stress in a stress-strain test. The interrelation of the sensors and the computer is discussed in Section 5.

In addition to the electronic transducers, mechanical gauges in the power pack monitor the actuator, confining-pressure pump, and test-cell pressures.

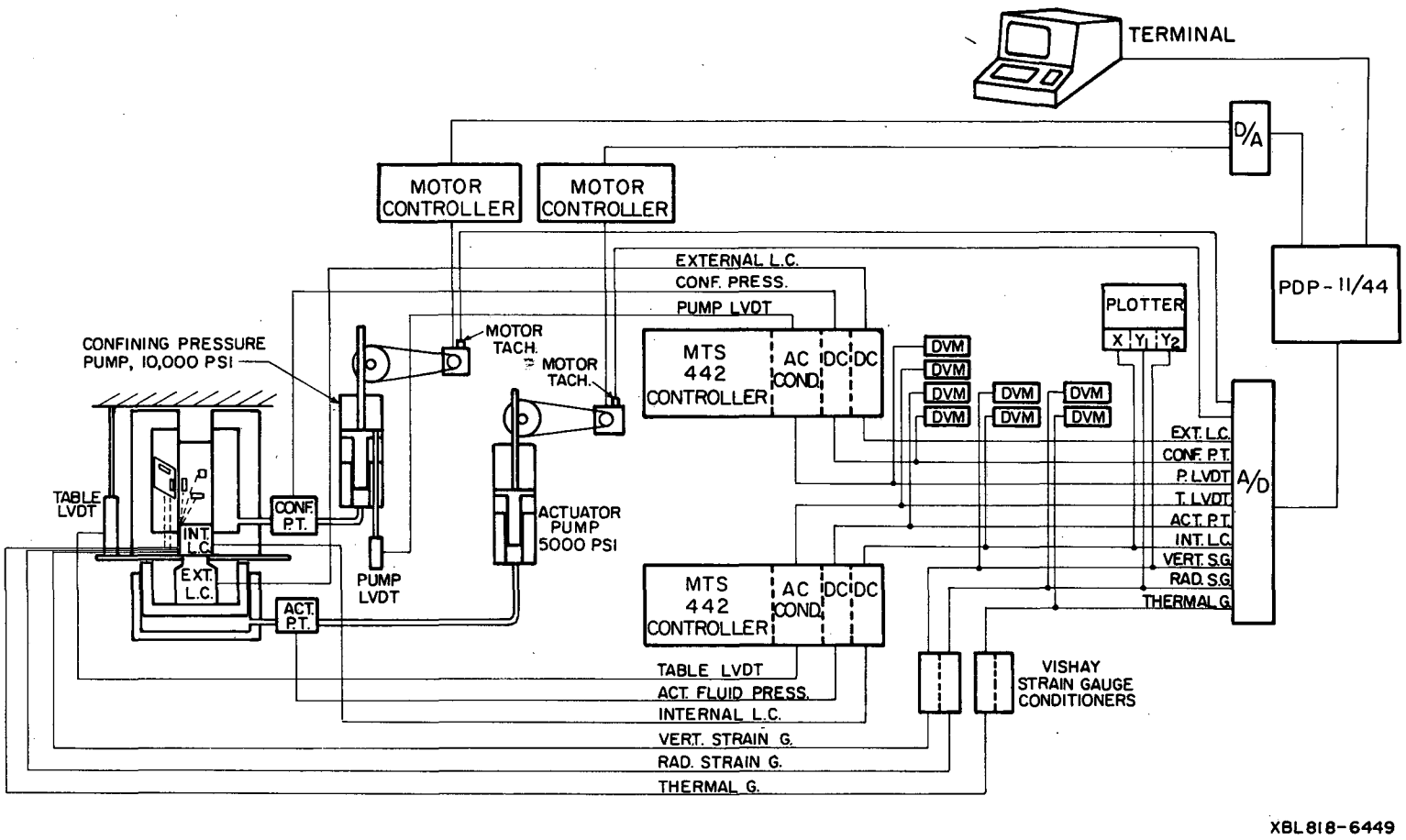

Fig. 9. Schematic illustration of instrumentation and feedback control system.

The individual transducers are described below, including their specifications, signal conditioning, and method of calibration. The calibration points were fit to a best-fit straight line for all calibrations. The slope and intercept of the best-fit line were the calibration constants used to convert transducer signals into engineering units. The calibration procedures to be described were used during machine development and in all testing to date. The calibration constant cited illustrate the procedures, but since these values are dependent upon transducer excitation and signal amplification levels, other values could occur in other tests.

4.1 Load Cells

As mentioned, axial load can be measured either by the internal load cell, which is in the lower test cell piston, or by the external load cell, which is part of the actuator assembly. The external load cell is a 2.2 MN (500,000-lb.)-capacity spool-type cell; the internal load cell (Fig. 4) has a modified spool and a 1 MN (220,000-lb.) capacity. Load is sensed in either cell by strain gauges oriented axially and circumferentially on the load cell core. These gauges are mounted in pairs at four points on the core circumference to average the effects of eccentric loading. All gauges are self-compensating to match the thermal expansion of the steel and thus provide a temperature-compensated measurement.

4.1.1 Signal Conditioning

Signal conditioning for each load cell is provided by a DC conditioner module of an MTS 442 controller. Excitation voltage is set at 3.0 volts for the external load cell and 2.5 volts for the internal load cell. A maximum excitation voltage of 5.0 V is recommended for both load cells. Amplifier

gains are adjustable from 0 to 5000 so that the load cells may be calibrated to read in engineering units.

4.1.2 Calibration of Load Cells

Both the internal and external load cells were calibrated by loading them in the test frame in series with a load cell with a calibration traceable to the National Bureau of Standards. Excitation to the cell was provided by a regulated ±5 V power supply, while output from the load cell being calibrated was monitored with a Fluke digital voltmeter. The MTS 442 controller provided excitation and signal conditioning for the internal and external load cells. Response of the cells was monitored through the computer-based data acquisition system. The first step in calibration was to load the cell and set the gain in the signal conditioner. For example, for the external load cell, the gain was set so that a 100 kN load resulted in an output of about 1 V. After setting this gain, load was increased in 10 steps to 0.44 MN (100,000-lbs) and then decreased to zero. The slope and intercept (if there is a zero offset) of the resulting curve were the calibration constants for the cell. For the external load cell, load was related to output voltage by the relation $\gamma = 98.48\ X - 0.04$, where γ is expressed in kN and X in volts. Both the internal and external load cells exhibited very linear, repeatable calibration curves. For example, the slope of the calibration curve of the internal load cell remained consistent between calibrations to within 0.2%.

4.2 Strain Gauges

Figure 10 illustrates the set-up developed for monitoring sample deformations using strain gauges. The sample mounted gauges were placed directly on the

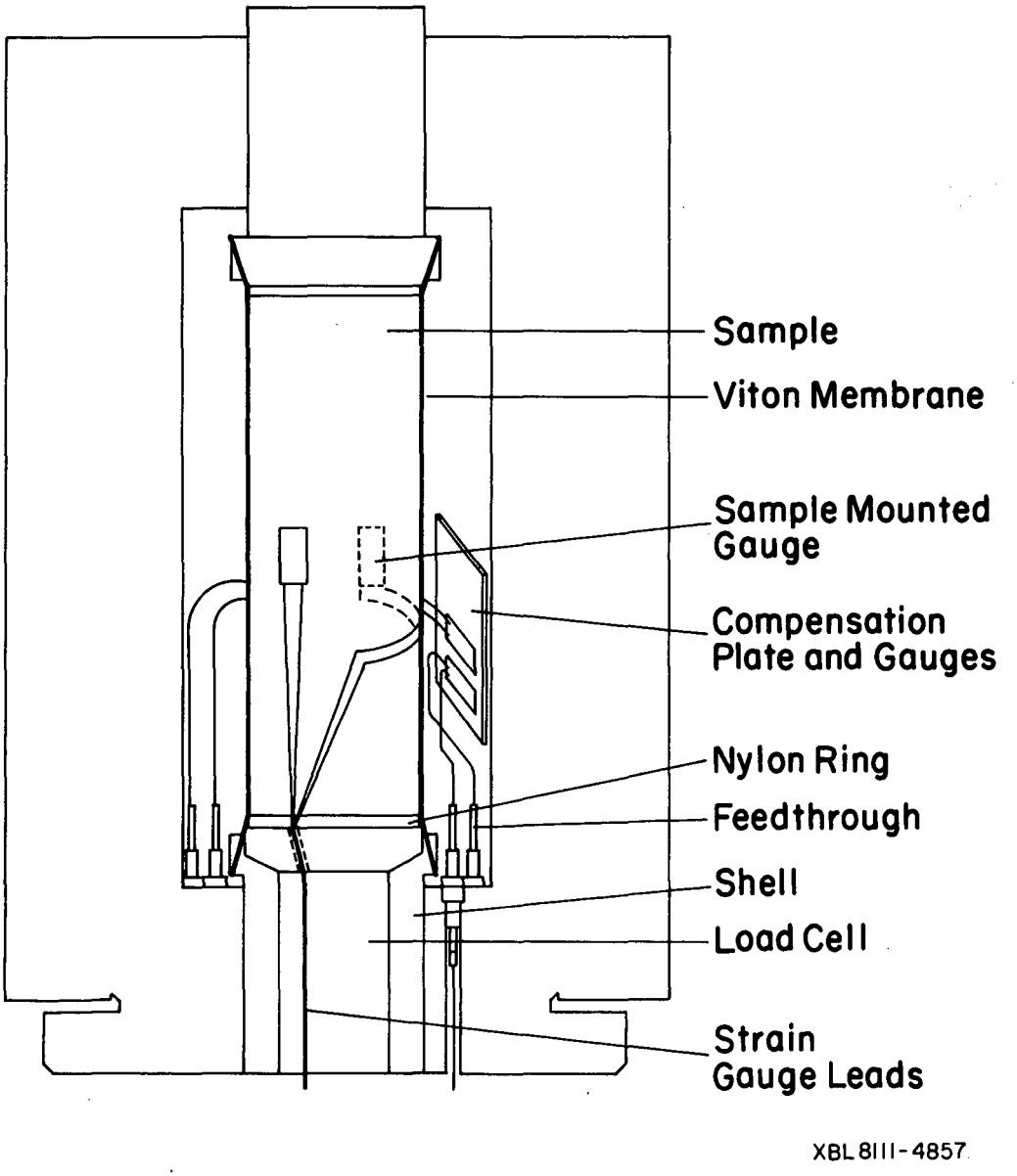

Fig. 10. Set-up for measurement of sample deformations by strain gauge instrumentation.

rock surface. Duplicate gauges were bonded to a compensation plate of titanium silicate glass, chosen for its low thermal expansion (α_ℓ = 0.03 X 10^{-6} mm/mm°C). The plate was mounted inside the triaxial cell during tests, where its near-zero thermal expansion permitted a true measurement of the thermally induced strain in the rock, thus compensating for the change in resistance with temperature of the conducting material in the gauges. The compensation-plate gauges were connected to the sample-mounted gauges to form a full Wheatstone bridge for measuring axial and radial strain on the rock sample (Fig. 11). As shown in Fig. 10, lead wires from the sample-mounted and compensating gauges were brought out of the cell by different paths, so the physical connection of the wires in the Wheatstone bridge took place outside the test cell.

4.2.1 Signal Conditioning

A Vishay model 2100 ten-channel, 1-12 volt DC power supply provides a regulated power source to the strain gauges. Normally, a 1-volt excitation is used to limit the deleterious effects of strain-gauge self-heating. The complementary Vishay 2120 conditioner contains the differential amplifiers needed to magnify the voltage output across the strain gauge bridge. A balance control allows for initial zeroing of the bridge. Amplifier gains of 50-1050 are possible.

4.2.2 Calibration

A calibration circuit is contained in the conditioner so that a fine adjustment of the amplifier gain can be performed before testing a sample. This circuit includes 17.5 kilohm shunt resistors that can be switched in to simulate 1000 microstrain offsets.

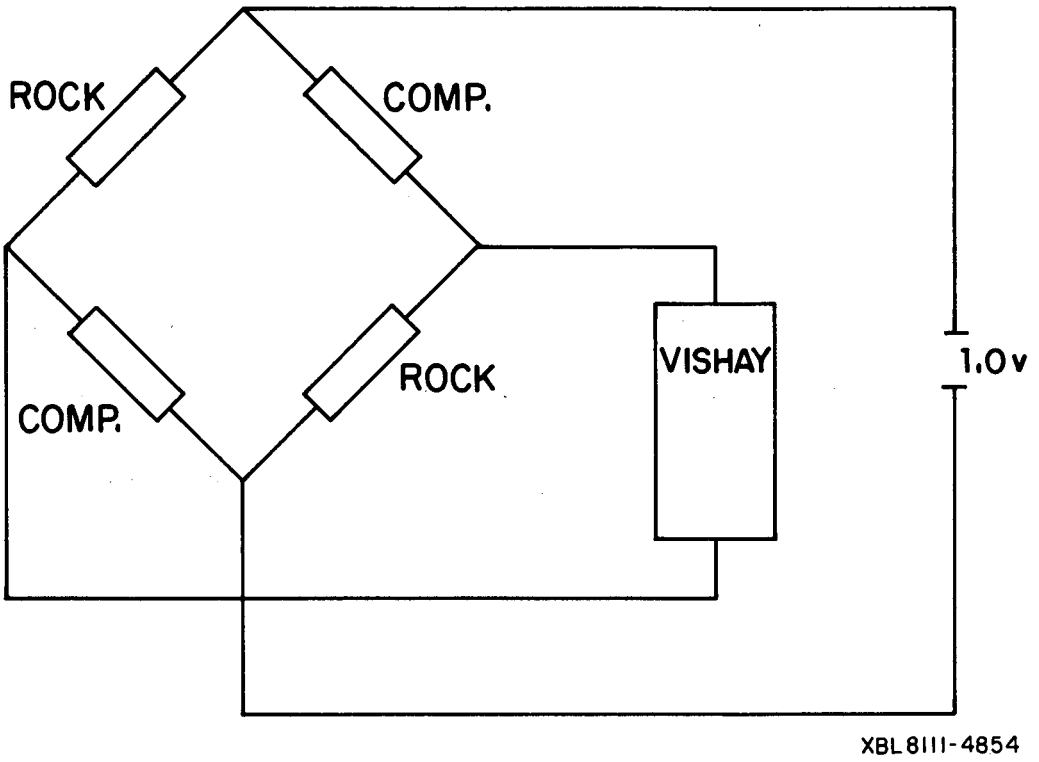

Fig. 11. Wheatstone bridge strain gauge circuit.

4.3 Temperature Sensor

Nickel-foil resistance temperature sensors bonded to the sample surface provide accurate monitoring of temperature. A Micromeasurements LST-10C/350B resistance network connected in series with the temperature sensor linearizes the output of the sensor with temperature. This network also forms a balanced bridge circuit by converting the resistance output to a convenient equivalent strain output that can be input to a Vishay strain gauge conditioner, as described above. In testing to date, a 1.0-V excitation voltage has been used to reduce erroneous readings from self-heating.

The zero balance control of the signal conditioner is used to attain a temperature sensor output equal to the ambient temperature. As the resistance network allows for an equivalency of 10 microstrain per 1°C, the calibration circuit in the Vishay signal conditioner is used to adjust output amplification so that a 10-mV output equals 1°C.

4.4 LVDTs

A Scheavitz DC-LVDT, the "table" LVDT, located on the testing table, measures the relative displacement between this table and the test frame. The displacement of the test table is directly proportional to the overall axial deformation of the rock sample, so the table LVDT supplements the deformation measurements of the axial strain gauges on the sample. Another DC-LVDT, the "pump" LVDT, attached to the piston of the confining pressure fluid pump. The piston moves in response to changes in test cell confining fluid volume so the LVDT supplements strain-gauge measurements of sample volumetric deformations. In tests conducted under constant confining pressure, confining fluid volume changes--and, therefore, pump LVDT readings--

should be proportional to the volumetric deformation of the rock sample. The linear displacement range of the table LVDT is ± 25 mm (1.0 inches), whereas that of the pump LVDT is ± 13 mm (0.50 inches). Output over these ranges is ± 10 V for a 15-V excitation. The manufacturer specified < 0.25% deviation from linearity and a temperature effect coefficient of 0.06%/°C over the operating range.

4.4.1 Signal Conditioning

The AC modules of the MTS 442 controller are used as the signal conditioning units for the two LVDTs. Since the LVDTs require only direct current power, the frequency modulation circuits of the AC units are bypassed. The available 10 volts (DC) from the controller provide the excitation. Amplifier gains are adjustable so that the LVDTs may be calibrated to read in engineering units.

4.4.2 Calibration

A mounted micrometer with a .06 mm (.0025-inch) vernier scale provided known displacements of the LVDT cores. The MTS controller provided excitation and signal conditioning for the LVDTs while LVDT response was monitored by the data acquisition system. Calibration was begun by setting the amplifier gain to approximately the proper level. For example, for the table LVDT, the gain was set so that a ± 0.25 mm (0.1 inch) displacement produced a ± 10.0 V response. After setting the gain, a precise calibration was carried out in which the LVDT core was moved incrementally in the positive and negative directions to the linear range limit. Output was recorded at each displacement increment. The slope and intercept of the resulting displacement-voltage curve are the required calibration constants. For example, for the table LVDT,

displacement was related to output voltage by the relation $\gamma = 0.0253\ X - 0.0007$, where γ is expressed in centimeters and X in volts.

Since the LVDTs were not attached directly to the sample, their response is affected by the compliance and thermal expansion of the end pieces and the test frame. To determine the contribution of system deformations to LVDT movement, a strain-gauged sample of known mechanical properties (aluminum) was subjected to the same test sequence as that planned for the rock sample. The results are reported in Section 6.

4.5 Pressure Transducers

Fluid pressure transducers (Data Instruments Inc.) monitor the test cell confining pressures and the fluid pressure acting on the actuator piston. These transducers are of a strain-gauged diaphragm type with a 70 MPa (0-10,000 psi) range and an output of 0-100 mV for a +5 V input. Accuracy is better than 0.5% at constant temperature and 1% over a range of 38°C. The pressure transducers are located on the test frame away from the heated test cell so that the temperature change of the fluid in contact with the transducers is small.

4.5.1 Signal Conditioning

DC conditioner units of the MTS 442 controller are used for power and signal amplification of the pressure transducers. For testing to date, excitation voltage has been set at 5 V. The recommended maximum is 6 V. Amplifier gains are adjustable so that the pressure transducers can be calibrated to read in engineering units.

4.5.2 Calibration

Calibration of both fluid pressure transducers was performed using an Ashcroft deadweight tester to provide a known pressure on the transducer, while the data acquisition system monitored transducer response. The transducers were initially pressurized to the working pressure limit, and the gain was set so that a 70 MPa pressure resulted in about a 7.0 V transducer output. A detailed calibration was then performed in which the transducer was loaded in 3.45 MPa (500 psi) increments up to 70 MPa and then unloaded in 3.45 MPa increments back to zero. The slope and intercept of this calibration curve are the required calibration constants. For example, for the confining pressure transducer, pressure was related to output voltage by the relation $\gamma = 10.05\ X - 0.169$, where γ is expressed in MPa and X in volts. Calibrations were repeatable to within 1% or better.

5.0 COMPUTER SERVOCONTROL AND DATA ACQUISITION

The design of the computer-based servocontrol and data acquisition system was based upon two general concepts. The first was that the system should be able to respond quickly (on the order of tenths of a second or less) to changes in test conditions while maintaining maximum flexibility in the type of control paths that could be generated. The computer hardware chosen to meet this criterion was a PDP-11/44 with two 20 megabyte disks in conjunction with two 16-channel analog-to-digital (A/D) converters and an 8 channel digital-to-analog (D/A) converter. Figure 9 details the lines of data acquisition, from the instrumentation to the A/D converter, and the lines of control from the D/A converter to the motor controllers.

The second design concept was that the control system should be interactive. Thus, the flexibility of either manual or automatic control of the motor-driven pumps was to be provided, and the operator was to be able to initiate and cancel control functions and data acquisition at his or her discretion. These criteria were met by structuring the control software in the following manner. Data acquisition proceeds continually at prescribed time intervals. For example, the output of all transducers is read into a common area every second. These data then become available for use in control. If the data are to be archived for future use, they are put on a permanent file. Otherwise the data in the common area are updated at each data acquistion time interval. Various control functions (for instance, keeping the confining pressure constant at a specified value) are programmed as subroutines that can be activated at the discretion of the operator. These control routines access the common area to obtain the current status of the transducers needed for control.

In the following two subsections, more specific detail is given on various aspects of the hardware and software for the servocontrol and data acquisition systems.

5.1 Data Acquisition and Archiving

The key elements of the data acquisition system were the two CAMAC 3510 A/D converters, which changed the analog voltage outputs of the sensors to digital numbers usable by the computer. The A/D converters had 11-bit (1 part in 2048) resolution, one over a $\pm$ 5 V range and the other over a $\pm$ 10 V range. Data lines from the instrumentation went into both A/D converters. When the amplified sensor voltage was less than 5 V, the low-range A/D was read; when voltage was higher, the alternate A/D channel was used. The instrumentation voltage was integrated over one 60 Hz power cycle to provide a minimum 40-dB suppression of any 60-Hz noise.

If data are to be transferred to a file for future reference, a software subroutine is activated by entering an "archive" command at the computer terminal (Fig. 9). As noted above, data are continually read into a common area in the computer. The archive subroutine initiates transferral of data from the common area to a permanent file at prescribed intervals. For example, to obtain 10 to 15 data points during loading in a stress-strain test, it may be sufficient to archive data every 25 seconds. To follow the temperature change of a sample being slowly heated, readings every minute may be sufficient. Besides transferring data to file, the "archive" subroutine outputs the data onto hard copy.

5.2 Servocontrol

As described in Section 3.1, the actuator and confining pressure pumps

are driven by electric motors. Speed and directional control are provided by Electro-Craft Model E710-BM motor controllers, which can be operated either manually or automatically. Under automatic operation, the motor controllers receive voltage level commands from the D/A converter and then transmit current pulses in proportion to these voltages to drive the motors.

Figure 12 illustrates the servocontrol logic by showing the steps in the motor feedback control for maintaining a constant confining pressure. The operator initiates automatic control by calling the "confining" subroutine and entering the desired pressure value. As described earlier, transducer voltage values are continually updated in the common area of the control program. Upon initiation of control, the "confining" subroutine looks at the most current value of confining pressure stored in the common area. It subtracts this value from the desired value and multiplies the difference by a feedback amplification factor. The D/A converter then changes the computer-determined correction to a voltage level command sent to the motor controllers. The voltage sent by the D/A converter remains constant until the interval time, typically 0.3 seconds, elapses, and a new feedback cycle is begun.

Because the pump motors run at a constant speed during a feedback cycle, it is necessary to select the amplification factor so that the pumps do not over- or undercompensate for the pressure difference. Overcompensation will cause the pressure to oscillate about the desired value, while under-compensation may cause the desired value to be approached too slowly.

Subroutines have also been written for maintaining constant axial load and for performing stress-strain tests. During a stress-strain test, the computer maintains an approximately constant rate of axial displacement by

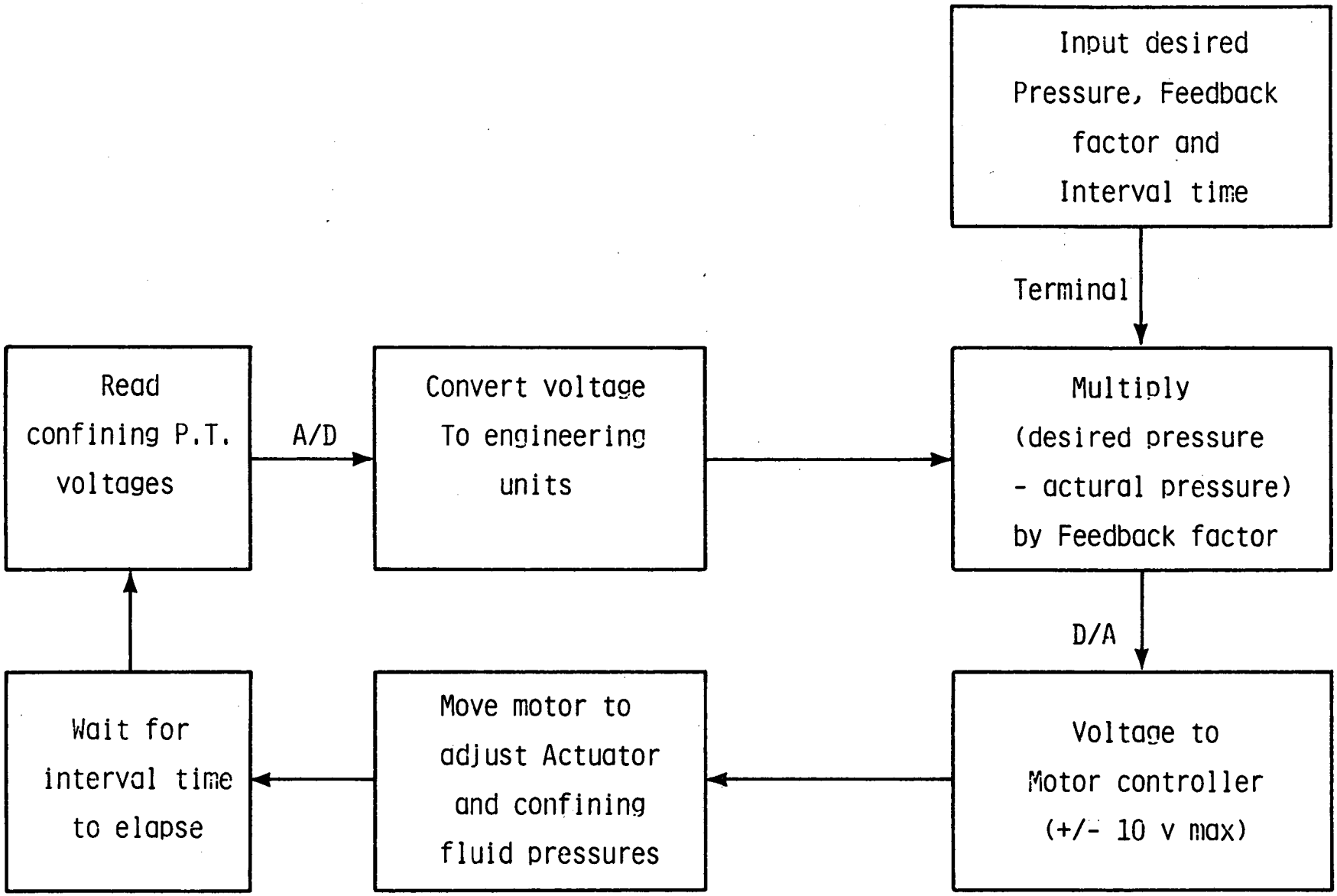

XBL 8210-2504

Fig. 12. Logic of feedback control loop for maintaining constant confining pressure.

operating the actuator pump motor at a fixed speed. When the specified peak axial load is obtained, motor rotation automatically reverses, and unloading begins. Tests to date have not required a more accurate control of axial displacement rate, though this could easily be provided by controlling the motor speed according to the sample displacement rate as monitored by the axial strain gauges.

As described above, the servocontrol program is interactive, permitting motor control and data acquisition parameters to be entered by the operator. Following is a list of the available interactive commands and a description of the function of each:

INTERVAL - Sets the time between readings of the transducer signals.

ARCHIVING - Turns the permanent data recording routine on or off. Data are stored at an "archiving" time interval specified by the operator.

FEEDBACK - Sets the magnitude of the feedback amplification factor, which controls the size of the command voltage signal from the D/A converter to the motor controllers. The value of the amplfication factor is set independently for each motor.

ACTUATOR - Sets the operating states, input as additional commands, of the actuator pump motor. The operating states are: DISPLACEMENT - provides a constant motor speed up to a specified axial stress, then reverses the motor until the axial stress equals the initial value. Peak stress and rate of loading are entered in this command. PRESSURE - maintains the axial stress at a constant specified level. NEUTRAL -

computer control of the actuator motor controller, while continuing data acquisition.

CONFINING - Similar to ACTUATOR, controls the confining pressure. Has all the same operating modes except for displacement.

BOTH - Sets both the actuator and the confining-pressure motors in either "neutral" or "pressure" mode.

STATUS - Provides updates of current program control parameters as well as current values (in engineering units) of all transducers. The information is output to the computer command terminal, as illustrated in Fig. 13.

EXIT - Exit from the program.

```
Triaxial Test Control System Status - 14:41:15 14-OCT-81

Main feedback loop interval:    0.30 seconds.
Data archiving interval:       20.   seconds.
Logging data on E164244.DAT                and TT 3: - current record: 300
Channels being read:      0 through 12
Channels being archived:  0 through 10
Actuator motor mode:   NEUTRAL   (    10.000     0.00000      0.00000     )
Confining motor mode:  NEUTRAL   (    10.000     0.00000      0.00000     )
Actuator feedback amplification factor:     0.50000
Confining feedback amplification factor:     2.0000

Latest data:
Channel  7 (external load cell):                  9.73959
Channel  1 (internal load cell):                  10.0083
Channel  0 (confining pressure transducer):       9.82303
Channel  2 (actuator pressure transducer):       0.828969
Channel  3 (table LVDT):                       -0.646650E-01
Channel  4 (pump LVDT):                        -0.488759E-01
Channel 11 (actuator motor tach):               0.244379E-02
Channel 12 (confining motor tach):              0.000000
Channel  5 (axial strain gauge):                0.122190E-05
Channel  6 (radial strain gauge):               0.000000
Channel 10 (temperature strain gauge):           17.3509
```

Figure 13. Example of information provided in response to STATUS command.

6. CALIBRATION WITH ALUMINUM SAMPLE

The purposes of performing a calibration test using an aluminum sample with known properties were to: (a) check the reliability over temperature of the strain gauge and load cell measuring system, and (b) determine an overall machine stiffness and thermal expansion coefficient to permit use of the table LVDT as a second strain-measuring device.

The aluminum sample was a cylinder 62 mm diameter x 186 mm long of the alloy 6061. The test procedure was similar to that of the thermomechanical rock properties testing program described in Part II. At a particular confining pressure the test temperature was raised in 25°C increments. At each increment, thermal equilibrium was established in the sample and thermal expansion measurements were made. Every 50°C, a stress-strain test was also performed. Upon reaching 200°C, the sample was cooled in 25°C increments, with stress-strain tests again performed at 50°C increments. After attaining room temperature, the confining pressure was changed and the thermal cycle repeated. Thermal cycles were performed at confining pressures of 2 MPa, 5 MPa, 15 MPa, and 30 MPa.

Neither confining pressure nor temperature cycling appeared to affect Young's modulus, E, and Poisson's ratio, ν, for the aluminum. Therefore, linear E and ν, measured for the loading curves at all the confining pressures and for both heat-up and cool-down, were combined to produce mean E and ν values as a function of temperature, these average values are listed in Table 1. As the standard deviations of E and ν at each of the temperatures were 2% or less, the repeatability of the measurement system appeared to be very good.

Table 1. Measured E and ν as a function of temperature for aluminum calibration sample. Each E and ν listed are the average of E and ν at each temperature for all confining pressures, for both the loading and unloading cycles of the stress-strain tests.

Sample Temperature (°C)	E mean val.	E std. dev.	ν mean val.	ν std. dev.
25	75.0	0.24	0.339	0.0037
69	73.8	0.31	0.340	0.0064
115	72.3	0.51	0.339	0.0102
159	70.4	0.61	0.339	0.0057
182	69.3	0.66	0.338	0.0027

Table 2. Effect of temperature on E and ν of aluminum, as given in literature.

Temperature (°C)	E*	ν+
25	75.0	0.33
69	74.1	
115	72.9	0.35
159	70.8	
182	69.5	0.34

*Based on percent reduction of room temperature E value as listed by Alcoa Structural Handbook (1960), p. 11. Assumes a 75.0 GPa room temperature value for E.

+Aerospace Structural Metals Handbook (1977), Vol. III, Fig. 3.061.

The elastic moduli determined in the rock testing machine were compared with those published in the literature for 6061 aluminum. The average room temperature values of Young's modulus, determined from the testing machine measurements, was 75.0 GPa. The typical Young's modulus for compression of aluminum 6061 at room temperature is 69.7 GPa (Alcoa Structural Handbook, 1960). Higher values for E of aluminum 6061 are listed in the Aerospace Structural Metals Handbook (1978), and the measured Young's modulus appears to be slightly dependent upon the thickness, with E = 73.8 GPa for extrusion thickness of 3.0-6.5 inches compared with E = 69.4 GPa for extrusion thickness of 0.075 - 0.375 inches. The higher value may be more applicable to the aluminum sample used in the test.

Temperature is known to decrease the value of Young's modulus. The temperature effect seen in the Young's modulus measurements on the aluminum (Table 1) was very similar to those noted in the literature (Table 2).

In addition to checking the Young's modulus obtained from the rock testing machine, the calibration verified the accuracy of the thermal expansion coefficient derived from the strain gauges. Table 3 lists the mean α_ℓ computed from the test data with published values for aluminum 6061. Deviation of measured values from expected values was 3% or less.

The table-mounted LVDT provided an alternative sample strain measuring system. However, as the LVDT was not directly attached to the rock, the displacements measured by the LVDT were not entirely attributable to the strain on the sample. In order to determine the Young's modulus of the sample from the LVDT data, it was necessary to determine the contribution to the LVDT measurements, of displacements due to the compliance of the end pieces

Table 3. Comparison of α_ℓ of aluminum calibration sample with published values for aluminum 6061.

	Temperature Range (°C)	Mean Value of α_ℓ over Temp. Range ($\times 10^{-6}$ cm/cm-°C)
Aluminum sample (30 MPa Conf. Pres.)	22 - 92	2.334
	22 - 183	2.449
Aluminum sample (2 MPa Conf. Pres.)	25 - 93	2.383
	25 - 180	2.491
Aluminum 6061 (Aerospace Structural Metals Handbook)	20 - 92	2.34
	20 - 183	2.41

and test frame. Displacement measured by the table LVDT was the sum of the sample deformation and the displacement due to the compliance of the axial loading system; hence

$$Dt = Da + Ds$$

where Dt is the total displacement measured by the LVDT, Da is the axial deformation of the aluminum sample, and Ds is the system deformation. Displacement is related to load, L, by the compliance, so

$$Da = Ka \times L,$$
$$Ds = Ks \times L,$$
$$\text{and } Dt = (Ka + Ks) \times L = Kt \times L,$$

where Ka, Ks, and Kt are, respectively, the compliances of the aluminum sample and the axial load system, and the total compliance as determined by the LVDT measurement. Thus the load system compliance can be expressed as

$$Ks = Kt - Ka .$$

The strain gauge measurements were assumed to represent the true sample deformations. Therefore, Ka was calculated from the strain gauge derived Young's modulus (Ea) by

$$Ka = (\ell/AEa)$$

where ℓ = sample length, and A = sample cross-sectional area. With Ks determined for each temperature and pressure state used in a test sequence, the Young's modulus of a rock sample could then be derived from the LVDT data. With Ks known and Kt derived from the LVDT measurement, Kr, the rock sample compliance, is

$$Kr = Kt - Ks$$

and the Young's modulus of the rock is

$$Er = (\ell/AKr)$$

The Ks for both the loading and unloading portions of the stress-strain curve are listed in Table 4 for the all the modulus measurements performed using the aluminum cylinder. Also given is the compliance of the aluminum sample, Ka, at 30 MPa confining pressure. Note that Ks is of the same order of magnitude as Ka. From the table, it is apparent that Ks can vary by 0.100 x 10^{-6} mn/N. Such a variation in Ks would affect the Young's modulus determined from the LVDT data by 11%.

A similar calibration was attempted to permit table LVDT measurements to be used for the thermal expansion determinations. However, the variation in the LVDT calibration data was too great to be useful. This large variation was probably the result of sticking of the LVDT core.

Table 4. Axial load system compliance with temperature and confining pressure measured in the calibration test.

Conf. Pres:	30		15		5		2		30^{II}		
Set Temp (°C)	Ks_ℓ ($\times 10^{-6}$) (mm/N)	$Ks_{u\ell}$ ($\times 10^{-6}$) (mm/N)	Ks_ℓ	$Ks_{u\ell}$	Ks_ℓ	$Ks_{u\ell}$	Ks_ℓ	$Ks_{u\ell}$	Ks_ℓ	$Ks_{u\ell}$	Ka_ℓ
25	1.012	0.970	1.011	0.938	0.932	0.931	1.009	1.021	0.904	0.917	0.818
75	0.903	0.950	0.908	0.987	0.851	0.901	0.831	1.062	0.928	0.895	0.840
125	0.892	0.972	0.952	0.928	0.778	0.899	0.922	1.106	0.856	0.872	0.862
175	1.002	0.913	0.578	0.934	0.696	1.019	0.467	1.064	0.654	0.925	0.892
200	0.504	0.885	0.688	0.977	0.950	1.009	0.465	1.002	0.598	0.925	0.899
175	0.830	0.896	0.936	0.995	0.900	0.918	0.888	1.072	0.875	0.986	0.878
125	0.941	0.899	0.960	0.908	0.934	0.856	0.967	1.061	0.977	0.910	0.859
75	1.033	0.912	0.973	0.937	0.945	0.883	1.011	1.024	1.014	0.895	0.838
25	0.984	0.904	1.007	0.951	0.972	0.934	1.059	0.971	1.058	0.916	0.826

Ka_ℓ = Compliance of aluminum sample measured by sample mounted strain gauges, during load cycle at 30 MPa confining pressure.

Ks_ℓ = Axial load system compliance during the load cycle of a stress-strain test.

$Ks_{u\ell}$ = Axial load system compliance during the unload cycle of a stress-strain test.

30^{II} = Results of a repeat thermal cycle at 30 MPa confining pressure.

7. SUMMARY

This report has described the work carried out in the first phase of the Stripa material properties investigations--the development and testing of a laboratory facility for thermomechanical rock property measurements. To meet the experimental design criteria, a system with the following capabilities was assembled: (1) a stiff load frame with an axial load capability of 1.4 MN, (2) a maximum confining pressure of 70 MPa, (3) a sample size of either 52- or 62-mm diameter with a 3-to-1 length to diameter ratio, (4) independent systems for controlled heating and cooling of the test cell with a maximum sustained test cell temperature of 200°C, (5) control of data acquisition and axial load and confining pressure by an electro-servocontrol system using a PDP-11/44 computer to close the feedback control loop. Axial load was monitored by spool-type electronic load cells; confining pressure by a strain-gauged diaphragm-type pressure transducer; sample deformations by strain gauges and LVDT's; and sample temperature by resistance temperature sensors.

In addition to calibration tests of individual transducers, a test was carried out on an aluminum sample to establish the overall reliability of the strain gauge and load cell measuring system under elevated temperatures. The test also provided data on the contribution of deformations of the test machine to property measurements and yielded an overall machine "stiffness" for use of the LVDT's as strain-measuring devices.

PART II: APPLICATION AND RESULTS

1. INTRODUCTION

Most of the Stripa iron ore mine lies in a Precambrian metavolcanic rock known as leptite (Olkiewicz et al., 1979). The underground test site was located in a granite body in contact with the leptite, and the actual heater experiments were located about 150 m from the contact at a depth of about 340 m (Thorpe, 1979). Although the rock from the test area is commonly referred to as "Stripa granite," the actual mineral composition is quartz monzonite (Wollenberg et al., 1981).

For proper analysis of the data from the in situ experiments, testing samples of the Stripa granite in the laboratory for their thermomechanical properties was necessary. The samples in this program were to consist of 52-mm and 62-mm diameter drill cores from the Stripa mine experimental area. Initially the tests were to investigate the effects of stress and temperature on the elastic moduli and the coefficients of thermal expansion for intact and fractured, and wet and dry, samples.

Part II of this report discusses results from six intact dry samples of 62-mm core obtained from instrumentation holes in the experimental area (Figs. 14a and 14b). The laboratory specimens thus came from the same holes in which in situ measurements of displacements and stresses had been performed. Although an effort was made to obtain samples from numerous locations in order to study the spatial variability of properties, only a few intact samples were available, and these were mostly from the time-scaled experiment area. Tests were performed over a range of temperatures (room to 200°C) and hydrostatic stress (2 MPa to 55 MPa) in order to bracket stresses and temperatures in the field. Because both the cool-down, and heat-up portions of the in

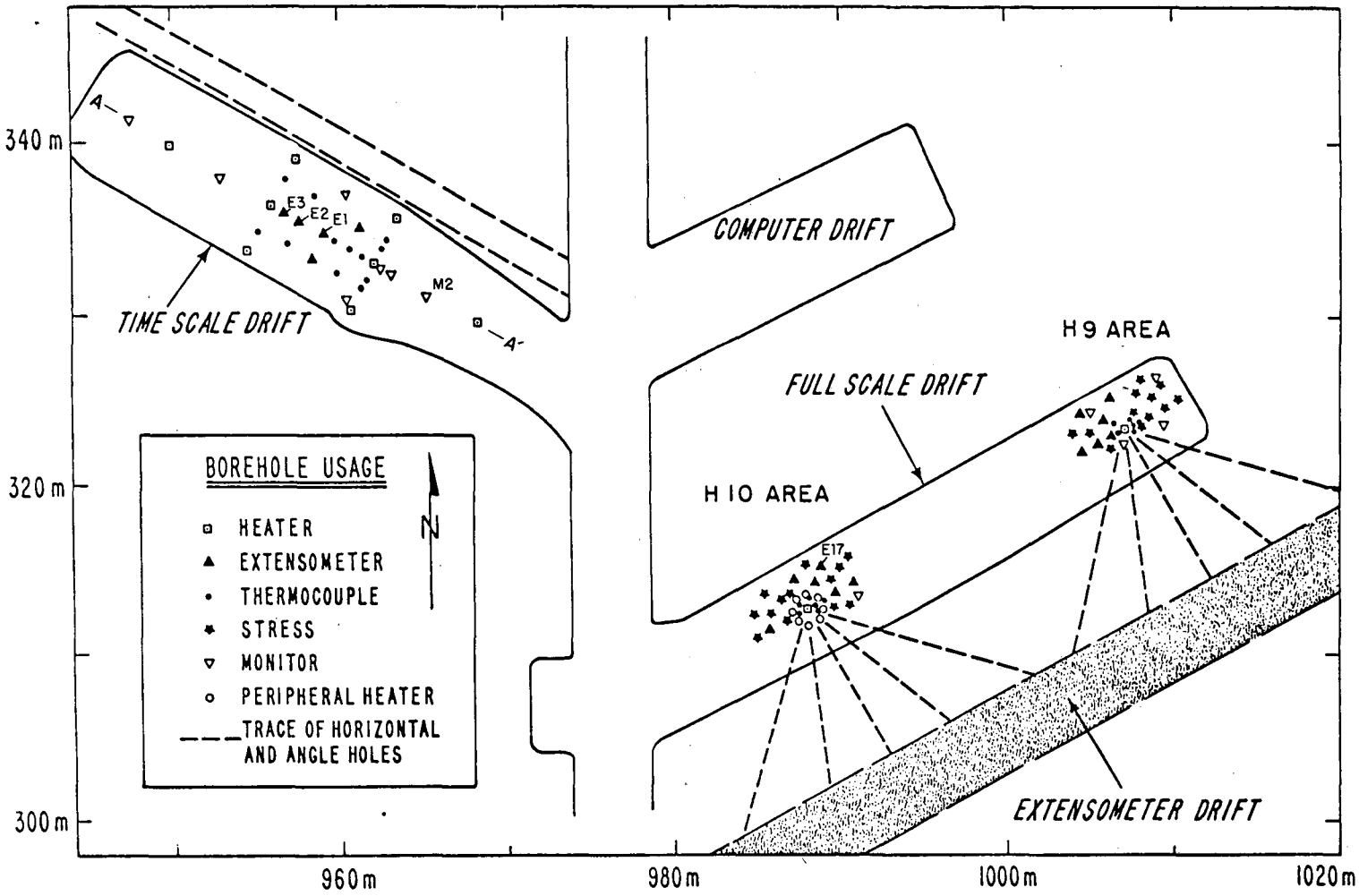

Fig. 14A. Plan view of Stripa experimental area indicating holes from which samples were taken.

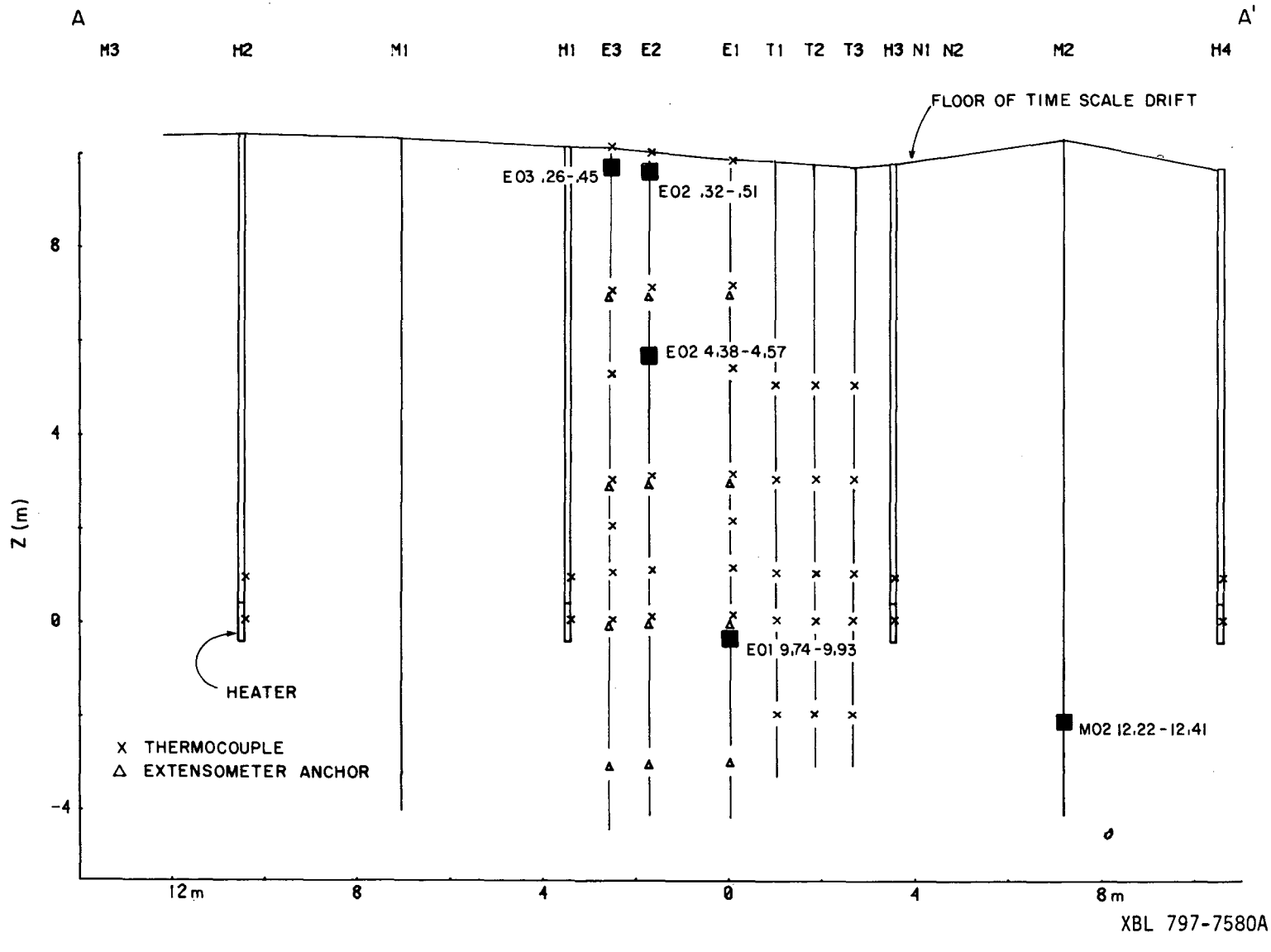

Fig. 14B. Cross section showing position of samples in holes.

situ experiment were to be modelled, properties were also measured during both heat up and cooldown of the samples.

2. SAMPLE PREPARATION

2.1 Surface Preparation

Most of the 62-mm-diameter core was neither smooth enough nor straight enough for testing without surface grinding. After cutting the samples roughly to length, they were ground to a cylindrical shape. Then the ends were ground parallel to each other and perpendicular to the sides. Tolerances for smoothness of sample ends and sample perpendicularity were as prescribed in ASTM standard D2664. Because of the grinding procedures, actual dimensions of the samples varied within a few millimeters of the nominal 186 mm length and 62 mm diameter.

2.2 Strain Gauging

Areas to be strain-gauged were coated with an epoxy chosen for its low cure temperature and high service temperature, 260°C (Micromeasurements 610). The coated samples were cured in an oven for 8 to 10 hours at a temperature of about 85°C. After the sample had cooled, gauges were applied using the epoxy, and the sample was cured for an additional 8 to 10 hours at about 85°C. By slowly heating the samples to cure temperature and maintaining this temperature at less than 100°C, damage due to microcrack growth was minimized during sample preparation.

Figure 15 illustrates a typical strain gauge pattern for a sample. Four strain gauges and a temperature sensor were placed approximately at sample midplane. Two gauges were oriented axially and placed diametrically opposite each other. The other two gauges were oriented circumferentially.

The grid area of the strain gauges measured 12.7 mm in length by 4.57 mm in width. As the grain size of Stripa granite was mostly less than 0.5 mm,

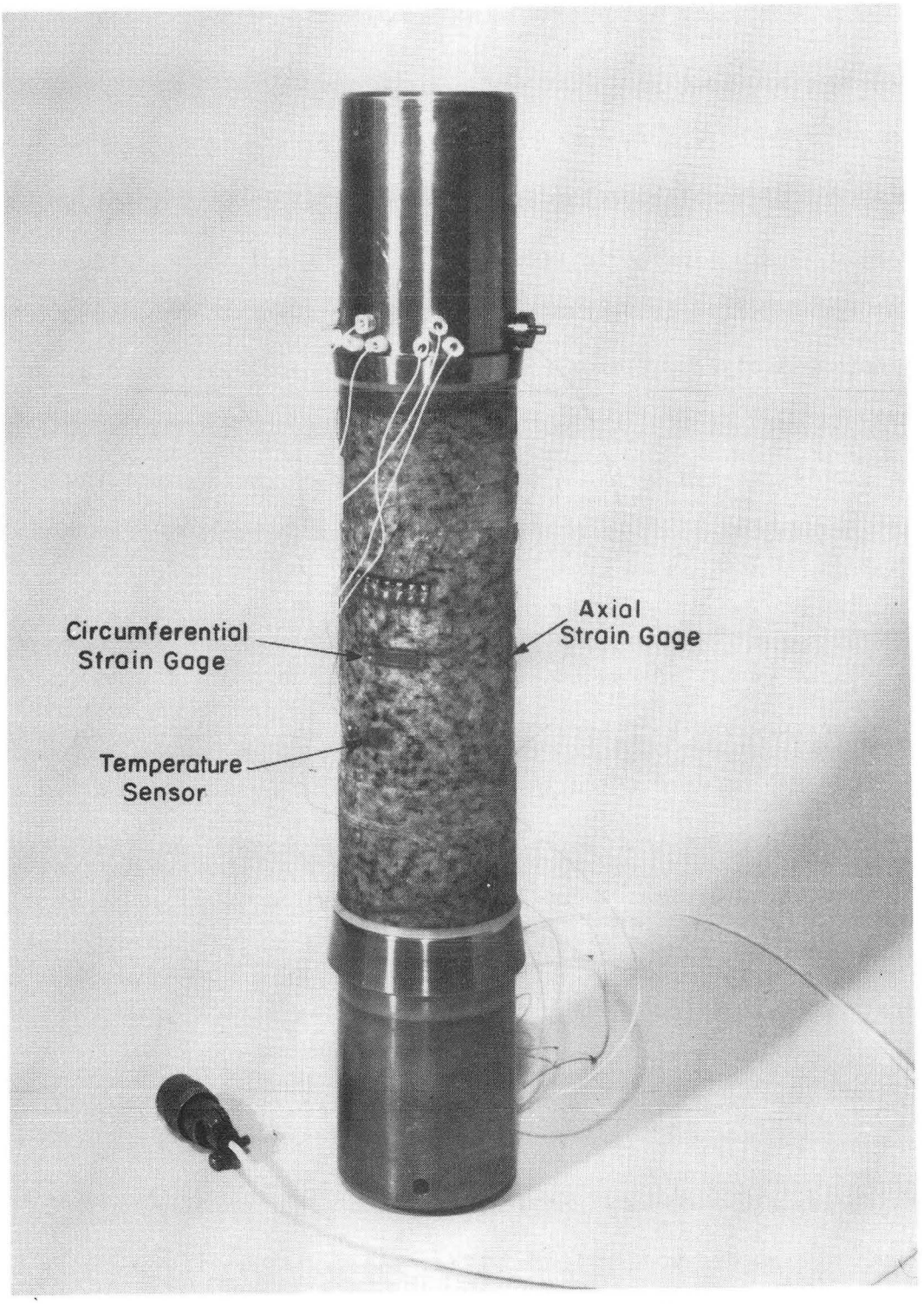

XBB 814-3291A

Fig. 15. Strain gauged sample mounted between loading pistons.

with very few grains in excess of 1 mm (Wollenberg et al., 1981), the strain gauges were large enough to insure that the measured strains represented the average strain of the aggregate material. This was further verified by testing a sample with 24.5 mm as well 12.7 grid length strain gauges. Differences in results were less than 1%.

Strain gauges were wired in two Wheatstone bridge configurations (see Part I), one bridge for the two axial gauges and another for the circumferential gauges. Gauges on the rock were active elements of the bridges, whereas gauges on a plate of titanium silicate in the test cell acted as compensating elements. Compensating gauges in the same environment as active gauges assured that effects of temperature and pressure on the gauges themselves would be cancelled and therefore not reflected in property measurements. Because titanium silicate has a near-zero coefficient of thermal expansion, the strain gauges on this plate would measure only the thermal expansion of the rock sample. This can be demonstrated formally as follows. The temperature-induced change in resistance of a strain gauge $(\Delta R/R)_{\Delta T}$ can be expressed as (Dally and Riley, 1965):

$$(\Delta R/R)_{\Delta T} = (\alpha - \beta)\, S_g\, \Delta T + \gamma \Delta T \quad ,$$

where α = coefficient of thermal expansion of material on which the gauge is mounted,

β = coefficient of thermal expansion of gauge material,

γ = temperature coefficient of resistivity of the gauge material, and

S_g = gauge factor of the gauge.

With identical gauges on the rock and the compensating plate, the change in output from the strain gauge bridge due to a change in temperature, ΔT, will be proportional to:

$$\frac{\Delta R}{R} - \frac{\Delta R'}{R} = (\alpha - \alpha') S_g \Delta T \quad ,$$

where primes refer to a compensation plate. Because α' (titanium silicate) is less than 1% of α (granite), the output of the bridge was assumed to be due totally to the thermal expansion of the rock.

2.3 Sample Jacketing

The final step of sample preparation was to jacket the specimen in a Viton sheath and place it in the test cell as shown in Fig. 16. Details of the jacket and sample axial loading assembly are found in Part I.

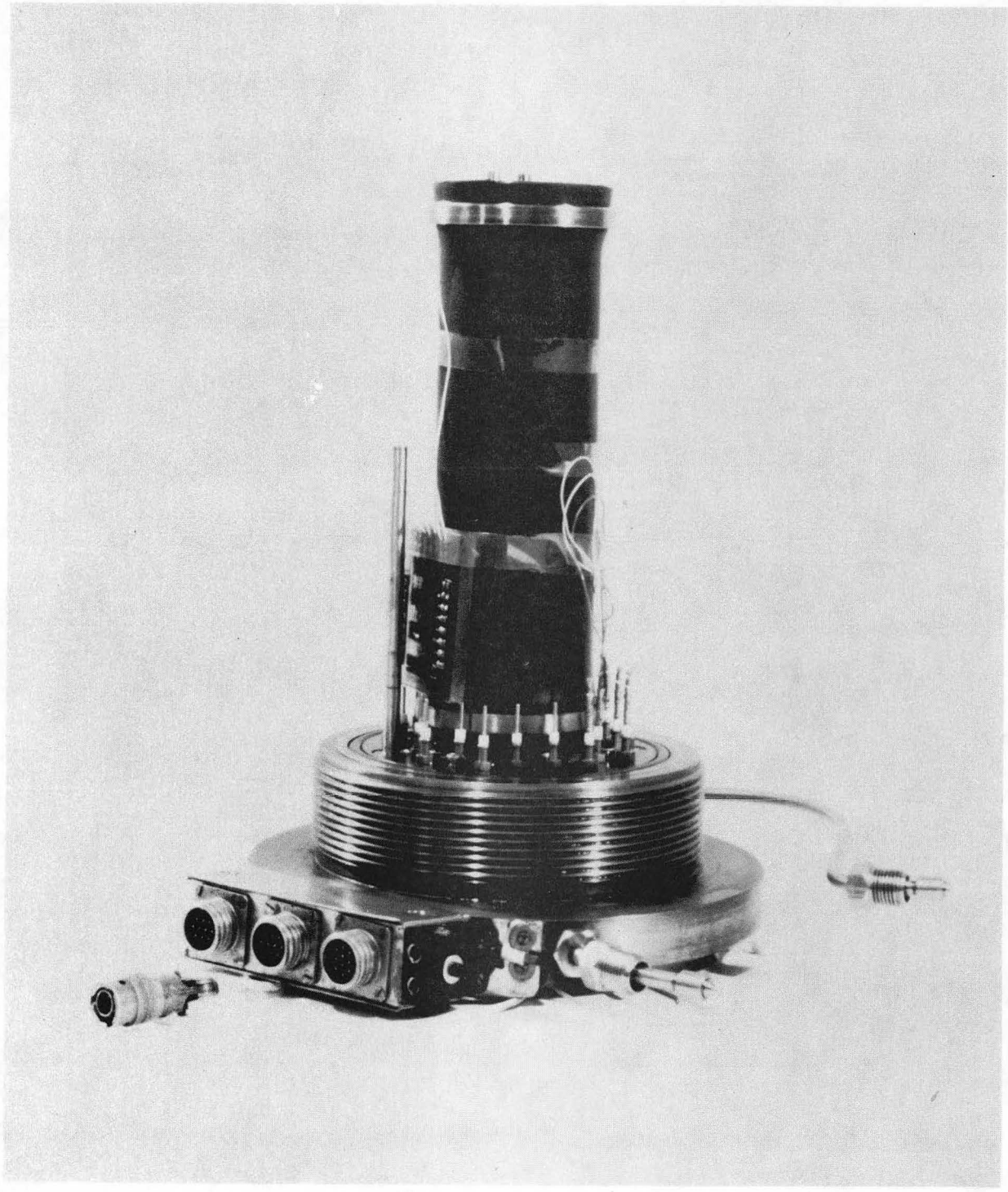

CBB 810-11474

Fig. 16. Sample in Viton jacket in test cell (different top position than shown in Fig. 15).

3. TEST PROCEDURES

3.1 Test State Matrix

The number of pressure-temperature (P-T) states at which properties were required would have demanded a great many samples for statistically meaningful data if a new sample had been used for tests at each P-T state. Each specimen tested was therefore subjected to a matrix of P-T states ranging from room temperature to 200°C and 2 MPa to 55 MPa confining pressure.

The manner in which testing proceeded through this matrix is illustrated by Fig. 17. First of all, hydrostatic stress on the sample was increased to 55 MPa. While maintaining a constant hydrostatic stress, the temperature was increased to 50°C and allowed to stabilize. Thermal expansion measurements were taken and the temperature increased to 75°C. At this temperature, both thermal expansion measurements and stress-strain measurements for elastic moduli determination were made. Stress-strain tests were performed under a constant rate of axial deformation of approximately 0.07%/min. The sequence of thermal expansion measurements every 25°C and stress-strain tests every 50°C was continued to 175°C. At 200°C both thermal expansion and stress-strain measurements were made. The sample was then cooled in steps of 25°C, with thermal expansion measurements made each 25°C and stress-strain tests done every 50°C from 175°C to 25°C. After each thermal cycle, the confining pressure was reduced to the next lower test pressure, and the sequence was repeated.

Performing a complete temperature cycle at each confining pressure resulted in a very lengthy test procedure that totaled about 120 hours to complete all five thermal cycles. Other investigators (e.g., Heard, 1980)

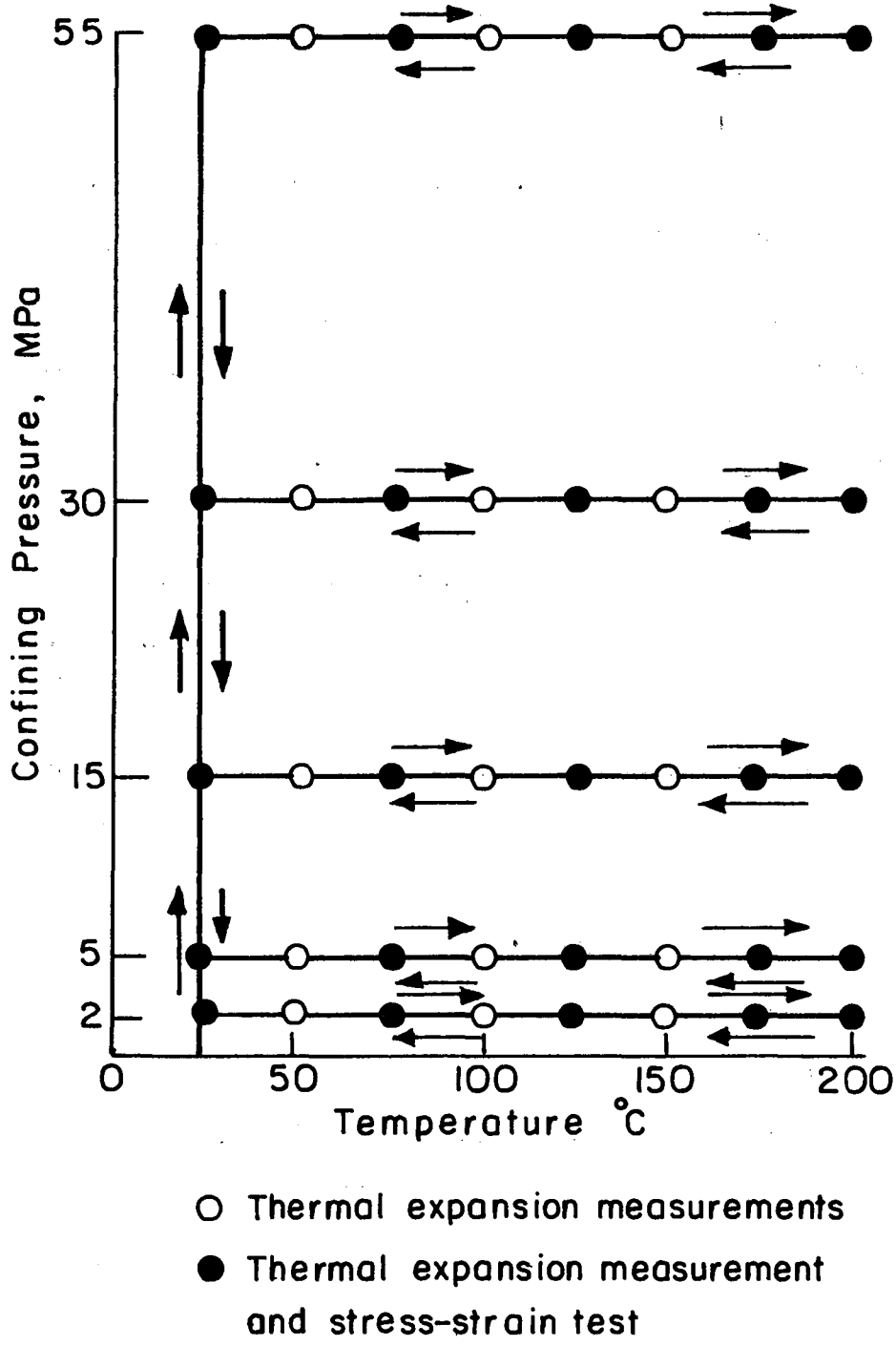

Fig. 17. Diagrammatic representation of test sequence showing pressure and temperature states at which measurements were made.

have made similar measurements using a much more rapid procedure in which hydrostatic stress states were cycled at various temperatures. Our approach was selected because it allowed a more direct, and therefore less uncertain, measurement of thermal expansion.

Table 5 presents a summary of the confining pressures, temperatures, and maximum deviator stresses used in testing. After four samples had been tested, it was noted that the sample-to-sample scatter in α_V and α_ℓ at any test pressure was greater than the effect, for any single sample, of varying the pressure over the entire test range. For thermomechanical modeling, these results indicated that studying the variability of the properties would be more important than determining, in detail, the pressure dependence of the parameters. The test procedure was therefore shortened by eliminating thermal cycles at 30 MPa and 2 MPa confining pressures. This shorter procedure allowed both testing of additional samples and more study of the variability of properties in the rock mass.

3.2 Stabilization Criteria

Accurate thermal expansion measurements also required thermal equilibrium in the sample before measurements were made. Theoretically, according to results calculated for an infinite cylinder with constant surface temperature (Carslaw and Jaeger, 1959), stabilization should occur about 9 minutes after the outside of the sample reaches the target temperature. In practice, stabilization criteria were based on strain gauge response. Stabilization was assumed if the change in axial and radial strain was equal to or less than 0.0005% in 10 to 15 minutes. This generally occurred about 30 minutes after the temperature of the exterior of the rock had stabilized and about 1-1/2 hours after the temperature change was initiated.

Table 5. Summary matrix of test states.

Confining Pressure (MPa)	Maximum deviator stress levels σ_d (MPa), at various temperatures				
	25°C	75°C	125°C	175°C	200°C
55	260	260	244	195	195
30	212	212	199	159	159
15	178	178	167	125	125
5	123	123	115	92	92
2	80	80	75	60	60

As a check on the uniformity of the temperature field within the sample, one test was run with a temperature sensor placed within one-half inch of each end of the sample as well as in the center plane. This test established that the ends of the sample were cooler than the center portions. At 75°C, the ends of the sample were 2°C to 4°C cooler than the midsection. At 200°C, this difference increased to between 8°C and 13°C. The difference in temperatures between the two ends did not exceed 3°C. Discrepancies between midplane and end temperatures were not altered by allowing greater stabilization time (e.g., overnight), indicating that although thermal gradients existed, steady state conditions were in effect. These thermal gradients did not affect data based on strain gauge measurements because the gauges measured deformations over a length of only one-half inch at the midplane.

3.3 Minimization of Sample Damage

A potential disadvantage of a testing a sample at many pressure-temperature states is that the sample may become damaged at some point, affecting its properties in subsequent tests. The major sources of sample damage in this study were expected to be (1) rate of sample heating, (2) repeated thermal cycling to 200°C, and (3) repeated application of deviator stresses. Steps taken to minimize these effects will now be discussed.

Thirumalai and Demou (1970) had observed microstructural damage in electron microscope photographs of a granodiorite heated at 5°C/min to 300°C. From acoustic emission studies, Richter and Simmons (1974) later concluded that simply heating a granite at a rate equal to or greater than 5°C/min caused cracking. These authors therefore recommended a rate of 2°C/min to minimize cracking due to the heating rate alone. For this study, both heating and cooling rates were maintained at 1.5°C/min or less.

Richter and Simmons (1974) also found a threshold cracking temperature. Above this temperature cracking occurs due to differental thermal expansion of the mineral grains, regardless of the heating rate. For Westerly granite, they determined this temperature to be between 260°C and 300°C. This indicated that little cracking should occur, given a slow heating rate, up to the maximum temperature (200°C) of this study. As a further precaution against damage from thermal cycling, the first cycle was at the highest confining pressure, with succeeding cycles at progressively lower pressures. It was felt that, if crack growth due to differential thermal expansion did occur, high confining pressures would limit crack growth more than low pressures.

Damage from stress-strain tests was minimized by keeping the maximum applied deviator stress equal to 40% of the rock strength at a given P-T state. Work by Brace et al. (1966) and later by Scholy (1968) had indicated that microfracturing of granite begins at approximately one-half of the failure stress. Thus the maximum deviator stress value was high enough to represent in situ stress conditions but low enough to prevent significant damage to the sample.

Data on the strength of intact Stripa granite was obtained from Swan (1978). Average values of the fracture stress at room temperature are plotted in Fig. 18 along with the stress levels used in this study. Strength at a confining pressure of 55 MPa was not available, so the data were extrapolated on the basis of the average strength at 20 MPa confinement. There is some scatter in the strength data, indicating that a deviator stress equal to 40% of the average strength may be greater or less than 40% of the sample strength. On the basis of standard deviations in sample strengths as determined

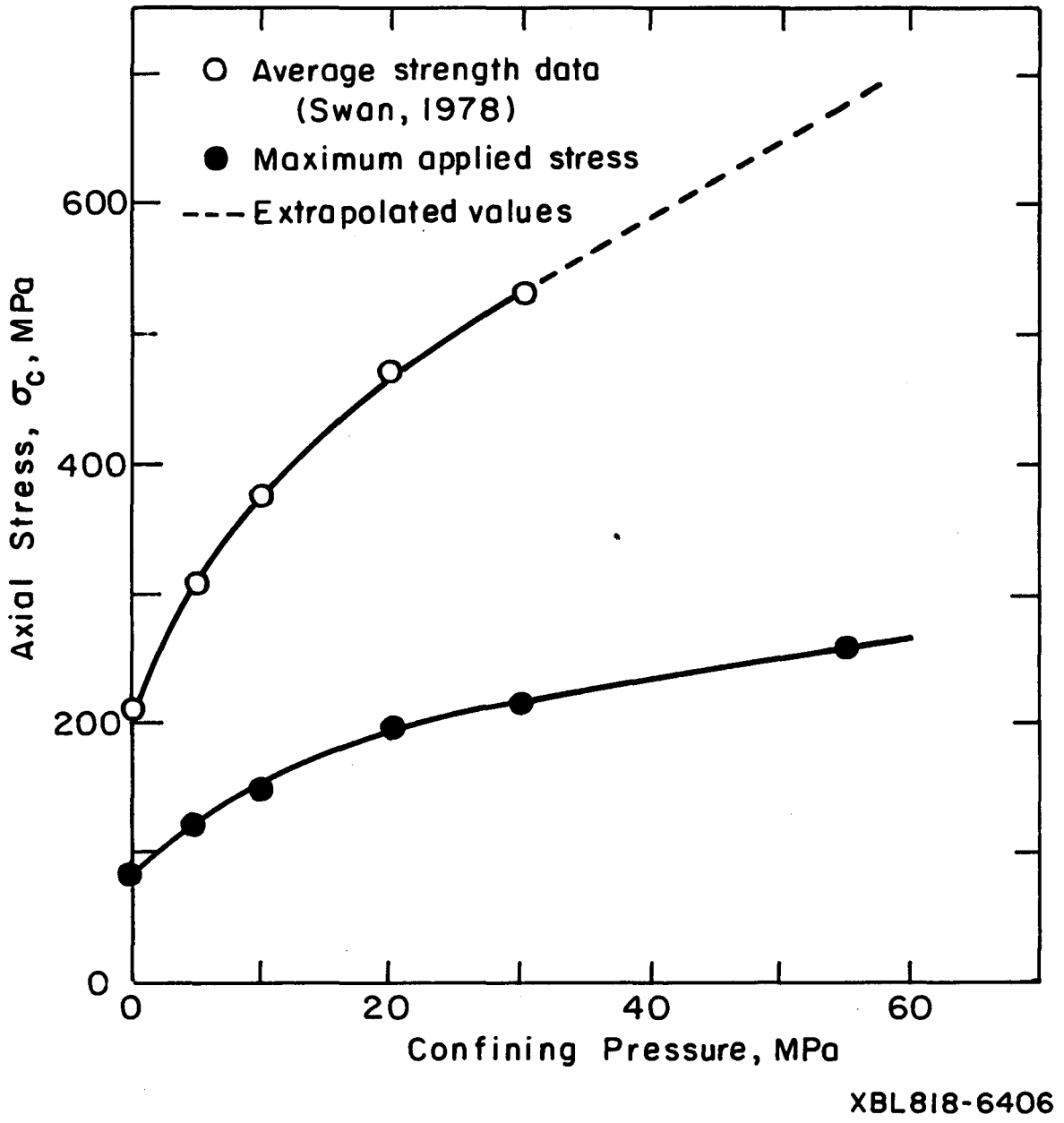

Fig. 18. Maximum axial stress levels used in this study compared with average strength data for Stripa granite.

by Swan (1978), it was concluded that at least 95% of the strength values should lie within $\pm$16% of the average. Swan (1978) also conducted unconfined strength tests at elevated temperatures. On the basis of this data, an additional strength reduction of 0.25% per °C for temperatures in excess of 100°C was assumed at all confining pressures.

One final check on the amount of damage sustained during the test sequence was provided by a repeat thermal cycle on each sample after cycles had been completed for each confining pressure. If properties measured in the repeat tests were nearly equal to those of the first test, it could be concluded that no damage significant enough to be reflected in the macroscopic material properties had occurred. Results of these repeat thermal cycles are discussed in Section 5.3.

4. DATA ACQUISITION AND REDUCTION PROCEDURES

Hardware aspects of the data acquisition system are discussed in Part I.

4.1 Data Acquisition Procedures

The frequency at which readings were taken depended upon the property being measured. After thermal stabilization at each step in the thermal cycle, at least three readings at 2-second intervals were taken for use in determining the thermal expansion. During stress-strain tests, the data acquisition frequency was such that at least 10 data points were taken during both loading and unloading phases. The analogue signals from the strain gauges and the internal load cell were also recorded by an X-Y-Y recorder during the stress-strain test.

Data was stored both as hardcopy output from the computer terminal and on disk files in the computer. The hardcopy output consisted of transducer voltages as read by the A/D converters. Data stored on the disk files consisted of integer numbers related to the bit patterns generated by the incoming signal in the A/D converter. These integer numbers represented the values of the conditioned transducer signals before application of any calibration constants and thus were considered to be the raw data.

4.2 Data Reduction Procedures

Separate computer programs were written for reduction of thermal expansion data and stress-strain data.

4.2.1 Stress-Strain Data

In the stress-strain reduction program, values of deviator stress, σ_d, $(\sigma_1 - \sigma_3)$, and corresponding values of axial strain, ε_a, and radial strain, ε_r, were computed using appropriate calibration constants. (Though circum-

ferential strain was measured, under the uniform loading conditions in the triaxial cell the radial strain is equal to the circumferential strain.) Tangent values of Young's modulus (E_T) and Poisson's ratio (ν) for loading and unloading were then found by performing a polynomial regression analysis of the data.

The first step in the regression analysis was to normalize the data with respect to the maximum values of stress and strain for the particular stress-strain test being analyzed. The normalized data were then fit by polynomials of the form

$$Y = f_0 + f_1 X + f_2 X^2 + f_3 X^3 + \ldots f_n X^n \ , \tag{4.1}$$

where f_0, f_1, f_2, ..., f_n are coefficients and Y and X are the dependent and independent variables. Assume that n data points were recorded for the loading portion of a stress-strain test, where Y_i was the ith value of normalized strain and X_i was the corresponding value of normalized deviator stress. Values of the coefficients were determined by minimizing the sum of squares:

$$S = \sum \left(Y_i - f_0 - f_1 X_1 - f_2 X_2^2 - \ldots - f_n X_n \right)^2 \ . \tag{4.2}$$

Details of the method can be found in Carnahan et al. (1969).

To determine E_T, the tangent Young's modulus, Y_i and X_i in Eq. (4.2) became

$$Y_i = \varepsilon_{ai} / \varepsilon_{amax}$$

and (4.3)

$$X_i = \sigma_{di} / \sigma_{dmax} \ .$$

The theory of regression analysis assumes that the variable Y is subject to random error and that values of X are known precisely. It was assumed that values of deviator stress were known more precisely than strain values, so strain values were assigned to the variable Y. Polynomials resulting from the regression analysis expressed normalized strain as a function of normalized stress. Thus,

$$\varepsilon_a = \varepsilon_{amax}\left[f_0 + \frac{f_1\,\sigma_d}{\sigma_{dmax}} + \frac{f_2(\sigma_d)^2}{(\sigma_{dmax})^2} + \ldots + \frac{f_n(\sigma_d)^n}{(\sigma_{dmax})^n}\right]. \qquad (4.4)$$

The derivative with respect to σ_d of the right hand side of Eq. (4.4) resulted in a value of the inverse of the tangent Young's modulus:

$$\frac{1}{E_T} = \frac{d\varepsilon_a}{d\sigma_d} = \varepsilon_{amax}\left[\frac{f_1}{\sigma_{dmax}} + \frac{2f_2\sigma_d}{(\sigma_{dmax})^2} + \ldots + \frac{nf_n(\sigma_d)^{n-1}}{\sigma_{dmax}^{\,n}}\right]. \qquad (4.5)$$

Equation (4.5), in general, gives E_T as a function of σ_d. For the case in which the stress-strain curve is linear, Eq. (4.5) simplifies to a constant value of E_T:

$$\frac{1}{E_T} = \frac{d\varepsilon_a}{d\sigma_d} = \frac{f_1}{\sigma_{dmax}} = \text{constant}.$$

To determine ν, the variables in Eq. (4.2) were replaced by:

$$Y_i = \varepsilon_{ri}/\varepsilon_{rmax}$$

and (4.6)

$$X_i = \sigma_{di}/\sigma_{dmax} \quad .$$

Thus polynomials were generated that expressed radial strain as a function of axial stress. The slope of the curve representing each such polynomial was a

compliance, $1/E_{rT}$, calculated from Eq. (4.4) by substituting ε_r for ε_a and ε_{rmax} for ε_{amax}. If the best-fit polynomial was a straight line, then

$$\nu = \frac{\varepsilon_r}{\varepsilon_a} = \frac{E_T}{E_{rT}} \quad . \tag{4.7}$$

If the stress-strain relations are nonlinear, incremental approximations can be made so that for a particular increment of stress $\Delta\sigma_d$,

$$\nu = \frac{\Delta\varepsilon_r}{\Delta\varepsilon_a} = \left(\frac{E_T}{E_{rT}}\right) \Delta\sigma_d \quad . \tag{4.8}$$

Selection of the polynomial providing the best fit of the data was done manually, based on two criteria. The first criterion required that the slope of the curve used to fit the stress-strain data should be either constant or constantly increasing within the range of the stresses applied to the sample. The second criterion required minimum variance in the data. From those polynomials meeting the first criterion, the polynomial about which the variance of the data was least was selected as the best fit-curve. The assumption that the stress-strain curve was constant or constantly increasing was verified by analogue plots of the load cell and strain gauge signals made on the X-Y-Y recorder during the stress-strain tests.

4.2.2 Thermal Expansion Data

Thermal expansion data was handled in a parallel fashion, using polynomials of the same form as Eq. (4.1) to fit the data for each thermal cycle. Data was normalized with respect to maximum strain and temperature. To determine the linear coefficient of thermal expansion α_ℓ, variables Y_i and X_i in Eq. (4.2) became:

$$Y_i = \frac{\varepsilon_{ai}}{\varepsilon_{amax}} \quad ,$$

$$X_i = \frac{T_i}{T_{max}} \quad , \tag{4.9}$$

where ε_{ai} and T_i are the ith values of the axial strain and temperature during a heat-up or cool-down cycle. Values of strain were assigned to the variable Y because strains were assumed to be less precisely known than temperatures. Regression analysis yielded best-fit curves, from which α_ℓ was determined by finding the slope of the curves. Thus,

$$\alpha_\ell = \frac{d\varepsilon_a}{dT} = \varepsilon_{amax} \left[\frac{f_1}{T_{max}} + \frac{2f_2 T}{(T_{max})^2} + \ldots + \frac{nf_n T^{n-1}}{(T_{max})^n} \right] . \qquad (4.10)$$

In the regression analysis for determining the volumetric coefficient of thermal expansion, α_v, the volumetric strain,

$$\varepsilon_v = \varepsilon_a + 2\varepsilon_r \quad ,$$

and the maximum volumetric strain,

$$\varepsilon_{vmax} = \left(\varepsilon_{amax} + 2\varepsilon_{rmax} \right) \quad ,$$

were substituted for ε_a and ε_{max} in Eq. (4.9). Then values of α_v were determined as in Eq. (4.10), substituting ε_v and ε_{vmax} for ε_a and ε_{amax}.

The best-fit polynomial was selected by visual inspection of regression analysis results, based on two criteria. In the first, α_v and α_ℓ were assumed to be either constant or always increasing with increasing temperature. This assumption was justified by the data, as will be discussed later. The second criterion, as in the stress-strain data, was for a minimum variance.

In addition to property values derived through regression analysis, "incremental" values of parameters were also determined by calculating the slope of the straight line connecting each pair of data points. This is illustrated in Fig. 19. The solid curve represents a hypothetical best-fit

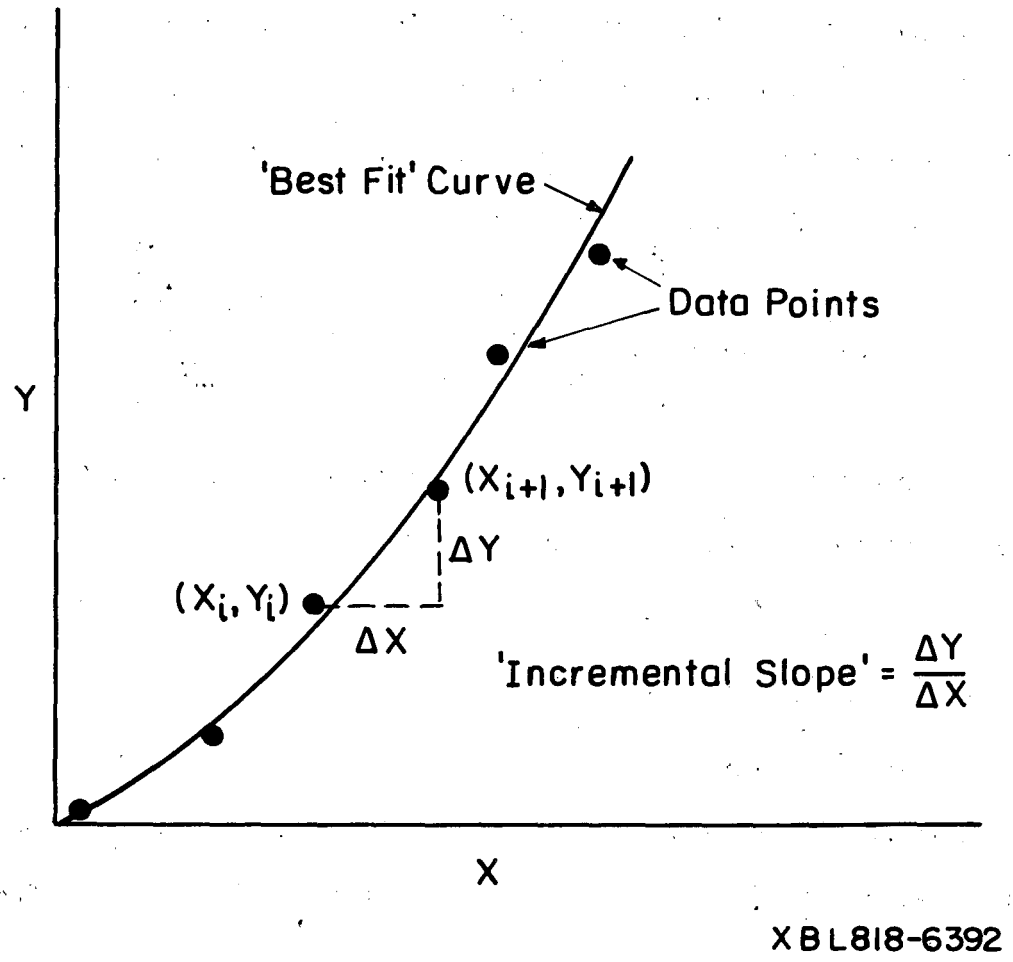

Fig. 19. Definition of "incremental" values of parameters.

line through the data points. If parameter Y is being plotted as a function of parameter X, then the "incremental" slope between two data points (X_i, Y_i), (X_{i+1}, Y_{i+1}) is

$$\frac{\left(Y_{i+1} - Y_i\right)}{\left(X_{i+1} - X_i\right)} \quad .$$

5. RESULTS AND DISCUSSION

5.1 Thermal Expansion Measurements

Thermal expansion measurements will be presented using results of polynomial regression analysis. The data could also have been discussed in terms of incremental values of the properties. A typical example of the difference in values between α_V from a polynomial regression analysis and α_V from incremental slopes is shown in Fig. 20. As shown, there is some scatter of the incremental slopes about the best-fit line. Clearly, however, the trends in the incremental slope data are reflected, as they should be, by the best-fit curves. Incremental values of the α_V and α_ℓ for all samples at each P-T state tested can be found in Appendix A, Table A-1.

5.1.1 Effects of Temperature and Pressure

Major trends in thermal expansion behavior of the intact Stripa granite are illustrated by summary curves in Figs. 21 and 22. Two confining pressures were eliminated from the experiment procedure for two samples, so curves for 55 MPa, 15 MPa, and 5 MPa confining pressures represent average results of six tests, whereas curves at 30 MPa and 2 MPa confinement represent average results of four tests. The correlation between average values calculated from regression analysis results and average values based on incremental slope values is illustrated by the discrete data points plotted for 5 MPa and 55 MPa confining pressure.

From Fig. 22 it can be seen that an average value of α_ℓ for Stripa granite between 20°C and 100°C at low confining pressure is about 9.5 x 10^{-6}/°C. For these pressure-temperature conditions, Stripa granite seems to

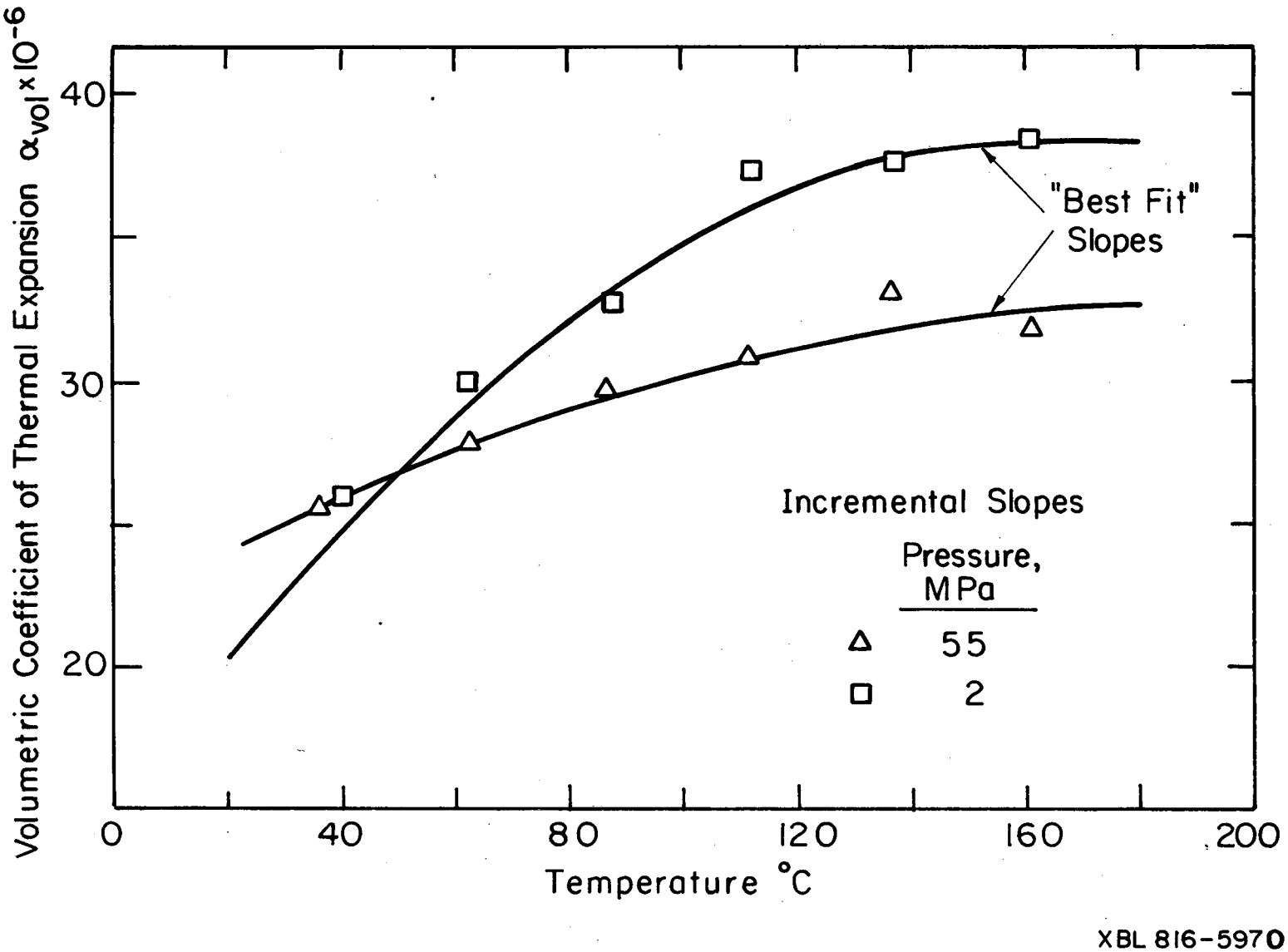

XBL 816-5970

Fig. 20. Comparison of best fit curve and incremental values for α_v from sample E020.32-0.51.

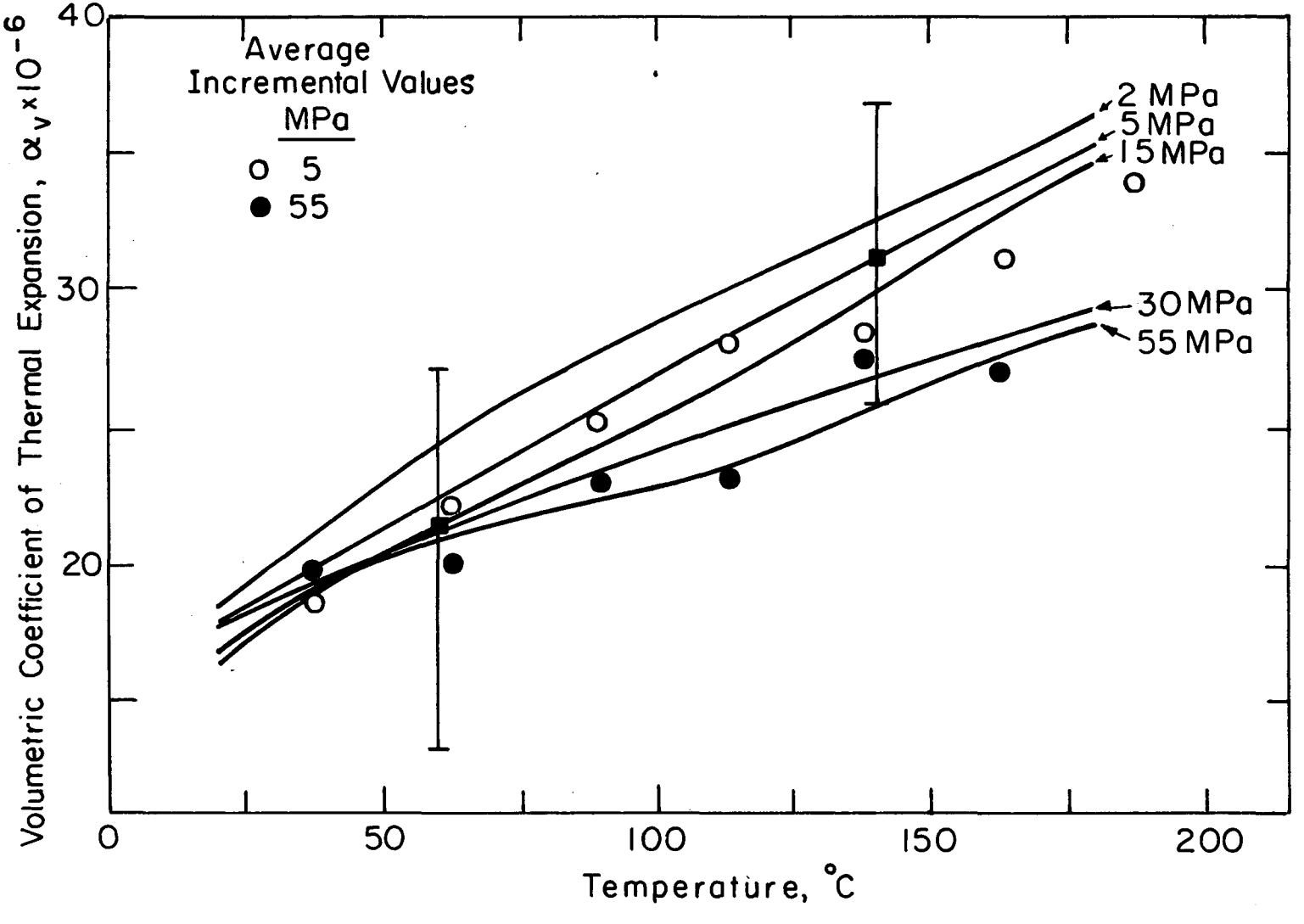

XBL 818-6393

Fig. 21. Average values of α_v for each confining pressure as a function of temperature.

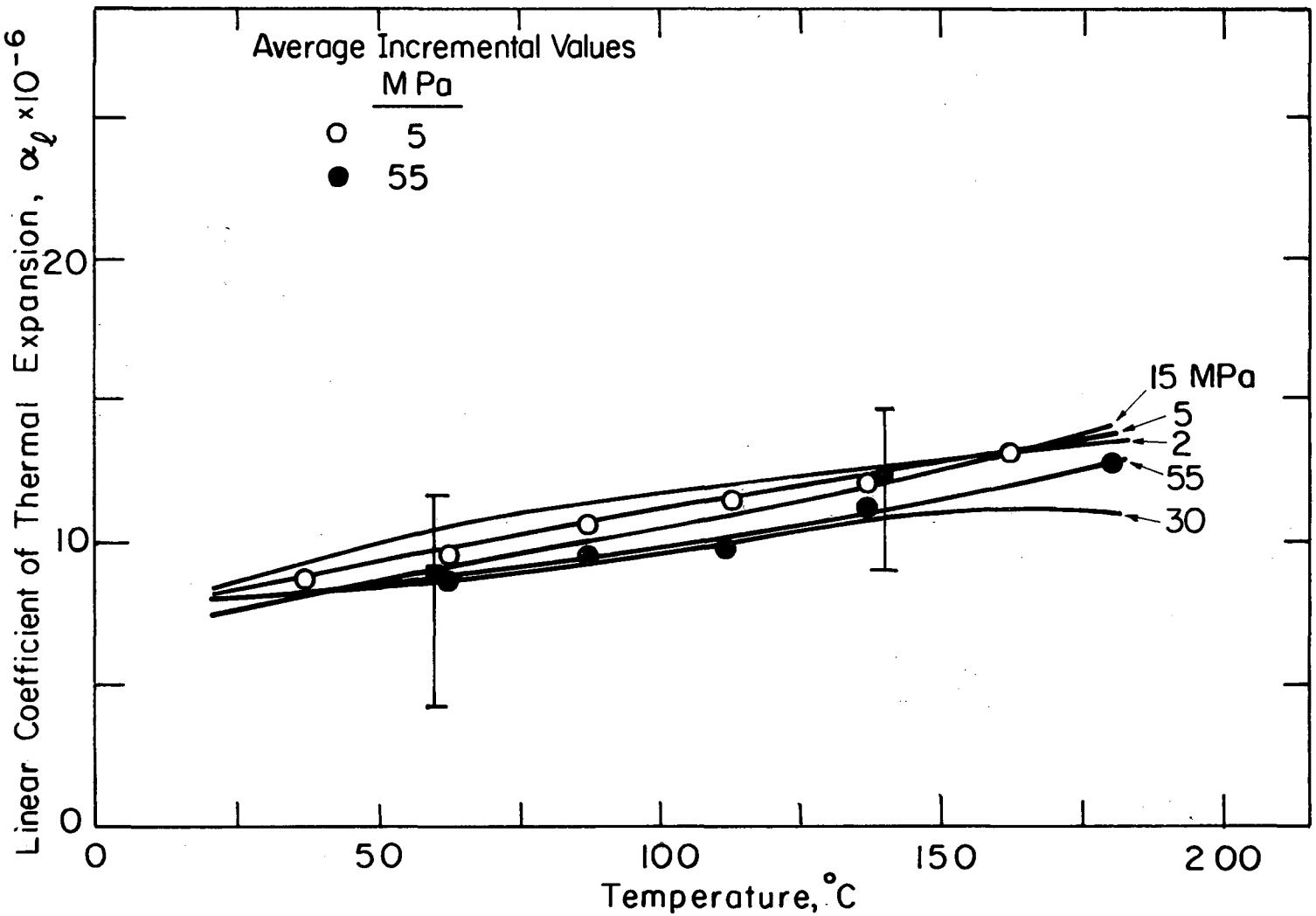

Fig. 22. Average vaulues of α_ℓ for each confining pressure as a function of temperature.

fall within the range of many granitic rocks. For example, Skinner (1966) found the average of 21 measurements for various granites to be 8 ± 3 x 10^{-6}/°C. More recent measurements by others--e.g., Cooper and Simmons (1977), Laubser and Bryden (1971), Bauer and Handin (1981), Page and Heard (1981), and Heard and Page (1981)--also fell within this range at low pressure and temperature.

The most significant trend shown by the average curves from tests on the Stripa core is an increase in the coefficient of thermal expansion (α_v or α_ℓ) for an isobaric temperature increase. Average values of α_v at 20°C were from 48% to 61% of those at 180°C, while average values of α_ℓ at 20°C ranged from 52% to 70% of those at 180°C. Since α_ℓ is a function of ε_a alone, while α_v is a function of the sum of ε_a and $2\varepsilon_r$, the larger decrease in α_ℓ with temperature indicates a slightly greater rate of change with temperature for ε_a than for ε_r. The scatter in the data, however, precludes drawing definite conclusions. The large effects of isobaric temperature increases observed in this work are similar to those observed previously by Cooper and Simmons (1977) for other granites. Though performed only at ambient pressure, their results for five different granites yielded values of α_ℓ at 20°C from 42% to 46% of α_ℓ values at 200°C. However, on tests of Climax quartz monzonite at confining pressures from 6.9 MPa to 55 MPa, Page and Heard (1981), observed almost no net increase in α_ℓ in isobaric heating from 20°C to 200°C.

Though not so pronounced in the average α_ℓ results, the α_v results clearly show a decrease in the temperature dependence at higher confining pressure. This trend has also been observed by Wong and Brace (1979), who

found that, above a confining pressure of about 50 MPa, Westerly granite exhibited a constant value of α_ℓ.

Curves of average values of α_V and α_ℓ shown in Figs. 21 and 22 are nearly linear, indicating a constant increase in both volumetric and linear thermal expansion with temperature. Though, on the average, curves were nearly linear, best-fit curves for individual samples exhibited a variety of shapes, as illustrated, for example, by Fig. 23. These shapes reflect the best-fit curve selection criterion mentioned in Section 4.2.2, by which α_V and α_ℓ were assumed to be constant or increasing with temperature. Examination of the incremental slope data indicated that, within the scatter of the data, this assumption was appropriate up to 175°C. Both Board (Appendix C) and Heard and Page (1981) observed a decrease in α at or above 200°C at various confining pressures. Data from the present study for the temperature interval of 175° to 200°C are not included in the figures because much of the information was lost due to drift in the strain gauges at temperatures above 190°C. Remaining data are inconclusive, with some values of α_V and α_ℓ decreasing between 175°C and 200°C and some increasing. For details of individual tests, refer to Appendix A. It should also be noted that the shapes of best-fit curves reflect selected polynomial functions that are based on statistical theory rather than on the physics of rock behavior. Curve fitting may be useful in defining trends, but it cannot substitute for sound theoretical work in defining functional relationships between variables.

Results of work by Board (Appendix C) and Heard and Page (1981) on Stripa granite are compared with results of this study in Figs. 24 and 25. In these figures, the curves from this study and from Board represent α_ℓ as

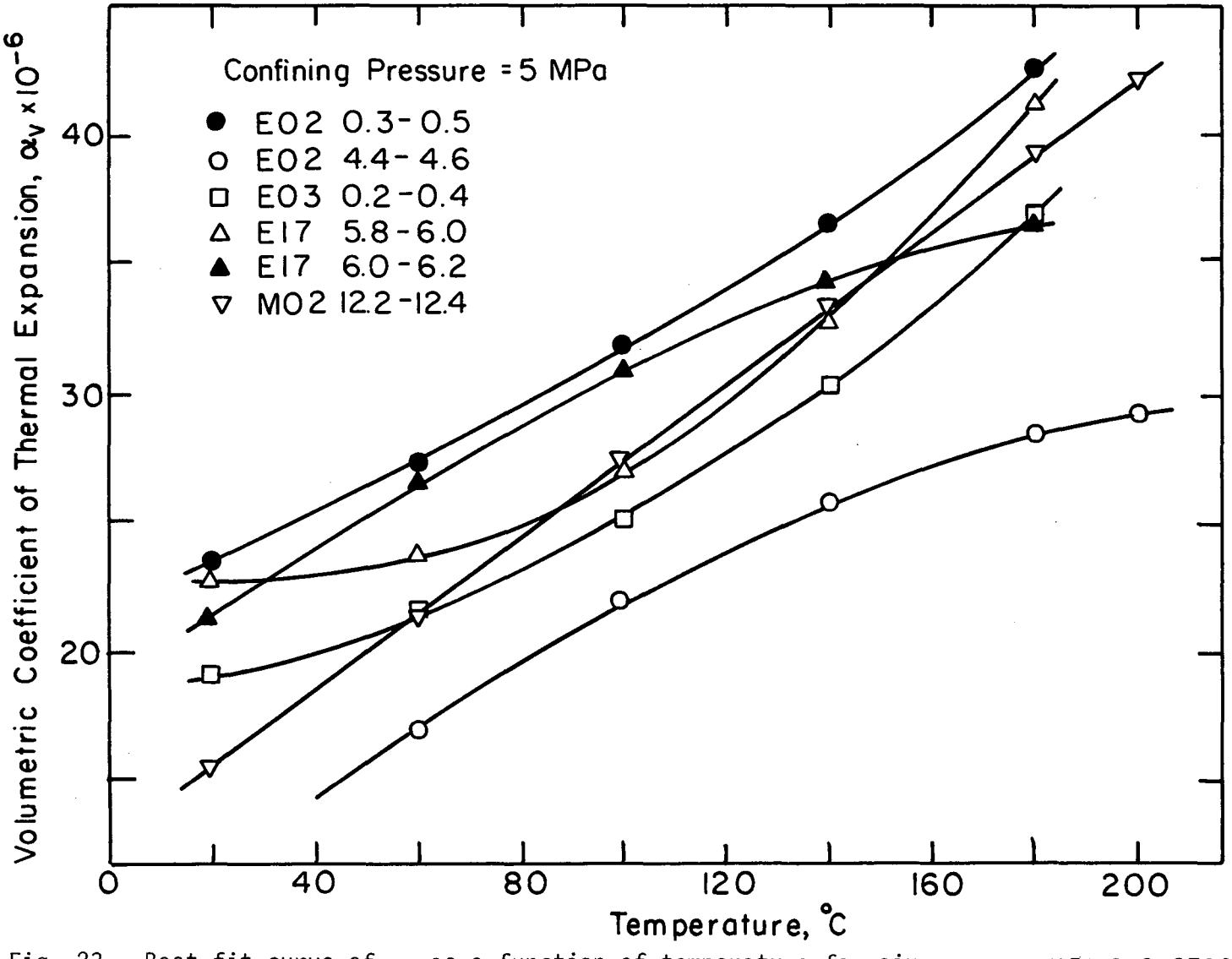

Fig. 23. Best fit curve of α_V as a function of temperature for six samples. Data points represent values of α_V calculated using the best fit polynomials.

XBL 818-6390

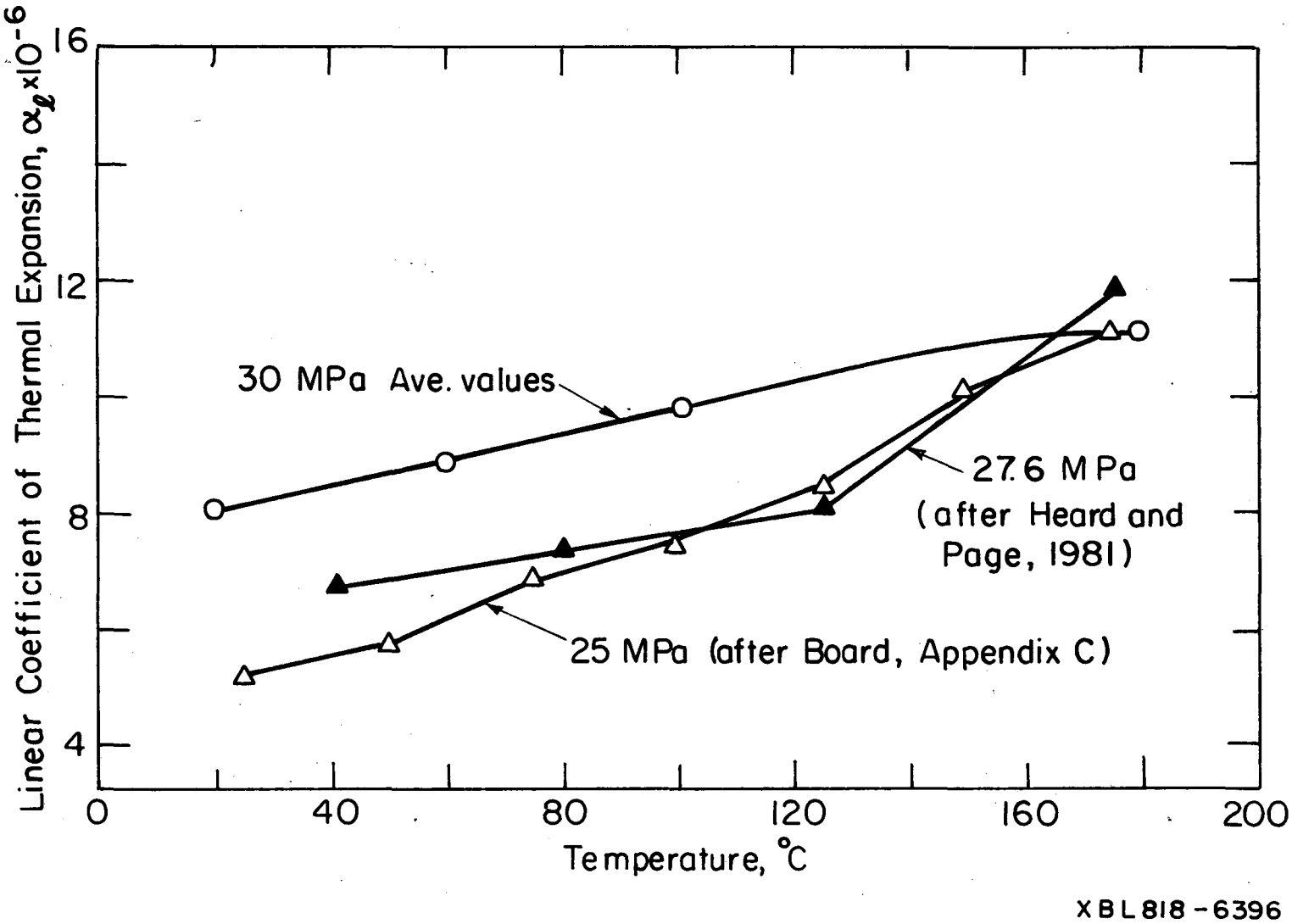

Fig. 24. Comparison of average values of α_ℓ at 30 MPa confining pressure with work by others.

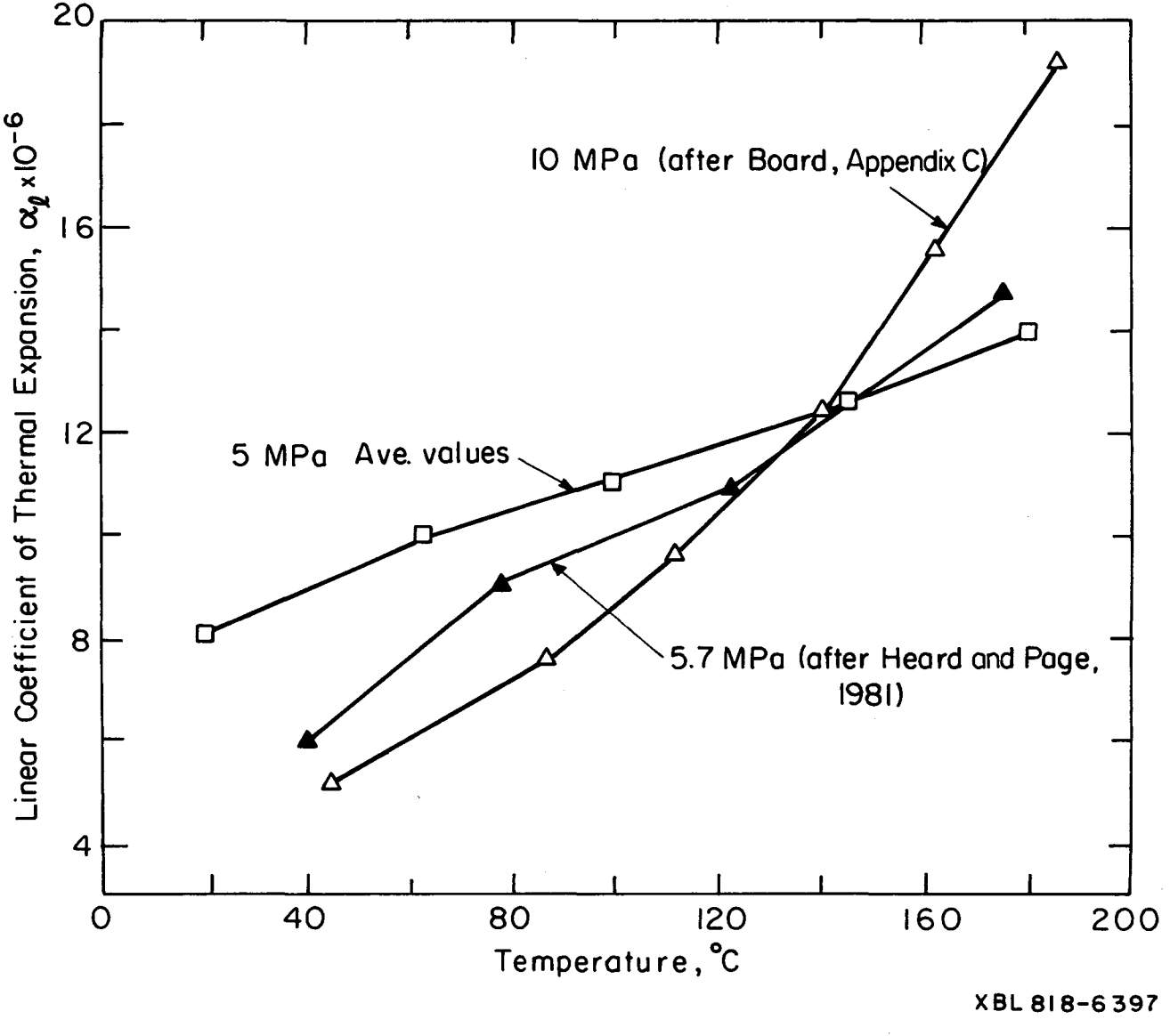

Fig. 25. Comparison of average values of α_ℓ at 5 MPa confining pressure with work by others.

as determined from regression analysis, while curves from Heard and Page represent average values of α_ℓ calculated from incremental slopes. The steeper slopes of Board and of Heard and Page show a greater influence of isobaric heating on rock thermal expansion than was observed in this study. Except for Board's values at 10 MPa, however, the data of the other investigators tended to converge at higher temperatures with those of this study.. The discrepancies at low temperatures may be related to differences in experimental technique, though this is speculative. Sample deformations were measured by Heard and Page and by Board with transducers outside the test cell, whereas the current work used strain gauges bonded to the rock. These rock-mounted gauges may have had greater sensitivity to the small deformations occurring at low temperatures.

At any given temperature, the difference between curves in Figs. 21 and 22 reflects the effect of changes in confining pressure on α_V and α_ℓ. For illustration, average results at 180°C and 20°C were replotted in Fig. 26 as a function of confining pressure. The average data indicated that an isothermal increase in confining pressure from 2 MPa to 55 MPa resulted in a 10% to 20% decrease in α_V. The greatest effect was noted at higher temperatures. The effect of the isothermal pressure increase on α_ℓ was only a 5% to 10% decrease in magnitude at most. The smaller change in α_ℓ with confining pressure indicated a smaller rate of change with confining pressure for ε_a than ε_r, but data scatter again prevented drawing of definite conclusions. Very little experimental data are available from other work on the effects of isothermal pressure increases on thermal expansion of granite. Page and Heard (1981) tested a quartz monzonite over a pressure range of 6.9 MPa to 55.2 MPa, and the same investigators (Heard and Page, 1981) tested Stripa

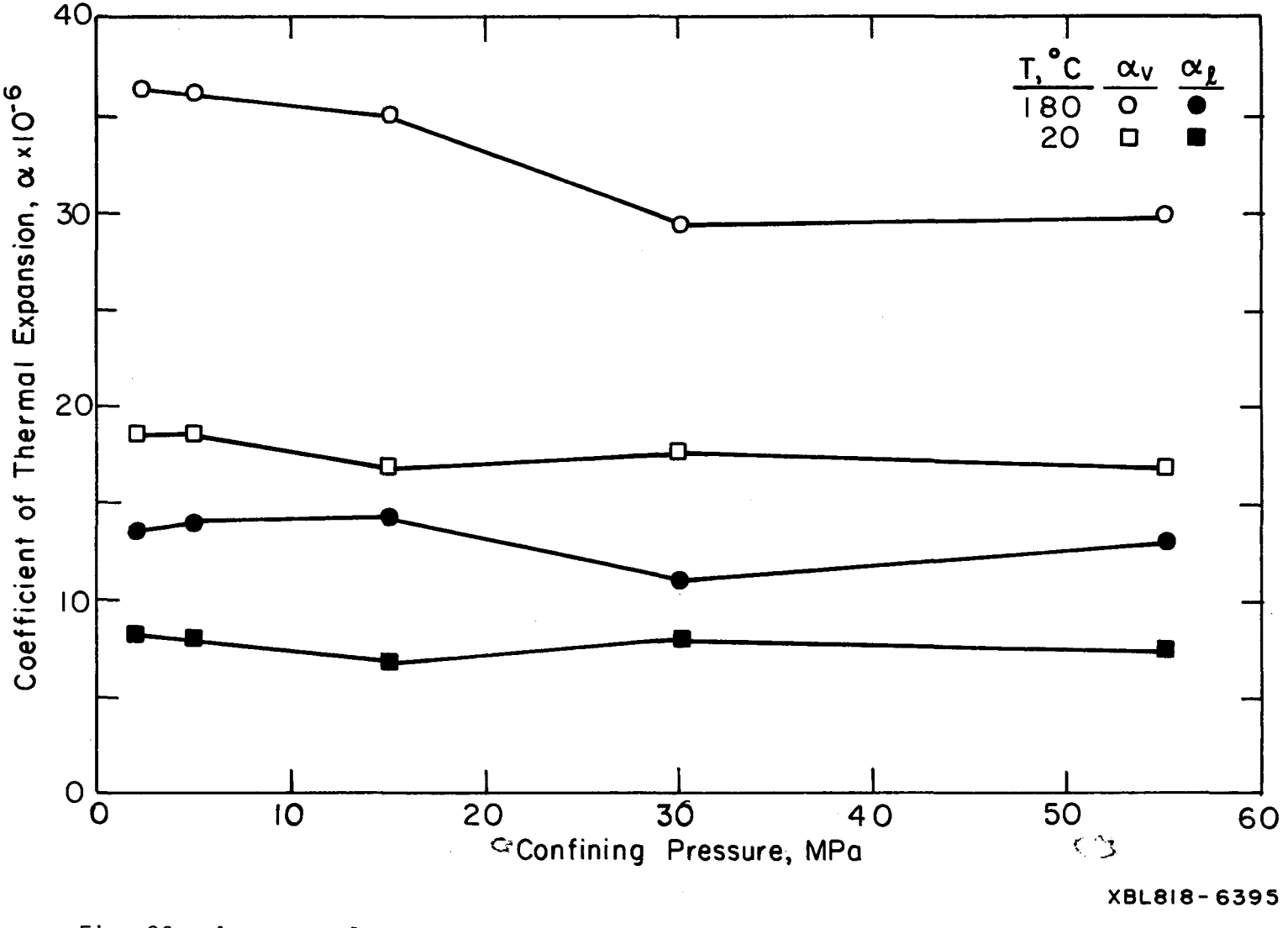

Fig. 26. Average values of α_v and α_ℓ at two temperatures as a function of confining pressure.

granite over the same range. In both cases, they found that an isothermal pressure increase resulted in a 20% to 30% decrease in α_ℓ.

5.1.2 Possible Anisotropy

In comparing the average data for α_V and α_ℓ, it was found that α_V was approximately 2.5 times α_ℓ. This may indicate some anisotropy in thermal expansion properties of Stripa granite because an isotropic homogeneous material should yield α_V equal to three times α_ℓ. All samples tested to date were from vertical core holes. Planned tests on samples from horizontal holes could not be performed because of budget constraints. Such tests would have enabled a better definition of anisotropy in thermal properties. Previous work by Swan (1978) on Stripa granite detected a slight but distinct trend in dilational wave velocities and in Young's modulus for a series of samples cut at different orientations from a single block. On the other hand, Heard and Page (1981) measured values of α_ℓ for samples from orthogonal directions and concluded Stripa granite was isotropic in α_ℓ.

5.1.3 Data Scatter

Error bars, representing typical scatter in results, are shown for selected data points in Figs. 21 and 22. Each bar shows the maximum variations in the data about the mean value, indicated by a filled-in square. Though scatter in the magnitudes of the parameters is large, data from each test reflected the same trends as seen in the average data. Aside from the natural variability of the rock, no explanations were found to satisfactorily explain the large scatter in the thermal expansion data. Measurement error could have contributed to scatter, but careful calibration tests using an aluminum "dummy" sample (see Part I) indicated that observed scatter was much larger than would result from this source. In the regression analyses,

it was noted that small changes in the goodness of fit of the strain vs. temperature curves resulted in significant changes in α_v or α_ℓ. However, regression analysis also produced less scatter in α_v or α_ℓ than if the coefficients had been calculated directly using incremental strain and temperature data.

Results on samples from one core hole suggested another possible source of scatter: the proximity of some samples to the excavation boundary. In hole E02, one sample was obtained at a depth of 0.3 meters, while another was obtained 4.4 m below the drill hole collar. The core holes were drilled from rooms excavated by blasting, and it was suspected that properties of samples from near the surface of the excavation would accordingly reflect damage. Differences in results for the two samples seemed to support this hypothesis. However, for all tests, grouping data according to the sample's proximity to the excavation boundary did not reduce scatter.

The large data scatter has important implications for the thermomechanical analysis. This will be discussed further in Section 5.4.

5.1.4 Hysteresis

Thermal contraction measurements were made during cool-down to study hysteresis in the thermal cycling. As a typical example, Fig. 27 is a plot of the volumetric strain as a function of temperature for the thermal cycle at 5 MPa confining pressure of sample M0212.23-12.43. As indicated by the figure, very little hysteresis in the thermal cycle was observed above 100°C. Below this temperature, hysteresis in volumetric strain amounted to 2 x 10^{-4} to 3 x 10^{-4}. This hysteresis, however, was "negative"--the sample was smaller in both length and diameter at the conclusion of the thermal cycle than at the beginning. This behavior is the opposite

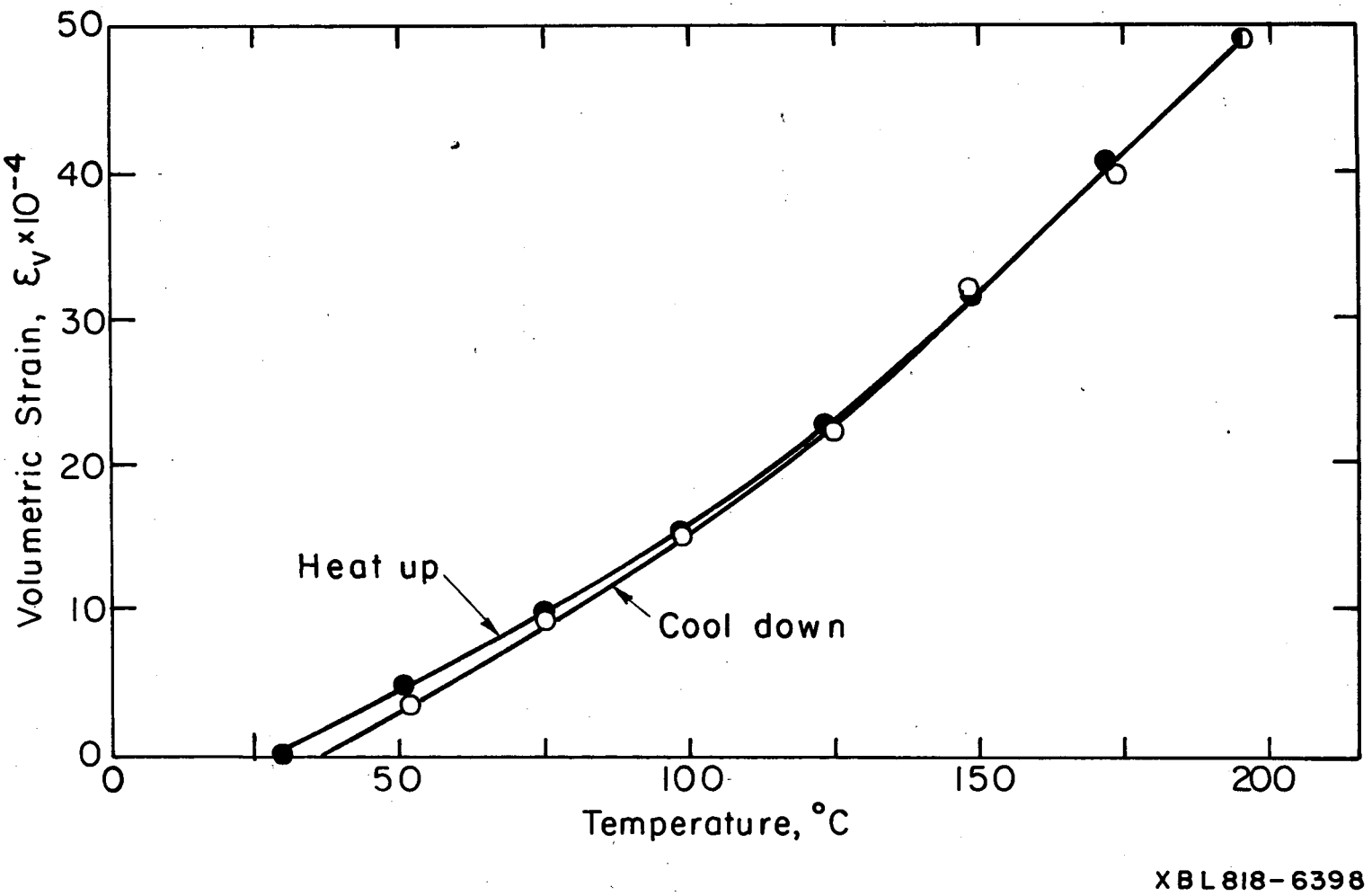

Fig. 27. Volumetric strain for heat-up and cool down at 5 MPa confining pressure for sample M0212.23-12.43.

of that observed by others (Richter and Simmons (1974), Board (Appendix C), and Bauer and Johnson (1979)) for typical thermal expansion tests. In this study, however, the thermal expansion tests were atypical in that stress-strain tests were performed during the thermal cycle. After completion of the usual pressure/temperature test matrix, one sample was repressurized to 15 MPa confining pressure and subjected to an additional thermal cycle during which no stress-strain tests were performed. The "negative" hysteresis was again observed. Another hypothesis is that consistent, cumulative measurement error produced this result, but calibration tests using a "dummy" aluminium sample (Part I) did not show such error. Regardless of the source, the hysteresis was small. As would be expected from the curves in Fig. 27, average values of α_v and α_ℓ for heat-up did not differ significantly from cool-down values.

5.1.5 Theoretical Estimates of Thermal Expansion Coefficients

The primary objective of this study was the acquisition of thermo-mechanical properties for input into theoretical model studies. Thus, theoretical interpretation of observed behavior was not emphasized. This section serves as a very basic introduction to such work by comparing measured values of the coefficients of thermal expansion with those predicted by two commonly used methods.

It is obvious that the mineral composition, and particularly the percentage of quartz, will affect the thermal expansion of the aggregate rock (Hockman and Kessler, 1950). The simplest approach to a predictive estimate of thermal expansions would be to assume that the volumetric expansion of the aggregate equals the weighted average of the volumetric expansion of the mineral constituents. Thus, α_v would be given by

$$\alpha_V = \Sigma\, \alpha_i\, V_i \quad , \tag{5.1}$$

where α_i is the volumetric thermal expansion of component i and V_i is the fractional volume of component i.

By assuming (1) distribution of components is isometric; (2) there is no crack development; (3) thermal deformation of each grain is equal to that of the aggregate, and (4) all microstresses are hydrostatic, it can be shown (Kingery, 1960) that α_V will be given by

$$\alpha_V = \frac{\Sigma\, \alpha_i\, k_i\, V_i}{\Sigma\, k_i\, V_i} \quad , \tag{5.2}$$

where k_i is the bulk modulus of component i. If the bulk moduli of all components are equal, Eq. (5.2) reduces to the volume average given by Eq. (5.1).

Calculations from both equations are compared with average values of measured α_V in Fig. 28. The modal compositions of the samples used in the thermomechanical testing were not determined. However, the composition of the other samples from boreholes in the experimental area was determined (Wollenberg et al., 1981), and a typical example of this data was used for calculation of α_V (Table 5). Thermal expansion coefficients and bulk moduli for single crystals were obtained from data reported by Swan (1978) and Simmons and Wang (1971) (Table 6). As can be seen in Fig. 28, values of α_V calculated from both Eqs. (5.1) and (5.2) lie within the scatter of the measurements. However, the difference in slopes indicate a much greater effect of temperature on α_V than is predicted by theory. This observation is consistent with previous work on Stripa and other granites (Heard and Page, 1981; Page and Heard, 1981), and supports the hypothesis that discrepencies between calculated and observed behavior are due to the effect of cracks on thermal expansion.

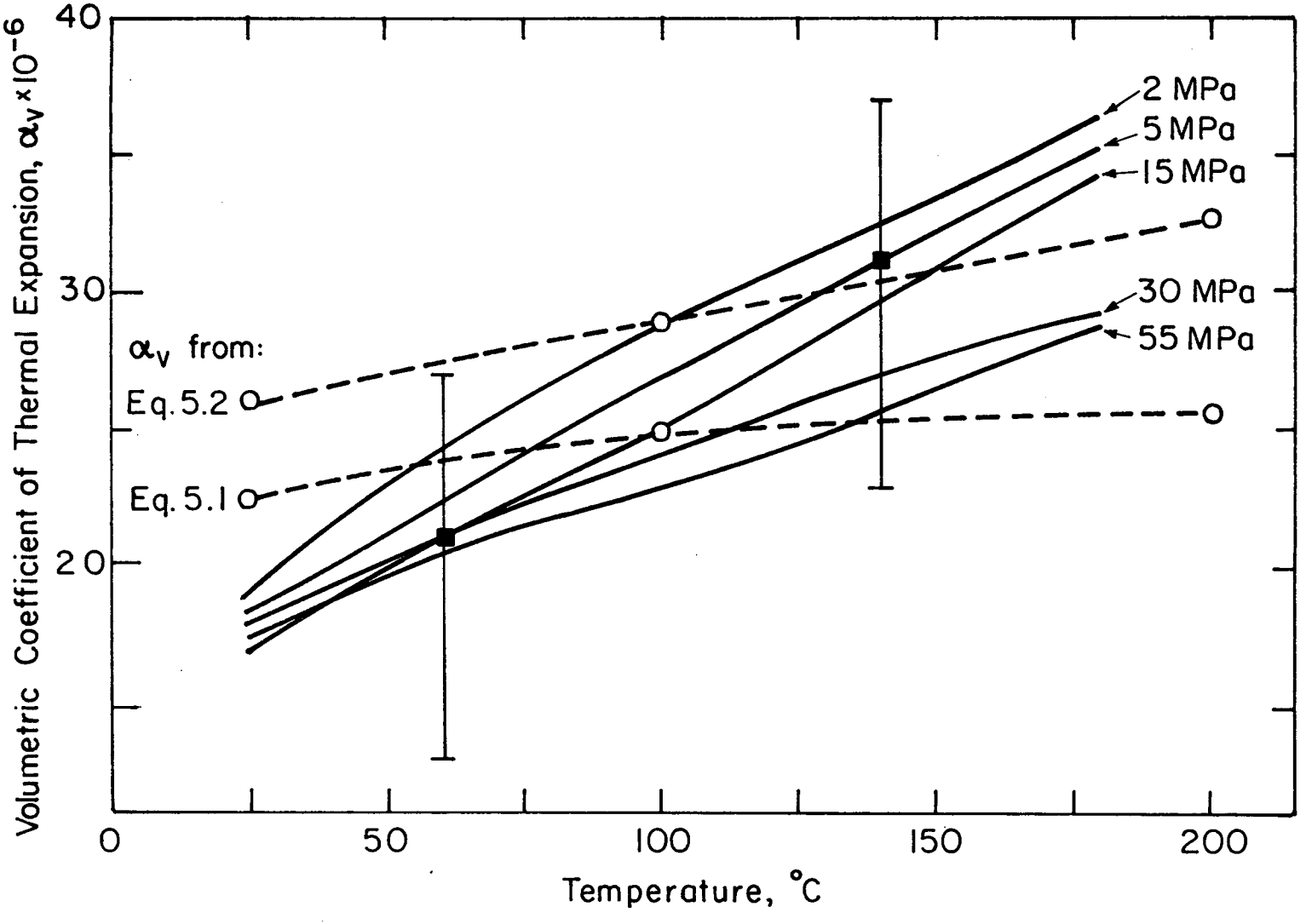

Fig. 28. Comparison of theoretically determined values of α_v with average measured values.

XBL8110-6840

Table 6. Typical modal composition of Stripa granite*

Mineral	Percentage by Volume
Quartz	41.10
Plagioclase	25.90
K-felspar	18.00
Muscovite Chlorite	12.50
Acc. Min.	2.50
TOTAL	100.00

*After Wollenberg et al., 1981.

Table 7. Mineral properties used for calculation of α_v.

Mineral	α_v* x 10^{-6}/°C			Bulk modulus†, K x 10^5 MPa		
	25°C	100°C	200°C	25°C	100°C	200°C
Quartz	34	38.76	44.20	0.2923	0.2923	0.2923
Plagioclase	13	13.52	14.57	0.1313	0.1313	0.1313
K-felspar	15	15.74	17.10	0.1911	0.1911	0.1911
Muscovite Chlorite	20	21.25	22.50	0.1806	0.1806	0.1806

*After Swan (1978), values at 100°C and 200°C interpolated using data at 25°C and 400°C.

†Based on single crystal elastic constants from Simmons and Wang (1971).

5.2 Elastic Moduli Measurements

As explained earlier, tangent values of elastic moduli were determined from polynomial regression analysis of the stress-strain data. Summary graphs will be presented herein, with complete tabulated data provided in Appendix B (Table B-1 and B-2). Entries in the tables can be used to generate the polynomial representing the best fit of the stress-strain data. Using Eq. (4.4), data in Table B-1 can be used to generate curves of axial strain as a function of deviator stress, and Table B-2 values can generate curves of radial strain as a function of deviator stress. Derivatives of these polynomials will then generate values of tangent moduli, as explained in Section 4.2.1. As for the thermal expansion results, values of parameters at 2 MPa and 30 MPa confinement represent the average of four tests, whereas values at all other confining pressures represent the average of six tests.

A great many measurements have been made of the elastic properties of granite at low temperature and pressure. A sampling given by Birch (1966) demonstrates the great variability in properties and thus the futility of discussing "average" elastic properties for granite. However, a comparison of the results on Stripa granite with these data does show that Stripa granite is stiffer in compression than most other granites. If Poisson's ratio can be used with Young's modulus to infer a reasonable shear stiffness, then the results also show that Stripa granite has a lower shear stiffness than most other granites.

5.2.1 Nonlinearity of Stress-Strain Curves

Nonlinearity in stress-strain tests is to be expected, particularly at low deviator stress levels. Classically, the initial portion of a stress-strain curve is convex upward, becoming nearly linear at higher deviator

stresses. Results of this study showed that both confining pressure and temperature affected the degree of nonlinearity of the stress-strain curve. At confining pressures of 30 MPa and 55 MPa, stress-strain curves were very nearly linear over the entire range of applied deviator stresses at all temperatures. At 15 MPa confinement, linear behavior was observed up to about 75°C, but at higher temperatures, nonlinear behavior, evidenced by increasing E_T with increasing deviator stress, was observed. At lower confining pressures, stress-strain curves were nonlinear at all temperatues. In general, the greatest nonlinearity was observed at the lowest confining pressure and highest temperature. For a typical example, Fig. 29 presents the axial and radial strains as a function of deviator stresss for one sample at 2 MPa confinement and 200°C temperature. As shown in the figure, E_T increased by about 30% over the deviator stress range of 2 MPa to 60 MPa. At the same time, the slope of E_r versus σ_d decreased by 28%, resulting in a variation of ν from 0.10 at a deviator stress of 2 MPa to 0.19 at 60 MPa. Reported data on the variation in moduli with increasing deviator stress levels is relatively scarce. For unconfined room temperature conditions, Haas (1981) reported a few results for granites showing an increase in E of 17% to 38% over a range of deviator stresses up to 97 MPa. Haas also reported increases in ν of 14% to 53% under the same conditions.

5.2.2 Effects of Temperature and Confining Pressure

Major effects of temperature and confining pressure on E_T are illustrated by Fig. 30. Because of the nonlinearities discussed above, the moduli not only vary as a function of confining pressure and temperature, but also as a function of the deviator stress magnitude. For consistency, all data were compared at a deviator stress of 60 MPa. This stress level corresponded to 40% of the estimated strength of the rock at a confining pressure of 2 MPa and temperatures in excess of 150°C.

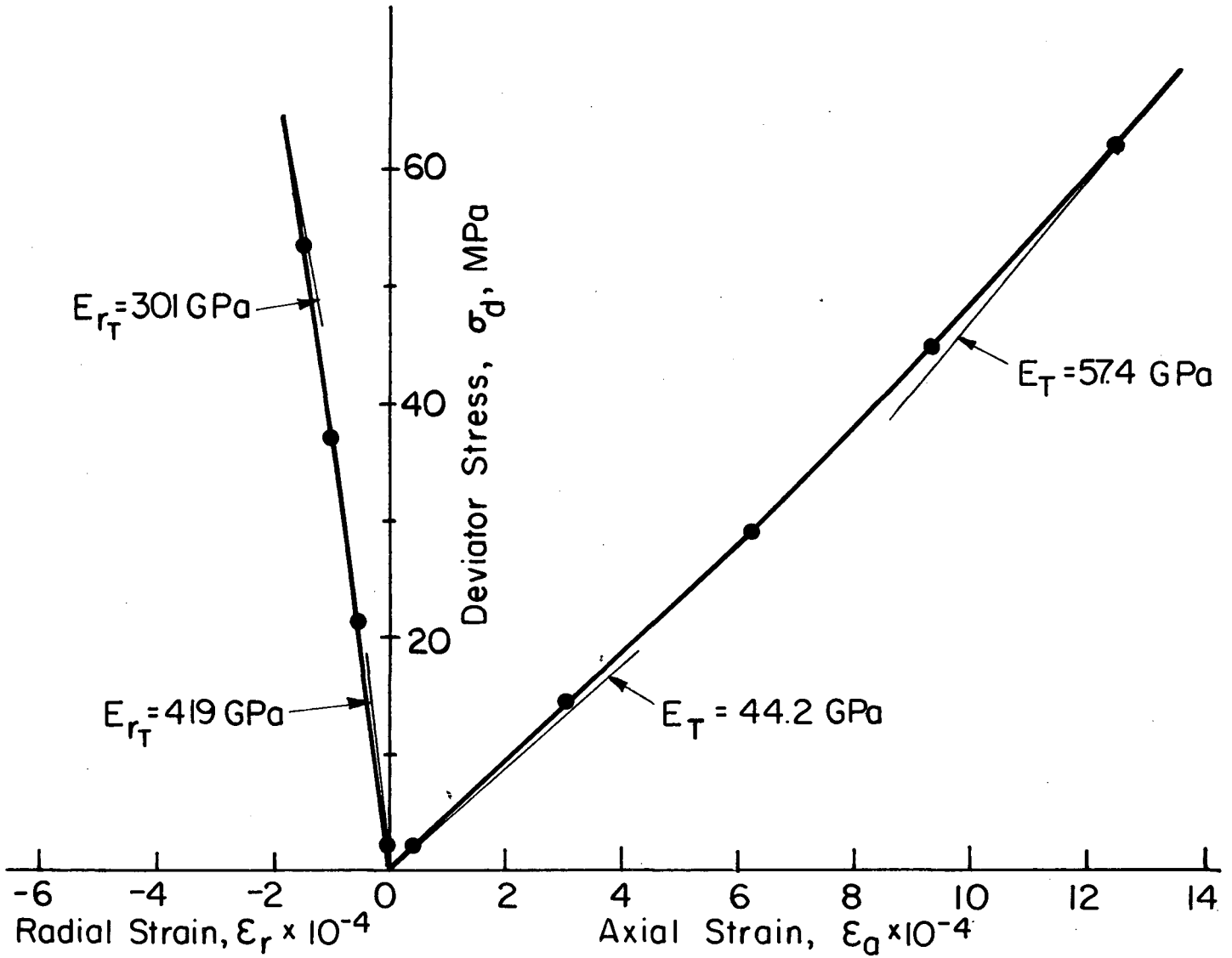

Fig. 29. Typical stress-strain curves for a sample (E020.32-0.51) at 2 MPa confinement and 200°C.

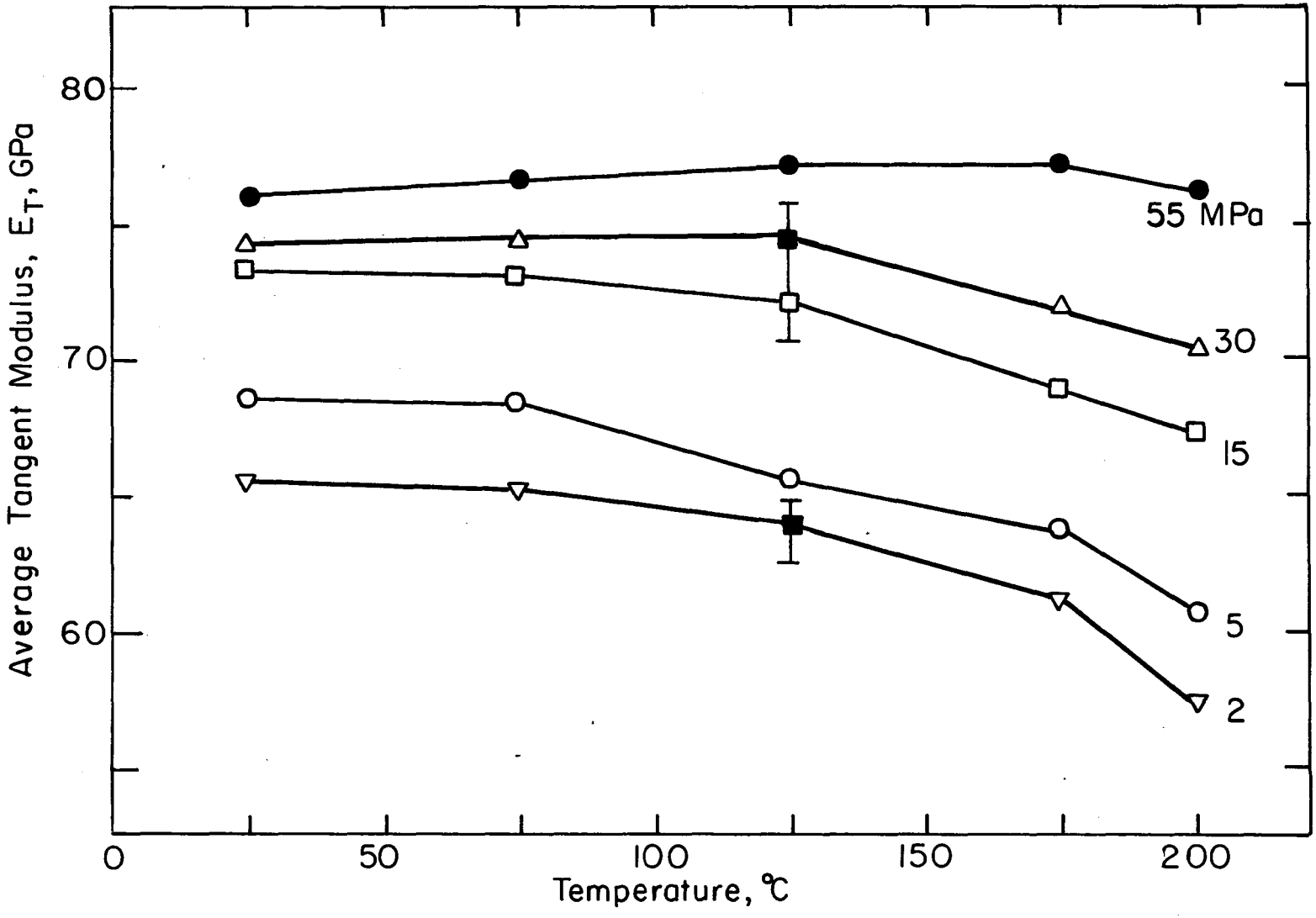

Fig. 30. Average values of tangent Young's modulus for each confining pressure as a function of temperature. All values obtained at a deviator stress of 60 MPa. XBL 818-6399

At 30 MPa and 55 MPa confining pressures the effects of isobaric temperature changes were small: increasing temperature from room to 200°C caused no more than a 5% difference between average maximum and minimum values of E_T. Interestingly, at these confining pressures average values of E_T increased slightly with increasing temperatures and then began to decrease. This behavior occurred in some, but not all, samples and is as yet unexplained. At confining pressures of 15 MPa and less, increasing temperature over the test range resulted in a decrease in average E_T values of 10% to 14%. At all confining pressures, the slope of the curves show that the greatest effect of temperature increases occurs above 125°C.

These results indicate a smaller overall temperature effect for Stripa granite than that observed by Swan (1978), who found a 23% decrease in secant Young's modulus over 175°C under unconfined conditions. Heard and Page (1981), however, found essentially no influence of temperature on secant Young's modulus up to 200°C for confining pressures from 5.9 MPa to 55.2 MPa.

The degree of temperature dependence of Young's modulus for granites varies widely in the literature. Data presented by Birch (1966) for three granites showed small effects of temperature, particularly at high confining pressures. At 50 MPa confinement, increasing temperature from 25°C to 200°C resulted in a modulus decrease of 3% to 11% for the reported tests. At a confining pressure of 500 MPa, however, Griggs et al. (1960) observed a 35% decrease in E between 25°C and 300°C. A large isobaric temperature effect was also noted by Page and Heard (1981) for Climax quartz monzonite. At 55.2 MPa confinement, they observed a 50% decrease in secant Young's modulus between 25°C and 200°C, compared to a 18% decrease over the same temperature interval at 6.9 MPa confinement. Finally, using sonic methods under

unconfined conditions, Wingquist (1969) noted a 49% decrease in Young's modulus in heating Charcoal Black granite from 24°C to 260°C.

The effect of isothermal pressure changes on E_T are illustrated in Fig. 31 for 25°C (room temperature) and 175°C. It can be seen that decreasing the confining pressure from 55 MPa to 2 MPa resulted in about a 20% decrease in E_T. This decline is much less than that observed by Heard and Page (1981), who found almost an 80% decrease in Young's modulus for Stripa granite when confining pressure fell from 55.2 MPa to 5.9 MPa. Page and Heard (1981) also observed a 40% to 60% reduction in secant Young's modulus for Climax quartz monzontie when isothermal pressure was decreased from 55.2 MPa to 6.9 MPa. Other researchers have observed behavior more in line with the results of this study. Birch (1966) presented data for Westerly granite at room temperature showing a 17% decrease in Young's modulus for an increase in confining pressure from 1 MPa to 100 MPa. Hughes and Jones (1950) dynamically tested two granites at 30°C and 3.46 MPa, and 100°C and 51.7 MPa. Young's modulus, calculated using their values for bulk and shear moduli, was 11% to 17% less at the lower tempeature-pressure state.

Figure 31 also shows a decreasing rate of change in E_T for a given temperature as confining pressure increases, suggesting that, at some higher confining pressure, E_T tends toward a constant value. Similar behavior has been observed by Brace (1965) for other granites. It appears to result from closure of microcracks as pressure is increased. The curve at 175°C exhibits a slower rate of change in E_T than the 25°C curve. This suggests, though the data is not conclusive, that the confining pressure required to attain a constant E_T would be higher at higher temperatures.

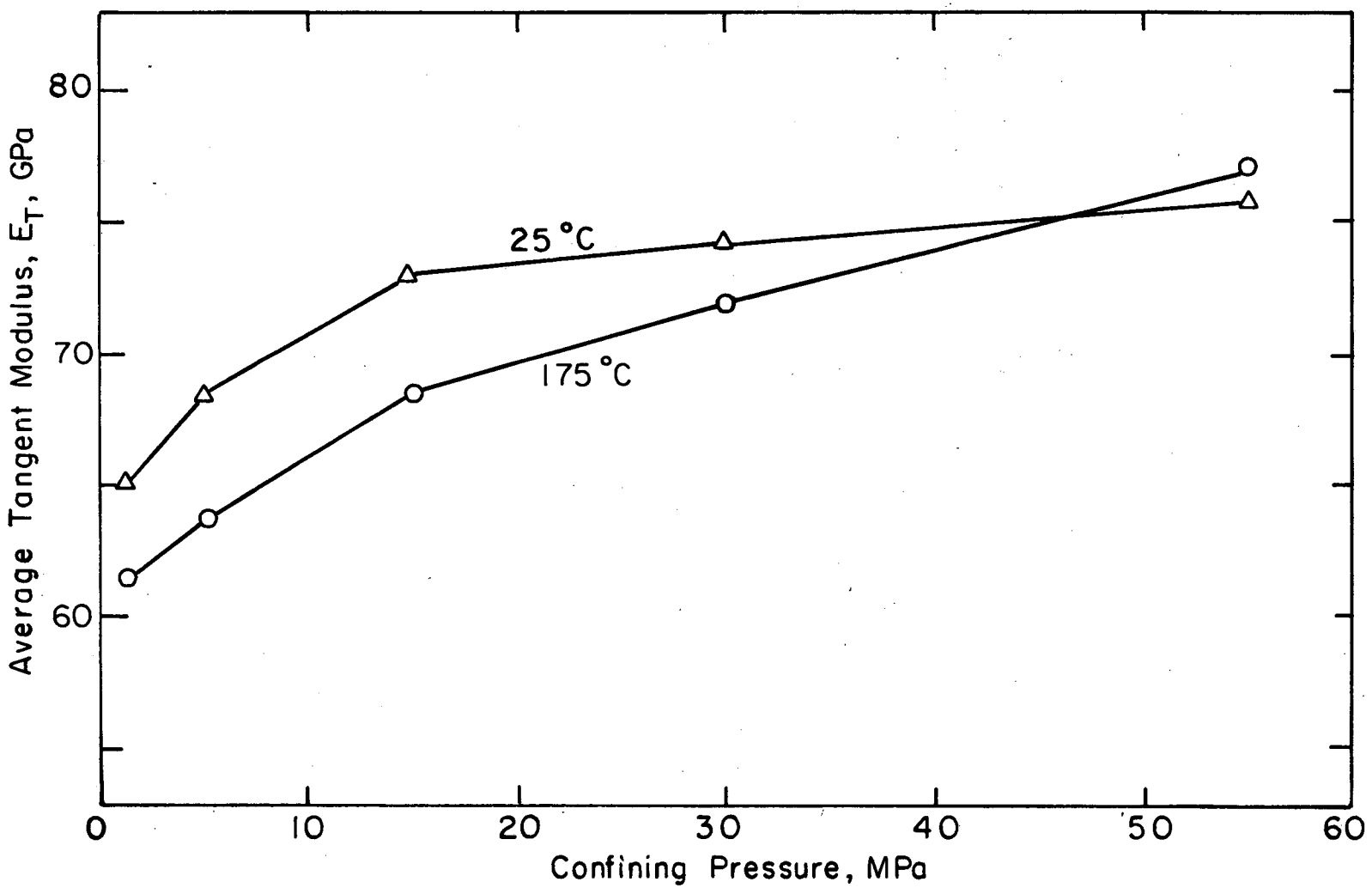

XBL 818-6401

Fig. 31. Average values of tangent Young's Modulus for two temperatures as a function of confining pressure. All values obtained at a deviator stress of 60 MPa.

Isobaric effects of temperature on Poisson's ratio, ν, are summarized in Fig. 32. As with the E_T results, increasing temperature had somewhat less effect at higher confining pressures. At 55 MPa confinement, average values of ν decreased by about 15% over the temperature range tested, compared to a 27% reduction at 2 MPa. There was some indication in the data, particularly at 30 MPa and 55 MPa, that the greatest reduction in ν occurred at temperatures over 150°C. Contrary to the E_T results, at the high confining pressures, values of ν did not increase in the temperature range of 25°C to 125°C.

The data did not yield conclusive trends on the effects of isothermal confining pressure changes on ν. At low temperatures, ν was independent of pressure change, though at high temperatures increasing confining pressure apparently led to as much as a 16% increase in ν.

Very little data are available on pressure and temperature effects on ν for other granites. Birch (1966) reported dynamic measurements that showed both a slight decrease (2%) and a slight increase (5%) in ν for a temperature interval of 25°C to 200°C at 50 MPa confining pressure. From sonic velocity measurements under unconfined conditions, Wingquist (1969), however, recorded an 85% decrease in ν in heating Charcoal granite from 24°C to 260°C. Birch (1966) also reported an increase of 40% in ν when isothermal pressure increased from 0.1 MPa to 100 MPa. Hughes and Jones (1950) observed a 1% increase in ν changing the temperature-pressure state from 30°C and 3.46 MPa.

5.2.3 Data Scatter

Error bars are shown for selected data points in Figs. 30 and 32 to represent typical scatter in the data. Each error bar shows the maximum

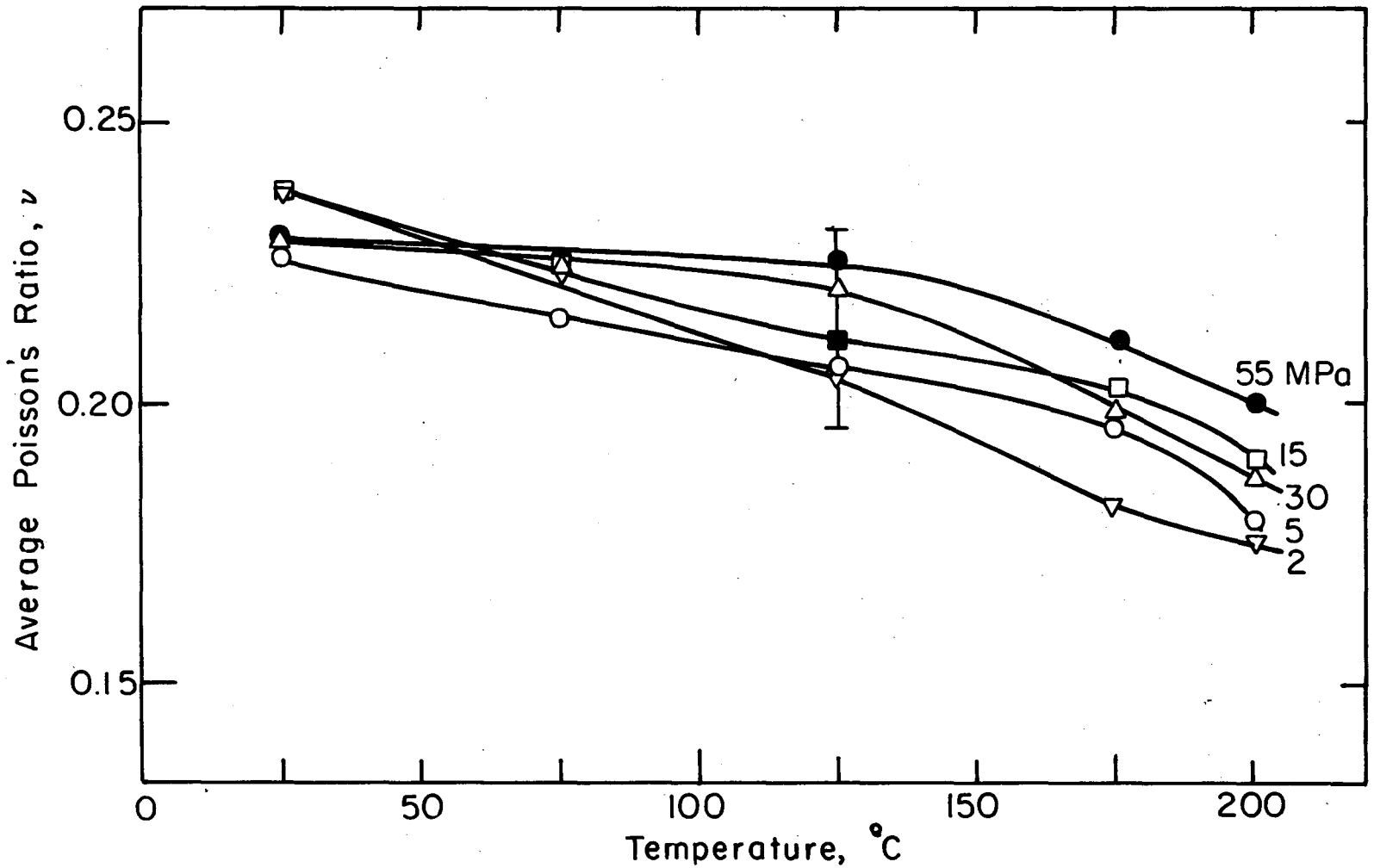

XBL 818-6391

Fig. 32. Average values of Poisson's ratio for each confining pressure as a function of temperature. All values obtained at a deviator stress of 60 MPa.

variation of the data about the mean value, represented by a filled-in square. Sample-to-sample scatter in moduli results was less than that in results for the coefficient of thermal expansion. Extreme values of either E_T or ν were within about 10% of the mean, whereas variations in α were up to approximately 25% of the mean. While isothermal pressure effects on ν were not large, scatter prevented delineation of any clear trends. For E_T results, isobaric temperature effects were clear in individual tests, but scatter between samples at any given pressure was greater than the total effect of increasing temperatures from room to 200°C.

5.2.4 Hysteresis in Stress-Strain Tests

Some hysteresis was observed in all stress-strain tests. As a typical example, Fig. 33 shows the results at 5 MPa confinement and 125°C. Arrows indicate direction of loading and unloading. Many stress-strain tests were repeated a second time, but the loading and unloading curves were often indistinguishable from the first test. Some tests exhibited a small non-recoverable deformation at zero deviator stress following the first loading-unloading cycle. Upon reloading, however, the stress-strain curve normally rejoined the original loading curve at some point before the maximum load was attained.

Hysteresis in the stress-strain data is reflected in the moduli data as illustrated by Fig. 34. At high confining pressure, there was very little difference in loading and unloading values of E_T, though values of the unloading modulus tended to be a little higher. At low confining pressure, values of the unloading modulus were about 10% higher than E_T loading. All comparisons were at a deviator stress of 60 MPa, which is a different proportion of the maximum applied stress at different confining pressures and temperatures. At low confining pressure and high temperature, 60 MPa deviator

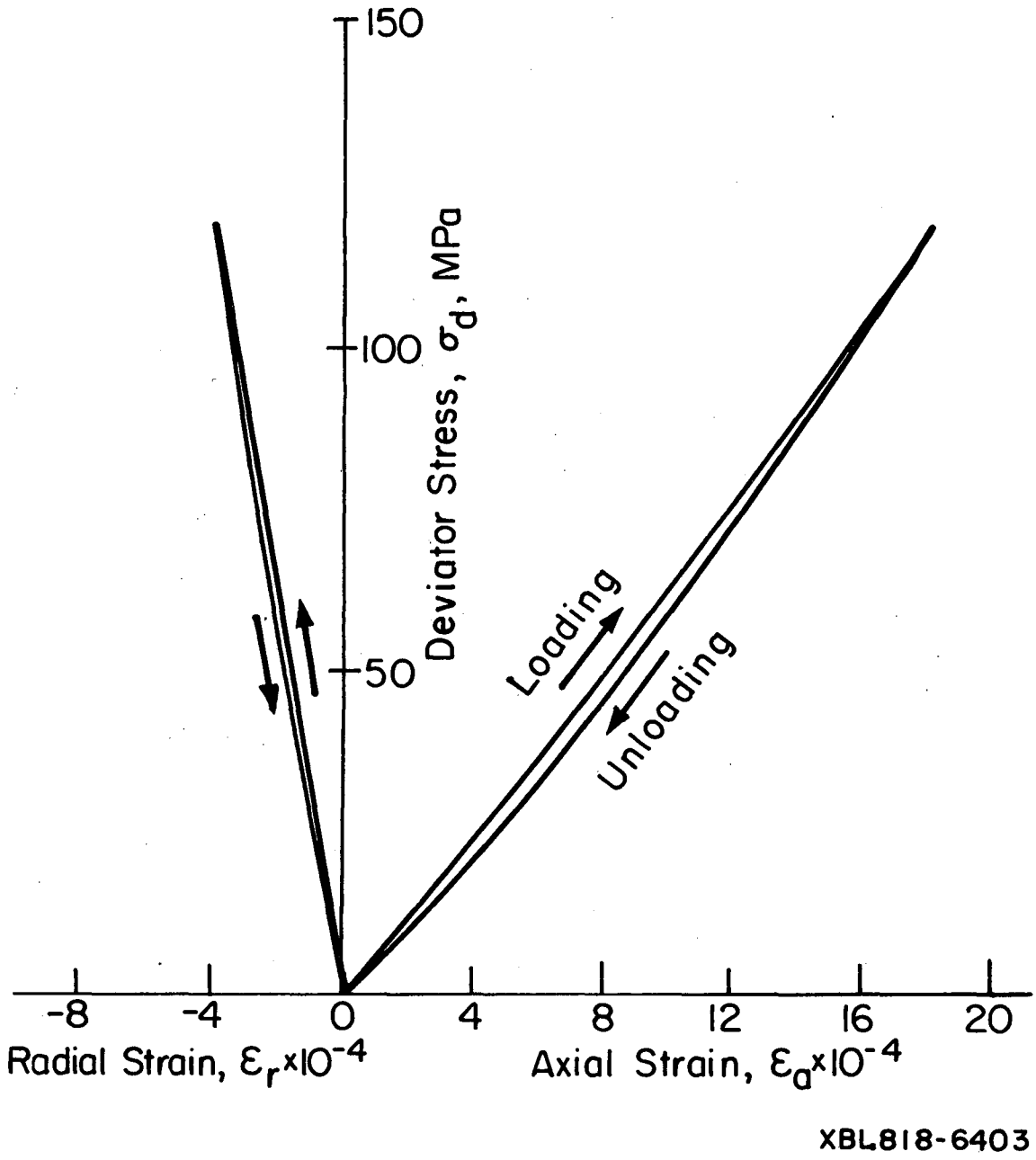

Fig. 33. Typical stress-strain test (sample E020.32-0.51, 5 Mpa confinement, 125°C) illustrating hysteresis in results.

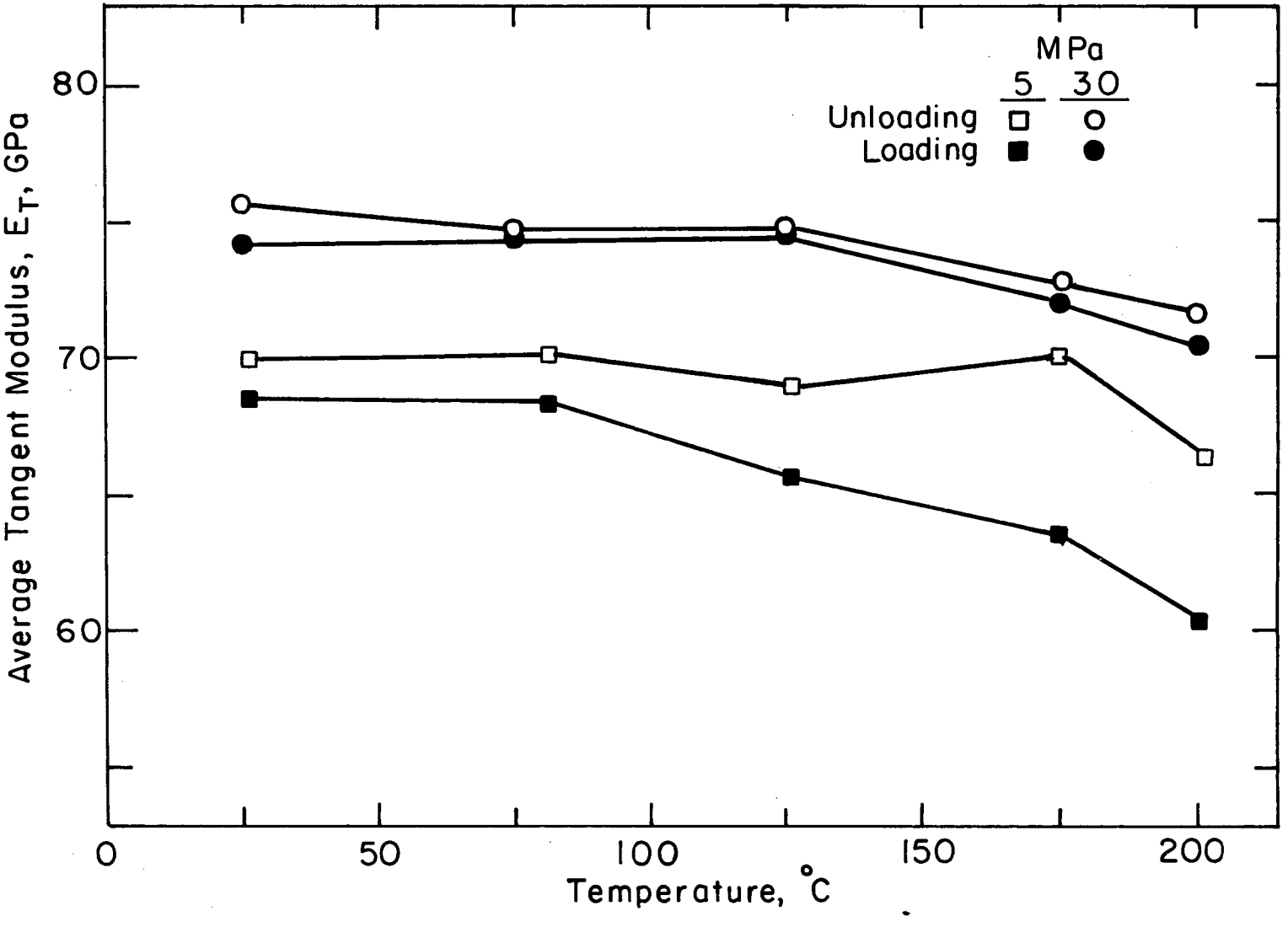

Fig. 34. Comparison of average E_T values for loading and unloading portions of the stress-strain tests. All values obtained at a deviator stress of 60 MPa.

stress is close to the maximum applied stress. From Fig. 34 it can be seen that the difference in slope between loading and unloading is greater near the maximum applied stress than at other points on the stress-strain curve. Thus the greater difference between loading and unloading values of E_T seen at low confining pressure may be due in part to the fact that for low confining pressures the deviator stress at which the modulus is calculated is nearer to the maximum applied stress. Within the data scatter, no difference was noted between loading and unloading values of ν. This may be because less hysteresis was observed in the radial strain data.

5.2.5 Comparison of Heat-up and Cool-down Values

Stress-strain tests were performed at the same temperature during the heat-up and cool-down portions of each thermal cycle. Comparison of the average values of the moduli during heat-up and cool-down did not yield large differences in behavior. At confining pressures from 5 MPa to 30 MPa, a consistent but small (10% or less) decrease in average E_T values was observed on cool-down (Fig. 35). At 2 MPa confinement, average values of E_T for heat-up and cool-down were essentially equal. At 55 MPa, average cool-down values were slightly higher than heat-up values. Differences in average values of ν for heat-up and cool-down were less than 10% and did not show any consistent trends.

5.3 Sample Damage Assessment

Sources of potential damage and procedures for minimizing damage to the sample during the test sequence were discussed in Section 3. Assuming that damage to the rock is reflected in changes in the aggregate mechanical properties of the sample, the results discussed above indicated that only a small amount of damage was done to a sample during any one thermal cycle.

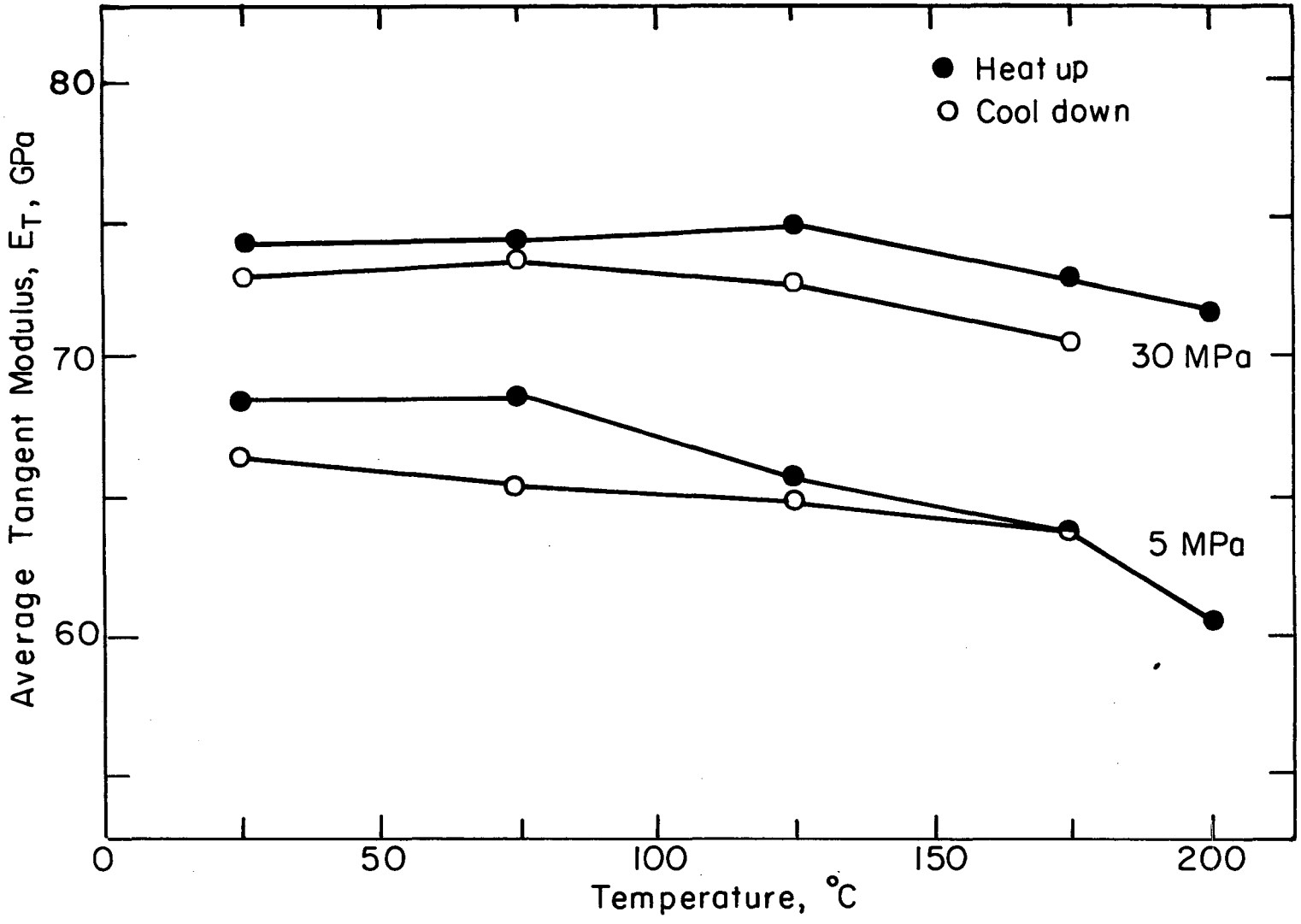

Fig. 35. Comparison of average values of E_T for heatup and cooldown portions of the thermal cycles. All values obtained at a deviator stress of 60 MPa.

XBL818-6405

That is, moduli from repeated stress-strain tests were nearly equal, and both thermal expansion coefficients and moduli varied little between heat-up and cool-down. As a further assessment of sample damage, a thermal cycle that included all stress-strain tests was repeated after completion of all P-T states of the test matrix. Thermomechanical properties were compared with those from the initial thermal cycle to detect any changes in property magnitudes or trends. Any changes would be macroscopic evidence of damage sustained by the sample during the entire test sequence.

The first sample for which a repeat thermal cycle was carried out at 30 MPa confinement exhibited behavior very nearly equal to that of the initial thermal cycle. Thermal cycles were repeated for two other samples at 55 MPa confinement. Though trends in the results of the repeat tests were the same as in the initial test, values of α_v, α_ℓ, and ν were higher, and values of E_T were lower. Moreover, these values were nearly the same as those obtained at 2 MPa confinement. Lower values of E_T were consistent with the hypothesis that the test sequence had caused microcrack growth and an increase in microcrack density, leading to a lower stiffness (Walsh, 1965). The mechanism responsible for the higher values of α_v and α_ℓ of the repeated thermal cycle is not understood. Other investigators (Richter and Simmons, 1974; Cooper and Simmons, 1977) have concluded that repeated thermal cycling should reduce the magnitude of the coefficient of thermal expansion, though Richter and Simmons (1974) have also reported data exhibiting the opposite behavior.

Whatever the mechanism, the finding that results of the repeat thermal cycle at 55 MPa were nearly equal to those at 2 MPa raised a question as to whether the observed effects of isothermal hydrostatic pressure changes were

due to the pressure change or to thermal cycling. The test procedure for one sample (MO212.23-12.43) was therefore altered to study changes in properties due to thermal cycling. Thermal cycles were performed at 55 MPa and 15 MPa following the usual test procedure. Then, instead of reducing the confining pressure again, the confining pressure was increased back up to 55 MPa and the thermal cycle repeated. Confining pressure was then reduced to 5 MPa and a thermal cycle was performed. As a final step, the confining pressure was increased again to 55 MPa and the thermal cycle repeated for a third time at this pressure.

Incremental values of α_V and best-fit values of E_T are shown for the three tests at 55 MPa in Figs. 36 and 37. Following the trend of earlier tests, the last thermal cycle at 55 MPa confinement yielded E_T values (Fig. 36) nearly equal to those from the thermal cycle at the the lowest confining pressure. In addition, the differences in values between the first two cycles at 55 MPa are much less than those between the second and third cycles. The same trend was noted in the thermal expansion results except for values at the highest temperature (Fig. 37). These results indicated that most sample damage occurred at confining pressures of 5 MPa and below. Thus, it was concluded that trends in the data for confining pressures of 5 MPa and above were not affected by previous thermal cycles.

5.4 Impact of Results on Model Predictions

Initial modeling of the in-situ experiments at Stripa was carried out with numerical programs using temperature- and pressure-independent material properties (Chan and Cook, 1979). By integrating temperature and pressure dependence of the properties into the programs, we hoped to enhance the

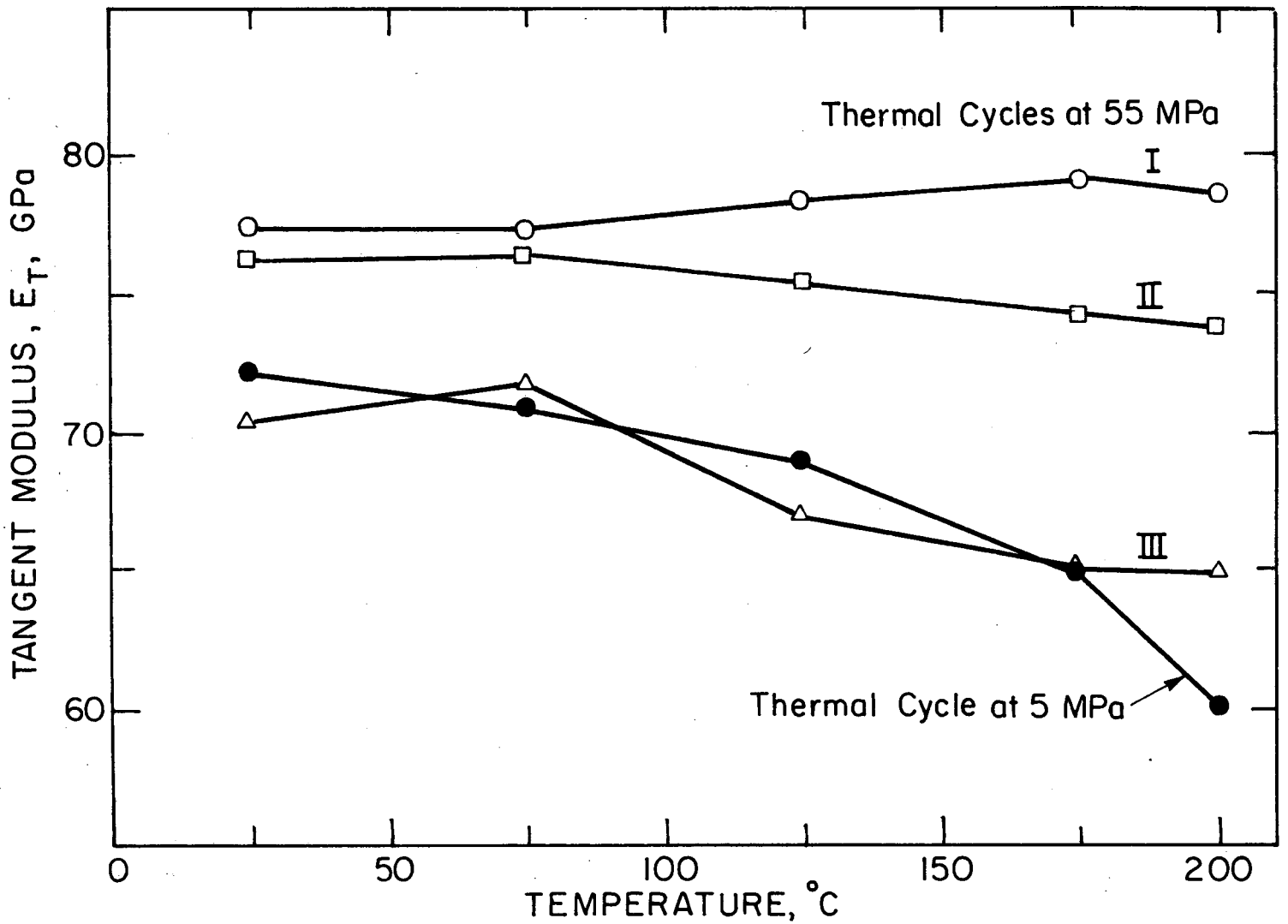

Fig. 36. Values of E_T at 55 MPa confinement for heatup portion of thermal cycles repeated at various times during test sequence of sample M0212.23-12.43.

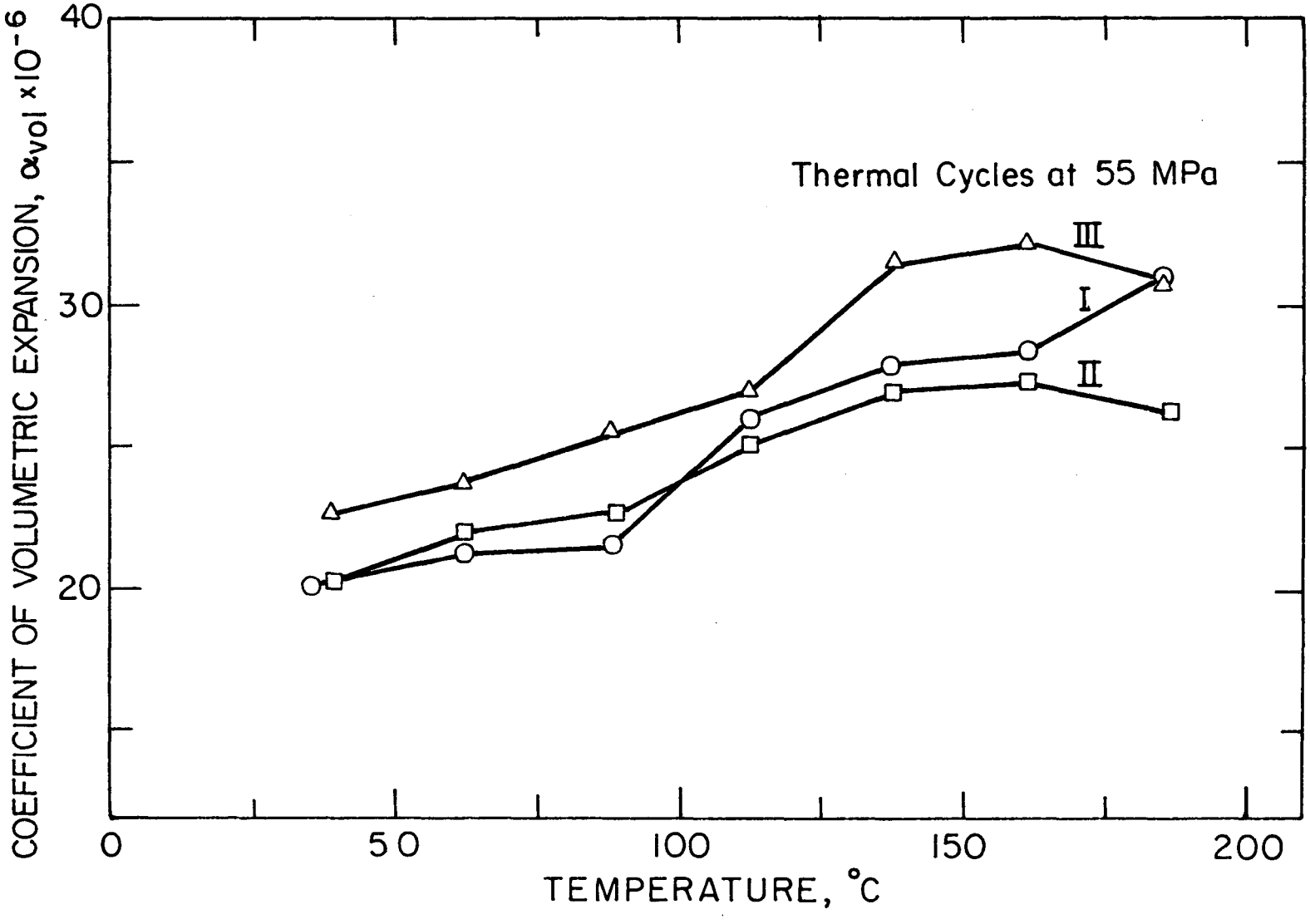

Fig. 37. Incremental values of α_v at 55 MPa confinement for heatup portion of thermal cycles repeated at various times during test sequence of sample M0212.23-12.43. XBL8111-6994

accuracy of the predictions. In this section, a preliminary assessment will be made of how much the predictions would change as a result of including temperature-dependent material properties. The impact on predictions of scatter in results will also be discussed.

Chan and Cook (1979) demonstrated that a reasonable approximation to the geometry of the heater experiments could be made by using an axisymmetric model centered about the heater. In fact, in the region where stresses were monitored, the presence of the excavations did not greatly affect thermal stresses induced by the heater experiments. Thus, for a restricted region, assumptions of plane strain conditions were also reasonable. For axisymmetric plain strain problems assuming linear thermoelasticity, Timoshenko and Goodier (1951) showed that thermally induced displacements and stresses vary directly with temperature and are proportional to two factors, D and S, where:

$$D = \alpha_\ell \left(\frac{1 + \nu}{1 - \nu}\right) \quad \text{for displacements,}$$

and

$$S = \left(\frac{\alpha_\ell E}{1 - \nu}\right) \quad \text{for stresses.}$$

Recognizing the limitations in assuming axisymmetric plain strain conditions, these factors were used to assess the effect on model predictions of assuming temperature-dependent (as opposed to temperature-independent) properties. Figure 38 plots D/D_0 and S/S_0 as a function of temperature, with D_0 and S_0 evaluated at 25°C. Data at 2 MPa confining pressure were used for illustration because temperature effects were most pronounced at this pressure. The case in which properties are temperature-independent is represented by the straight lines $D/D_0 = 1$ and $S/S_0 = 1$. The difference

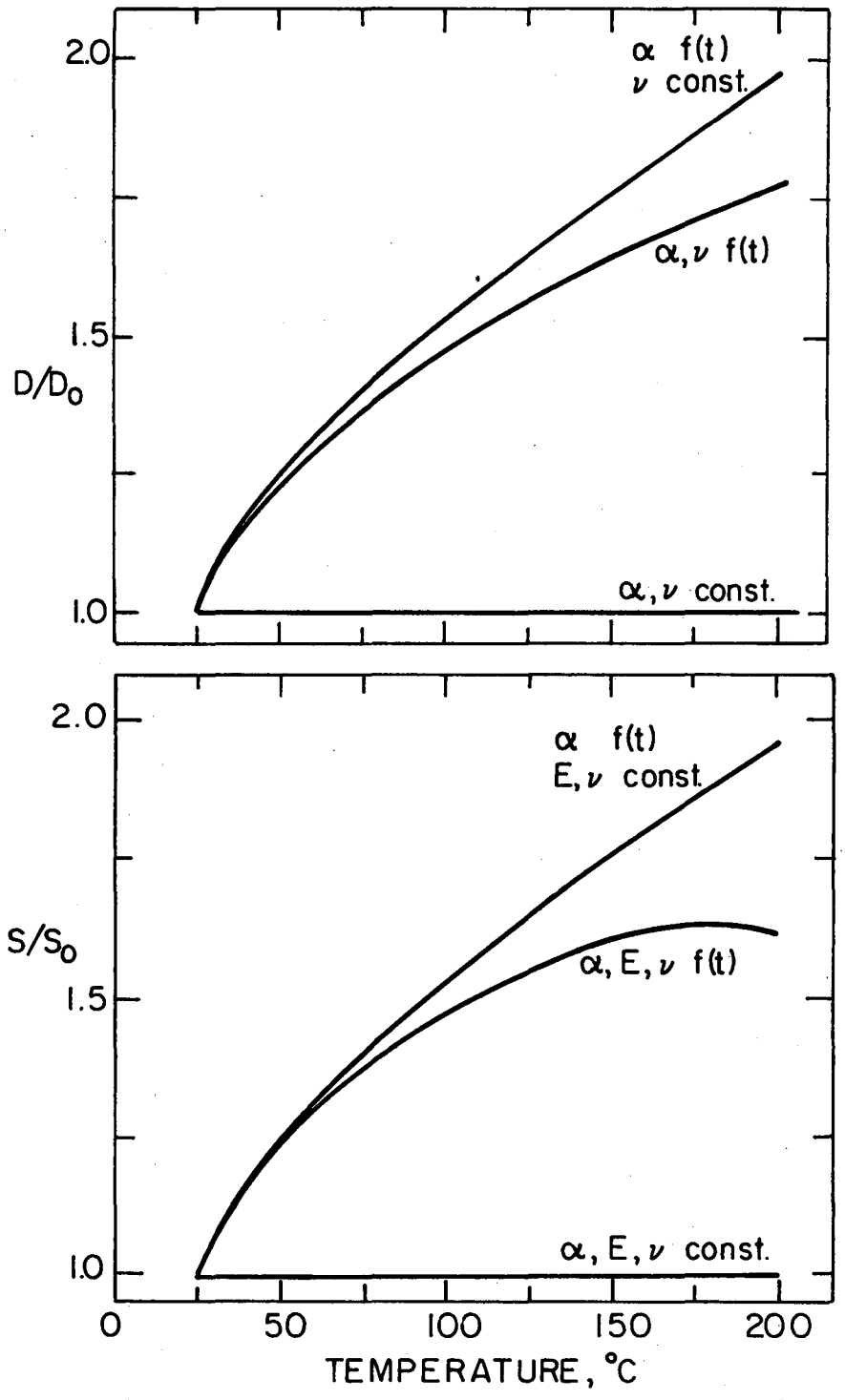

Normalized displacement factor, D/D_o, for average data at 2 MPa confining pressure.

Normalized stress factor, S/S_o, for average data at 2 MPa confining pressure

Fig. 38 (A&B)

XBL8111-6995

between the other curves and these straight lines reflects the difference in predictions resulting from assuming temperature-dependent properties. For example, if constant values of E and ν are assumed and if the stress dependence of α_ℓ is ignored, using α_ℓ (25°C) for computations of a problem at 200°C would result in stresses and displacements in error by a factor of almost 2. It is clear that model predictions would be affected most by incorporating the temperature dependence of α_V or α_ℓ. Interestingly, Fig. 38 shows that if the temperature dependence of E and ν is included as well as α, smaller differences between predictions based on temperature-independent properties and those based on temperature dependent properties would result. This is because the values of ν and E decrease with temperature, while the values of α increase. The factors D and S continue to increase with temperature because of the strong temperature dependency of α, but the rate of increase is less due to the influence of changes in E and ν.

This discussion demonstrates how incorporating the temperature dependence of the parameters would enhance model predictions. From a practical standpoint, however, the uncertainty due to scatter in the laboratory data should also be considered when deciding whether to include temperature- or pressure-dependent properties. The increased accuracy of solution gained by incorporating pressure or temperaure dependence may be offset by uncertainities in the value of the parameter. Consider, for example, the pressure dependence of α_V and α_ℓ. In Figs. 21 and 22, the data scatter at any one confining pressure is greater than the maximum effect of isothermal pressure changes. Including the pressure dependence of either α_V or α_ℓ would result in, at most, a 20% difference from predictions that assume pressure-independent α. This difference would be much less than the difference that would result from using the high and low extremes of the data scatter for α. The degree of data

scatter, nevertheless, is not necessarily a deciding factor in all circumstances. For example, in studying not only the magnitude but the form of the stress distribution, it would be necessary to include temperature- and pressure-dependent properties.

6. SUMMARY AND CONCLUSIONS

Thermomechanical modeling of the in situ experiments at Sweden requires a characterization of the material properties of the rock mass. A basis for this characterization was formed by the study of the thermomechanical properties of dry, intact, 62-mm-diameter samples taken from holes in the experimental area. To bracket stresses and temperatures prevailing in the field, tests were performed over a range of temperatures (room to 200°C) and hydrostatic stresses (2 MPa to 55 MPa). Results of six tests were used to evaluate the effects of temperature and pressure on the coefficient of thermal expansion and on the elastic moduli of the intact rock.

The most significant trend in the thermal expansion results was the effect of isobaric temperature increases on the coefficients of thermal expansion. Average values of α_v at 20°C, for instance, varied from 16.5 x 10^{-6}/°C to 19.4 x 10^{-6}/°C, depending on pressure, while at 180°C average values varied from 28.8 x 10^{-6}/°C to 36.5 x 10^{-6}/°C. The magnitude of this temperature effect is similar to that observed for various granites by other investigators but is much greater than predicted by some theories for isotropic, crack-free rock. Average results indicated that the rate of increase in the thermal expansion coefficients was nearly constant within the temperature range of 25°C to 180°C.

Isothermal pressure changes had a less pronounced effect on thermal expansion. The average results showed a 10% to 20% decrease in α_v and only a 5% to 10% decrease in α_ℓ for isothermal pressure increases from 2 MPa to 55 MPa. The same trend of increasing α_v and α_ℓ with increasing pressure was apparent in the data from individual tests, but variations in the magnitudes of α_v and α_ℓ between tests at one pressure were greater than the total effect of changing pressure from 2 MPa to 55 MPa.

A surprising result of the thermal expansion testing was that the volumetric coefficient of thermal expansion was approximately 2.5 times larger than the linear coefficient. This result implies some anisotropy in the thermal expansion behavior of the rock, and further work is needed to study this possibility.

Coefficients of thermal expansion determined from cool-down portions of the thermal cycle did not differ significantly from those measured during heat-up. The implication of this result for modeling of the in situ experiments is that the same thermal properties could be used in simulating both heat-up and cool-down.

Nonlinear stress-strain behavior evidenced by increasing values of ν and E_T with increasing deviator stress levels was observed. However, the degree of nonlinearity was affected by both confining pressure and temperature. In general, nonlinearity increased with increasing temperature and decreased with increasing confining pressure. At confining pressures above 15 MPa, stress-strain curves were very nearly linear.

The most significant trend in measurements of tangent Young's modulus was the effect of isothermal confining pressure changes. Average values of E_T at 2 MPa confining pressure varied from 57.3 GPa to 65.6 GPa, depending on temperature, whereas average values at 55 MPa ranged from 76.5 GPa to 77.2 GPa. The data also exhibited a decreasing rate of change in E_T at higher confining pressures. Effects of isobaric temperature changes were minimal at 30 MPa confinement and above. At confining pressures of 15 MPa or less, increasing temperature over the test range resulted in a decrease in average E_T values of 10% to 14%.

For Poisson's ratio, the most significant trends were due to the effects of isobaric temperature changes. As was the case for E_T results, increasing temperature had somewhat less effect at higher confining pressures. At 55 MPa, average values of ν decreased by about 15% over the temperature range tested, while at 2 MPa the reduction was about 27%. Results were not conclusive as to the effects of isothermal confining pressure increases on ν.

A small amount of hysteresis was observed in all stress-strain tests, but it resulted in less than 10% difference in moduli between loading and unloading portions of the stress-strain tests. The effect of thermal cycling on moduli values was also small, though a consistent decrease of 10% or less was observed for average E_T values on cool-down at confining pressures from 5 MPa to 30 MPa.

Thermal cycles were repeated at various times during the test procedure to determine if results at lower confining pressures were influenced by testing at the preceding pressure. It was concluded that measurements at 5 MPa confinement and above were not affected by previous thermal cycles.

A preliminary assessment was made of how model prediction would be affected by incorporating temperature and pressure dependence of the material properties. The greatest impact on predictions would result from incorporating the temperature dependence of α_V or α_ℓ alone. Including the temperature dependence of E and ν as well as of α would reduce somewhat the differences between predictions.

REFERENCES

Aerospace Structural Metals Handbook, 1978. Vol., III, Pub. Mechanical Properties Data Center, Traverse City, Mich., for Department of Defense.

Alcoa Structural Handbook, 1960. Aluminum Company of America, Pittsburgh, Penn.

Bauer, S.J. and J. Handin, 1981. "Thermal Expansion of Three Water-Saturated Igneous Rocks to 800°C at Effective Confining Pressures of 5 and 50 MPa" Trans. Amer. Geophys. Union, Vol. 62, No. 17, p. 393.

Bauer, S.J. and B. Johnson, 1979. "Effects of Slow Uniform Heating on the Physical Properties of Westerly and Charcoal Granites," in Proceedings of the 20th U.S. Symposium on Rock Mechanics. Austin, Texas, pp. 7-18.

Birch, F., 1966. "Compressibility; Elastic Constants," in Handbook of Physical Constants. (Clark, S.P., Jr., ed.), Geological Society of American Memoir 97, p. 97.

Brace, W.F., 1965. "Some New Measurements of Linear Compressibility of Rocks," Journ. Geophys. Res., Vol. 70, No. 2, pp. 391-398.

Brace, W.F., B.W. Paulding, Jr., and C. Scholy, 1966. "Dilatency in the Fracture of Crystalline Rocks," Jour. Geophys. Res., Vol. 79, No. 16, pp. 3939-3953.

Carnahan, B., H.A. Luther, and J.O. Wilkes, 1969. Applied Numerical Methods. John Wiley & Sons, Inc., New York., p. 573.

Carslaw, H.S. and J.C. Jasper, 1959. Conduction of Heat in Solids. Clarendon Press, Oxford, p. 200.

Chan, T. and N.G.W. Cook, 1979. Calculated Thermally Induced Displacements and Stresses for Heater Experiments at Stripa, Sweden. Lawrence Berkeley Laboratory report LBL-7061, SAC-22. Berkeley, California.

Cook, N.G.W., 1981. "Stiff Testing Machines, Stick Slip Sliding and Stability of Rock Deformation," in The Mechanical Behavior of Rocks, N.L. Carter, et al., eds., Geophysical Monograph no. 24, American Geophysical Union, Washington, D.C.

Cooper, H.W. and G. Simmons, 1977. "The Effect of Cracks on the Thermal Expansion of Rocks," Earth and Planetary Sci. Lett., Vol. 36, pp. 404-412.

Dally, J. and W. Riley, 1965. Experimental Stress Analysis. McGraw-Hill, New York., p. 366.

Griggs, D.T., F.J. Turner and H.C. Heard, 1960. "Deformation of Rocks at 500°C to 800°C," Chapter 4 in Rock Deformation, D.T. Griggs and J. Handin, eds., Geological Society of America Memoir 79, pp. 39-104.

Haas, C.J., 1981. "Static Stress-Strain Relationships," in Physical Properties of Rocks and Minerals, Y.S. Toblockian, W.R. Judd, and R.F. Roy, eds.) McGraw-Hill/CINDAS Data Series on Material Properties, Vol. II-2. McGraw-Hill, New York, p. 123.

Heard, H.C., 1980. "Thermal Expansion and Inferred Permeability of Climax Quartz Monzonite to 300°C and 27.6 MPa," Int. Journ. Rock Mech. and Min. Sci., Vol. 17, pp. 289-296.

Heard, H.C. and L. Page, 1981. "Elastic Moduli, Thermal Expansion, and Infrared Permeability of Two Granites to 350°C and 55 MPa," J. Geophys. Res. (in preparation).

Hockman, A. and D.W. Kessler, 1950. "Thermal and Moisture Expansion Studies of Some Domestic Granites," NBS Jour. Res., Vol. 44, No. 4, pp. 395-410.

Hughes, D.S. and H.J. Jones, 1950. "Variation of Elastic Moduli of Igneous Rocks with Pressure and Temperature," Bull. Geol. Soc. Amer., Vol. 61, pp. 843-856.

Kingery, W.D., 1960. Introduction to Ceramics. John Wiley & Sons, Inc. New York, p. 478.

Laubser, P.J. and J.G. Bryden, 1971. "An Apparatus for Determining the Coefficient of Thermal Expansion of Rocks, Mortars and Concretes," in Mag. Concrete Res., Vol. 24, No. 79, pp. 97-100.

Olkiewicz, A., J.E. Gale, R. Thorpe, and B. Paulsson, 1979. Geology and Fracture System at Stripa, Lawrence Berkeley Laboratory report LBL-8907, SAC-21. Berkeley, California.

Page, L. and H. Heard, 1981. "Elastic Moduli, Thermal Expansion, and Inferred Permeability of Climax Quartz Monzonite and Sudbury Gabbro at 500°C and 55 MPa," in Proc. 22nd Symp. on Rock Mechanics. MIT Press, Cambridge, Mass., pp. 97-104.

Pratt, H.R., T.A. Schrauf, L.A. Bills, and W.A. Hustrulid, 1977. Thermal and Mechanical Properties of Granite, Stripa, Sweden. Terra Tek Report TR 77-92, October. Salt Lake City, Utah.

Richter, D. and G. Simmons, 1974. "Thermal Expansion Behavior of Igneous Rocks," in Int. J. Rock Mech. Min. Sci. & Geomech. Abstr., Vol. 11, pp. 403-411.

Scholy, C.H., 1968. "Microfracturing and the Inelastic Deformation of Rock in Compression," Journ. Geophys. Res., Vol. 73, No. 4, pp. 1417-1432.

Simmons, G. and H. Wang, 1971. Single Crystal Elastic Constants and Calculated Aggregate Properties: A Handbook. MIT Press, Cambridge, Mass., 370 pp.

Skinner, B.J., 1966. "Thermal Expansion," in Handbook of Physical Constants (Clark, S.P., Jr., ed.), Geol. Soc. of Amer. Memoir 97, p. 76.

Swan, G., 1978. The Mechanical Properties of Stripa Granite. Lawrence Berkeley Laboratory report LBL-7074, SAC-03. Berkeley, California.

Thirumalai, K., and S.G. Demou, 1970. "Effect of Reduced Pressure on Thermal Expansion Behavior of Rocks and its Significance to Thermal Fragmentation," Journ. Appl. Phys.,Vol. 49, No. 13, pp. 5147-5151.

Thorpe, R., 1979. Characterization of Discontinuities in the Stripa Granite --Time-Scale Heater Experiment. Lawrence Berkeley Laboratory report LBL-7083, SAC-20. Berkeley, California, p. 9.

Timoshenko, S.P. and J.W. Goodier, 1951. Theory of Elasticity, 3rd ed., McGraw Hill, New York, pp. 441-452.

Walsh, J.B., 1965. "The Effect of Cracks on the Uniaxial Elastic Compression of Rocks," Journ. Geophys. Res.,Vol. 70, No. 2, pp. 399-411.

Wingquist, L.F., 1969. Elastic Moduli of Rock at Elevated Temperatures. U.S. Bureau of Mines Report of Investigations RI 7269.

Wollenberg, H.A., S. Flexser and L. Andersson, 1981. Petrology and Radiogeology of the Stripa Pluton. Lawrence Berkeley Laboratory report LBL-11654, SAC-36. Berkeley, California (in preparation).

Wong, T.F. and W.F. Brace, 1979. "Thermal Expansion of Rocks: Some Measurements at High Pressure," Tectonophysics, Vol. 57, pp. 95-117.

APPENDIX A: THERMAL EXPANSION RESULTS FOR INDIVIDUAL TESTS

For each sample, results are given for both heat-up and cool-down portions of the thermal cycle. Those values labeled "Best-Fit Tangent Values" were determined by taking the exact derivative, at the specified temperature, of the polynomial which best-fit the data. Results labeled "Incremental Values" were determined by calculating the slope of the straight line connecting each pair of data points. Thus, values are given for the specified temperature interval. See Section 5.2.2 for details of data reduction procedures.

Table A-1.

E01 9.74-9.93 HEAT-UP

BEST FIT TANGENT VALUES

TEMP (deg C)	CONFINING PRESSURE (MPa) 55	15	5	55	**	**	x 10E-6
20	14.81	16.44	18.99	18.24	*****	*****	alpha-v
	6.64	8.50	7.92	7.54	*****	*****	alpha-l
60	17.03	17.59	21.54	20.57	*****	*****	alpha-v
	7.30	7.01	9.08	8.64	*****	*****	alpha-l
100	19.25	20.57	24.10	22.90	*****	*****	alpha-v
	7.96	8.20	10.24	9.75	*****	*****	alpha-l
140	21.47	25.38	26.65	25.22	*****	*****	alpha-v
	8.63	10.41	11.40	10.85	*****	*****	alpha-l
180	23.69	32.02	29.20	27.55	*****	*****	alpha-v
	9.29	11.95	12.56	11.95	*****	*****	alpha-l
200	24.80	36.03	30.48	28.71	*****	*****	alpha-v
	9.63	11.94	13.14	12.50	*****	*****	alpha-l

INCREMENTAL VALUES

TEMP (deg C)	CONFINING PRESSURE (MPa) 55	15	5	55	**	**	x 10E-6
25 - 50	17.04	16.74	18.69	19.15	*****	*****	alpha-v
	7.54	7.37	8.35	7.90	*****	*****	alpha-l
50 - 75	17.22	17.86	20.00	20.12	*****	*****	alpha-v
	7.09	7.32	8.72	8.42	*****	*****	alpha-l
75 -100	18.18	19.82	24.28	21.01	*****	*****	alpha-v
	7.74	7.91	10.10	8.71	*****	*****	alpha-l
100 -125	19.26	20.34	25.30	23.08	*****	*****	alpha-v
	8.09	8.41	10.77	10.77	*****	*****	alpha-l
125 -150	20.84	24.19	27.86	29.27	*****	*****	alpha-v
	8.07	9.65	11.28	11.85	*****	*****	alpha-l
150 -175	23.26	32.85	29.90	25.87	*****	*****	alpha-v
	9.50	12.69	12.30	10.93	*****	*****	alpha-l
175 -200	25.05	30.00	24.16	23.97	*****	*****	alpha-v
	9.57	11.20	12.01	10.97	*****	*****	alpha-l

E01 9.74-9.93 COOL-DOWN

BEST FIT TANGENT VALUES

TEMP (deg C)	CONFINING PRESSURE (MPa) 55	15	5	55	**	**	x 10E-6
20	15.52	16.74	15.20	18.65	*****	*****	alpha-v
	6.30	7.28	6.37	7.20	*****	*****	alpha-l
60	17.93	20.38	20.28	20.79	*****	*****	alpha-v
	7.24	8.27	8.03	7.94	*****	*****	alpha-l
100	20.34	24.02	25.35	22.93	*****	*****	alpha-v
	8.18	9.25	9.68	8.68	*****	*****	alpha-l
140	22.75	27.66	30.42	25.06	*****	*****	alpha-v
	9.12	10.24	11.34	9.41	*****	*****	alpha-l
180	25.17	31.30	35.50	27.20	*****	*****	alpha-v
	10.05	11.22	12.99	10.15	*****	*****	alpha-l
200	26.37	33.12	38.03	28.27	*****	*****	alpha-v
	10.52	11.72	13.82	10.52	*****	*****	alpha-l

INCREMENTAL VALUES

TEMP (deg C)	CONFINING PRESSURE (MPa) 55	15	5	55	**	**	x 10E-6
25 - 50	18.62	20.50	20.62	21.39	*****	*****	alpha-v
	7.00	8.06	7.89	8.42	*****	*****	alpha-l
50 - 75	18.50	21.03	21.69	21.28	*****	*****	alpha-v
	7.42	8.28	8.08	7.88	*****	*****	alpha-l
75 -100	19.36	21.85	22.86	21.81	*****	*****	alpha-v
	8.56	9.04	8.96	8.41	*****	*****	alpha-l
100 -125	19.24	22.91	24.82	21.51	*****	*****	alpha-v
	7.53	9.31	9.83	7.63	*****	*****	alpha-l
125 -150	21.93	30.66	29.45	25.56	*****	*****	alpha-v
	8.52	10.45	11.39	10.28	*****	*****	alpha-l
150 -175	22.79	26.44	32.08	26.27	*****	*****	alpha-v
	9.31	9.79	11.98	9.88	*****	*****	alpha-l
175 -200	30.99	34.95	41.01	29.33	*****	*****	alpha-v
	12.09	12.61	13.80	10.49	*****	*****	alpha-l

E02 0.32-0.51 HEAT-UP

BEST FIT TANGENT VALUES

TEMP (deg C)	CONFINING PRESSURE (MPa) 57	30	15	5	2	57	x 10E-6
20	22.96	22.85	23.08	23.29	21.80	24.82	alpha-v
	9.21	11.52	13.12	10.11	12.10	11.95	alpha-l
60	26.68	27.09	27.16	27.21	28.95	30.43	alpha-v
	11.39	11.89	13.12	11.82	13.04	13.10	alpha-l
100	28.48	30.03	31.24	31.66	34.36	34.81	alpha-v
	12.10	12.26	13.12	13.32	13.97	14.25	alpha-l
140	30.19	32.23	35.32	36.64	38.03	37.95	alpha-v
	12.29	12.63	13.12	14.64	14.90	15.40	alpha-l
180	33.61	34.24	39.40	42.14	39.96	39.85	alpha-v
	12.89	13.00	13.12	15.76	15.84	16.55	alpha-l
200	36.53	35.34	41.44	45.09	40.27	40.34	alpha-v
	13.65	13.19	13.12	16.24	16.30	17.12	alpha-l

INCREMENTAL VALUES

TEMP (deg C)	CONFINING PRESSURE (MPa) 57	30	15	5	2	57	x 10E-6
25 - 50	24.44	24.78	22.54	24.53	25.58	28.96	alpha-v
	10.09	10.57	9.66	10.77	11.39	12.16	alpha-l
50 - 75	26.51	27.29	30.92	27.17	29.87	29.76	alpha-v
	11.33	11.92	13.24	11.86	12.87	12.80	alpha-l
75 -100	28.31	30.22	27.53	30.44	32.57	32.62	alpha-v
	12.05	12.58	11.53	12.88	14.01	13.87	alpha-l
100 -125	28.79	29.13	36.42	34.22	37.21	36.61	alpha-v
	12.16	12.24	14.73	13.78	14.71	15.60	alpha-l
125 -150	30.17	33.06	35.03	34.99	37.41	39.32	alpha-v
	12.23	13.26	14.02	14.30	15.47	15.54	alpha-l
150 -175	31.85	33.34	36.78	40.26	38.37	37.78	alpha-v
	12.56	13.34	14.23	15.99	15.84	15.44	alpha-l
175 -200	*****	34.24	38.95	43.59	41.15	40.20	alpha-v
	*****	11.35	13.81	15.49	14.29	16.41	alpha-l

E02 0.32-0.51 COOL-DOWN

BEST FIT TANGENT VALUES

TEMP (deg C)	CONFINING PRESSURE (MPa) 57	30	15	5	2	57	x 10E-6
20	23.90	24.15	25.09	28.10	24.62	27.09	alpha-v
	10.31	10.13	9.77	9.85	10.78	11.08	alpha-l
60	26.55	27.05	27.81	29.26	28.92	28.62	alpha-v
	11.07	10.85	11.00	11.42	11.90	11.51	alpha-l
100	28.36	29.95	30.54	31.41	33.23	30.15	alpha-v
	11.75	11.93	12.23	12.99	12.75	11.93	alpha-l
140	30.43	32.85	33.26	35.20	37.53	31.68	alpha-v
	12.60	13.39	13.46	14.56	14.23	12.36	alpha-l
180	33.85	35.76	35.99	41.29	41.84	33.21	alpha-v
	13.84	15.21	14.69	16.13	17.28	12.79	alpha-l
200	36.41	37.21	37.35	45.40	43.99	33.98	alpha-v
	14.70	16.26	15.31	16.92	19.68	13.00	alpha-l

INCREMENTAL VALUES

TEMP (deg C)	CONFINING PRESSURE (MPa) 57	30	15	5	2	57	x 10E-6
25	25.27	27.28	22.87	29.39	30.21	30.04	alpha-v
- 50	10.77	10.55	8.90	11.53	11.41	11.96	alpha-l
50	27.18	24.82	28.53	28.96	28.81	25.39	alpha-v
- 75	11.10	10.07	11.37	11.82	11.67	10.49	alpha-l
75	27.33	31.25	30.94	30.99	31.60	30.93	alpha-v
-100	11.51	12.79	12.28	12.79	13.30	12.61	alpha-l
100	29.48	30.03	31.57	32.34	32.94	30.50	alpha-v
-125	12.18	12.17	12.92	12.88	12.35	11.07	alpha-l
125	30.19	31.59	36.68	35.65	38.18	33.21	alpha-v
-150	12.44	12.73	14.30	14.44	14.85	13.62	alpha-l
150	32.41	35.96	35.64	37.76	40.58	32.42	alpha-v
-175	13.39	14.48	14.97	14.84	16.09	12.12	alpha-l
175	*****	35.94	30.50	43.36	45.04	31.48	alpha-v
-200	*****	15.90	12.33	17.93	18.26	12.38	alpha-l

E02 4.38-4.57 HEAT-UP

BEST FIT TANGENT VALUES

TEMP (deg C)	CONFINING PRESSURE (MPa) 55*	30	15	5	2	**	x 10E-6
20	5.07	7.77	6.48	10.82	14.59	*****	alpha-v
	2.07	4.04	2.51	3.92	5.86	*****	alpha-l
60	10.49	13.45	13.15	16.95	18.95	*****	alpha-v
	4.05	5.06	4.31	6.27	6.78	*****	alpha-l
100	15.92	18.01	19.82	21.91	23.32	*****	alpha-v
	6.04	6.07	6.80	7.93	7.69	*****	alpha-l
140	21.34	21.44	26.49	25.70	27.69	*****	alpha-v
	8.02	7.08	9.97	8.91	8.61	*****	alpha-l
180	26.77	23.75	33.17	28.31	32.05	*****	alpha-v
	10.00	8.10	13.84	9.21	9.53	*****	alpha-l
200	29.48	24.49	36.50	29.17	34.24	*****	alpha-v
	11.00	8.60	16.03	9.10	9.99	*****	alpha-l

INCREMENTAL VALUES

TEMP (deg C)	CONFINING PRESSURE (MPa) 55	30	15	5	2	**	x 10E-6
25	10.91	11.48	10.35	13.29	16.91	*****	alpha-v
- 50	3.80	3.75	3.13	4.64	5.70	*****	alpha-l
50	12.15	13.05	11.51	17.24	21.45	*****	alpha-v
- 75	4.86	4.93	4.14	6.57	6.97	*****	alpha-l
75	20.37	15.92	16.86	19.73	19.94	*****	alpha-v
-100	7.91	5.73	5.82	7.35	7.09	*****	alpha-l
100	20.44	18.01	21.35	22.78	23.15	*****	alpha-v
-125	7.57	6.41	7.40	7.84	8.00	*****	alpha-l
125	23.78	23.16	26.23	25.11	28.94	*****	alpha-v
-150	8.78	7.95	9.54	8.80	9.68	*****	alpha-l
150	*****	21.83	31.20	29.02	32.33	*****	alpha-v
-175	*****	7.14	11.49	9.93	9.98	*****	alpha-l
175	*****	23.23	30.69	26.52	29.23	*****	alpha-v
-200	*****	6.99	14.04	8.44	6.75	*****	alpha-l

E02 4.38-4.57 COOL-DOWN

BEST FIT TANGENT VALUES

TEMP (deg C)	CONFINING PRESSURE (MPa) 55	30	15	5	2	**	x 10E-6
20	21.66	13.82	8.95	11.15	11.85	*****	alpha-v
	6.25	3.84	2.87	3.73	3.27	*****	alpha-l
60	21.66	13.93	15.79	15.11	15.60	*****	alpha-v
	6.25	4.36	4.69	5.07	5.24	*****	alpha-l
100	21.66	16.85	18.89	19.24	19.36	*****	alpha-v
	6.25	5.65	6.51	6.41	6.48	*****	alpha-l
140	21.66	22.59	23.61	23.56	23.11	*****	alpha-v
	6.25	7.71	8.33	7.75	7.64	*****	alpha-l
180	21.66	31.14	35.29	28.07	26.86	*****	alpha-v
	6.25	10.55	10.15	9.08	9.39	*****	alpha-l
200	21.66	36.48	45.42	30.39	28.74	*****	alpha-v
	6.25	12.25	11.06	9.75	10.69	*****	alpha-l

INCREMENTAL VALUES

TEMP (deg C)	CONFINING PRESSURE (MPa) 55	30	15	5	2	**	x 10E-6
25	10.43	13.62	13.10	12.29	13.30	*****	alpha-v
- 50	3.34	3.96	3.91	4.09	4.15	*****	alpha-l
50	13.67	13.59	14.16	15.36	15.71	*****	alpha-v
- 75	3.47	4.24	4.35	5.05	5.27	*****	alpha-l
75	15.42	16.37	18.07	18.11	17.97	*****	alpha-v
-100	5.16	5.36	6.02	6.04	6.08	*****	alpha-l
100	16.16	16.62	19.71	20.36	20.10	*****	alpha-v
-125	5.62	5.80	6.70	6.88	6.60	*****	alpha-l
125	74.57	23.21	24.90	22.76	22.83	*****	alpha-v
-150	6.87	7.76	8.47	7.59	7.76	*****	alpha-l
150	*****	24.61	25.00	25.08	25.58	*****	alpha-v
-175	7.60	8.33	8.07	8.05	8.28	*****	alpha-l
175	46.31	32.20	39.09	29.44	26.60	*****	alpha-v
-200	12.67	11.02	11.77	9.44	9.69	*****	alpha-l

E03 0.26-0.45 HEAT-UP

BEST FIT TANGENT VALUES

TEMP (deg C)	CONFINING PRESSURE (MPa) 55	30	15	5	2	30	x 10E-6
20	17.67	17.54	17.34	19.21	19.23	16.68	alpha-v
	8.79	8.35	8.85	8.95	9.21	8.57	alpha-l
60	19.69	19.55	20.28	21.41	22.38	20.21	alpha-v
	9.47	9.13	9.27	9.70	10.08	9.63	alpha-l
100	21.71	22.32	23.79	25.08	25.52	23.74	alpha-v
	10.15	10.12	10.55	10.94	10.94	10.70	alpha-l
140	23.73	25.86	27.87	30.20	28.67	27.28	alpha-v
	10.83	11.33	12.03	12.67	11.81	11.76	alpha-l
180	25.75	30.16	32.52	36.79	31.81	30.81	alpha-v
	11.51	12.75	13.06	14.89	12.68	12.83	alpha-l
200	26.76	32.59	35.06	40.63	33.39	32.57	alpha-v
	11.85	13.54	13.20	16.19	13.11	13.36	alpha-l

INCREMENTAL VALUES

TEMP (deg C)	CONFINING PRESSURE (MPa) 55	30	15	5	2	30	x 10E-6
25	22.73	18.15	18.94	19.83	20.35	18.78	alpha-v
- 50	11.02	8.63	8.94	9.17	9.45	9.22	alpha-l
50	18.29	19.90	20.50	21.52	22.64	19.84	alpha-v
- 75	8.81	9.16	9.36	9.66	10.02	9.38	alpha-l
75	21.67	21.89	22.23	24.35	25.48	23.20	alpha-v
-100	10.36	10.10	10.09	10.89	11.30	10.78	alpha-l
100	21.30	22.79	25.89	25.85	26.20	24.39	alpha-v
-125	9.74	10.19	11.19	10.95	10.92	10.61	alpha-l
125	25.15	25.99	27.27	30.18	27.31	27.92	alpha-v
-150	11.25	11.38	11.79	12.84	11.27	12.18	alpha-l
150	23.93	28.04	30.20	33.21	31.44	28.28	alpha-v
-175	11.19	12.07	12.72	13.64	12.77	11.93	alpha-l
175	*****	*****	*****	*****	*****	*****	alpha-v
-200	*****	*****	*****	*****	*****	*****	alpha-l

E03 0.26-0.45 COOL-DOWN

BEST FIT TANGENT VALUES

TEMP (deg C)	CONFINING PRESSURE (MPa) 55	30	15	5	2	30	x 10E-6
20	15.45	16.93	19.17	17.39	17.54	18.98	alpha-v
	7.67	8.02	8.02	7.30	7.99	7.83	alpha-l
60	18.08	19.58	20.42	20.93	20.75	19.38	alpha-v
	8.27	8.64	8.71	9.04	8.87	8.55	alpha-l
100	20.71	22.24	22.64	24.47	23.96	21.62	alpha-v
	8.88	9.26	9.39	10.23	9.75	9.27	alpha-l
140	23.34	24.89	25.83	28.02	27.18	25.71	alpha-v
	9.48	9.87	10.04	10.88	10.62	10.00	alpha-l
180	25.97	27.54	29.98	31.56	30.39	31.64	alpha-v
	10.09	10.49	10.67	10.97	11.50	10.72	alpha-l
200	27.29	28.87	32.41	33.33	32.00	35.29	alpha-v
	10.39	10.80	10.98	10.82	11.94	11.08	alpha-l

INCREMENTAL VALUES

TEMP (deg C)	CONFINING PRESSURE (MPa) 55	30	15	5	2	30	x 10E-6
25	18.56	19.21	20.39	19.86	19.64	18.60	alpha-v
- 50	8.25	8.38	8.61	8.71	8.53	8.63	alpha-l
50	17.87	18.07	19.57	19.85	20.18	19.78	alpha-v
- 75	8.17	8.10	8.48	8.51	8.64	8.64	alpha-l
75	18.42	22.86	22.24	23.94	23.42	21.29	alpha-v
-100	8.20	9.81	9.29	10.11	9.66	9.11	alpha-l
100	21.54	21.86	23.47	26.18	24.64	20.69	alpha-v
-125	9.46	8.87	9.39	10.56	9.98	8.25	alpha-l
125	24.51	25.15	25.78	28.01	27.29	27.12	alpha-v
-150	10.05	10.25	10.40	11.07	10.75	10.91	alpha-l
150	23.84	26.19	27.52	28.83	28.37	27.64	alpha-v
-175	8.89	9.79	10.05	10.66	10.71	10.37	alpha-l
175	*****	*****	*****	*****	*****	*****	alpha-v
-200	*****	*****	*****	*****	*****	*****	alpha-l

E17 6.04-6.22 HEAT-UP

BEST FIT TANGENT VALUES

TEMP (deg C)	CONFINING PRESSURE (MPa) 55	30	15	5	2	55	x 10E-6
20	20.67	22.34	20.96	21.12	19.82	25.43	alpha-v
	9.36	10.05	8.43	9.37	8.50	10.70	alpha-l
60	23.13	24.13	24.70	26.50	27.96	26.32	alpha-v
	9.87	10.67	10.76	11.46	11.95	11.54	alpha-l
100	25.58	25.91	28.43	30.89	31.85	28.83	alpha-v
	11.06	11.28	11.94	13.06	13.55	12.37	alpha-l
140	28.04	27.70	32.16	34.28	35.68	32.94	alpha-v
	12.92	11.90	13.11	14.17	14.61	13.21	alpha-l
180	30.49	29.48	35.89	36.68	43.67	38.66	alpha-v
	15.45	12.51	15.42	14.80	16.44	14.04	alpha-l
200	31.72	30.37	37.76	37.51	50.53	42.13	alpha-v
	16.96	12.82	17.37	14.94	18.05	14.46	alpha-l

INCREMENTAL VALUES

TEMP (deg C)	CONFINING PRESSURE (MPa) 55	30	15	5	2	55	x 10E-6
25	21.78	22.79	22.40	23.28	23.57	26.40	alpha-v
- 50	8.88	9.60	9.62	10.32	10.08	11.13	alpha-l
50	23.38	24.59	24.85	27.03	28.07	25.27	alpha-v
- 75	10.32	11.61	10.67	11.49	11.93	11.03	alpha-l
75	26.29	24.37	27.54	28.59	30.43	28.75	alpha-v
-100	11.19	10.17	11.58	12.44	13.20	13.44	alpha-l
100	21.71	26.74	28.99	33.79	32.63	28.81	alpha-v
-125	10.43	11.77	12.32	13.80	13.55	11.25	alpha-l
125	32.96	28.76	30.38	32.01	34.97	33.43	alpha-v
-150	13.30	12.47	12.71	13.60	14.64	13.38	alpha-l
150	27.53	26.78	35.60	36.40	38.56	33.40	alpha-v
-175	14.01	11.19	14.05	14.74	15.19	14.11	alpha-l
175	*****	*****	*****	*****	*****	*****	alpha-v
-200	*****	*****	*****	*****	*****	*****	alpha-l

E17 6.04-6.22 COOL-DOWN

BEST FIT TANGENT VALUES

TEMP (deg C)	CONFINING PRESSURE (MPa) 55	30	15	5	2	55	x 10E-6
20	19.69	22.79	26.68	22.38	23.64	26.55	alpha-v
	8.23	8.58	10.20	8.83	9.59	10.41	alpha-l
60	22.10	23.97	27.22	25.91	27.51	28.16	alpha-v
	9.29	10.01	10.75	10.32	11.13	11.00	alpha-l
100	24.50	26.59	27.75	29.43	31.38	29.76	alpha-v
	10.36	11.43	11.30	11.82	12.68	11.59	alpha-l
140	26.91	30.66	28.28	32.96	35.25	31.36	alpha-v
	11.42	12.86	11.86	13.31	14.23	12.19	alpha-l
180	29.32	36.18	28.81	36.48	39.12	32.97	alpha-v
	12.48	14.28	12.41	14.80	15.78	12.78	alpha-l
200	30.52	39.48	29.08	38.25	41.05	33.77	alpha-v
	13.01	14.99	12.68	15.55	16.55	13.08	alpha-l

INCREMENTAL VALUES

TEMP (deg C)	CONFINING PRESSURE (MPa) 55	30	15	5	2	55	x 10E-6
25	23.86	23.01	26.66	27.00	26.46	27.37	alpha-v
- 50	10.50	9.28	10.17	10.68	10.56	11.37	alpha-l
50	23.69	24.42	26.40	24.59	24.71	26.03	alpha-v
- 75	9.41	10.25	10.48	9.73	9.78	10.46	alpha-l
75	19.12	25.76	28.31	28.54	33.94	27.23	alpha-v
-100	7.81	10.99	11.63	11.37	14.27	10.59	alpha-l
100	24.85	26.07	27.67	28.86	30.74	38.38	alpha-v
-125	11.14	10.94	11.19	11.78	12.39	13.27	alpha-l
125	28.49	32.49	30.40	32.73	33.85	23.80	alpha-v
-150	12.27	13.71	12.43	13.43	13.00	10.04	alpha-l
150	29.40	31.59	25.40	36.70	38.13	32.91	alpha-v
-175	11.93	13.21	11.15	14.40	15.86	13.97	alpha-l
175	*****	*****	*****	*****	*****	*****	alpha-v
-200	*****	*****	*****	*****	*****	*****	alpha-l

M02 12.23-12.43 HEAT-UP

BEST FIT TANGENT VALUES

TEMP (deg C)	CONFINING PRESSURE (MPa) 55	15	55	5	55	**	x 10E-6
20	20.18	17.58	19.62	15.43	20.78	*****	alpha-v
	7.88	7.17	7.90	8.06	9.25	*****	alpha-l
60	20.56	22.05	21.70	21.38	23.72	*****	alpha-v
	8.32	8.35	8.37	9.12	9.55	*****	alpha-l
100	23.77	26.52	23.77	27.32	26.67	*****	alpha-v
	8.77	9.53	8.84	10.17	9.85	*****	alpha-l
140	27.71	30.99	25.85	33.26	29.62	*****	alpha-v
	9.21	10.71	9.31	11.23	10.15	*****	alpha-l
180	30.27	35.45	27.93	39.20	32.56	*****	alpha-v
	9.66	11.89	9.78	12.29	10.45	*****	alpha-l
200	30.37	37.69	28.97	42.17	34.04	*****	alpha-v
	9.88	12.47	10.01	12.82	10.60	*****	alpha-l

INCREMENTAL VALUES

TEMP (deg C)	CONFINING PRESSURE (MPa) 55	15	55	5	55	**	x 10E-6
25 - 50	19.95	19.81	20.19	20.48	22.65	*****	alpha-v
	7.87	7.57	7.93	8.28	9.29	*****	alpha-l
50 - 75	21.20	20.99	21.67	20.36	23.70	*****	alpha-v
	8.00	7.62	8.36	8.65	9.20	*****	alpha-l
75 -100	21.49	28.54	22.53	23.15	25.41	*****	alpha-v
	8.82	10.64	8.51	9.75	9.81	*****	alpha-l
100 -125	25.92	25.50	25.07	27.40	26.82	*****	alpha-v
	9.05	9.31	9.33	11.15	10.10	*****	alpha-l
125 -150	27.77	31.55	26.96	36.67	31.10	*****	alpha-v
	9.65	11.17	9.52	11.39	10.73	*****	alpha-l
150 -175	28.39	34.38	27.11	40.74	32.15	*****	alpha-v
	9.54	11.05	9.40	11.82	10.18	*****	alpha-l
175 -200	31.08	34.63	26.22	31.53	30.72	*****	alpha-v
	8.65	11.74	9.50	11.23	9.71	*****	alpha-l

M02 12.23-12.43 COOL-DOWN

BEST FIT TANGENT VALUES

TEMP (deg C)	CONFINING PRESSURE (MPa) 55	15	55	5	**	**	x 10E-6
20	17.76	20.36	*****	20.65	*****	*****	alpha-v
	6.40	7.71	*****	8.36	*****	*****	alpha-l
60	20.70	22.79	*****	23.81	*****	*****	alpha-v
	7.27	8.05	*****	8.62	*****	*****	alpha-l
100	23.64	26.40	*****	27.86	*****	*****	alpha-v
	8.14	8.97	*****	9.55	*****	*****	alpha-l
140	26.58	31.19	*****	32.79	*****	*****	alpha-v
	9.01	10.46	*****	11.14	*****	*****	alpha-l
180	29.53	37.15	*****	38.60	*****	*****	alpha-v
	9.88	12.53	*****	13.38	*****	*****	alpha-l
200	31.00	40.58	*****	41.84	*****	*****	alpha-v
	10.32	13.78	*****	14.75	*****	*****	alpha-l

INCREMENTAL VALUES

TEMP (deg C)	CONFINING PRESSURE (MPa) 55	15	55	5	**	**	x 10E-6
25	21.78	21.26	*****	21.35	*****	*****	alpha-v
- 50	8.37	7.69	*****	8.19	*****	*****	alpha-l
50	20.54	23.38	*****	25.37	*****	*****	alpha-v
- 75	6.90	8.33	*****	8.80	*****	*****	alpha-l
75	22.82	24.98	*****	26.59	*****	*****	alpha-v
-100	7.82	8.56	*****	9.32	*****	*****	alpha-l
100	23.35	27.59	*****	26.89	*****	*****	alpha-v
-125	8.16	9.24	*****	9.85	*****	*****	alpha-l
125	25.58	31.49	*****	34.95	*****	*****	alpha-v
-150	8.45	10.56	*****	11.12	*****	*****	alpha-l
150	29.16	33.71	*****	34.51	*****	*****	alpha-v
-175	9.64	11.47	*****	11.76	*****	*****	alpha-l
175	31.90	38.58	*****	39.30	*****	*****	alpha-v
-200	11.32	12.92	*****	14.10	*****	*****	alpha-l

APPENDIX B: STRESS STRAIN DATA FOR INDIVIDUAL TESTS

For each sample, results are reported for the loading and unloading portion of the stress strain tests during both heat-up and cool-down phases of the thermal cycles. Values of the polynomial coefficients can be used to generate curves of strain as a function of stress as discussed in Sections 5.2 and 5.2.1. Derivatives of these polynomials will then generate tangent values of Young's modulus (Table B-1) and Poisson's ratio (Table B-2).

Table B1.

E01 9.74-9.93 TANGENT YOUNG'S MODULUS LOADING

CONF PRES (MPa)	TEMP (deg C)	MAX DEV STRESS (MPa)	MAX AXIAL STRAIN x 10E-2	POLYNOMIAL COEFFICIENTS F0	F1	F2	F3	F4
55	24	149.9	0.1812	0.3697E-01	-0.1030E+01			
55	74	151.3	0.1837	0.2805E-01	-0.1024E+01			
55	126	139.2	0.1685	0.3355E-01	-0.1034E+01			
55	174	102.1	0.1246	0.3517E-01	-0.1036E+01			
55	198	102.3	0.1262	0.2209E-01	-0.1022E+01			
55	174	102.1	0.1242	0.2462E-01	-0.1026E+01			
55	126	133.5	0.1641	0.9613E-02	-0.1007E+01			
55	76	151.1	0.1823	0.2864E-01	-0.1024E+01			
55	21	151.2	0.1821	0.3492E-01	-0.1027E+01			
15	20	119.9	0.1503	0.4149E-02	-0.1005E+01			
15	74	112.0	0.1398	0.4993E-02	-0.1006E+01			
15	124	112.1	0.1409	0.3215E-02	-0.1034E+01	0.2980E-01		
15	174	81.2	0.1119	0.4495E-03	-0.1006E+01			
15	199	78.3	0.1168	0.9661E-03	-0.1058E+01	0.2560E-01	0.3092E-01	
15	174	81.1	0.1182	0.5671E-02	-0.1122E+01	0.1161E+00		
15	124	113.0	0.1593	-0.7728E-02	-0.1005E+01			
15	76	117.7	0.1613	-0.2180E-02	-0.1075E+01	0.7771E-01		
15	27	121.2	0.1621	0.7070E-02	-0.1073E+01	0.6717E-01		
5	26	116.7	0.1595	-0.1347E-02	-0.1087E+01	0.9059E-01		
5	74	117.6	0.1635	0.1180E-02	-0.1151E+01	0.2238E+00	-0.7363E-01	
5	124	110.0	0.1605	-0.3852E-03	-0.1123E+01	0.1260E+00		
5	172	87.1	0.1386	0.6893E-02	-0.1111E+01	0.5129E-01	0.5429E-01	
5	198	86.3	0.1496	0.2773E-02	-0.1178E+01	0.1763E+00		
5	173	86.8	0.1456	0.3929E-02	-0.1288E+01	0.4208E+00	-0.1380E+00	
5	125	109.7	0.1695	-0.3000E-01	-0.9883E+00			
5	74	117.8	0.1750	-0.3971E-02	-0.1136E+01	0.1457E+00		
5	27	117.2	0.1702	0.1197E-03	-0.1197E+01	0.3494E+00	-0.1982E+00	0.4571E-01
55	28	152.7	0.2153	0.1671E-01	-0.1133E+01	0.1174E+00		
55	73	152.1	0.2173	-0.9664E-02	-0.1003E+01			
55	124	140.3	0.2076	-0.1575E-01	-0.1003E+01			
55	172	102.1	0.1649	0.2332E-01	-0.1216E+01	0.1940E+00		
55	198	101.1	0.1673	0.1971E-01	-0.1212E+01	0.1947E+00		
55	175	101.1	0.1640	0.2000E-01	-0.1208E+01	0.1887E+00		
55	125	138.1	0.2059	0.1050E-01	-0.1149E+01	0.1427E+00		
55	75	152.3	0.2230	0.8289E-02	-0.1119E+01	0.1145E+00		
55	23	146.6	0.2136	-0.1299E-01	-0.9909E+00			

E01 9.74-9.93 TANGENT YOUNG'S MODULUS UNLOADING

CONF PRES (MPa)	TEMP (deg C)	MAX DEV STRESS (MPa)	MAX AXIAL STRAIN x 10E-2	POLYNOMIAL COEFFICIENTS F0	F1	F2	F3	F4
55	24	149.9	0.1812	-0.8331E-02	-0.9958E+00			
55	74	151.3	0.1837	-0.8017E-03	-0.1000E+01			
55	126	139.2	0.1685	0.3192E-02	-0.1003E+01			
55	174	102.1	0.1246	0.2638E-02	-0.1005E+01			
55	198	102.3	0.1262	0.8915E-03	-0.1006E+01			
55	174	102.1	0.1242	0.6343E-02	-0.1010E+01			
55	126	133.5	0.1641	-0.8801E-02	-0.9895E+00			
55	76	151.1	0.1823	0.4515E-02	-0.1005E+01			
55	21	151.2	0.1821	0.1132E-02	-0.1005E+01			
15	20	119.9	0.1503	-0.6026E-02	-0.1049E+01	0.5501E-01		
15	74	112.0	0.1398	-0.1071E-02	-0.1036E+01	0.3756E-01		
15	124	112.1	0.1412	-0.1001E-01	-0.9948E+00			
15	174	81.2	0.1119	0.4268E-03	-0.1122E+01	0.1214E+00		
15	199	78.3	0.1168	-0.2064E-01	-0.1137E+01	0.1623E+00		
15	174	81.1	0.1182	-0.1345E-01	-0.1154E+01	0.1692E+00		
15	124	113.0	0.1593	-0.1444E-01	-0.1136E+01	0.1508E+00		
15	76	117.7	0.1613	-0.1587E-01	-0.1108E+01	0.1269E+00		
15	27	121.2	0.1621	-0.4177E-02	-0.1104E+01	0.1097E+00		
5	26	116.7	0.1595	-0.1053E-01	-0.1201E+01	0.4034E+00	-0.2698E+00	0.7809E-01
5	74	117.6	0.1635	-0.6889E-02	-0.1263E+01	0.6164E+00	-0.5551E+00	0.2088E+00
5	124	110.0	0.1605	-0.1650E-01	-0.1173E+01	0.1923E+00		
5	172	87.1	0.1386	-0.1326E-01	-0.1248E+01	0.2645E+00		
5	198	86.3	0.1496	-0.1654E-01	-0.1387E+01	0.5862E+00	-0.1830E+00	
5	173	86.8	0.1456	-0.1522E-01	-0.1484E+01	0.9745E+00	-0.7044E+00	0.2292E+00
5	125	109.7	0.1695	-0.2658E-01	-0.1378E+01	0.9102E+00	-0.7746E+00	0.2691E+00
5	74	117.8	0.1750	-0.2218E-01	-0.1313E+01	0.7615E+00	-0.6629E+00	0.2374E+00
5	27	117.2	0.1702	-0.2164E-01	-0.1284E+01	0.7170E+00	-0.6675E+00	0.2552E+00
55	28	152.7	0.2153	-0.1675E-01	-0.1080E+01	0.9945E-01		
55	73	152.1	0.2173	-0.1055E-01	-0.1114E+01	0.1291E+00		
55	124	140.3	0.2076	-0.1084E-01	-0.1154E+01	0.1687E+00		
55	172	102.1	0.1649	-0.2105E-01	-0.1193E+01	0.2154E+00		
55	198	101.1	0.1673	-0.2708E-01	-0.1175E+01	0.2035E+00		
55	175	101.1	0.1640	-0.2377E-01	-0.1185E+01	0.2101E+00		
55	125	138.1	0.2059	-0.1744E-01	-0.1140E+01	0.1629E+00		
55	75	152.3	0.2230	-0.2887E-01	-0.1091E+01	0.1219E+00		
55	23	146.6	0.2136	-0.5072E-01	-0.1053E+01	0.1027E+00		

E02 0.32-0.51 TANGENT YOUNG'S MODULUS LOADING

CONF PRES (MPa)	TEMP (deg C)	MAX DEV STRESS (MPa)	MAX AXIAL STRAIN x 10E-2	POLYNOMIAL COEFFICIENTS F0	F1	F2	F3	F4
57	17	215.2	0.2816	0.2734E-01	-0.1018E+01			
57	75	208.8	0.2724	0.2055E-01	-0.1013E+01			
57	126	202.1	0.2624	0.2147E-01	-0.1018E+01			
57	175	151.1	0.1940	0.2270E-01	-0.1018E+01			
57	201	150.9	0.1965	0.2040E-01	-0.1015E+01			
57	177	150.7	0.1933	0.1846E-01	-0.1013E+01			
57	128	201.0	0.2629	0.1536E-01	-0.1010E+01			
57	77	216.9	0.2845	0.2042E-01	-0.1013E+01			
57	29	215.7	0.2810	0.2325E-01	-0.1016E+01			
31	28	191.5	0.2533	0.1307E-01	-0.1005E+01			
31	77	192.7	0.2558	0.1230E-01	-0.1006E+01			
31	128	180.4	0.2373	0.9989E-02	-0.1007E+01			
31	177	139.2	0.1842	0.1451E-01	-0.1017E+01			
31	203	139.2	0.1911	0.4949E-02	-0.1009E+01			
31	179	139.2	0.1895	-0.2162E-02	-0.1003E+01			
31	129	180.8	0.2420	0.2935E-02	-0.1003E+01			
31	78	192.6	0.2569	0.1139E-01	-0.1007E+01			
31	27	191.3	0.2556	0.1680E-01	-0.1012E+01			
15	26	171.3	0.2327	0.5321E-02	-0.1005E+01			
15	75	160.6	0.2249	0.1704E-03	-0.1003E+01	0.4232E-02		
15	128	162.6	0.2229	0.3571E-02	-0.1038E+01	0.3498E-01		
15	177	118.4	0.1691	0.7979E-02	-0.1068E+01	0.6031E-01		
15	202	118.4	0.1779	0.4801E-02	-0.1063E+01	0.2559E-01	0.3392E-01	
15	175	118.3	0.1746	0.4320E-02	-0.1135E+01	0.1787E+00	-0.4821E-01	
15	128	162.3	0.2320	-0.1797E-02	-0.1064E+01	0.6865E-01		
15	77	172.6	0.2441	-0.5640E-03	-0.1027E+01	0.3030E-01		
15	19	171.0	0.2436	0.2236E-02	-0.1020E+01	0.1893E-01		
5	18	124.2	0.1850	0.1189E-02	-0.1064E+01	0.6422E-01		
5	75	125.1	0.1864	-0.3140E-02	-0.1065E+01	0.6974E-01		
5	126	117.9	0.1814	-0.1127E-02	-0.1116E+01	0.1203E+00		
5	175	93.7	0.1560	0.6303E-02	-0.1148E+01	0.1489E+00	-0.6554E-02	
5	201	94.0	0.1661	0.4531E-02	-0.1152E+01	0.1487E+00		
5	176	93.7	0.1619	0.4794E-02	-0.1239E+01	0.3314E+00	-0.9630E-01	
5	125	117.3	0.1869	0.1000E-01	-0.1236E+01	0.4212E+00	-0.2506E+00	0.5627E-01
5	78	125.0	0.1991	-0.3623E-02	-0.1103E+01	0.1121E+00		
5	31	124.2	0.1958	-0.1010E-02	-0.1080E+01	0.8410E-01		
2	31	82.2	0.1355	0.5243E-02	-0.1193E+01	0.3173E+00	-0.1285E+00	
2	77	77.6	0.1301	0.3532E-02	-0.1198E+01	0.2992E+00	-0.1036E+00	
2	127	78.2	0.1363	0.5367E-02	-0.1196E+01	0.2390E+00	-0.4863E-01	
2	176	62.5	0.1186	0.6872E-02	-0.1133E+01	0.1105E+00	0.1606E-01	
2	202	62.6	0.1245	0.5635E-02	-0.1102E+01	0.2983E-01	0.6748E-01	
2	178	62.6	0.1220	0.3934E-02	-0.1172E+01	0.1380E+00	0.3125E-01	
2	129	99.4	0.1732	0.7597E-02	-0.1435E+01	0.9629E+00	-0.7876E+00	0.2519E+00
2	76	82.7	0.1421	0.2569E-02	-0.1201E+01	0.2905E+00	-0.9201E-01	
2	27	82.0	0.1396	0.3440E-03	-0.1140E+01	0.1792E+00	-0.3800E-01	
57	26	215.5	0.3355	-0.2114E-01	-0.9823E+00			
57	76	217.0	0.3399	-0.1767E-01	-0.9924E+00			
57	125	201.6	0.3278	-0.2602E-01	-0.9844E+00			
57	176	150.7	0.2564	-0.1247E-01	-0.1007E+01			
57	199	150.5	0.2635	0.1209E-01	-0.1196E+01	0.1891E+00		
57	175	150.4	0.2534	-0.5807E-02	-0.1013E+01			
57	127	201.6	0.3353	-0.7644E-02	-0.1139E+01	0.1562E+00		
57	76	216.9	0.3521	-0.2390E-01	-0.9880E+00			
57	28	215.7	0.3416	-0.1092E-01	-0.1001E+01			

E02 0.32-0.51 TANGENT YOUNG'S MODULUS UNLOADING

CONF PRES (MPa)	TEMP (deg C)	MAX DEV STRESS (MPa)	MAX AXIAL STRAIN x 10E-2	POLYNOMIAL COEFFICIENTS F0	F1	F2	F3	F4
57	17	215.2	0.2816	-0.9159E-02	-0.1004E+01			
57	75	217.3	0.2847	-0.1168E-01	-0.9939E+00			
57	126	202.1	0.2624	-0.1021E-01	-0.9964E+00			
57	175	151.1	0.1940	-0.1259E-01	-0.1001E+01			
57	201	150.9	0.1965	-0.3453E-01	-0.9775E+00			
57	177	150.7	0.1933	-0.1502E-01	-0.9952E+00			
57	128	201.0	0.2629	-0.1800E-01	-0.9894E+00			
57	77	216.9	0.2845	-0.1182E-01	-0.9963E+00			
57	29	215.7	0.2810	-0.7407E-02	-0.1007E+01			
31	28	191.5	0.2533	-0.1160E-01	-0.9979E+00			
31	77	192.7	0.2558	-0.6479E-02	-0.1040E+01	0.4647E-01		
31	128	180.4	0.2373	-0.1071E-01	-0.9980E+00			
31	177	139.2	0.1842	-0.5333E-02	-0.1069E+01	0.7388E-01		
31	203	139.2	0.1911	-0.2100E-01	-0.1083E+01	0.1033E+00		
31	179	139.2	0.1895	-0.1678E-01	-0.1075E+01	0.9149E-01		
31	129	180.8	0.2420	-0.1722E-01	-0.1045E+01	0.6172E-01		
31	78	192.6	0.2569	-0.9344E-02	-0.1039E+01	0.4744E-01		
31	27	191.3	0.2556	-0.1331E-01	-0.9970E+00			
15	26	171.3	0.2327	-0.1250E-02	-0.1086E+01	0.8739E-01		
15	75	160.6	0.2249	-0.1344E-01	-0.1088E+01	0.1338E+00		
15	128	162.6	0.2229	-0.4386E-02	-0.1144E+01	0.2028E+00	-0.5510E-01	
15	177	118.4	0.1691	-0.4903E-02	-0.1183E+01	0.2576E+00	-0.6994E-01	
15	202	118.4	0.1779	-0.1482E-01	-0.1217E+01	0.3121E+00	-0.8120E-01	
15	175	118.3	0.1746	-0.1194E-01	-0.1223E+01	0.3437E+00	-0.1091E+00	
15	128	162.3	0.2320	-0.1937E-01	-0.1172E+01	0.2801E+00	-0.9043E-01	
15	77	172.6	0.2441	-0.1294E-01	-0.1126E+01	0.1960E+00	-0.5898E-01	
15	19	171.0	0.2436	-0.5169E-02	-0.1113E+01	0.1179E+00		
5	18	124.2	0.1850	-0.6513E-02	-0.1155E+01	0.1627E+00		
5	75	125.1	0.1864	-0.6264E-03	-0.1334E+01	0.8054E+00	-0.7832E+00	0.3131E+00
5	126	117.9	0.1814	-0.2024E-02	-0.1384E+01	0.8670E+00	-0.7651E+00	0.2841E+00
5	175	93.7	0.1560	-0.1461E-01	-0.1313E+01	0.5591E+00	-0.3596E+00	0.1283E+00
5	201	94.0	0.1661	-0.2037E-01	-0.1374E+01	0.6432E+00	-0.3414E+00	0.9262E-01
5	176	93.7	0.1619	-0.1631E-01	-0.1409E+01	0.7556E+00	-0.4757E+00	0.1451E+00
5	125	117.3	0.1869	-0.1084E-01	-0.1356E+01	0.7364E+00	-0.5557E+00	0.1862E+00
5	78	125.0	0.1991	-0.1634E-01	-0.1334E+01	0.7952E+00	-0.7006E+00	0.2565E+00
5	31	124.2	0.1958	-0.1337E-01	-0.1299E+01	0.7155E+00	-0.6855E+00	0.2825E+00
2	31	82.2	0.1355	-0.1012E-01	-0.1398E+01	0.9496E+00	-0.8481E+00	0.3079E+00
2	77	77.6	0.1301	-0.1777E-01	-0.1371E+01	0.8774E+00	-0.8087E+00	0.3202E+00
2	127	78.2	0.1363	-0.1906E-01	-0.1491E+01	0.1160E+01	-0.1050E+01	0.3997E+00
2	176	62.5	0.1186	-0.1678E-01	-0.1351E+01	0.5207E+00	-0.2195E+00	0.6718E-01
2	202	62.6	0.1245	-0.2046E-01	-0.1343E+01	0.5092E+00	-0.1957E+00	0.4993E-01
2	178	62.6	0.1220	-0.1836E-01	-0.1353E+01	0.4950E+00	-0.1236E+00	
2	129	99.4	0.1732	-0.2190E-01	-0.1534E+01	0.1271E+01	-0.1135E+01	0.4199E+00
2	76	82.7	0.1421	-0.2452E-01	-0.1356E+01	0.7830E+00	-0.6418E+00	0.2399E+00
2	27	82.0	0.1396	-0.2894E-01	-0.1303E+01	0.6926E+00	-0.5675E+00	0.2073E+00
57	26	215.5	0.3355	-0.3926E-01	-0.1123E+01	0.1643E+00		
57	76	217.0	0.3399	-0.2641E-01	-0.1173E+01	0.2036E+00		
57	125	201.6	0.3278	-0.4108E-01	-0.1190E+01	0.2367E+00		
57	176	150.7	0.2564	-0.3494E-01	-0.1249E+01	0.2894E+00		
57	199	150.5	0.2635	-0.8460E-01	-0.9562E+00			
57	175	150.4	0.2534	-0.2143E-01	-0.1270E+01	0.2987E+00		
57	127	201.6	0.3353	-0.5164E-01	-0.1184E+01	0.2396E+00		
57	76	216.9	0.3521	-0.3572E-01	-0.1194E+01	0.2338E+00		
57	27	215.7	0.3416	-0.2753E-01	-0.1187E+01	0.2171E+00		

E02 4.38-4.57 TANGENT YOUNG'S MODULUS LOADING

CONF PRES (MPa)	TEMP (deg C)	MAX DEV STRESS (MPa)	MAX AXIAL STRAIN x 10E-2	POLYNOMIAL COEFFICIENTS F0	F1	F2	F3	F4
55	123	178.4	0.2238	0.3011E-01	-0.1023E+01			
55	172	133.4	0.1665	0.2659E-01	-0.1021E+01			
55	197	132.9	0.1755	0.1842E-01	-0.1011E+01			
55	170	133.2	0.1706	0.2555E-01	-0.1024E+01			
55	123	178.4	0.2297	0.2053E-01	-0.1016E+01			
55	73	191.3	0.2484	0.2084E-01	-0.1017E+01			
55	25	189.6	0.2458	0.2458E-01	-0.1020E+01			
30	25	168.4	0.2273	0.7088E-02	-0.1005E+01			
30	72	170.0	0.2280	0.5448E-02	-0.1006E+01			
30	123	160.0	0.2169	-0.4145E-02	-0.9983E+00			
30	170	122.6	0.1777	-0.1659E-01	-0.9941E+00			
30	193	122.5	0.1781	-0.2049E-01	-0.9902E+00			
30	170	122.6	0.1743	-0.1430E-01	-0.9953E+00			
30	122	159.3	0.2197	-0.2033E-02	-0.1035E+01	0.3892E-01		
30	74	169.9	0.2309	0.2078E-02	-0.1001E+01			
30	24	168.4	0.2300	0.6259E-02	-0.1005E+01			
15	22	149.1	0.2153	-0.2022E-02	-0.1058E+01	0.6190E-01		
15	72	150.6	0.2159	0.2056E-02	-0.1148E+01	0.2856E+00	-0.1398E+00	
15	121	142.1	0.2069	-0.6340E-02	-0.1085E+01	0.9639E-01		
15	169	103.4	0.1591	0.8634E-02	-0.1209E+01	0.3046E+00	-0.1038E+00	
15	194	103.0	0.1622	0.7528E-02	-0.1193E+01	0.2575E+00	-0.7211E-01	
15	172	104.6	0.1626	0.2376E-02	-0.1165E+01	0.1668E+00		
15	122	141.1	0.2026	-0.6870E-02	-0.1080E+01	0.8951E-01		
15	71	150.0	0.2122	-0.3525E-02	-0.1045E+01	0.5094E-01		
15	22	149.5	0.2156	-0.4648E-02	-0.1039E+01	0.4473E-01		
5	21	108.1	0.1678	-0.2739E-02	-0.1139E+01	0.1457E+00		
5	74	111.0	0.1746	-0.5992E-02	-0.1171E+01	0.1839E+00		
5	122	103.1	0.1678	-0.3376E-02	-0.1207E+01	0.2166E+00		
5	172	84.8	0.1456	0.3320E-02	-0.1194E+01	0.1921E+00		
5	195	81.8	0.1440	0.2859E-02	-0.1145E+01	0.1021E+00	0.4071E-01	
5	172	81.7	0.1420	0.1601E-02	-0.1178E+01	0.4292E-01	0.3119E+00	-0.1794E+00
5	123	103.6	0.1698	-0.4781E-02	-0.1207E+01	0.2188E+00		
5	74	109.7	0.1734	-0.7766E-02	-0.1174E+01	0.1893E+00		
5	24	108.2	0.1717	-0.5682E-02	-0.1162E+01	0.1739E+00		
2	23	71.6	0.1208	0.2939E-02	-0.1233E+01	0.3184E+00	-0.8787E-01	
2	73	72.3	0.1258	-0.1724E-03	-0.1325E+01	0.5001E+00	-0.1742E+00	
2	125	68.1	0.1236	0.1798E-02	-0.1226E+01	0.7740E-02	0.5449E+00	-0.3283E+00
2	172	58.1	0.1108	0.4700E-02	-0.1139E+01	0.7498E-01	0.6125E-01	
2	196	54.6	0.1072	0.5377E-02	-0.1123E+01	0.1176E+00		
2	171	54.8	0.1064	0.3117E-02	-0.1151E+01	0.1066E+00	0.4317E-01	
2	124	67.9	0.1249	0.3437E-02	-0.1336E+01	0.4819E+00	-0.1484E+00	
2	71	72.0	0.1270	-0.2663E-02	-0.1248E+01	0.2569E+00		
2	25	71.8	0.1225	0.2903E-02	-0.1267E+01	0.3880E+00	-0.1220E+00	

E02 4.38-4.57 TANGENT YOUNG'S MODULUS UNLOADING

CONF PRES (MPa)	TEMP (deg C)	MAX DEV STRESS (MPa)	MAX AXIAL STRAIN x 10E-2	POLYNOMIAL COEFFICIENTS F0	F1	F2	F3	F4
55	123	178.4	0.2238	-0.3826E-02	-0.1003E+01			
55	172	133.4	0.1665	0.7966E-03	-0.1013E+01			
55	197	132.9	0.1755	-0.4016E-01	-0.9788E+00			
55	170	133.2	0.1706	-0.1134E-01	-0.1018E+01			
55	123	178.4	0.2297	-0.1205E-01	-0.1009E+01			
55	73	191.3	0.2484	-0.1094E-01	-0.1009E+01			
55	25	189.6	0.2458	-0.1022E-01	-0.1014E+01			
30	25	168.4	0.2273	-0.1349E-01	-0.9939E+00			
30	72	170.0	0.2280	-0.9504E-02	-0.9987E+00			
30	123	160.0	0.2169	-0.1765E-01	-0.9921E+00			
30	170	122.6	0.1777	-0.4872E-01	-0.9684E+00			
30	193	122.5	0.1781	-0.4261E-01	-0.9783E+00			
30	170	122.6	0.1743	-0.2628E-01	-0.9910E+00			
30	122	158.9	0.2157	-0.3602E-02	-0.9992E+00			
30	74	169.9	0.2309	-0.1319E-01	-0.1039E+01	0.5192E-01		
30	24	168.4	0.2300	-0.1886E-01	-0.9914E+00			
15	22	149.1	0.2153	-0.1307E-01	-0.1096E+01	0.1123E+00		
15	72	150.6	0.2159	-0.1839E-01	-0.1094E+01	0.1158E+00		
15	121	142.1	0.2069	-0.1582E-01	-0.1135E+01	0.1580E+00		
15	169	103.4	0.1591	-0.4451E-02	-0.1211E+01	0.2223E+00		
15	194	103.0	0.1622	-0.9890E-02	-0.1212E+01	0.2266E+00		
15	172	104.6	0.1626	-0.1451E-01	-0.1199E+01	0.2192E+00		
15	122	141.1	0.2026	-0.4950E-02	-0.1158E+01	0.1693E+00		
15	71	150.0	0.2122	-0.8750E-02	-0.1095E+01	0.1078E+00		
15	22	149.5	0.2156	-0.1772E-01	-0.1089E+01	0.1105E+00		
5	21	108.1	0.1678	-0.1248E-01	-0.1203E+01	0.2221E+00		
5	74	111.0	0.1746	-0.2142E-01	-0.1212E+01	0.2431E+00		
5	122	103.1	0.1678	-0.1301E-01	-0.1506E+01	0.1235E+01	-0.1110E+01	0.3940E+00
5	172	84.8	0.1456	-0.7055E-02	-0.1385E+01	0.6400E+00	-0.3088E+00	0.5995E-01
5	195	81.8	0.1440	-0.1104E-01	-0.1367E+01	0.6344E+00	-0.3533E+00	0.9730E-01
5	172	81.7	0.1420	-0.4377E-01	-0.1159E+01	0.2020E+00		
5	123	103.6	0.1698	-0.2412E-01	-0.1241E+01	0.2706E+00		
5	74	109.7	0.1734	-0.2684E-01	-0.1202E+01	0.2374E+00		
5	24	108.2	0.1717	-0.2744E-01	-0.1189E+01	0.2248E+00		
2	23	71.6	0.1208	-0.3588E-02	-0.1443E+01	0.9002E+00	-0.6341E+00	0.1805E+00
2	73	72.3	0.1258	-0.1436E-01	-0.1539E+01	0.1206E+01	-0.9569E+00	0.3043E+00
2	125	68.1	0.1236	-0.1499E-01	-0.1472E+01	0.8976E+00	-0.5597E+00	0.1488E+00
2	172	58.1	0.1108	-0.1235E-01	-0.1308E+01	0.4333E+00	-0.1690E+00	0.5712E-01
2	196	54.6	0.1072	-0.1795E-01	-0.1275E+01	0.3590E+00	-0.6536E-01	
2	171	54.8	0.1064	-0.1007E-01	-0.1322E+01	0.4358E+00	-0.1025E+00	
2	124	67.9	0.1249	-0.2397E-01	-0.1456E+01	0.8903E+00	-0.5675E+00	0.1568E+00
2	71	72.0	0.1270	-0.2471E-01	-0.1512E+01	0.1150E+01	-0.8936E+00	0.2800E+00
2	25	71.8	0.1225	-0.2196E-01	-0.1330E+01	0.3740E+00		

E03 0.26-0.45 TANGENT YOUNG'S MODULUS LOADING

CONF PRES (MPa)	TEMP (deg C)	MAX DEV STRESS (MPa)	MAX AXIAL STRAIN x 10E-2	POLYNOMIAL COEFFICIENTS F0	F1	F2	F3	F4
55	21	187.9	0.2626	0.8218E-02	-0.1003E+01			
55	76	191.1	0.2632	0.1593E-01	-0.1010E+01			
55	125	178.1	0.2434	0.1977E-01	-0.1014E+01			
55	173	128.7	0.1716	0.2303E-01	-0.1014E+01			
55	122	194.3	0.1584	-0.1935E+00	-0.8626E+00			
55	76	198.1	0.2543	-0.4642E-01	-0.8853E+00			
55	27	200.7	0.2517	-0.3817E-01	-0.9176E+00			
30	26	168.2	0.2327	0.1264E-01	-0.1006E+01			
30	76	169.0	0.2363	0.5280E-02	-0.1002E+01			
30	126	159.0	0.2225	0.5194E-02	-0.1001E+01			
30	173	122.6	0.1743	0.2231E-02	-0.1004E+01			
30	124	158.9	0.2240	0.4821E-02	-0.1001E+01			
30	75	220.9	0.2364	-0.1181E+00	-0.9244E+00			
30	28	221.1	0.2345	-0.1123E+00	-0.9427E+00			
15	27	150.3	0.2131	0.2518E-02	-0.9832E+00	-0.1813E-01		
15	76	151.9	0.2181	0.3371E-03	-0.9904E+00	-0.9194E-02		
15	124	143.0	0.2084	0.9354E-03	-0.1022E+01	0.3296E-01	-0.1014E-01	
15	173	104.3	0.1585	0.3728E-02	-0.1053E+01	0.4894E-01		
15	125	143.1	0.2110	0.1343E-03	-0.1060E+01	0.9598E-01	-0.3587E-01	
15	75	151.6	0.2196	-0.1534E-02	-0.9986E+00			
15	27	150.3	0.2141	0.5761E-02	-0.1005E+01			
5	21	109.3	0.1655	-0.1007E-02	-0.1060E+01	0.6368E-01		
5	75	110.1	0.1690	-0.1106E-01	-0.9944E+00			
5	126	103.9	0.1622	0.1653E-02	-0.1098E+01	0.1284E+00	-0.3104E-01	
5	172	73.0	0.1234	0.8967E-03	-0.1109E+01	0.1185E+00	-0.8839E-02	
5	125	103.9	0.1672	-0.2242E-02	-0.1125E+01	0.1316E+00		
5	76	110.4	0.1713	-0.2746E-02	-0.1105E+01	0.1123E+00		
5	27	109.1	0.1646	0.7364E-04	-0.1067E+01	0.7002E-01		
2	27	72.7	0.1154	0.3677E-02	-0.1133E+01	0.1918E+00	-0.6190E-01	
2	76	72.8	0.1201	0.2222E-02	-0.1178E+01	0.2601E+00	-0.8338E-01	
2	125	68.5	0.1183	0.1451E-02	-0.1129E+01	0.1184E+00	0.1222E-01	
2	172	55.3	0.1004	0.5964E-02	-0.1088E+01	0.7880E-01		
2	124	87.5	0.1472	-0.9139E-04	-0.1181E+01	0.1862E+00		
2	76	74.8	0.1235	-0.2583E-03	-0.1157E+01	0.1614E+00		
2	26	72.3	0.1175	0.1848E-03	-0.1141E+01	0.1455E+00		
30	27	168.6	0.2344	0.9160E-02	-0.1002E+01			
30	76	169.7	0.2379	0.7183E-02	-0.1003E+01			
30	125	159.2	0.2240	0.2644E-02	-0.1001E+01			
30	124	158.8	0.2213	0.7417E-02	-0.1004E+01			
30	74	169.4	0.2366	0.7911E-02	-0.1004E+01			
30	26	167.5	0.2313	0.1057E-01	-0.1005E+01			

E03 0.26-0.45 TANGENT YOUNG'S MODULUS UNLOADING

CONF PRES (MPa)	TEMP (deg C)	MAX DEV STRESS (MPa)	MAX AXIAL STRAIN x 10E-2	POLYNOMIAL COEFFICIENTS F0	F1	F2	F3	F4
55	21	195.8	0.2626	-0.8514E-01	-0.8392E+00			
55	76	191.1	0.2632	-0.2372E-01	-0.9892E+00			
55	125	178.1	0.2434	-0.1956E-01	-0.9908E+00			
55	173	132.9	0.1779	-0.1524E-01	-0.9973E+00			
55	122	128.1	0.1702	0.2331E-02	-0.1104E+01	0.9596E-01		
55	76	187.5	0.2543	-0.8938E-02	-0.1009E+01			
55	27	200.6	0.2517	-0.6860E-01	-0.8876E+00			
30	26	223.7	0.2327	-0.8601E-01	-0.1013E+01			
30	76	169.0	0.2363	-0.2205E-01	-0.9904E+00			
30	126	159.0	0.2225	-0.2389E-01	-0.9894E+00			
30	173	122.6	0.1743	-0.3119E-01	-0.9862E+00			
30	124	158.9	0.2240	-0.2924E-01	-0.9845E+00			
30	75	169.1	0.2364	-0.1972E-01	-0.9929E+00			
30	28	167.8	0.2345	-0.2031E-01	-0.9917E+00			
15	27	236.9	0.2131	-0.1278E+00	-0.1049E+01			
15	76	151.9	0.2181	-0.1144E-01	-0.1091E+01	0.1038E+00		
15	124	143.0	0.2084	-0.1680E-01	-0.1108E+01	0.1264E+00		
15	173	104.3	0.1585	-0.1621E-01	-0.1158E+01	0.1765E+00		
15	125	143.1	0.2110	-0.2218E-01	-0.1119E+01	0.1431E+00		
15	75	151.6	0.2196	-0.3365E-01	-0.9840E+00			
15	27	150.3	0.2141	-0.1905E-01	-0.9965E+00			
5	21	109.3	0.1655	-0.9671E-02	-0.1244E+01	0.4174E+00	-0.1655E+00	
5	75	110.1	0.1690	-0.1414E-01	-0.1319E+01	0.7684E+00	-0.6868E+00	0.2514E+00
5	126	103.9	0.1622	-0.7001E-02	-0.1366E+01	0.8387E+00	-0.7402E+00	0.2744E+00
5	172	73.0	0.1234	-0.4924E-01	-0.1206E+01	0.3660E+00	-0.1110E+00	
5	125	103.9	0.1672	-0.2959E-01	-0.1198E+01	0.2345E+00		
5	76	110.4	0.1713	-0.2652E-01	-0.1157E+01	0.1892E+00		
5	27	109.1	0.1646	-0.2631E-01	-0.9968E+00			
2	27	72.7	0.1154	-0.2407E-02	-0.1362E+01	0.7807E+00	-0.6542E+00	0.2387E+00
2	76	72.8	0.1201	-0.2550E-01	-0.1217E+01	0.2496E+00		
2	125	68.5	0.1183	-0.2008E-01	-0.1344E+01	0.5586E+00	-0.1947E+00	
2	172	55.3	0.1004	-0.1310E-01	-0.1279E+01	0.3716E+00	-0.7088E-01	-0.8956E-02
2	124	87.5	0.1472	-0.3130E-01	-0.1238E+01	0.2761E+00		
2	76	74.8	0.1235	-0.2400E-01	-0.1394E+01	0.9067E+00	-0.7445E+00	0.2559E+00
2	26	72.3	0.1175	-0.2160E-01	-0.1376E+01	0.8938E+00	-0.7788E+00	0.2828E+00
30	27	168.6	0.2344	-0.1489E-01	-0.1000E+01			
30	76	169.7	0.2379	-0.2540E-01	-0.9903E+00			
30	125	159.2	0.2240	-0.2929E-01	-0.9878E+00			
30	124	158.8	0.2213	-0.2033E-01	-0.9942E+00			
30	74	169.4	0.2366	-0.2566E-01	-0.9890E+00			
30	26	167.5	0.2313	-0.1766E-01	-0.9943E+00			

E17 6.04-6.22 TANGENT YOUNG'S MODULUS LOADING

Conf Pres (MPa)	TEMP (des C)	MAX DEV STRESS (MPa)	MAX AXIAL STRAIN x 10E-2	Polynomial Coefficients F_0	F_1	F_2	F_3	F_4
55	20	210.4	.2746	$.4220\times10^{-2}$	$-.1006\times10^{1}$	--	--	--
55	73	137.6	.1744	$.2491\times10^{-1}$	$-.1021\times10^{1}$	--	--	--
55	123	118.1	.1499	$.1578\times10^{-1}$	$-.1018\times10^{1}$			
55	170	86.3	.1098	$.2510\times10^{-1}$	$-.1024\times10^{1}$			
55	194	83.3	.1058	$.3448\times10^{-1}$	$-.1034\times10^{1}$			
55	170	83.2	.1082	$-.5153\times10^{-2}$	-.9957			
55	123	120.2	.1558	$.1660\times10^{-2}$	-.9984			
55	74	132.1	.1709	$.3873\times10^{-2}$	$-.1000\times10^{1}$			
55	23	130.7	.1684	$.2075\times10^{-1}$	$-.1017\times10^{1}$			
30	73	126.6	.1651	$.2877\times10^{-2}$	$-.1006\times10^{1}$			
30	123	115.6	.1505	$.8294\times10^{-2}$	$-.1011\times10^{1}$			
30	170	85.7	.1163	$.5390\times10^{-2}$	$-.1010\times10^{1}$			
30	194	85.5	.1212	$.7489\times10^{-2}$	$-.1013\times10^{1}$			
30	170	85.7	.1205	$-.3954\times10^{-2}$	$-.1006\times10^{1}$			
30	125	115.5	.1609	$-.3492\times10^{-1}$	-.9709			
30	74	125.5	.1682	$-.4207\times10^{-2}$	-.9981			
30	23	125.5	.2685	$.2929\times10^{-2}$	$-.1007\times10^{1}$			
15	73	115.1	.1594	$.5273\times10^{-2}$	$-.1085\times10^{1}$	$.8289\times10^{-1}$		
15	122	98.0	.1531	$.8252\times10^{-2}$	$-.1109\times10^{1}$	.1030		
15	168	77.1	.1184	$.5935\times10^{-2}$	$-.1094\times10^{1}$	$.8637\times10^{-1}$		
15	195	76.4	.1278	$-.1228\times10^{-2}$	$-.1064\times10^{1}$	$-.1434\times10^{1}$	$.7934\times10^{-1}$	
15	171	76.0	.1248	$.2467\times10^{-2}$	$-.1143\times10^{1}$	.1417		
15	123	107.3	.1667	$.8447\times10^{-2}$	$-.1200\times10^{1}$	.2727	-.8071x10-1	
15	75	116.3	.1769	$.8951\times10^{-2}$	$-.1172\times10^{1}$	.2351	-.7143x10-1	
15	26	116.1	.1776	$.2793\times10^{-2}$	$-.1112\times10^{1}$	.1113		
5	26	116.9	.1814	$.5467\times10^{-2}$	$-.1294\times10^{1}$	.6747	-.6560	.2509
5	73	116.9	.1848	$.6295\times10^{-2}$	$-.1354\times10^{1}$	.8486	-.7909	.2899
5	122	108.8	.1768	$.2304\times10^{-2}$	$-.1185\times10^{1}$	.1854		
5	169	83.0	.1433	$-.2575\times10^{-2}$	$-.1180\times10^{1}$	.1846		
5	194	84.6	.1562	$.8586\times10^{-2}$	$-.1275\times10^{1}$	.3404	$-.7390\times10^{-1}$	
5	171	84.6	.1516	$.9423\times10^{-2}$	$-.1323\times10^{1}$	.4546	-.1423	
5	123	108.3	.1798	$.1023\times10^{-1}$	$-.1361\times10^{1}$	.7516	-.5441	.1787
5	74	117.0	.1904	$-.5471\times10^{-2}$	$-.1163\times10^{1}$	.1733		
5	25	117.0	.1933	$-.2128\times10^{-1}$	$-.1124\times10^{1}$	.1471		
2	23	76.0	.1334	$.1622\times10^{-3}$	$-.1180\times10^{1}$	.1830		
2	72	76.6	.1373	$.2877\times10^{-2}$	$-.1284\times10^{1}$	.3925	-.1117	
2	121	69.0	.1260	$.2072\times10^{-2}$	$-.1391\times10^{1}$	.8200	-.6769	.2451
2	170	55.5	.1221	$.2567\times10^{-2}$	$-.1192\times10^{1}$	.1482	$.4312\times10^{-1}$	
2	194	54.7	.1148	$.8727\times10^{-2}$	$-.1219\times10^{1}$	.2101		
2	169	55.0	.1139	$.6370\times10^{-2}$	$-.1274\times10^{1}$	.3030	$-.3487\times10^{-1}$	
2	124	71.7	.1513	$-.0121\times10^{-2}$	$-.1025\times10^{1}$	$.5299\times10^{-1}$		
2	74	76.4	.1431	$.1537\times10^{-2}$	$-.1321\times10^{1}$	.4743	-.1550	
2	26	76.6	.1400	.5323x10-2	-.1261x101	.3422	-.8684x10-1	

E17 6.04-6.22 TANGENT YOUNG'S MODULUS UNLOADING

Conf Pres (MPa)	TEMP (des C)	MAX DEV STRESS (MPa)	MAX AXIAL STRAIN x 10E-2	Polynomial Coefficients F_0	F_1	F_2	F_3	F_4
55	20	210.4	.2746	$-.9837\times10^{-2}$	-.9951			
55	73	137.6	.1744	$-.3628\times10^{-2}$	$-.1005\times10^{1}$			
55	122	118.1	.1499	$-.1293\times10^{-1}$	-.9929			
55	170	86.3	.1098	$-.1165\times10^{-1}$	$-.1000\times10^{1}$			
55	194	83.3	.1058	$-.1010\times10^{-1}$	$-.1006\times10^{1}$			
55	170	83.2	.1082	$-.3624\times10^{-1}$	-.9797			
55	123	117.6	.1496	$-.5384\times10^{2}$	$-.1000\times10^{1}$			
55	74	132.1	.1709	-.2406x10-1	-.9838			
55	23	130.7	.1684	$-.1231\times10^{-1}$	-.9955			
30	73	126.6	.1651	$-.1671\times10^{-1}$	$-.9917\times10^{1}$			
30	123	115.6	.1505	$-.9587\times10^{-2}$	-.9990			
30	170	85.6	.1163	$-.1924\times10^{-1}$	-.9916			
30	194	85.5	.1212	$-.2770\times10^{-1}$	-.9869			
30	170	85.7	.1205	$-.2696\times10^{-1}$	-.9898			
30	125	115.5	.1609	$-.6343\times10^{-1}$	-.9455			
30	74	125.5	.1682	$-.2681\times10^{-1}$	-.9803			
30	23	125.5	.1685	$-.1934\times10^{-1}$	-.9904			
15	73	115.1	.1594					
15	122	108.0	.1531	$-.5633\times10^{-2}$	$-.1172\times10^{1}$	.2407	$-.6325\times10^{1}$	
15	168	77.1	.1184	$-.1275\times10^{-1}$	$-.1156\times10^{1}$	.1688		
15	195	76.4	.1278	$-.6038\times10^{-1}$	-.9589			
15	171	76.0	.1248	$-.1560\times10^{-1}$	$-.1258\times10^{1}$	.3800	-.1067	
15	123	107.3	.1667	$-.1190\times10^{-1}$	$-.1251\times10^{1}$	.3810	-.1195	
15	75	116.3	.1769	$-.1105\times10^{-1}$	$-.1170\times10^{1}$	.1839		
15	26	116.1	.1776	$-.2920\times10^{-1}$	$-.1123\times10^{1}$	.1546		
5	26	116.9	.1814	$-.1942\times10^{-1}$	$-.1188\times10^{1}$	-.2126		
5	73	116.9	.1848	$-.3554\times10^{-1}$	$-.1142\times10^{1}$	.1815		
5	122	108.8	.1768	$-.2417\times10^{-1}$	$-.1223\times10^{1}$	.2523		
5	169	83.0	.1433	$-.4234\times10^{-2}$	$-.14078\times10^{1}$	.6253	-.2149	
5	194	84.6	.1562	$-.1104\times10^{-1}$	$-.1411\times10^{1}$	.5609	$-.9537\times10^{-1}$	$-.4410\times10^{-1}$
5	171	84.6	.1516	$-.1306\times10^{-2}$	$-.1571\times10^{1}$	$.1218\times10^{1}$	$-.1003\times10^{1}$	.3572
5	123	108.3	.1798	$-.1996\times10^{-1}$	-.1250x101	.2760		
5	74	117.0	.1904	$-.1047\times10^{-1}$	$-.1471\times10^{1}$	$.1161\times10^{1}$	$-.1071\times10^{1}$	.3927
5	25	117.0	.1933	$-.5546\times10^{-1}$	-.1355 10^{1}	.1938		
2	23	76.0	.1334	$-.1214\times10^{-1}$	$-.1563\times10^{1}$	$.1447\times10^{-1}$	$-.440\times10^{1}$	.5678
2	72	76.6	.1373	$-.2484\times10^{-1}$	$-.1525\times10^{1}$	$.1282\times10^{1}$	$-.1165\times10^{1}$	.4320
2	121	69.0	.1260	$-.2030\times10^{-1}$	$-.1523\times10^{1}$	$.1168\times10^{1}$	-.9504	.3252
2	170	55.5	.1121	$-.8637\times10^{-2}$	$-.1354\times10^{1}$	.3778	$.8277\times10^{-1}$	$-.9802\times10^{-1}$
2	194	54.7	.1282	$-.9910\times10^{-2}$	.8127	.2018		
2	169	55.0	.1139	$-.1418\times10^{-1}$	$-.1349\times10^{1}$	.3206	.1815	-.1381
2	124	71.7	.1500					
2	74	76.4	.1431	$-.4392\times10^{-1}$	$-.1496\times10^{1}$	$.1249\times10^{1}$	$-.111\times10^{1}$	.4014
2	26	76.6	.1400	$-.4110\times10^{-1}$	$-.1231\times10^{1}$	.2875		

M02 12.23-12.43 TANGENT YOUNG'S MODULUS LOADING

CONF PRES (MPa)	TEMP (deg C)	MAX DEV STRESS (MPa)	MAX AXIAL STRAIN x 10E-2	POLYNOMIAL COEFFICIENTS F0	F1	F2	F3	F4
55	19	203.9	0.2593	0.1858E-01	-0.1018E+01			
55	75	203.4	0.2614	0.6536E-02	-0.1008E+01			
55	124	187.4	0.2368	0.1476E-01	-0.1012E+01			
55	174	136.2	0.1721	0.3907E-03	-0.1002E+01			
55	198	136.0	0.1731	0.2947E-04	-0.1002E+01			
55	176	136.1	0.1737	-0.8790E-03	-0.1002E+01			
55	125	185.3	0.2356	0.2377E-02	-0.1000E+01			
55	76	200.8	0.2534	0.8035E-03	-0.1001E+01			
55	27	195.5	0.2456	0.2536E-02	-0.9990E+00			
15	26	162.7	0.2129	0.1991E-03	-0.1026E+01	0.2681E-01		
15	75	155.1	0.2049	-0.3577E-03	-0.1040E+01	0.4237E-01		
15	124	150.7	0.2051	-0.1884E-04	-0.1069E+01	0.7035E-01		
15	174	105.7	0.1545	0.1275E-02	-0.1129E+01	0.1513E+00	-0.2267E-01	
15	197	107.9	0.1627	0.1814E-02	-0.1119E+01	0.1190E+00		
15	174	108.2	0.1616	0.2736E-02	-0.1167E+01	0.2309E+00	-0.6583E-01	
15	124	150.0	0.2091	-0.2492E-02	-0.1096E+01	0.9990E-01		
15	75	162.0	0.2197	0.6713E-03	-0.1058E+01	0.5807E-01		
15	27	158.3	0.2134	0.6041E-03	-0.1054E+01	0.7395E-01	-0.2098E-01	
55	27	199.2	0.2619	-0.5398E-02	-0.9968E+00			
55	76	197.9	0.2592	-0.2276E-02	-0.9998E+00			
55	125	183.7	0.2436	-0.3215E-02	-0.1001E+01			
55	175	136.1	0.1826	-0.3063E-02	-0.1003E+01			
55	124	184.8	0.2516	-0.1084E-01	-0.9953E+00			
55	75	197.3	0.2623	-0.7494E-02	-0.9977E+00			
55	26	195.9	0.2553	-0.2403E-02	-0.9998E+00			
5	25	114.5	0.1646	-0.2771E-02	-0.1103E+01	0.1090E+00		
5	74	111.2	0.1621	0.2120E-03	-0.1231E+01	0.5067E+00	-0.4048E+00	0.1294E+00
5	123	106.9	0.1644	-0.3196E-02	-0.1165E+01	0.1725E+00		
5	171	84.1	0.1408	0.3288E-02	-0.1205E+01	0.2426E+00	-0.3991E-01	
5	195	84.0	0.1461	0.3847E-02	-0.1179E+01	0.1766E+00		
5	172	84.4	0.1440	0.3161E-02	-0.1226E+01	0.2668E+00	-0.4377E-01	
5	124	108.0	0.1710	-0.3655E-02	-0.1188E+01	0.1982E+00		
5	75	116.1	0.1757	-0.1033E-02	-0.1153E+01	0.1576E+00		
5	28	116.1	0.1724	0.2031E-02	-0.1151E+01	0.1928E+00	-0.4423E-01	
55	28	203.3	0.2815	-0.6011E-02	-0.1001E+01			
55	75	203.4	0.2874	-0.1325E-01	-0.9963E+00			
55	126	187.5	0.2749	-0.2590E-01	-0.9872E+00			
55	173	138.3	0.2110	-0.1047E-01	-0.1009E+01			
55	198	138.2	0.2109	-0.5351E-02	-0.1013E+01			

M02 12.23-12.43 TANGENT YOUNG'S MODULUS UNLOADING

CONF PRES (MPa)	TEMP (deg C)	MAX DEV STRESS (MPa)	MAX AXIAL STRAIN x 10E-2	POLYNOMIAL COEFFICIENTS F0	F1	F2	F3	F4
55	19	203.9	0.2593	-0.1137E-01	-0.9944E+00			
55	75	203.4	0.2614	-0.2097E-01	-0.9872E+00			
55	124	187.4	0.2368	-0.1275E-01	-0.9962E+00			
55	174	136.2	0.1721	-0.2033E-01	-0.9989E+00			
55	198	136.0	0.1731	-0.1901E-01	-0.9995E+00			
55	176	136.1	0.1737	-0.2460E-01	-0.9977E+00			
55	125	185.3	0.2356	-0.1813E-01	-0.9951E+00			
55	76	200.8	0.2534	-0.2667E-01	-0.9881E+00			
55	27	195.5	0.2456	-0.3287E-01	-0.9814E+00			
15	26	162.7	0.2129	-0.2475E-02	-0.1119E+01	0.1500E+00	-0.3004E-01	
15	75	155.1	0.2049	-0.9566E-02	-0.1098E+01	0.1545E+00	-0.4735E-01	
15	124	150.7	0.2051	-0.8071E-02	-0.1110E+01	0.1186E+00		
15	174	105.7	0.1545	-0.3251E-03	-0.1177E+01	0.1800E+00		
15	197	107.9	0.1627	-0.2487E-02	-0.1195E+01	0.2003E+00		
15	174	108.2	0.1616	-0.8005E-02	-0.1260E+01	0.4052E+00	-0.1379E+00	
15	124	150.0	0.2091	-0.1424E-01	-0.1162E+01	0.2658E+00	-0.9088E-01	
15	75	162.0	0.2197	-0.6302E-02	-0.1138E+01	0.1961E+00	-0.5223E-01	
15	27	158.3	0.2134	-0.1687E-01	-0.1105E+01	0.1525E+00	-0.3185E-01	
55	27	199.2	0.2619	-0.2914E-01	-0.1034E+01	0.6249E-01		
55	76	197.9	0.2592	-0.3085E-01	-0.9790E+00			
55	125	183.7	0.2436	-0.2965E-01	-0.9795E+00			
55	175	136.1	0.1826	-0.2441E-01	-0.9948E+00			
55	124	184.8	0.2516	-0.3778E-01	-0.9848E+00			
55	75	197.3	0.2623	-0.3621E-01	-0.9859E+00			
55	26	195.9	0.2553	-0.3394E-01	-0.9909E+00			
5	25	114.5	0.1646	-0.1437E-01	-0.1299E+01	0.7632E+00	-0.7408E+00	0.2909E+00
5	74	111.2	0.1621	-0.2139E-01	-0.1271E+01	0.7094E+00	-0.6976E+00	0.2810E+00
5	123	106.9	0.1644	-0.1077E-01	-0.1399E+01	0.9071E+00	-0.7669E+00	0.2693E+00
5	171	84.1	0.1408	-0.7865E-02	-0.1335E+01	0.4911E+00	-0.1489E+00	
5	195	84.0	0.1461	-0.1092E-01	-0.1339E+01	0.4921E+00	-0.1425E+00	
5	172	84.4	0.1440	-0.1506E-01	-0.1364E+01	0.6120E+00	-0.3049E+00	0.7140E-01
5	124	108.0	0.1710	-0.2531E-01	-0.1211E+01	0.2407E+00		
5	75	116.1	0.1757	-0.1143E-01	-0.1334E+01	0.7496E+00	-0.6420E+00	0.2364E+00
5	28	116.1	0.1724	-0.1622E-01	-0.1306E+01	0.7573E+00	-0.7308E+00	0.2957E+00
55	28	203.3	0.2815	-0.3110E-01	-0.9874E+00			
55	75	203.4	0.2874	-0.3764E-01	-0.9784E+00			
55	126	187.5	0.2749	-0.5177E-01	-0.9716E+00			
55	173	138.3	0.2110	-0.5023E-01	-0.9692E+00			
55	198	138.2	0.2109	-0.3926E-01	-0.9847E+00			

Table B2.

E01 9.74-9.93 TANGENT POISSON'S RATIO LOADING

CONF PRES (MPa)	TEMP (deg C)	MAX DEV STRESS (MPa)	MAX RADIAL STRAIN x 10E-3	POLYNOMIAL COEFFICIENTS F0	F1	F2	F3	F4
55	24	149.9	0.4568	-0.4536E-01	0.1033E+01			
55	74	151.3	0.4543	-0.2816E-01	0.1018E+01			
55	126	139.2	0.4055	-0.4024E-01	0.1036E+01			
55	174	102.1	0.2894	-0.4533E-01	0.1043E+01			
55	198	102.3	0.2894	-0.2273E-01	0.1024E+01			
55	174	102.1	0.3029	-0.1947E-01	0.1020E+01			
55	126	133.5	0.4030	-0.1247E-01	0.1015E+01			
55	76	151.1	0.4653	-0.2986E-01	0.1032E+01			
55	21	151.2	0.4739	-0.3007E-01	0.1022E+01			
15	20	119.9	0.3896	-0.6564E-04	0.9536E+00	0.4656E-01		
15	74	112.0	0.3554	0.9942E-02	0.9492E+00	0.3934E-01		
15	124	112.1	0.3468	0.7470E-03	0.9781E+00	0.2050E-01		
15	174	81.2	0.2711	-0.8421E-03	0.1003E+01			
15	199	78.3	0.2601	0.6146E-02	0.9895E+00			
15	174	81.1	0.2809	0.7604E-02	0.1093E+01	-0.1017E+00		
15	124	113.0	0.4543	0.7964E-02	0.1231E+01	-0.2514E+00		
15	76	117.7	0.4555	0.7301E-02	0.1163E+01	-0.1741E+00		
15	27	121.2	0.4543	0.1121E-02	0.1114E+01	-0.1173E+00		
5	26	116.7	0.4213	0.2785E-02	0.1057E+01	-0.6541E-01		
5	74	117.6	0.4470	0.1143E-01	0.1156E+01	-0.1745E+00		
5	124	110.0	0.4250	0.1833E-01	0.1194E+01	-0.2186E+00		
5	172	87.1	0.3236	0.1559E-01	0.1152E+01	-0.1707E+00		
5	198	86.3	0.2919	0.1008E-02	0.9896E+00	-0.6805E-01	0.7959E-01	
5	173	86.8	0.3151	-0.2192E-02	0.1077E+01	-0.7484E-01		
5	125	109.7	0.4702	0.1641E-01	0.1305E+01	-0.3350E+00		
5	74	117.8	0.5142	0.1988E-01	0.1312E+01	-0.3442E+00		
5	27	117.2	0.5081	0.6619E-04	0.1421E+01	-0.8640E+00	0.6636E+00	-0.2216E+00
55	28	152.7	0.6277	0.2966E-01	0.9900E+00			
55	73	152.1	0.6461	0.4103E-01	0.9870E+00			
55	124	140.3	0.6302	0.7512E-01	0.9595E+00			
55	172	102.1	0.4910	0.4802E-01	0.1018E+01			
55	198	101.1	0.4885	0.5321E-01	0.1007E+01			
55	175	101.1	0.4836	0.8047E-01	0.9631E+00			
55	125	138.1	0.5960	0.6852E-01	0.9500E+00			
55	75	152.3	0.6693	0.5747E-01	0.9692E+00			
55	23	146.6	0.6424	0.3759E-01	0.9809E+00			

E01 9.74-9.93 TANGENT POISSON'S RATIO UNLOADING

CONF PRES (MPa)	TEMP (deg C)	MAX DEV STRESS (MPa)	MAX RADIAL STRAIN x 10E-3	POLYNOMIAL COEFFICIENTS F0	F1	F2	F3	F4
55	24	149.9	0.4568	0.1152E-01	0.9920E+00			
55	74	151.3	0.4543	0.6931E-02	0.9933E+00			
55	126	139.2	0.4055	-0.1711E-01	0.1018E+01			
55	174	102.1	0.2894	-0.4955E-02	0.1006E+01			
55	198	102.3	0.2894	-0.1742E-01	0.1021E+01			
55	174	102.1	0.3029	0.1332E-01	0.9878E+00			
55	126	133.5	0.4030	0.1714E-01	0.9838E+00			
55	76	151.1	0.4653	0.2612E-01	0.9730E+00			
55	21	151.2	0.4739	0.2047E-01	0.9821E+00			
15	20	119.9	0.3896	0.3688E-01	0.9795E+00	-0.1731E-01		
15	74	112.0	0.3554	0.2073E-01	0.1021E+01	-0.4330E-01		
15	124	112.1	0.3468	0.3239E-01	0.9735E+00			
15	174	81.2	0.2711	0.7637E-01	0.9909E+00	-0.6705E-01		
15	199	78.3	0.2601	0.5945E-01	0.9413E+00			
15	174	81.1	0.2809	0.1627E-01	0.9992E+00			
15	124	113.0	0.4543	0.2999E-01	0.1243E+01	-0.2796E+00		
15	76	117.7	0.4555	0.4052E-01	0.1173E+01	-0.2207E+00		
15	27	121.2	0.4543	0.2025E-01	0.1176E+01	-0.1987E+00		
5	26	116.7	0.4213	0.2277E-01	0.1065E+01	-0.9012E-01		
5	74	117.6	0.4470	0.3698E-01	0.1093E+01	-0.1333E+00		
5	124	110.0	0.4250	0.1653E-01	0.1136E+01	-0.1526E+00		
5	172	87.1	0.3236	0.8010E-01	0.8443E+00	0.7995E-01		
5	198	86.3	0.2919	0.7142E-01	0.7834E+00	0.1455E+00		
5	173	86.8	0.3151	-0.2248E-01	0.6284E+00	0.1089E+01	-0.1001E+01	0.3042E+00
5	125	109.7	0.4702	-0.9911E-02	0.1290E+01	-0.2860E+00		
5	74	117.8	0.5142	0.3236E-01	0.1263E+01	-0.3033E+00		
5	27	117.2	0.5081	0.5075E-01	0.1199E+01	-0.2543E+00		
55	28	152.7	0.6253	0.7496E-01	0.9470E+00			
55	73	152.1	0.6461	0.8381E-01	0.9433E+00			
55	124	140.3	0.6302	0.9446E-01	0.9354E+00			
55	172	102.1	0.4910	0.6108E-01	0.9733E+00			
55	198	101.1	0.4885	0.3420E-01	0.1009E+01			
55	175	101.1	0.4836	0.6296E-01	0.9776E+00			
55	125	138.1	0.5960	0.6322E-01	0.9711E+00			
55	75	152.3	0.6693	0.1068E+00	0.9155E+00			
55	23	146.6	0.6424	0.1165E+00	0.9076E+00			

E02 0.32-0.51 TANGENT POISSON'S RATIO LOADING

CONF PRES (MPa)	TEMP (deg C)	MAX DEV STRESS (MPa)	MAX RADIAL STRAIN x 10E-3	POLYNOMIAL COEFFICIENTS F0	F1	F2	F3	F4
57	17	215.2	0.6425	-0.3884E-01	0.1023E+01			
57	75	208.8	0.6125	-0.1760E-01	0.9087E+00	0.1114E+00		
57	126	202.1	0.5925	-0.9967E-02	0.9436E+00	0.6395E-01		
57	175	151.1	0.4262	-0.1996E-01	0.9424E+00	0.7430E-01		
57	201	150.9	0.4150	-0.1240E-01	0.9289E+00	0.8263E-01		
57	177	150.7	0.4200	-0.8315E-02	0.9232E+00	0.8575E-01		
57	128	201.0	0.5825	-0.2812E-01	0.1014E+01			
57	77	216.9	0.6388	-0.1806E-01	0.9838E+00			
57	29	215.7	0.6488	0.1071E+03	-0.2303E+00			
31	28	191.5	0.5950	-0.5826E-02	0.8909E+00	0.1149E+00		
31	77	192.7	0.5850	-0.1112E-01	0.9219E+00	0.9002E-01		
31	128	180.4	0.5313	-0.1137E-01	0.9176E+00	0.9480E-01		
31	177	139.2	0.3950	-0.1451E-01	0.9222E+00	0.9296E-01		
31	203	139.2	0.3975	-0.1559E-01	0.9323E+00	0.8376E-01		
31	179	139.2	0.4000	-0.6737E-02	0.9602E+00	0.4705E-01		
31	129	180.8	0.5513	-0.1390E-01	0.1008E+01			
31	78	192.6	0.6013	-0.2024E-01	0.1008E+01			
31	27	191.3	0.6200	-0.9403E-02	0.9294E+00	0.7746E-01		
15	26	171.3	0.5637	-0.8545E-02	0.9127E+00	0.9812E-01		
15	75	160.6	0.5423	-0.5935E-03	0.9565E+00	0.4025E-01		
15	128	162.6	0.5000	-0.1863E-01	0.9572E+00	0.6414E-01		
15	177	118.4	0.3663	-0.2155E-01	0.1035E+01	-0.1387E-01		
15	202	118.4	0.3600	-0.5922E-02	0.9854E+00	0.1853E-01		
15	175	118.3	0.3563	-0.6288E-02	0.1009E+01			
15	128	162.3	0.5562	-0.1376E-01	0.1164E+01	-0.2510E+00	0.1012E+00	
15	77	172.6	0.5988	-0.8801E-02	0.1135E+01	-0.1977E+00	0.7125E-01	
15	19	171.0	0.6125	0.6354E-02	0.9937E+00			
5	18	124.2	0.4250	-0.6805E-02	0.9326E+00	0.7698E-01		
5	75	125.1	0.4300	0.2520E-02	0.9516E+00	0.4732E-01		
5	126	117.9	0.3813	-0.7869E-02	0.9028E+00	0.1097E+00		
5	175	93.7	0.2963	-0.5798E-02	0.9859E+00	0.2059E-01		
5	201	94.0	0.2838	0.6627E-02	0.7076E+00	0.7182E+00	-0.7736E+00	0.3396E+00
5	176	93.7	0.2775	-0.1688E-02	0.8841E+00	0.1238E+00		
5	125	117.3	0.4850	0.8910E-03	0.1282E+01	-0.2921E+00		
5	78	125.0	0.5300	-0.1144E-01	0.1522E+01	-0.9575E+00	0.5676E+00	-0.1198E+00
5	31	124.2	0.5325	-0.1629E-02	0.1355E+01	-0.5637E+00	0.2213E+00	-0.1041E-01
2	31	82.2	0.3250	-0.7598E-03	0.8505E+00	0.3914E+00	-0.2432E+00	
2	77	77.6	0.3475	-0.3385E-02	0.1133E+01	0.2854E+00	-0.8168E+00	0.3994E+00
2	127	78.2	0.3362	-0.1167E-02	0.1131E+01	0.6007E+00	-0.1439E+01	0.7091E+00
2	176	62.5	0.2138	0.5661E-02	0.9045E+00	0.2295E+00	-0.1407E+00	
2	202	62.6	0.1787	0.4321E-02	0.8235E+00	0.1708E+00		
2	178	62.6	0.1625	-0.3099E-02	0.7630E+00	0.2425E+00		
2	129	99.4	0.3500	-0.1592E-01	0.1026E+01	-0.7907E-02		
2	76	82.7	0.4050	-0.7876E-02	0.1467E+01	-0.6587E+00	0.1993E+00	
2	27	82.0	0.3900	-0.3625E-02	0.1220E+01	-0.1803E+00	-0.3892E-01	
57	26	215.5	0.8925	0.5190E-01	0.9672E+00			
57	76	217.0	0.8937	0.5435E-01	0.9725E+00			
57	125	201.6	0.8312	0.7742E-01	0.9522E+00			
57	176	150.7	0.6500	0.6424E-01	0.9825E+00			
57	199	150.5	0.6450	0.6879E-01	0.9764E+00			
57	175	150.4	0.6525	0.2342E-01	0.1385E+01			
57	127	201.6	0.8075	0.8730E-01	0.9548E+00			
57	76	216.9	0.8788	0.6924E-01	0.9635E+00			
57	28	215.7	0.8750	0.3915E-01	0.9844E+00			

E02 0.32-0.51 TANGENT POISSON'S RATIO UNLOADING

CONF PRES (MPa)	TEMP (deg C)	MAX DEV STRESS (MPa)	MAX RADIAL STRAIN x 10E-3	POLYNOMIAL COEFFICIENTS F0	F1	F2	F3	F4
57	17	215.2	0.6425	-0.1756E-02	0.1018E+01			
57	75	217.3	0.6413	0.5895E-02	0.1005E+01			
57	126	202.1	0.5925	0.5688E-02	0.1006E+01			
57	175	151.1	0.4262	0.9915E-02	0.1011E+01			
57	201	150.9	0.4150	-0.3428E-01	0.1054E+01			
57	177	150.7	0.4200	0.5339E-02	0.1008E+01			
57	128	201.0	0.5825	-0.7975E-02	0.1017E+01			
57	77	216.9	0.6388	-0.9276E-03	0.1060E+01	-0.5029E-01		
57	29	215.7	0.6488	0.7821E-02	0.1009E+01			
31	28	191.5	0.5950	0.1490E-01	0.1062E+01	-0.7062E-01		
31	77	192.7	0.5850	0.4932E-02	0.1062E+01	-0.6170E-01		
31	128	180.4	0.5313	-0.7303E-02	0.1052E+01	-0.3898E-01		
31	177	139.2	0.3950	-0.1597E-02	0.1012E+01			
31	203	139.2	0.3975	0.2391E-01	0.9856E+00			
31	179	139.2	0.4000	-0.2369E-01	0.1060E+01	-0.3279E-01		
31	129	180.8	0.5513	-0.9586E-02	0.1026E+01			
31	78	192.6	0.6013	-0.6521E-02	0.1084E+01	-0.7191E-01		
31	27	191.3	0.6200	0.1812E-01	0.1000E+01			
15	26	171.3	0.5637	-0.1585E-02	0.1107E+01	-0.9735E-01		
15	75	160.6	0.5423	0.2049E-01	0.1080E+01	-0.9576E-01		
15	128	162.6	0.5000	-0.6908E-02	0.1091E+01	-0.7567E-01		
15	177	118.4	0.3663	0.4855E-01	0.9597E+00			
15	202	118.4	0.3600	0.7202E-01	0.9091E+00	0.2535E-01		
15	175	118.3	0.3563	-0.2219E-01	0.1031E+01			
15	128	162.3	0.5562	-0.1097E-01	0.1224E+01	-0.2094E+00		
15	77	172.6	0.5988	0.1811E-01	0.1142E+01	-0.1601E+00		
15	19	171.0	0.6125	0.1241E-03	0.1152E+01	-0.1507E+00		
5	18	124.2	0.4250	-0.1194E-01	0.1084E+01	-0.6065E-01		
5	75	125.1	0.4300	0.3927E-03	0.1077E+01	-0.6790E-01		
5	126	117.9	0.3813	-0.8083E-03	0.9961E+00	0.1249E-01		
5	175	93.7	0.2963	0.7468E-01	0.7252E+00	0.3434E+00	-0.1406E+00	
5	201	94.0	0.2838	0.1266E+00	0.6579E+00	0.5259E+00	-0.4882E+00	0.1779E+00
5	176	93.7	0.2775	-0.3261E-01	0.8683E+00	0.1555E-01	0.3975E+00	-0.2480E+00
5	125	117.3	0.4850	-0.1077E-01	0.1301E+01	-0.2939E+00		
5	78	125.0	0.5300	0.1029E-01	0.1549E+01	-0.1295E+01	0.1192E+01	-0.4556E+00
5	31	124.2	0.5325	0.3999E-01	0.1247E+01	-0.2919E+00		
2	31	82.2	0.3250	-0.1904E-01	0.1108E+01	-0.7784E-01		
2	77	77.6	0.3475	-0.1013E-01	0.1265E+01	-0.2555E+00		
2	127	78.2	0.3362	0.9164E-02	0.7180E+00	0.8296E+00	-0.5618E+00	
2	176	62.5	0.2138	0.7317E-01	0.6479E+00	0.1986E+00	0.8201E-01	
2	202	62.6	0.1787	0.1471E+00	0.5742E+00	0.7510E+00	-0.7435E+00	0.2709E+00
2	178	62.6	0.1625	-0.3584E-01	0.6996E+00	0.9391E+00	-0.1052E+01	0.4487E+00
2	129	99.4	0.3500	-0.5482E-01	0.9828E+00	0.8085E-01		
2	76	82.7	0.4050	-0.5861E-02	0.1498E+01	-0.7362E+00	0.2458E+00	
2	27	82.0	0.3900	0.1709E-02	0.1326E+01	-0.3340E+00		
57	26	215.5	0.8925	0.8415E-01	0.9511E+00			
57	76	217.0	0.8937	0.5370E-01	0.9834E+00			
57	125	201.6	0.8312	0.1727E-02	0.1036E+01			
57	176	150.7	0.6500	-0.3584E-02	0.1048E+01			
57	199	150.5	0.6450	-0.2465E-02	0.1039E+01			
57	175	150.4	0.6525	0.2651E-01	0.1016E+01			
57	127	201.6	0.8075	-0.4788E-02	0.1036E+01			
57	76	216.9	0.8788	0.1771E-01	0.1017E+01			
57	27	215.7	0.8750	0.5444E-01	0.9839E+00			

E02 4.38-4.57 TANGENT POISSON'S RATIO LOADING

CONF PRES (MPa)	TEMP (deg C)	MAX DEV STRESS (MPa)	MAX RADIAL STRAIN x 10E-3	POLYNOMIAL COEFFICIENTS F0	F1	F2	F3	F4
55	123	178.4	0.5288	-0.4092E-01	0.1026E+01			
55	172	133.4	0.3920	-0.2505E-01	0.1013E+01			
55	197	132.9	0.2846	-0.1366E+00	0.1070E+01			
55	170	133.2	0.3739	-0.3515E-01	0.1028E+01			
55	123	178.4	0.5327	-0.2765E-01	0.1016E+01			
55	73	191.3	0.5862	-0.3419E-01	0.1024E+01			
55	25	189.6	0.5973	-0.3244E-01	0.1022E+01			
30	25	168.4	0.5655	-0.9593E-02	0.9951E+00			
30	72	170.0	0.5435	-0.1841E-01	0.1006E+01			
30	123	160.0	0.4971	-0.1889E-01	0.1009E+01			
30	170	122.6	0.3481	-0.1674E-01	0.1001E+01			
30	193	122.5	0.3175	-0.3757E-01	0.1019E+01			
30	170	122.6	0.3481	-0.2125E-01	0.1007E+01			
30	122	159.3	0.4800	-0.2140E-01	0.1005E+01			
30	74	169.9	0.5374	-0.2655E-01	0.1014E+01			
30	24	168.4	0.5595	-0.2354E-01	0.1009E+01			
15	22	149.1	0.5010	-0.9027E-02	0.9050E+00	0.1083E+00		
15	72	150.6	0.4910	-0.1372E-02	0.8823E+00	0.1186E+00		
15	121	142.1	0.4372	-0.4301E-02	0.8738E+00	0.1328E+00		
15	169	103.4	0.2894	0.3097E-02	0.8614E+00	0.1346E+00		
15	194	103.0	0.2711	-0.2707E-01	0.1007E+01			
15	172	104.6	0.2748	0.8042E-02	0.8404E+00	0.1510E+00		
15	122	141.1	0.4275	-0.2142E-02	0.8826E+00	0.1222E+00		
15	71	150.0	0.4800	-0.2328E-01	0.1011E+01			
15	22	149.5	0.5081	0.2423E-02	0.8792E+00	0.1181E+00		
5	21	108.1	0.3591	-0.2098E-03	0.8574E+00	0.1928E+00	-0.5047E-01	
5	74	111.0	0.3346	0.5133E-02	0.7859E+00	0.2098E+00		
5	122	103.1	0.2882	0.3865E-02	0.7167E+00	0.3584E+00	-0.7919E-01	
5	172	84.8	0.2125	0.3818E-02	0.8527E+00	0.6980E-01	0.7481E-01	
5	195	81.8	0.1942	0.3491E-02	0.8743E+00	-0.8470E-02	0.1336E+00	
5	172	81.7	0.1881	0.8522E-02	0.7850E+00	0.1361E+00	0.6957E-01	
5	123	103.6	0.2626	-0.3735E-02	0.6824E+00	0.3309E+00		
5	74	109.7	0.3163	-0.2140E-02	0.7511E+00	0.2504E+00		
5	24	108.2	0.3346	-0.2352E-02	0.8389E+00	0.1632E+00		
2	23	71.6	0.2137	0.3402E-02	0.8473E+00	0.2135E+00	-0.6468E-01	
2	73	72.3	0.1917	-0.5007E-02	0.7991E+00	0.1515E+00	0.5452E-01	
2	125	68.1	0.1649	0.1318E-02	0.9848E+00	-0.6140E+00	0.1153E+01	-0.5269E+00
2	172	58.1	0.1270	0.4209E-02	0.9917E+00	-0.2355E+00	0.2449E+00	
2	196	54.6	0.1099	0.6017E-02	0.8227E+00	0.1700E+00		
2	171	54.8	0.1148	0.1185E-01	0.8939E+00	-0.6454E-01	0.1610E+00	
2	124	67.9	0.1466	0.8803E-02	0.6467E+00	0.3483E+00		
2	71	72.0	0.1832	0.4650E-02	0.7211E+00	0.2754E+00		
2	25	71.8	0.2040	0.1401E-02	0.8562E+00	0.1414E+00		

E02 4.38-4.57 TANGENT POISSON'S RATIO UNLOADING

CONF PRES (MPa)	TEMP (deg C)	MAX DEV STRESS (MPa)	MAX RADIAL STRAIN x 10E-3	POLYNOMIAL COEFFICIENTS F0	F1	F2	F3	F4
55	123	178.4	0.5288	-0.1708E-01	0.1023E+01			
55	172	133.4	0.3920	0.8803E-02	0.1003E+01			
55	197	132.9	0.2846	-0.1511E+00	0.1057E+01			
55	170	133.2	0.3739	-0.3414E-01	0.1061E+01			
55	123	178.4	0.5327	-0.3557E-02	0.1026E+01			
55	73	191.3	0.5862	0.8576E-02	0.1014E+01			
55	25	189.6	0.5973	0.1800E-01	0.1010E+01			
30	25	168.4	0.5655	0.4313E-01	0.9693E+00			
30	72	170.0	0.5435	0.4205E-02	0.1006E+01			
30	123	160.0	0.4971	-0.8082E-02	0.1014E+01			
30	170	122.6	0.3481	-0.4014E-01	0.1039E+01			
30	193	122.5	0.3175	-0.1330E+00	0.1131E+01			
30	170	122.6	0.3481	-0.3450E-01	0.1035E+01			
30	122	158.9	0.4861	-0.2255E-01	0.1012E+01			
30	74	169.9	0.5374	-0.2041E-01	0.1071E+01	-0.4782E-01		
30	24	168.4	0.5595	0.1618E-01	0.9954E+00			
15	22	149.1	0.5010	-0.1624E-01	0.1070E+01	-0.4918E-01		
15	72	150.6	0.4910	-0.8143E-02	0.1052E+01	-0.4082E-01		
15	121	142.1	0.4372	-0.5984E-02	0.1003E+01			
15	169	103.4	0.2894	0.2682E-01	0.8924E+00	0.8346E-01		
15	194	103.0	0.2711	0.1305E-01	0.8514E+00	0.1912E+00	-0.5377E-01	
15	172	104.6	0.2748	-0.3502E-01	0.9454E+00	0.9175E-01		
15	122	141.1	0.4275	0.2544E-02	0.9668E+00	0.3578E-01		
15	71	150.0	0.4800	-0.5650E-02	0.1025E+01	-0.1744E-01		
15	22	149.5	0.5081	0.2281E-01	0.1037E+01	-0.5845E-01		
5	21	108.1	0.3591	0.5066E-01	0.9201E+00	0.3602E-01		
5	74	111.0	0.3346	-0.9851E-02	0.9629E+00	0.5363E-01		
5	122	103.1	0.2882	0.4429E-02	0.7750E+00	0.4337E+00	-0.2670E+00	0.5375E-01
5	172	84.8	0.2125	0.5480E-01	0.7757E+00	0.1714E+00		
5	195	81.8	0.1942	0.7650E-01	0.6753E+00	0.3226E+00	-0.7364E-01	
5	172	81.7	0.2162	-0.2225E+00	0.1505E+01	-0.4583E+00		
5	123	103.6	0.2626	-0.6803E-01	0.9099E+00	0.1652E+00		
5	74	109.7	0.3163	-0.3221E-01	0.9360E+00	0.1019E+00		
5	24	108.2	0.3346	-0.7985E-02	0.9719E+00	0.4148E-01		
2	23	71.6	0.2137	0.2813E-01	0.8826E+00	0.9443E-01		
2	73	72.3	0.1917	-0.6103E-02	0.8363E+00	0.1755E+00		
2	125	68.1	0.1649	0.1437E-01	0.8165E+00	0.1154E-02	0.3944E+00	-0.2269E+00
2	172	58.1	0.1270	0.6891E-01	0.6559E+00	0.3758E+00	-0.1012E+00	
2	196	54.6	0.1099	-0.2845E-01	0.9481E+00	0.7352E-01		
2	171	54.8	0.1148	0.5268E-01	0.6725E+00	0.2748E+00		
2	124	67.9	0.1466	-0.7870E-01	0.7929E+00	0.2946E+00		
2	71	72.0	0.1832	-0.2613E-01	0.6816E+00	0.7484E+00	-0.5723E+00	0.1686E+00

E03 0.26-0.45 TANGENT POISSON'S RATIO LOADING

CONF PRES (MPa)	TEMP (deg C)	MAX DEV STRESS (MPa)	MAX RADIAL STRAIN x 10E-3	POLYNOMIAL COEFFICIENTS F0	F1	F2	F3	F4
55	21	187.9	0.5813	-0.3072E-01	0.1012E+01			
55	76	191.1	0.5789	-0.2371E-01	0.1001E+01			
55	125	178.1	0.5252	-0.2953E-01	0.1013E+01			
55	173	128.7	0.3505	-0.3596E-01	0.1019E+01			
55	122	194.3	0.3493	0.2004E+00	0.8490E+00			
55	76	198.1	0.5655	0.3534E-01	0.8860E+00			
55	27	200.7	0.5691	0.2603E-01	0.9231E+00			
30	26	168.2	0.5435	-0.1989E-01	0.1001E+01			
30	76	169.0	0.5215	-0.1814E-01	0.9992E+00			
30	126	159.0	0.4824	0.2562E-02	0.8808E+00	0.1146E+00		
30	173	122.6	0.3420	-0.2054E-01	0.9957E+00			
30	124	158.9	0.4702	-0.2858E-01	0.1009E+01			
30	75	220.9	0.5215	0.9815E-01	0.9277E+00			
30	28	221.1	0.5300	0.9400E-01	0.9519E+00			
15	27	150.3	0.4910	-0.2303E-02	0.8631E+00	0.1368E+00		
15	76	151.9	0.4751	-0.3126E-01	0.1010E+01			
15	124	143.0	0.4299	-0.1116E-02	0.7433E+00	0.3811E+00	-0.1288E+00	
15	173	104.3	0.2870	-0.3671E-02	0.7999E+00	0.2007E+00		
15	125	143.1	0.4128	-0.5401E-02	0.8102E+00	0.2005E+00		
15	75	151.6	0.4678	-0.2749E-01	0.1002E+01			
15	27	150.3	0.4726	-0.4892E-01	0.1033E+01			
5	21	109.3	0.3236	-0.2743E-02	0.7024E+00	0.4086E+00	-0.1102E+00	
5	75	110.1	0.3200	-0.4126E-02	0.7351E+00	0.2703E+00		
5	126	103.9	0.2772	0.1556E-02	0.6400E+00	0.5138E+00	-0.1581E+00	
5	172	73.0	0.1844	0.1221E-02	0.7066E+00	0.3721E+00	-0.8333E-01	
5	125	103.9	0.2565	-0.1535E-02	0.6319E+00	0.3781E+00		
5	76	110.4	0.3029	-0.6885E-02	0.7085E+00	0.3034E+00		
5	27	109.1	0.3212	-0.3503E-02	0.7823E+00	0.2230E+00		
2	27	72.7	0.1991	0.3474E-02	0.7515E+00	0.2284E+00	0.8112E-01	-0.6829E-01
2	76	72.8	0.1771	0.1946E-02	0.5827E+00	0.5290E+00	-0.1147E+00	
2	125	68.5	0.1551	0.8623E-02	0.6710E+00	0.3514E+00	-0.3154E-01	
2	172	55.3	0.1099	0.5432E-02	0.7473E+00	0.2429E+00		
2	124	87.5	0.1881	-0.1518E-02	0.5495E+00	0.4573E+00		
2	76	74.8	0.1710	-0.1422E-02	0.6021E+00	0.4040E+00		
2	26	72.3	0.1808	-0.3107E-02	0.6710E+00	0.3396E+00		
30	27	168.6	0.5337	-0.1705E-01	0.9935E+00			
30	76	169.7	0.5288	-0.2679E-01	0.1005E+01			
30	125	159.2	0.4787	-0.1595E-01	0.9910E+00			
30	124	158.8	0.4763	-0.2788E-01	0.1007E+01			
30	74	169.4	0.5191	-0.2401E-01	0.1002E+01			
30	26	167.5	0.5288	-0.2328E-01	0.1001E+01			

E03 0.26-0.45 TANGENT POISSON'S RATIO UNLOADING

CONF PRES (MPa)	TEMP (deg C)	MAX DEV STRESS (MPa)	MAX RADIAL STRAIN x 10E-3	POLYNOMIAL COEFFICIENTS F0	F1	F2	F3	F4
55	21	195.8	0.5813	-0.2616E-01	0.1662E+01	-0.8237E+00		
55	76	191.1	0.5789	0.8925E-02	0.1009E+01			
55	125	178.1	0.5252	-0.1013E-01	0.1027E+01			
55	173	132.9	0.3639	-0.3763E-01	0.1052E+01			
55	122	128.1	0.3749	0.3505E-01	0.9848E+00			
55	76	187.5	0.5655	-0.5572E-03	0.1098E+01	-0.8513E-01		
55	27	200.6	0.5691	0.6773E-01	0.8786E+00			
30	26	223.7	0.5435	0.1031E+00	0.9959E+00			
30	76	169.0	0.5215	0.1036E-01	0.1007E+01			
30	126	159.0	0.4824	0.5045E-02	0.1012E+01			
30	173	122.6	0.3420	-0.1634E-01	0.1028E+01			
30	124	158.9	0.4702	-0.2131E-01	0.1037E+01			
30	75	169.1	0.5215	0.1008E-01	0.1009E+01			
30	28	167.8	0.5300	0.1584E-01	0.1002E+01			
15	27	236.9	0.4910	0.1537E+00	0.1022E+01			
15	76	151.9	0.4751	0.5790E-02	0.1009E+01			
15	124	143.0	0.4299	-0.6501E-02	0.1045E+01	-0.3076E-01		
15	173	104.3	0.2870	0.1045E-01	0.9884E+00			
15	125	143.1	0.4128	-0.3945E-01	0.1096E+01	-0.4993E-01		
15	75	151.6	0.4678	-0.1006E-01	0.1028E+01			
15	27	150.3	0.4726	-0.3505E-02	0.1023E+01			
5	21	109.3	0.3236	-0.1639E-01	0.1006E+01	0.1677E-01		
5	75	110.1	0.3200	-0.3047E-02	0.8103E+00	0.6161E+00	-0.5753E+00	0.1522E+00
5	126	103.9	0.2772	-0.1519E-01	0.7775E+00	0.5247E+00	-0.3179E+00	0.3114E-01
5	172	73.0	0.1844	0.7055E-01	0.7810E+00	0.1648E+00		
5	125	103.9	0.2565	-0.7342E-01	0.9487E+00	0.1361E+00		
5	76	110.4	0.3029	-0.3949E-01	0.9845E+00	0.6375E-01		
5	27	109.1	0.3212	-0.9540E-02	0.9925E+00	0.2330E-01		
2	27	72.7	0.1991	0.3664E-01	0.5565E+00	0.1332E+01	-0.1572E+01	0.6475E+00
2	76	72.8	0.1771	-0.2953E-01	0.8483E+00	0.1918E+00		
2	125	68.5	0.1551	0.1285E-01	0.5724E+00	0.8101E+00	-0.4194E+00	0.2366E-01
2	172	55.3	0.1099	0.6114E-01	0.5688E+00	0.5813E+00	-0.2100E+00	
2	124	87.5	0.1881	-0.8027E-01	0.8326E+00	0.2624E+00		
2	76	74.8	0.1710	-0.7855E-01	0.8500E+00	0.2396E+00		
2	26	72.3	0.1808	-0.2502E-01	0.7156E+00	0.6511E+00	-0.3428E+00	
30	27	168.6	0.5337	0.2415E-01	0.9993E+00			
30	76	169.7	0.5288	0.1429E-01	0.1010E+01			
30	125	159.2	0.4787	0.9248E-02	0.1011E+01			
30	124	158.8	0.4763	0.5313E-02	0.1011E+01			
30	74	169.4	0.5191	-0.2295E-02	0.1024E+01			
30	26	167.5	0.5288	0.1940E-01	0.9995E+00			

E17 6.04-6.22 TANGENT POISSON'S RATIO LOADING (Young's Modulus)

Conf Pres (MPa)	TEMP (des C)	MAX DEV STRESS (MPa)	MAX AXIAL STRAIN x 10E-2	Polynomial Coefficients F_0	F_1	F_2	F_3	F_4
55	20	210.4	.5862	$-.1571\times10^{-1}$	$-.1011\times10^{1}$	--	--	--
55	73	137.6	.3652	$-.3607\times10^{-1}$	$-.1027\times10^{1}$			
55	123	118.1	.3127	$-.2462\times10^{-1}$	$-.1021\times10^{1}$			
55	170	86.3	.2149	$-.4408\times10^{-1}$	$-.1042\times10^{1}$			
55	194	83.3	.2027	$-.4655\times10^{-1}$	$-.1039\times10^{1}$			
55	170	83.2	.2076	$-.1147\times10^{-1}$	$.1004\times10^{1}$			
55	123	120.2	.3163	$-.1777\times10^{-1}$	$.1012\times10^{1}$			
55	74	132.1	.3554	$-.9084\times10^{-2}$	$-.1000\times10^{1}$			
55	23	130.7	.3566	$-.2916\times10^{-1}$	$.1025\times10^{1}$			
30	73	126.6	.3334	$-.2262\times10^{-1}$	$-.1022\times10^{1}$			
30	123	115.6	.2980	$-.3694\times10^{-1}$	$-.1033\times10^{1}$			
30	170	85.6	.2140	$-.2940\times10^{-1}$	$-.1027\times10^{1}$			
30	194	85.5	.2065	$-.2778\times10^{-1}$	$-.1023\times10^{1}$			
30	170	85.7	.2065	$-.2049\times10^{-1}$	$.1012\times10^{1}$			
30	125	115.5	.3010	$-.1437\times10^{-1}$	$.1011\times10^{1}$			
30	74	125.5	.3445	$-.1128\times10^{-1}$	$-.1008\times10^{1}$			
30	23	125.5	.3556	$.1922\times10^{-1}$	$-.1018\times10^{1}$			
15	73	115.1	.3128	$-.2144\times10^{-1}$	-.9832	$.3802\times10^{-1}$		
15	122	108.0	.2910	$-.7253\times10^{-2}$	$-.1025\times10^{1}$	-.1112	$.9014\times10^{1}$	
15	168	77.1	.1980	$-.2427\times10^{-2}$	.7550	.4362	-.1884	
15	195	76.4	.1930	$-.2488\times10^{-1}$	.9069	.1108		
15	171	76.0	.2285	$-.1037\times10^{-1}$	.9824	$.3242\times10^{1}$		
15	123	107.3	.3885	$-.1504\times10^{-1}$	$-.1298\times10^{1}$	-.3995	.1148	
15	75	116.3	.4118	$-.1195\times10^{-1}$	$-.1172\times10^{1}$	-.1605		
15	26	116.1	.4191	$-.6430\times10^{-2}$	$-.1125\times10^{1}$	-.1215		
5	26	116.9	.3935	$-.9131\times10^{-2}$	$-.1034\times10^{1}$	$-.2071\times10^{-1}$		
5	73	116.9	.4215	$-.3647\times10^{-2}$	$-.1169\times10^{1}$	-.1641		
5	122	108.8	.4055	$-.1585\times10^{-1}$	$-.1319\times10^{1}$	-.3047		
5	169	83.0	.2760	$-.1770\times10^{-1}$	-.08578	.1675		
5	194	84.6	.2410	$.4553\times10^{-2}$	.6280	.3710		
5	171	84.6	.2995	$-.6476\times10^{-1}$	$.1330\times10^{1}$	-.2556		
5	123	108.3	.4300	$-.1358\times10^{-1}$	$.1646\times10^{1}$	-.9140	.2837	
5	74	117.0	.4742	$-.2045\times10^{-1}$	$-.1574\times10^{1}$	-.8703	.3157	
5	25	117.0	.4885	$-.5797\times10^{-1}$	$.1373\times10^{1}$	-.3198		
2	23	76.0	.3139	$-.7502\times10^{-2}$	$.1048\times10^{1}$	$-.3705\times10^{-1}$		
2	72	76.6	.3591	$-.1217\times10^{-1}$	$-.1395\times10^{1}$	-.3826		
2	121	69.0	.2833	-.1100	$-.1450\times10^{1}$	-.3359		
2	170	55.5	.1661	$.2314\times10^{-3}$	.5705	.6087	-.1799	
2	194	54.7	.1282	$-.9910\times10^{-2}$	.8127	.2018		
2	169	55.0	.1417	$.2019\times10^{-1}$	.4969	.4708		
2	124	71.7	.2443	$-.2697\times10^{-1}$	$-.2207\times10^{1}$	$-.1288\times10^{1}$		
2	74	76.4	.3566	$-.1278\times10^{-1}$	$-.1679\times10^{1}$	-.8676	.2005	
2	26	76.6	.3798	$-.7092\times10^{-2}$	$-.1293\times10^{1}$	-.2869		

E17 6.04-6.22 Tangent Poisson's ratio unloading

Conf Pres (MPa)	TEMP (des C)	MAX DEV STRESS (MPa)	MAX AXIAL STRAIN x 10E-2	Polynomial Coefficients F_0	F_1	F_2	F_3	F_4
55	20	210.4	.5862	$.6029 \times 10^{-2}$	$.1005 \times 10^{1}$			
55	73	137.6	.3652	$.1904 \times 10^{-3}$	$.1011 \times 10^{1}$			
55	122	118.1	.3127	$.2254 \times 10^{-1}$	.9840			
55	170	86.3	.2149	$.8427 \times 10^{-2}$	$.1003 \times 10^{1}$			
55	194	83.3	.2027	$.2694 \times 10^{-2}$	$.1013 \times 10^{1}$			
55	170	83.2	.2076	$.6931 \times 10^{-2}$	$.1007 \times 10^{1}$			
55	123	117.6	.3041	$-.5497 \times 10^{2}$	$.1014 \times 10^{1}$			
55	74	132.1	.3554	$.8365 \times 10-2$	$.1000 \times 10^{1}$			
55	23	130.7	.3566	$.5588 \times 10^{-2}$	$.1003 \times 10^{1}$			
30	73	126.6	.3334	$-.5508 \times 10^{-2}$	$.1016 \times 10^{1}$			
30	123	115.6	.2980	$-.7246 \times 10^{-2}$	$.1021 \times 10^{1}$			
30	170	85.6	.2140	$-.3525 \times 10^{-2}$	$.1003 \times 10^{1}$			
30	194	85.5	.2065	$-.8058 \times 10^{-2}$	$.1009 \times 10^{1}$			
30	170	85.7	.2065	$-.5784 \times 10^{-1}$	$.1063 \times 10^{1}$			
30	125	115.5	.3010	$-.3748 \times 10^{-1}$	$.1042 \times 10^{1}$			
30	74	125.5	.3445	$-.8748 \times 10^{-2}$	$.1016 \times 10^{1}$			
30	23	125.5	.3556	$.1203 \times 10^{-1}$	$.1002 \times 10^{1}$			
15	73	115.1	.3128					
15	122	108.0	.2910	$.1944 \times 10^{-1}$	.9863			
15	168	77.1	.1980	$.2898 \times 10^{-1}$	.8518	.1304		
15	195	76.4	.1930	$.6054 \times 10^{-1}$	.6343	.4868	-.1766	
15	171	76.0	.2285	$-.7432 \times 10^{-1}$	$.1255 \times 10^{1}$	-.1792		
15	123	107.3	.3885	$.3762 \times 10^{-1}$	$.1008 \times 10^{1}$			
15	75	116.3	.4118	$-.1614 \times 10^{-2}$	$.1304 \times 10^{1}$	-.3046		
15	26	116.1	.4191	$.2576 \times 10^{-1}$	$.1208 \times 10^{1}$	-.2390		
5	26	116.9	.3935	$.3544 \times 10^{-2}$	$.1167 \times 10^{1}$	.1667		
5	73	116.9	.4215	$.2620 \times 10^{-1}$	$.1292 \times 10^{1}$	-.3251		
5	122	108.8	.4055	$.2873 \times 10^{-2}$	$.1221 \times 10^{1}$	-.2272		
5	169	82.9	.2760	$.5154 \times 10^{-2}$	.8572	.1525		
5	194	84.6	.2410	$.3795 \times 10^{-1}$	.5389	.6971	-.2675	
5	171	84.8	.3045	$.7353 \times 10^{-1}$	$.1217 \times 10^{1}$	-.1444		
5	123	108.3	.4300	$-.1561 \times 10^{-1}$	$.1314 \times 101$	-.3111		
5	74	117.0	.4742	$-.2954 \times 10^{-2}$	$.1384 \times 10^{1}$	-.3914		
5	25	117.0	.4885	$-.1952 \times 10^{-1}$	$.1549\ 10^{1}$	-.5980		
2	23	76.0	.31339	$-.1875 \times 10^{-1}$	$.1336 \times 10^{1}$	-.3181		
2	72	76.6	.3591	$-.7891 \times 10^{-2}$	$.1331 \times 10^{1}$	-.3254		
2	121	69.0	.2833	$-.9662 \times 10^{-2}$	.9372	$.8935 \times 10^{1}$		
2	170	55.5	.1661	$-.6883 \times 10^{-1}$	$.1004 \times 10^{1}$			
2	194	54.7	.1282	$-.3754 \times 10^{-2}$	.9400	-.1582	.2148	
2	169	55.0	.1417	$-.9608 \times 10^{-2}$	.6106	.4049		
2	124	71.7	.2443					
2	74	76.5	.3566	$-.8197 \times 10^{-1}$	$.1488 \times 10^{1}$	-.4081		
2	26	76.6	.3798	$.2417 \times 10^{-1}$	$.1501 \times 10^{1}$	-.7499	.2265	

M02 12.23-12.43 TANGENT POISSON'S RATIO LOADING

CONF PRES (MPa)	TEMP (deg C)	MAX DEV STRESS (MPa)	MAX RADIAL STRAIN x 10E-3	POLYNOMIAL COEFFICIENTS F0	F1	F2	F3	F4
55	19	203.9	0.6192	-0.3188E-01	0.1027E+01			
55	75	203.4	0.6339	-0.1952E-01	0.1015E+01			
55	124	187.4	0.5557	-0.3636E-01	0.1021E+01			
55	174	136.2	0.3994	-0.1587E-01	0.1007E+01			
55	198	136.0	0.3945	-0.1137E-01	0.1002E+01			
55	176	136.1	0.3994	-0.1013E-01	0.1003E+01			
55	125	185.3	0.5594	-0.1051E-01	0.9925E+00			
55	76	200.8	0.5948	-0.1099E-01	0.1001E+01			
55	27	195.5	0.5887	-0.1069E-01	0.1001E+01			
15	26	162.7	0.5325	0.7671E-03	0.9413E+00	0.5540E-01		
15	75	155.1	0.4971	-0.1735E-02	0.9078E+00	0.9801E-01		
15	124	150.7	0.4885	-0.9708E-02	0.9127E+00	0.1008E+00		
15	174	105.7	0.3371	-0.5328E-02	0.9210E+00	0.8723E-01		
15	197	107.9	0.3090	-0.1467E-01	0.8261E+00	0.1976E+00		
15	174	108.2	0.3212	-0.8029E-02	0.8900E+00	0.1227E+00		
15	124	150.0	0.4885	-0.7955E-02	0.9669E+00	0.4266E-01		
15	75	162.0	0.5471	-0.3771E-02	0.9855E+00	0.2053E-01		
15	27	158.3	0.5447	-0.2614E-02	0.9914E+00	-0.3116E-01	0.4142E-01	
55	27	199.2	0.6497	-0.6327E-04	0.9964E+00			
55	76	197.9	0.6473	-0.1064E-01	0.1005E+01			
55	125	183.7	0.6131	-0.1232E-01	0.1006E+01			
55	175	136.1	0.4458	-0.9647E-02	0.1002E+01			
55	124	184.8	0.6436	0.7386E-02	0.9939E+00			
55	75	197.3	0.6681	0.5164E-02	0.9965E+00			
55	26	195.9	0.6326	-0.1198E-01	0.1017E+01			
5	25	114.5	0.4091	-0.5545E-03	0.8827E+00	0.3066E+00	-0.3348E+00	0.1467E+00
5	74	111.2	0.3945	-0.1881E-02	0.9663E+00	0.3678E-01		
5	123	106.9	0.3578	-0.9852E-03	0.8082E+00	0.6251E+00	-0.8123E+00	0.3811E+00
5	171	84.1	0.2443	0.3937E-02	0.6883E+00	0.8917E+00	-0.1051E+01	0.4660E+00
5	195	84.0	0.2406	0.3641E-02	0.6506E+00	0.1077E+01	-0.1391E+01	0.6612E+00
5	172	84.4	0.2345	-0.1149E-01	0.7870E+00	0.2292E+00		
5	124	108.0	0.3639	-0.3250E-01	0.9056E+00	0.1334E+00		
5	75	116.1	0.4678	-0.3443E-02	0.1176E+01	-0.1754E+00		
5	28	116.1	0.4507	-0.6629E-03	0.1108E+01	-0.1092E+00		
55	28	203.3	0.7413	0.7454E-02	0.1003E+01			
55	75	203.4	0.7658	0.1479E-01	0.9979E+00			
55	126	187.5	0.7487	0.1232E-01	0.1004E+01			
55	173	138.3	0.5899	0.7215E-02	0.1012E+01			
55	198	138.2	0.5655	-0.3168E-01	0.1049E+01			

M02 12.23-12.43 TANGENT POISSON'S RATIO UNLOADING

CONF PRES (MPa)	TEMP (deg C)	MAX DEV STRESS (MPa)	MAX RADIAL STRAIN x 10E-3	POLYNOMIAL COEFFICIENTS F0	F1	F2	F3	F4
55	19	203.9	0.6192	0.1435E-01	0.1001E+01			
55	75	203.4	0.6339	0.4420E-01	0.9722E+00			
55	124	187.4	0.5557	0.1314E-01	0.1012E+01			
55	174	136.2	0.3994	0.5581E-01	0.9703E+00			
55	198	136.0	0.3945	0.3524E-01	0.1008E+01			
55	176	136.1	0.3994	0.5246E-01	0.9797E+00			
55	125	185.3	0.5594	0.4959E-01	0.9745E+00			
55	76	200.8	0.5948	0.2959E-01	0.9924E+00			
55	27	195.5	0.5887	0.3475E-01	0.9833E+00			
15	26	162.7	0.5325	0.2413E-01	0.1105E+01	-0.1252E+00		
15	75	155.1	0.4971	0.1180E-02	0.1148E+01	-0.1460E+00		
15	124	150.7	0.4885	0.2135E-01	0.1096E+01	-0.1132E+00		
15	174	105.7	0.3371	0.1034E+00	0.8937E+00	0.9317E-02		
15	197	107.9	0.3090	0.1004E-01	0.9746E+00	0.2005E-01		
15	174	108.2	0.3212	-0.4227E-01	0.1066E+01	-0.2052E-01		
15	124	150.0	0.4885	-0.3597E-01	0.1198E+01	-0.1607E+00		
15	75	162.0	0.5471	0.2228E-02	0.1179E+01	-0.1824E+00		
15	27	158.3	0.5447	0.1463E-01	0.1123E+01	-0.1368E+00		
55	27	199.2	0.6497	0.5092E-01	0.9626E+00			
55	76	197.9	0.6473	0.5795E-01	0.9596E+00			
55	125	183.7	0.6131	0.6327E-01	0.9578E+00			
55	175	136.1	0.4458	0.6109E-01	0.9711E+00			
55	124	184.8	0.6436	0.3924E-01	0.1000E+01			
55	75	197.3	0.6681	0.5554E-01	0.9810E+00			
55	26	195.9	0.6326	0.2743E-01	0.1015E+01			
5	25	114.5	0.4091	0.2896E-01	0.1045E+01	0.3420E-01	-0.1085E+00	
5	74	111.2	0.3945	0.2905E-01	0.1158E+01	-0.1837E+00		
5	123	106.9	0.3578	0.2273E-02	0.9854E+00	-0.1205E+00	0.1290E+00	
5	171	84.1	0.2443	0.1968E-01	0.9777E+00	0.4117E-02		
5	195	84.0	0.2406	-0.1660E-01	0.9802E+00	0.5673E-01		
5	172	84.4	0.2345	-0.4655E-01	0.9575E+00	0.9720E-01		
5	124	108.0	0.3639	-0.7258E-01	0.1223E+01	-0.1469E+00		
5	75	116.1	0.4678	0.6837E-02	0.1488E+01	-0.9934E+00	0.7862E+00	-0.2872E+00
5	28	116.1	0.4507	0.7719E+02	-0.2568E+00			
55	28	203.3	0.7413	0.4696E-01	0.9910E+00			
55	75	203.4	0.7658	0.6697E-01	0.9665E+00			
55	126	187.5	0.7487	0.9003E-01	0.9585E+00			
55	173	138.3	0.5899	0.1076E+00	0.9297E+00			
55	198	138.2	0.5655	0.5539E-01	0.9920E+00			

APPENDIX C
SUMMARY OF THERMAL EXPANSION TESTS PERFORMED AT TERRA TEK

Mark Board
Terra Tek, Inc.
Salt Lake City, Utah

INTRODUCTION

This appendix reviews all of the measurements of the linear coefficient of expansion of Stripa granite as determined to date at Terra Tek. Seven tests were conducted on various core sizes over a range of temperatures and confining pressures, as shown in Table C-1.

LABORATORY TESTS

Tests 1 and 2 were conducted at the beginning of the Stripa project. The device used to measure the expansion is shown in Fig. C-1.

The sample expansion was measured by two LVDT's mounted to a bracket attached to the oven exterior. A small amount of error is probably introduced here due to oven expansion. Two fused quartz linkage rods were attached at each side of the sample. One was a quartz tube referenced to an aluminum disc on the sample surface and connected to the LVDT barrel. The other solid rod passed inside the hollow tube and was referenced to the sample bottom. This rod was connected to the LVDT core. The arrangement thus allowed the effects of expansion of the linkage from the sample top to the LVDT to be eliminated. A correction was added for the expansion of the fused quartz rod across the sample length.

The furnace temperature was raised and allowed to stabilize for approximately one hour. Voltage readings of the two LVDT's were then taken and converted to displacement using the LVDT calibration. The plot of strain for the first temperature cycle of test 1 is given in Fig. C-2. This first cycle attained a maximum sample temperature of 237°C; a second cycle attained a temperature of 230°C. Initially, the heat-up portion of the curve was not presented as it took a long time for the strains to stabilize with temperature,

Table C-1. Terra Tek thermal expansion tests.

Test No.	When Performed	Core Dimensions (in.)	Temp. Range (°C)	Conf. Pressure (MPa)	Heat Rate (°C/min)
1	9/1977	1φ x 2L	24-230	0	unknown
2	9/1977	1φ x 6L	22-217	0	unknown
3	9/1979	2φ x 4L	30-204	10	2
4	9/1979	2φ x 4L	40-203	10	2
5	9/1979	2φ x 4L	20-300	25	2
6	1/1980	2φ x 4L	8-350	25	2
7	2/1980	1φ x 2L	60-395	25	2

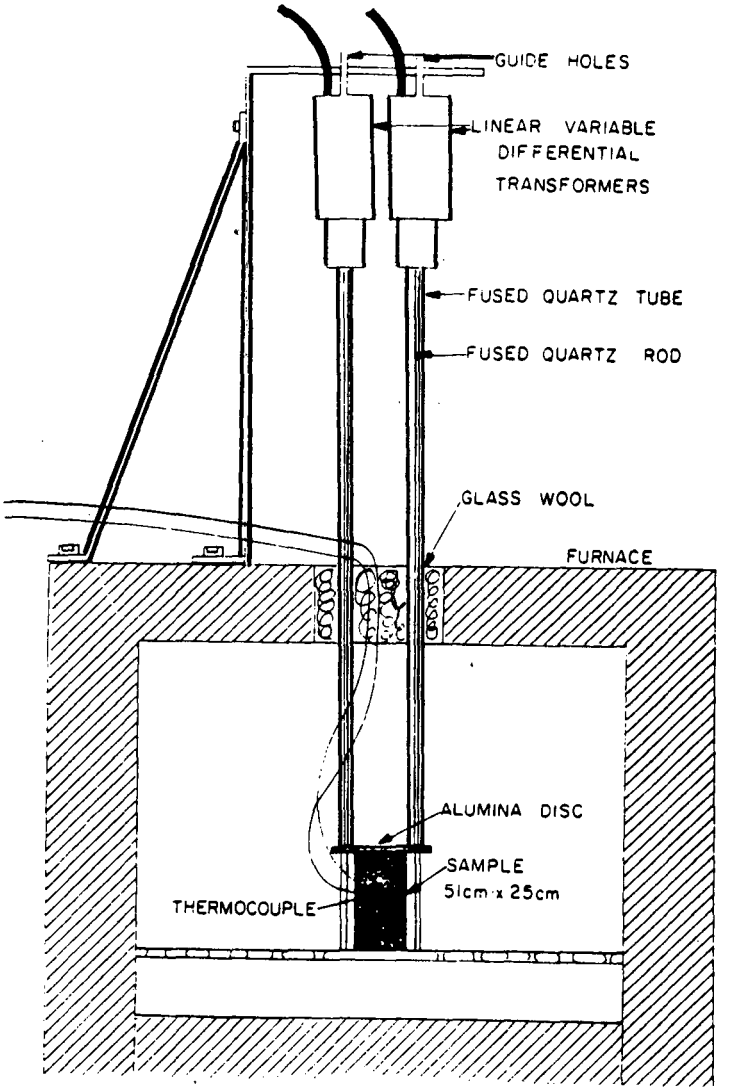

XBL 8112-12953

Fig. C1. Apparatus for determination of expansion coefficient, tests 1 and 2.

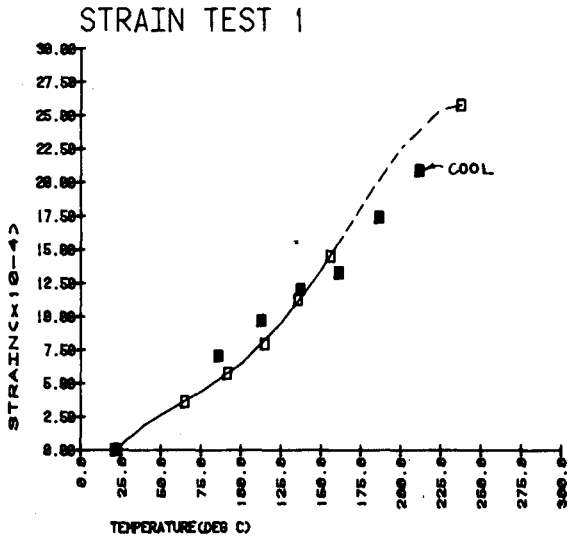

Fig. C2. Thermal strain as a function of temperature, test 1.

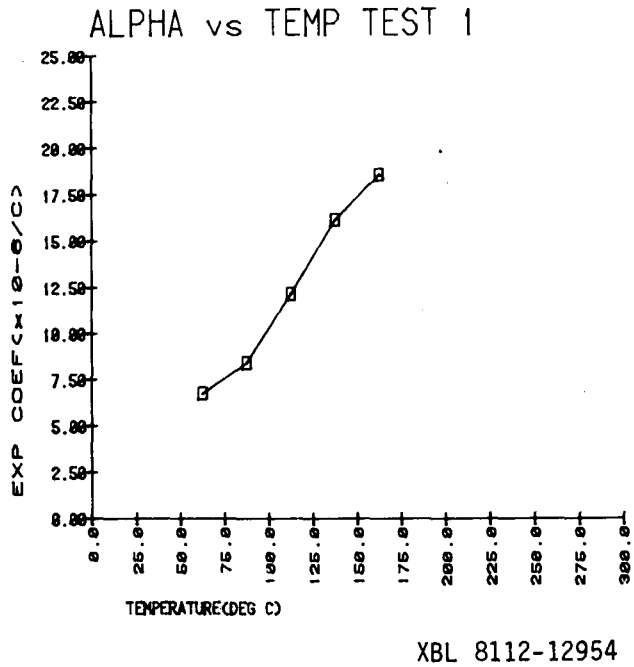

Fig. C3. Alpha as a function of temperature, test 1.

and only the cool-down slope was given (Pratt et al., 1977). Here, the heat-up curve is given and shows a nonlinear increase in strain as a function of temperature (Fig. C-2), whereas the cool-down displacements are roughly linear. The expansion coefficient was calculated by subtracting strains at successive temperatures divided by the temperature change for that interval. The value of α is plotted in Fig. C-3 at the midpoint of each temperature interval. Figure C-3 shows an increase in α from about 6 to 18 x 10^{-6}/°C from 20-150°C.

The second test was performed with the same apparatus as in test 1, but with a 6.3-inch-long sample. The sample strain as a function of temperature is shown in Fig. C-4. The behavior was similar to that in test 1, showing a nonlinear change with temperature. Sample strains over equivalent temperature ranges were nearly the same for both tests. Again, the cooling strains did not follow the heating path and showed a small amount of hysteresis. The coefficient of expansion, as determined by simple subtraction of successive strains, yielded a highly erratic behavior. This points up the measurement error associated with the simple device used to perform these tests, because small inconsistencies in determination of the strain can result in large differences in the calculated α. To overcome this problem, a smooth curve was fit to the strain vs. temperature data, using a cubic polynomial fit. For example, the strain vs. temperature data from test 2 can be fitted with the following polynomial:

$$\varepsilon(T) = -1.54 \times 10^{-4} + 7.122 \times 10^{-6}T - 1.65 \times 10^{-8}T^2 + 1.67 \times 10^{-10}T^3$$

with a correlation coefficient of 0.998. The continuous plot generated by this function is the curve drawn through the data points in Fig. C-4. The

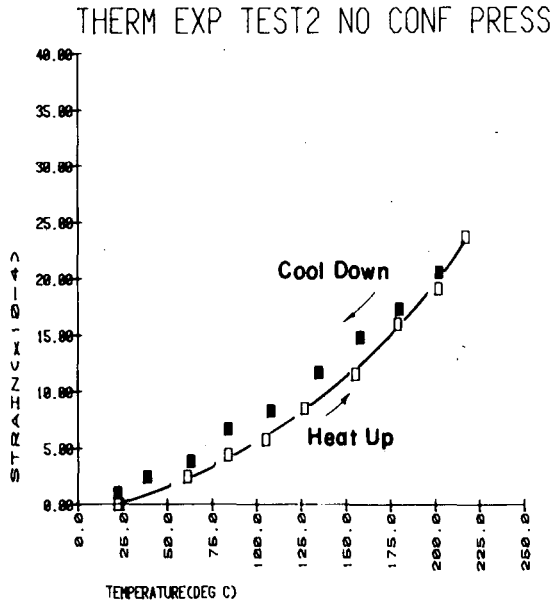

Fig. C4. Thermal strain as a function of temperature, test 2.

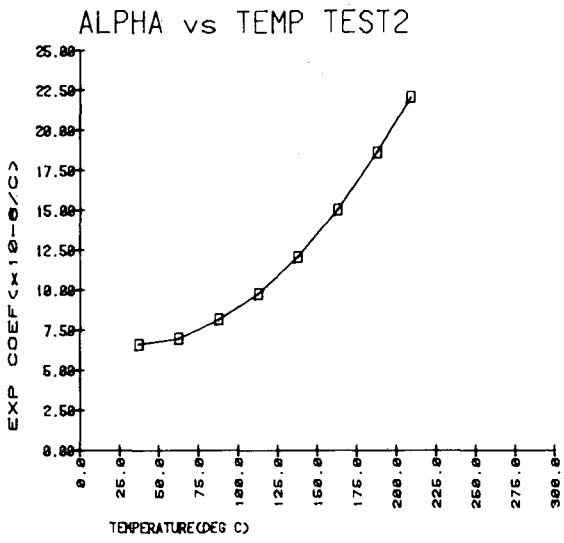

XBL 8112-12955

Fig. C5. Alpha as a function of temperature, test 2.

expansion coefficient was then calculated at 25°C intervals from the smooth curve, resulting in the plot given in Fig. C-5.

Tests 3-7 were all conducted on the "geothermal" testing machine at Terra Tek. This machine can be used for expansion measurements at confining pressure. The test set-up is shown in Fig. C-6. Samples were located in the upper portion of the test vessel. Ceramic insulation on each sample ends minimized the longitudinal temperature gradients. Heating elements were coiled about the lower aluminium insulator and the lower portion of the sample. A cylindrical ceramic shroud was placed over the sample and the coiled heater to localize the fluid convection currents. Convection within the vessel was further minimized by a second all-encompassing ceramic shroud. These ceramic convection baffles enabled temperatures of 535°C to be reached within the inner shroud while allowing the fluid surrounding the exterior shroud to remain at less than ~100°C, well below the maximum allowable for the internal instrumentation and pressure seal.

All non-sample stack components exposed to the high-temperature environment were fused quartz, with a thermal expansion coefficient of 0.5×10^{-6} cm/cm°C. Fused quartz endcaps and a fused quartz stack spacer supported the sample. Quartz rods attached to the top of the test sample suspended the core elements of the LVDT transformers at the base. The expansion of the rods and stack components tended to offset one another except for the expansion of the sample. System expansion consisted of the expansion of the fused quartz rods over a distance equal to the sample length. Compared to the rock expansion ($5\text{-}20 \times 10^{-6}$ cm/cm°C), the expansion of the quartz is small.

1. UPPER BRACKET ASSY
2. SHROUD RING
3. UPPER ENDCAP
4. INNER SHROUD
5. SILICONE JACKET
6. SAMPLE
7. HEATER
8. LOWER ENDCAP
9. HEAT DAM
10. PEDESTAL ASSY
11. LOWER BRACKET ASSY
12. COLUMN BASE

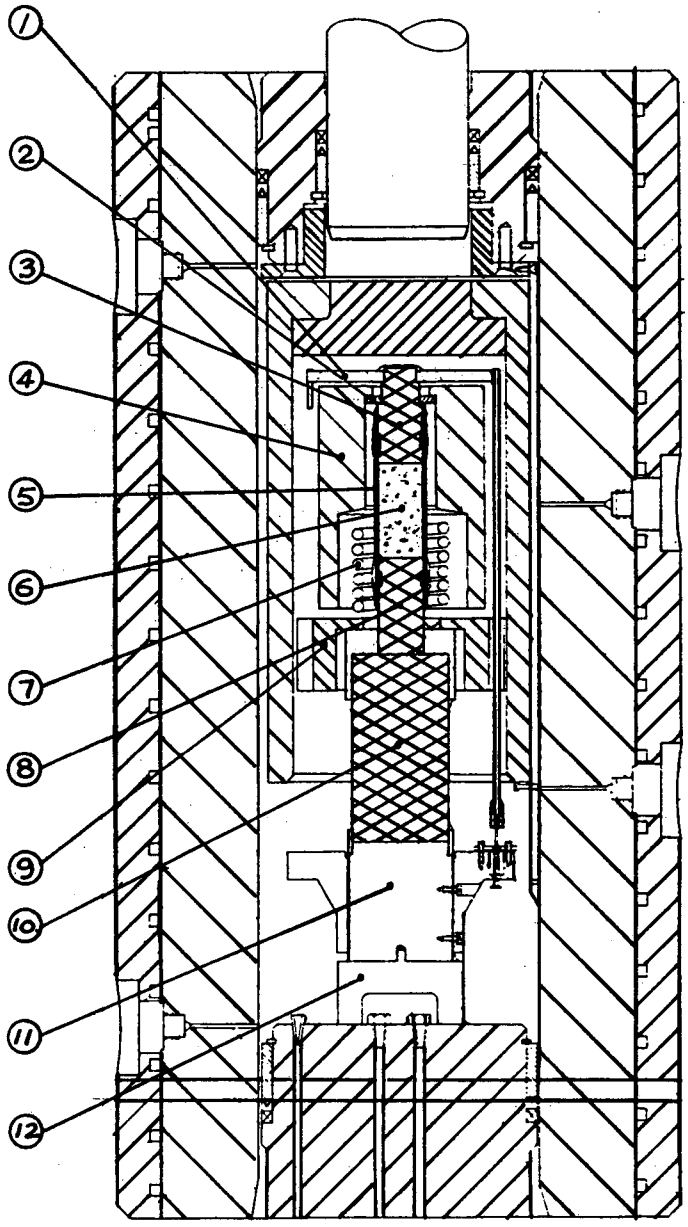

XBL 8112-12956

Fig. C6. Test set-up for thermal expansion.

High-resolution LVDT's located near the base of the stack measured the axial strain induced by sample temperature change. Thermal strains of up to $\pm$ 2.5 x 10^{-2}cm could be measured with an accuracy of $\pm$ 6.2 x 10^{-5} cm. Averaging the outputs of the two LVDT's removed any false strain due to tilting. Calibration was accomplished with three materials: fused quartz, steel, and aluminum. With the use of accepted expansion coefficients for these materials, the system expansion was determined as the expansion in excess of published values for the calibration samples. The system expansion is typically 0.5 x 10^{-6} cm/cm°C, and is repeatable regardless of the sample material.

Temperature was monitored by a thermocouple placed at midpoint on the sample, continually in contact with the sample jacket. Temperature was increased at a rate of 2°C/min.

Samples were 2 inches in diameter and 4 inches in length (unless otherwise noted), with the ends ground flat and parallel to within 2.5 x 10^{-3} cm. Before jacketing, the samples were bonded to the endcaps, with a minimum sized peripheral ring of adhesive along the interface line. A prestretched silicone jacket was sealed to the fused quartz endcaps by lock wire. Silicone jackets are preferred to copper in this type of testing because of the low Young's modulus of the silicone.

Tests 3 and 4 were run at 10 MPa hydrostatic pressure and in a cyclic (temperature) manner. The axial and confining stresses were first brought together to the desired level to avoid a large deviatoric stress that might contribute to fracturing. Next, the temperature was increased in 25°C intervals, with the temperature and expansion allowed to stabilize for 30 minutes at each temperature. A heating rate of 2°C/min was used.

The sample for test 3 was a section of core from hole E13 (6.283 m - 6.385 m). The sample was unfractured, with a fairly regular grain size of about 1/8 inch. A few pyrite flakes of 1/16-inch diameter were also present. The sample temperature was raised in four cycles from 30°C to 203°C. The raw data is plotted in Fig. C-7. The form of this curve and the magnitude of the thermal strains are very similar to those shown previously for test 2. A fourth-order fit of all of the heat-up strains was made and is shown as the smooth curve in Fig. C-7. From this curve, the value of α was calculated over successive 25°C intervals by taking differences in the strain and dividing by the change in temperature over the interval. The resultant values of α are plotted in Fig. C-8 at the midpoints of these intervals. This curve is similar to that of test 2, with values ranging from approximately 6.5 x 10^{-6}/°C over the interval of 25°C-100°C to about 21 x 10^{-6}/°C at 200°C.

Hysteresis of approximately 1 x 10^{-4} in./in. was obtained after a temperature of 98°C was reached in cycle 2. Subsequent cycles show increasing magnitudes of hysteresis (e.g., cycle 3 shows a hysteresis of about 2 x 10^{-4}in./in.; the final cycle obtained a low temperature of only 75°C). This appears to be contrary to work by others (Richter and Simmons, 1974; and Heard, 1980) who saw little or no permanent strains until temperature cycling of over 300°C. However, recent work at Texas A&M (Bauer & Johnson, 1979) may have shown significant permanent volumetric strains ($\Delta v/v$) in Charcoal Black granite when heated above 100°C and in Westerly granite above temperatures of 200 to 250°C. The hysteresis seen in those studies increases as a function of the maximum temperature achieved during the cycling and is of the same magnitude as that seen here.

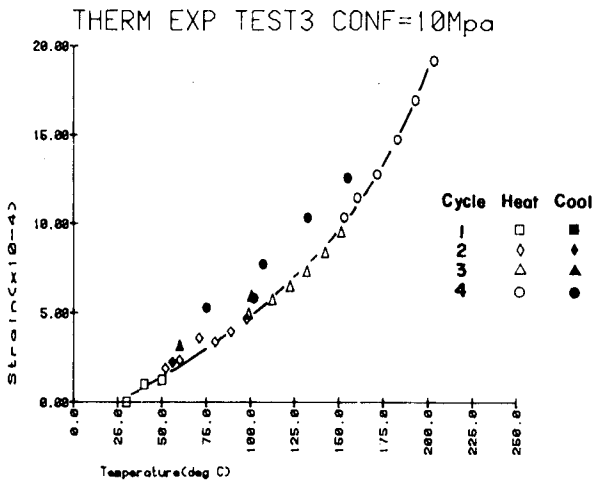

Fig. C7. Thermal strain as a function of temperature, test 3.

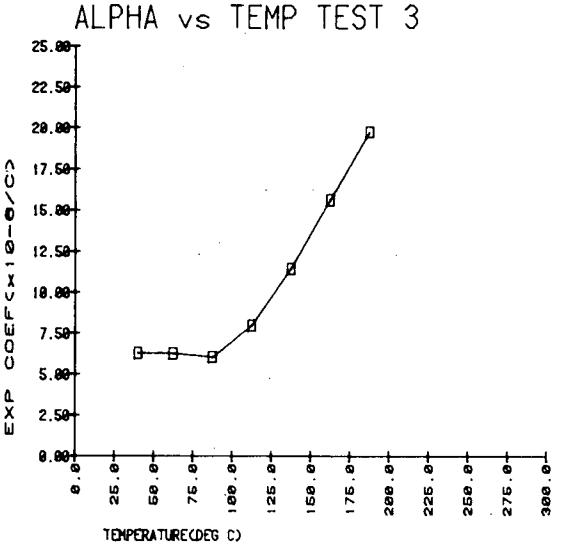

XBL 8112-12957

Fig. C8. Alpha as a function of temperature, test 3.

Test 4 was conducted identically to test 3. Sample 4 was taken from borehole E13, 5.138 m - 5.24 m; and was highly fractured. A fracture zone 3/4 to 1-1/4 inch thick, consisting of chlorite with a small amount of calcite, dipped at approximately 30° to the core axis. As seen in Fig. C-9, it appears that the highly fractured nature of the core had little effect on the resulting thermal strains. Strain magnitudes at temperatures lower than 100°C were slightly lower with this sample, but strains at the higher temperatures were nearly identical. Whereas in test 3, the hysteresis increased at the completion of each successive cycle, it seemed to be random in test 4. Fig. C-10 is a plot of α vs. temperature over the same intervals as before. In this case, a fourth-order polynomial was fit to the strains and expansion coefficients were determined as before.

Three additional tests were conducted at hydrostatic pressures of 25 MPa with the intent of examining the expansion coefficient at low (<25°C) and high (>200°C) temperature ranges. These final tests were performed in one temperature cycle to avoid inducing damage in the sample during thermal cycling. The sample temperature was raised at a rate of 2°C/min, with the temperature and strain allowed to stabilize for 30 minutes at 25°C intervals. The axial and confining stresses were brought up together to avoid a large deviatoric stress.

Test 5 was conducted on a core sample from hole E13 (8.22 m - 8.322 m). This sample had one continuous chlorite-filled fracture (approx. 1/16 in. thick) across its midplane. The thermal strains are plotted in Fig. C-11. The calculation of α was accomplished by taking a straight difference

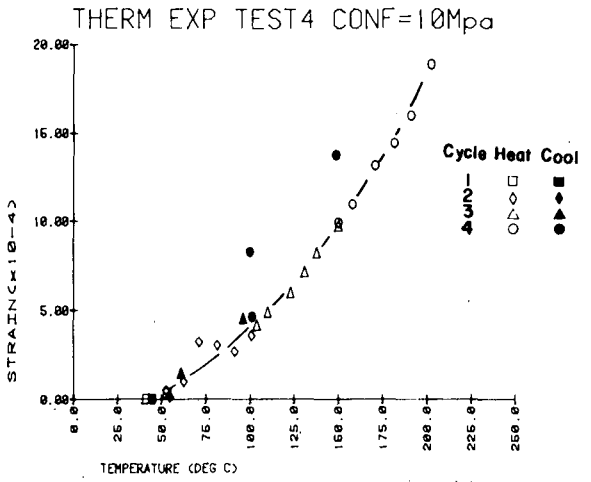

Fig. C9. Thermal strain as a function of temperature, test 4.

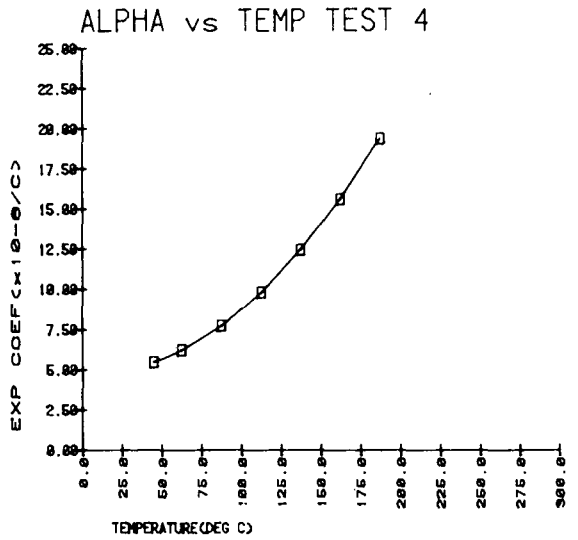

XBL 8112-12958

Fig. C10. Alpha as a function of temperature, test 4.

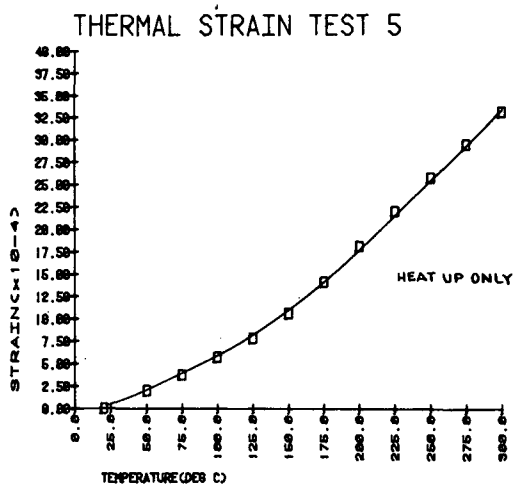

Fig. C11. Thermal strain as a function of temperature, test 5.

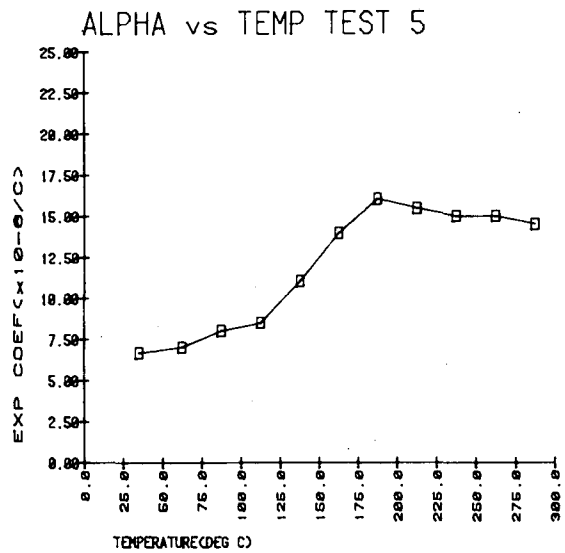

XBL 8112-12959

Fig. C12. Alpha as a function of temperature, test 5.

of the successive strains given in Fig. C-11. The expansion coefficient (Fig. C-12) closely follows those generated from other tests. However, there is a sharp break in slope at the temperature interval of 200°C-225°C, followed by a relatively constant α of approximately 14-14.5 x 10^{-6}/°C thereafter.

Test 6 was originally planned to run from a temperature of 10°C to 400°C. However, problems were encountered at about 300°C, when a teflon heat-shrunk confining jacket failed and the tests was terminated. In order to determine α at low temperatures, the confining fluid reservoir as well as the pressure vessel were cooled with dry ice for several hours until the temperature stabilized at 10°C. A plot of the raw data and the best fit curve drawn through the data are given in Fig. C-13. The calculation of α from this curve resulted in a behavior very different from that seen in the earlier tests (Fig. C-14). At temperatures below 125°C, the data are similar to previous tests, yielding an α of approximately 5.5 x 10^{-6}/°C from about 10° - 30°C, increasing to approximately 7.5 x 10^{-6}/°C at 125°C. From this point, the curve becomes much flatter than previous cases, reaching a maximum of about 12.5 x 10^{-6}/°C at 275°C and remaining stable thereafter. This is the type of effect one might expect in response to increasing confining pressure: i.e., as the confining pressure increases, the value of α tends toward a more uniform value, with less variation due to damage caused by microcracks.

Test 7 yielded similar behavior to test 6. As many problems with jacket failure at higher temperatures occurred, a new jacketing material was used. The material was TFE Teflon which is rated at 400°C. As the TFE was available only in a 1-inch ID tube, the core size for this test was reduced to

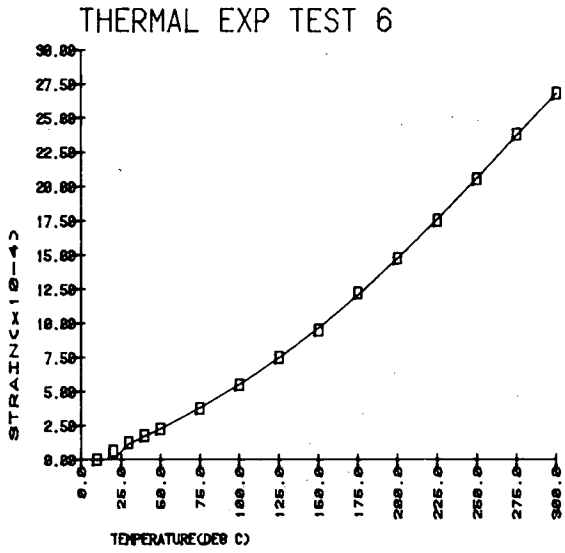

Fig. C13. Thermal strain as a function of temperature, test 6.

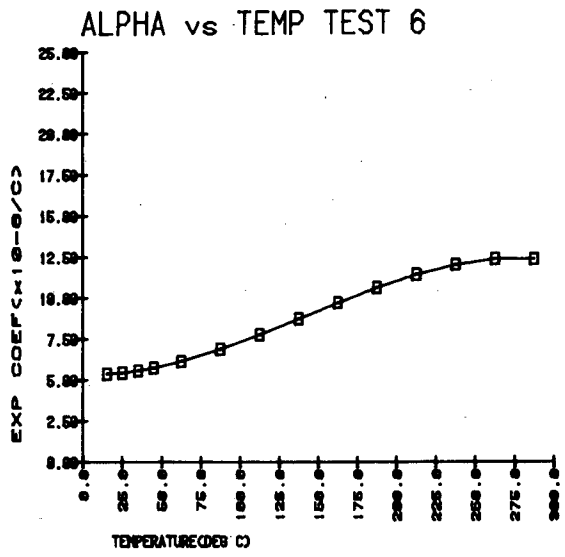

XBL 8112-12960

Fig. C14. Alpha as a function of temperature, test 6.

1 inch diameter by 2 inches in length. This test was to be run to as high a temperature as possible (499°C max) in one temperature cycle so as to determine α at the highest temperature range at Stripa. Again, this test was not without problems. Figure C-15 shows the sample strain as a function of temperature. An increase in strain very similar to that shown for test 6 was seen. After the sample was allowed to stabilize at 325°C, the temperature was again increased at a rate of 2°C/min to 350°C. Both LVDT's, however, showed no increase in sample strain, even when the temperature was allowed to stabilize at 350° and 375°C for 30 minutes. When the sample temperature was increased from 375°C to 396°C, both LVDT's showed a large increase in sample strain. Although the general consensus is that this phenomenon is a result of sticking of the displacement transducers until sufficient strain had occurred to free them, there is no convincing evidence for this explanation. Thus, a dashed line has been shown from 325° to 396°C on Fig. C-15.

The calculation of α was made from the smoothed data as discussed previously (Fig. C-16). The calculations were only performed through 325°C and show the same behavior as that for test 6.

DISCUSSION

Overlays of α vs. temperature for all tests and for those performed at 25 MPa confinement are given in Fig. C-17a and C-17b. The data shown in these figures was averaged for each group of tests at a given confining pressure (this was a simple average) and is plotted as a function of temperature in Fig. C-18. Both averaged and unaveraged data are given in these three figures because so few data points made averaging questionable.

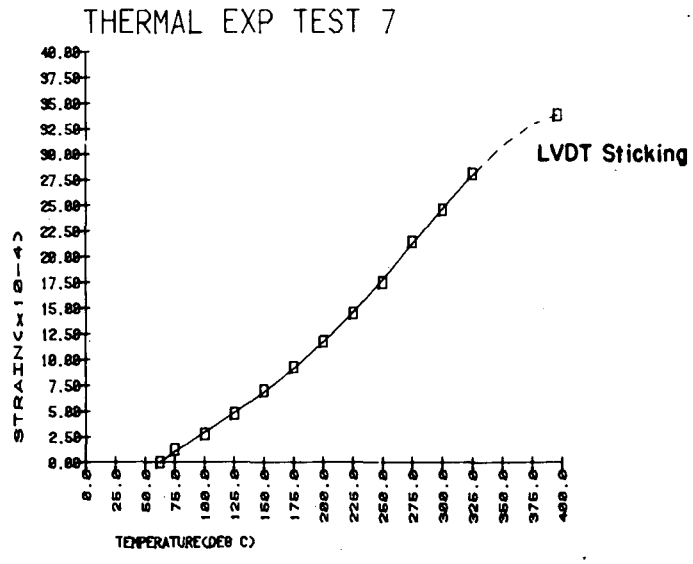

Fig. C15. Thermal strain as a function of temperature, test 7.

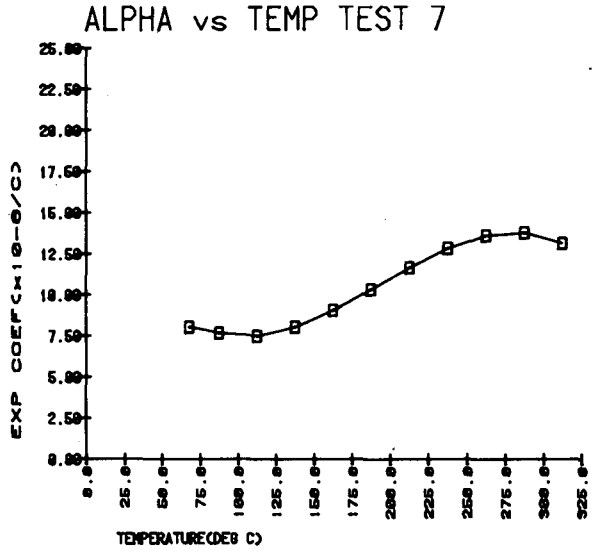

XBL 8112-12961

Fig. C16. Alpha as a function of temperature, test 7.

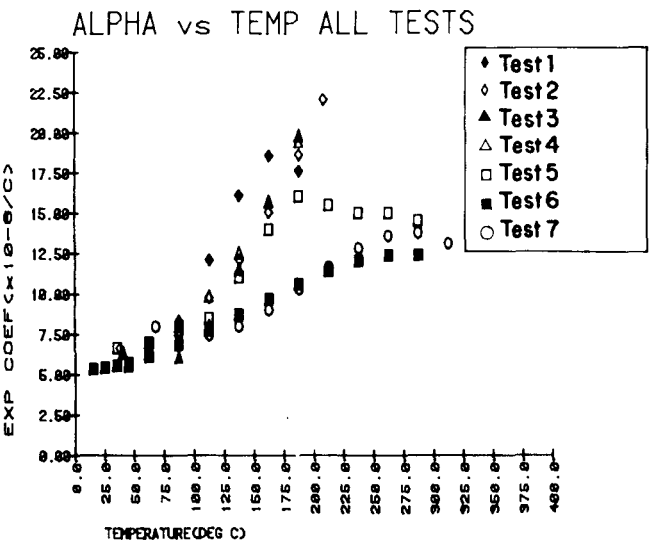

Fig. C17a. Overlay of α vs. temperature for all tests.

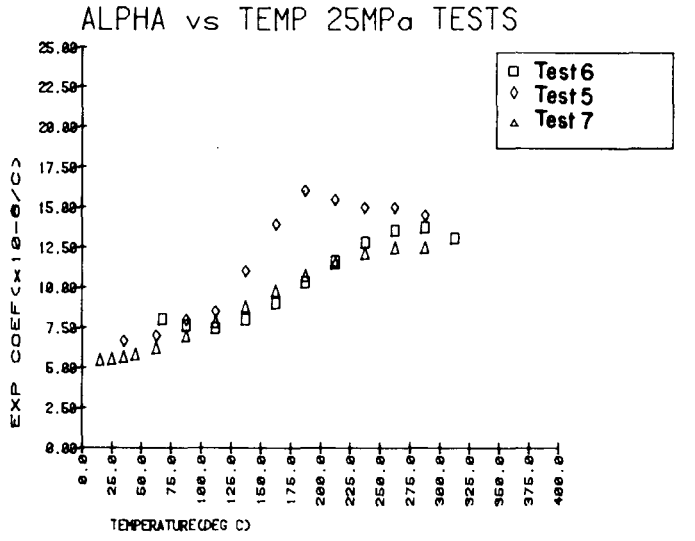

XBL 8112-12962

Fig. C17b. Overlay of α vs. temperature for 25MPa confinement only.

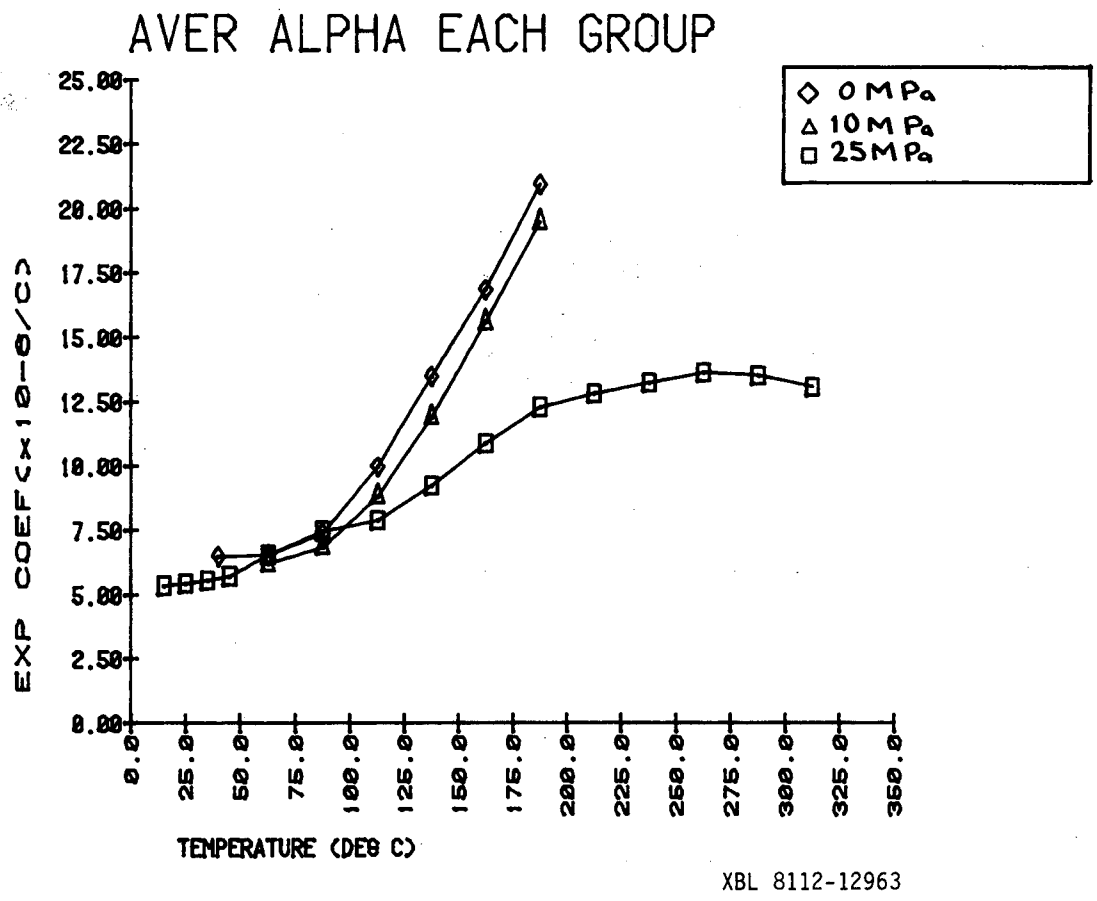

Fig. C18. Alpha vs. temperature for averaged data.

The behavior in the tests performed at 0 and 10 MPa hydrostatic loading were very similar, with the values for 10 MPa falling slightly below those for the unconfined tests. This varies from testing performed on the Climax Stock (Heard, 1980) where a large difference in magnitude of α was noted when moving from 0 to 13.8 MPa. Heard also saw the 13.8 MPa curve "turn over," as is seen here for the 25 MPa case at temperatures between 200 and 250°C (Fig. C-18). In this case, very few samples were tested, and they were tested with different apparatus. The tests at 0 and 10 MPa show a drastic increase in α starting at a temperature between 75°C and 100°C. Bauer and Johnson (1979) noted an irreversible change in longitudinal seismic velocity as well as the onset of acoustic emission for samples of Westerly and Charcoal granite when heated to 75°C or greater. This behavior has been attributed to the onset of thermal cracking, which is primarily a result of differential expansion of neighboring quartz and feldspar grains. Further heating creates new microcracks and widens old fractures. The rapid change in thermal strain at around 100°C could also be related to boiling of pore water. If the sample pores are not fully saturated, pore water will not be under the same confining stress as the matrix, which would allow boiling at 100°C even at confining stress.

One might expect a more dramatic effect of confinement on the difference in magnitude of α when moving from 0 to 10 MPa, as confinement will tend to inhibit microcrack development and growth. The possibility that α was artificially increased in tests 3 and 4 due to the cyclic temperature loading is downgraded somewhat, as others (Richter and Simmons, 1974, and Heard, 1980) saw little permanent change in expansion with cycling until temperatures over 250°C were reached. Another interesting point is that the strain showed very little offset when raised to the previous maximum temperature at each new cycle during tests 3 and 4.

The expansions for the final tests are given in Fig. C-17b, with averaged values in Fig. C-18. Although these tests have some conflicting results, they appear to indicate a definite effect of confinement similar to that seen by Heard. These tests followed the same general expansion behavior as previous testing until a temperature of 75-100°C was reached, when tests 6 and 7 diverged from the rest and showed a more gradual increase in thermal strain. This behavior conforms with the work by Bauer and Johnson and suggests that extensive microcracking began at this point. The confining pressure tended to inhibit growth of cracking, resulting in smaller strains. Why test 5 did not follow this behavior is not known. Test results did not indicate a leak of the confining jacket or any other phenomenon that could account for this behavior. A distinct break in the α vs. temperature curve was seen between 200° and 250°C. This break was also seen by Heard for tests on Climax Stock quartz monzonite at 13.8 and 27.6 MPa confining pressure, as well as by Bauer and Johnson. They observed a break in slope of the longitudinal wave velocities of Westerly and Charcoal granite samples temperature-cycled to 250°C. This temperature also corresponded to the point at which significant permanent volumetric strains were recorded and at which permeability displayed a change in its relationship to linear porosity. The authors were uncertain as to the cause of this behavior, but noted a reduction in the rate of microcrack development between 200 and 500°C for Charcoal granite as determined from SEM surveys of polished thin sections. The cause might be determined by examining the expansion characteristics of quartz and feldspar over this temperature range.

This report is part of a cooperative Swedish-American project supported by the U.S. Department of Energy and/or the Swedish Nuclear Fuel Supply Company. Any conclusions or opinions expressed in this report represent solely those of the author(s) and not necessarily those of The Regents of the University of California, the Lawrence Berkeley Laboratory, the Department of Energy, or the Swedish Nuclear Fuel Supply Company.

TECHNICAL INFORMATION DEPARTMENT
LAWRENCE BERKELEY LABORATORY
UNIVERSITY OF CALIFORNIA
BERKELEY, CALIFORNIA 94720